TABLE OF CONTENTS

CHAPTER 4.0

REACTOR

TABLE OF CONTENTS (Continued)

TABLE OF CONTENTS (Continued)

TABLE OF CONTENTS (Continued)

TABLE OF CONTENTS (Continued)

TABLE OF CONTENTS (Continued)

LIST OF TABLES

TABLE OF CONTENTS (Continued)

LIST OF TABLES

CHAPTER 4 - LIST OF FIGURES

*Refer to Section 1.6 and Table 1.6-3. Controlled drawings were removed from the USAR at Revision 17 and are considered incorporated by reference.

CHAPTER 4 - LIST OF FIGURES

*Refer to Section 1.6 and Table 1.6-3. Controlled drawings were removed from the USAR at Revision 17 and are considered incorporated by reference.

CHAPTER 4 - LIST OF FIGURES

*Refer to Section 1.6 and Table 1.6-3. Controlled drawings were removed from the USAR at Revision 17 and are considered incorporated by reference.

Figure #	Sheet	Title	Drawing #*
4.3-27		Deleted	
4.3-28		Deleted	
4.3-29		Deleted	
4.3-30		Deleted	
4.3-31		Deleted	
4.3-32		Deleted	
4.3-33		Deleted	
4.3-34		Deleted	
4.3-35		Deleted	
4.3-36		Rod Cluster Control Assembly Pattern	
4.3-37		Example Differential and Integral Rod Worth Versus Steps Withdrawn at MOL, HZP, HFP, EQ Xenon Banks D, C, and B Moving With 113 Step Overlap	
4.3-38		Design Trip Curve	
4.3-39		Typical Normalized Rod Worth Versus Percent Insertion, All Rods Out But One	
4.3-40		Axial Offset Versus Time, PWR Core With A 12 Foot Height and 121 Assemblies	
4.3-41		X-Y Xenon Test Thermocouple Response Quadrant Tilt Difference Versus Time	
4.3-42		Calculated and Measured Doppler Defect and Coefficients at BOL, 2-Loop Plant, 121 Assemblies, 12 Foot Core	
4.3-43		Comparison of Calculated and Measured Boron Concentration 2-Loop Plant, 121 Assemblies, 12 Foot Core	
4.3-44		Comparison of Calculated and Measured C_B, 2-Loop Plant, 121 Assemblies, 12 Foot Core	
4.3-45		Comparison of Calculated and Measured C_B, 3-Loop Plant, 157 Assemblies, 12 Foot Core	
4.3-46		Typical Boron Letdown Curve	
4.4-1		Deleted	
4.4-2		Deleted	
4.4-3		Deleted	
4.4-4		TDC Versus Reynolds Number for 26 Inch Grid Spacing	
4.4-5		Normalized Radial Flow and Enthalpy Distribution at 4 Foot Elevation	

CHAPTER 4 - LIST OF FIGURES

*Refer to Section 1.6 and Table 1.6-3. Controlled drawings were removed from the USAR at Revision 17 and are considered incorporated by reference.

CHAPTER 4.0

REACTOR

4.1 SUMMARY DESCRIPTION

This chapter describes: 1) the mechanical components of the reactor and reactor core, including the fuel rods and fuel assemblies, 2) the nuclear design, and 3) the thermal-hydraulic design.

The reactor core is composed of an array of fuel assemblies that are similar in mechanical design, but different in fuel enrichment. Within each fuel assembly, all rods are of the same enrichment. Three different enrichments were employed in the first core. The enrichments for Cycle 1 at Wolf Creek were 2.10 (Region 1), 2.60 (Region 2), and 3.10 (Region 3) weight percent. The average enrichments were increased in subsequent reloads in order to achieve an eighteen month cycle. This began in Cycle 2 and Cycle 4 was the first eighteen month cycle. Enrichments up to 5.0 weight percent may be used for reload fuel when credit is taken for integral fuel burnable absorbers (IFBA) or 4.6 weight percent without credit of IFBA.

The Westinghouse 17x17 low-parasitic (LOPAR) fuel design was used during cycle 1 and for the fresh fuel loaded in Cycles 2 and 3 as well. Cycle 4 fresh fuel incorporated the anti-snag grid design into the LOPAR fuel design. Cycle 5 fresh fuel added the reconstitutable top nozzle (RTN) and debris filter bottom nozzle (DFBN) features to the WCGS fuel design. Cycle 6 fresh fuel incorporated the low pressure drop Zircaloy mid grid feature as described in Reference 1. With the incorporation of the Zircaloy mid grids, the WCGS fuel design changed from the LOPAR design to the Westinghouse VANTAGE 5H (V5H)fuel design. Cycle 7 fresh fuel incorporated the Zircaloy Intermediate Mixing Vane Grids (IFM), as described in Reference 1, to provide additional coolant mixing in the upper fuel regions. An Inconel Protective Bottom Grid (PBG) was added to Cycle 8 fresh fuel to provide an additional debris barrier and increased fretting resistance. Cycle 9 fresh fuel incorporated the Integral Fuel Burnable Absorber (IFBA) design, as described in Reference 1, as an alternative to discrete burnable absorbers. Cycle 10 fresh fuel incorporated fully enriched annular axial blankets and the use of ZIRLO® as the material for the manufacture of the fuel clad, guide thimble and instrumentation tubes, mid grids, and IFM grids. With the incorporation of the ZIRLO material, the WCGS fuel design changed to the Westinghouse VANTAGE 5H with Performance + features (V5H P+) fuel design. The V5H P+ design is the .374" outside diameter rod equivalent to the VANTAGE+ design discussed in Reference 2. The Cycle 10 fresh fuel also included 8 demonstration assemblies of the Robust Fuel Assembly (RFA) design. The differences between the V5H P+ design and the RFA design are discussed in Reference 4. The Cycle 12 fresh fuel incorporated a revised rod design that increases the void volume available in the fuel rod and is referred to as the low rod internal pressure fuel rod design. The low rod internal pressure fuel rod design is discussed in Reference 5. With the incorporation of the low rod internal pressure fuel rod design the WCGS fuel design changed to the Westinghouse VANTAGE 5H with Performance + features, ZIRLO^{+2} (V5H P+Z^{+2}) fuel design.

The Cycle 13 fresh fuel incorporated the features of the Robust Fuel Assembly design, including modified mid-grids, modified IFM grids, and thicker wall guide thimble and instrument tubes, into the V5H P+Z^{+2} design. With the incorporation of

---

these features the WCGS fuel design changed to the Westinghouse Standard Fuel Rod Robust Fuel Assembly ZIRLO^{+2} (STD RFA Z^{+2} or RFA Z^{+2}) design. The Cycle 13 fresh fuel also included 4 demonstration assemblies that incorporated the RFA-2 mid-grid design and the Integral Clamp Top Nozzle (ICTN) design. The RFA-2 mid-grid is an improved mid-grid that provides increased margin for fretting wear, while maintaining the RFA mid-grids performance in other areas such as DNB and pressure drop. The key difference between the RFA and RFA-2 mid-grid design is the increased spring and dimple contact area with the fuel rod. The complete discussion of the differences between the modified mid-grid used in the RFA Z^{+2} design and RFA-2 mid-grid is contained in Reference 6. The ICTN includes a modified top nozzle casting that includes the spring clamps. The springs are located with pins that are welded in place (to the integral clamp) but do not react to the spring force. The ICTN design eliminates the potential for the fracture of the hold down spring screws by the removal of the spring screws in the ICTN design. The modification increases the fuel assembly integrity and eliminates the potential for loose parts from fractured spring screws entering the RCS during normal operations or during fuel movement during refueling outages. The features of the Integral Clamp Top Nozzle are discussed in Reference 7.

The Cycle 14 fresh fuel incorporated the features of the 17x17 RFA-2 (second generation Robust Fuel Assembly) design, including modified mid-grids, modified IFM grids, and thicker wall guide thimble and instrument tubes. The RFA-2 design is identical to the RFA design except for the mid-grid. The key difference between the RFA and RFA-2 mid-grid design is the increased spring and dimple contact area with the fuel rod. There is no change to the fuel assembly length, envelope or fuel rod design relative to the RFA design. The RFA-2 mid-grid is an improved mid-grid that provides increased margin for fretting wear while maintaining the RFA mid-grids performance in others areas such as DNB and pressure drop. The complete discussion of the differences between the RFA-2 Z^{+2} modified mid-grid design and the RFA-2 Z^{+2} mid-grid design is contained in Reference 6.

The Cycle 16 fresh fuel incorporates the Westinghouse Integral Nozzle (WIN) top nozzle and a Performance+ feature of fuel rod oxide coating. The WIN top nozzle was previously known as the Integral Clamp Top Nozzle (ICTN) and was introduced in four demonstration assemblies in Cycle 13. The features of the WIN top nozzle are discussed in Reference 8. The fuel rod has an oxide coating at the bottom end of the fuel rod. The extra layer of oxide coating provides additional debris induced rod fretting wear protection. The features of the fuel rod oxide coating are discussed in Reference 9.

The Cycle 21 fresh fuel incorporates a Standardized Debris Filter Bottom Nozzle (SDFBN) and a Robust Protective Grid. The Robust Protective Grid is provided as part of the Combination Grid which also included the bottom grid. This change will impact the location of the Protective Grid centerline in relation to the bottom of the fuel stack and the elevation of the Protective Grid to the bottom of the bottom nozzle. The SDFBN evaluation is discussed in Reference 10 and later in Section 4.2.2.2.1. The Robust Protective Grid is discussed in Reference 11 and Section 4.2.2.2.4.

Starting with Cycle 23 ZIRLO High Performance Fuel Optimized Cladding material will be utilized to contain the slightly enriched uranium dioxide fuel. The Optimized ZIRLO Cladding material is further described in Reference 12.

The core may consist of any combination of LOPAR, V5H, V5H P+, RFA, V5H P+ Z^{+2}, RFA Z^{+2} and RFA-2 Z^{+2} fuel assemblies as described in Subsection 4.2.2. The fuel is arranged in a checkered low-leakage pattern.

A fuel assembly is composed of 264 fuel rods in a 17 x 17 square array, except that limited substitution of filler rods for fuel rods may be made (Reference 3). The center position in the fuel assembly is reserved for incore instrumentation. The additional 24 positions in the fuel assembly have guide thimbles for the rod cluster control assemblies (RCCAs). The guide thimbles are joined to the bottom nozzles of the fuel assembly and also serve to support the fuel grids. The fuel grids consist of an "egg-crate" arrangement of interlocked straps that maintain lateral spacing between the rods. The straps have spring fingers and dimples which grip and support the fuel rods. The grids also have coolant-mixing vanes. The fuel rods consist of slightly enriched uranium, in the form of cylindrical pellets of uranium dioxide, contained in Zircaloy-4/ZIRLO tubing. The tubing is plugged and seal-welded at the ends to encapsulate the fuel. All fuel rods are pressurized internally with helium during fabrication to reduce clad creepdown during operation and thereby to increase fatigue life.

Depending on the position of the assembly in the core, the guide thimbles are used for rod cluster control assemblies (RCCAs), neutron source assemblies, or burnable absorber assemblies. If none of these are required, the guide thimbles may be fitted with plugging devices to limit bypass flow.

The bottom nozzle is a box-like structure which serves as the lower structural element of the fuel assembly and directs the coolant flow distribution to the assembly. The top nozzle assembly serves as the upper structural element of the fuel assembly and provides a partial protective housing for the RCCA or other components.

The RCCAs consist of 24 absorber rods fastened at the top end to a common hub or spider assembly. Each absorber rod consists of either all hafnium or an alloy of silver-indium-cadmium clad in stainless steel. The RCCAs are used to control relatively rapid changes in reactivity and to control the axial power distribution.

The reactor core is cooled and moderated by light water at a pressure of 2250 psia. Soluble boron in the moderator/coolant serves as a neutron absorber. The concentration of boron is varied to control reactivity changes that occur relatively slowly, including the effects of fuel burnup and transient xenon. Burnable absorber rods were also employed in the first core and subsequent reloads to limit the amount of soluble boron required and thereby maintain the desired range of reactivity coefficients. Either the borosilicate glass burnable absorber, the Wet Annular Burnable Absorber (WABA), or the Integral Fuel Burnable Absorber (IFBA) are included in subsequent reloads.

The nuclear design analyses established the core locations for control rods and burnable absorbers and define design parameters, such as fuel enrichments and boron concentration in the coolant. The nuclear design analyses established that the reactor core and the reactor control system satisfy all design criteria, even if the highest reactivity worth RCCA is in the fully withdrawn position. The core has inherent stability against diametral and azimuthal power oscillations. Axial power oscillations which may be induced by load changes and resultant transient xenon may be suppressed by the use of the control rods (RCCAs).

The thermal-hydraulic design analyses established that adequate heat transfer is provided between the fuel clad and the reactor coolant. The thermal design takes into account local variations in dimensions, power generation, flow distribution, and mixing. The mixing vanes incorporated in the fuel assembly spacer grid design induce additional flow-mixing between the various flow channels within a fuel assembly as well as between adjacent assemblies.

The performance of the core is monitored by fixed neutron detectors outside of the core, movable neutron detectors within the core, and thermocouples at the outlet of selected fuel assemblies. The ex-core nuclear instrumentation provides input to automatic control functions.

Table 4.1-1 presents the principal nuclear, thermal-hydraulic, and mechanical design parameters of WCGS.

The analytical techniques employed in the core design are tabulated in Table 4.1-2. The mechanical loading conditions considered for the core internals and components are tabulated in Table 4.1-3. Specific or limiting loads considered for design purposes of the various components are listed as follows: fuel assemblies in Section 4.2.1.5 and neutron absorber rods, burnable absorber rods, neutron source rods, and thimble plug devices in Section 4.2.1.6. The dynamic analyses, input forcing functions, and response loadings are presented in Section 3.9(N).

4.1.1 REFERENCES

1. Davidson, S. L., (Ed.), et al., "VANTAGE 5 Fuel Assembly Reference Core Report," WCAP-10444-P-A, September 1985, and Addendum 2A, February 1989.

2 Davidson, S. L., and Nuhfer, D. L. (Eds.), "VANTAGE+ Fuel Assembly Report," WCAP-12610-P-A, April 1995.

3. Slagle, W. H. (Ed.), "Westinghouse Fuel Assembly Reconstitution Evaluation Methodology," WCAP-13060-P-A, July 1993.

4. O'Cain, M.B., (Ed.), "17 x 17 Wolf Creek Robust Fuel Assembly Final Design Review Package," DR-97-2 (Proprietary), July 1997.

5. Shah, H., (Ed), "Low RIP Fuel Rod Design," DR-98-04 (Proprietary), October 1998.

6. Seel, D. D. (Ed.), "17 x 17 Robust Fuel Assembly with RFA-2 Mid-Grid Final Design Review Package", DR-01-5 (Proprietary), October 2001.

7. Maurer, B.F., "Generic – Implementation of Integral Clamp Top Nozzle (ICTN) Design Change – 15 x 15 and 17 x 17, 12 Foot Fuel Assemblies", EVAL-01-067, November 2001.

8. Kitchen, T. J., "Generic – Implementation of the Westinghouse Integral Nozzle (WIN) for 15x15 and 17x17, 12 foot Fuel Assemblies," EVAL-04-10, February 2004.

9. Kitchen, T. J., "Revision to Generic PERFORMANCE+ Fuel Assembly Safety Evaluation – SECL-92-305, Rev. 0," EVAL-03-127, May 2004.

10. Solomon, D. K., "17x17 Standardized Debris Filter Bottom Nozzle with Flow Hole Elimination – Impact on Best Estimate Flow (BEF) Calculations", EVAL-09-8, Revision 9, December 2013.

11. Solomon, D. K., "Generic – 17x17 Robust Protective Grid (RPG)", EVAL-10-12, Revision 4, October 2012.

12. Shah, H. H., "Optimized ZIRLO, WCAP-12610-P-A & CENPD-404-P-A, Addendum 1-A, July 2006.

TABLE 4.1-1

REACTOR DESIGN TABLE

Thermal and Hydraulic Design Parameters	WCGS
1. Reactor core heat output, MWt	3,565 *
2. Reactor core heat output, 10^6 Btu/hr	12,164
3. Heat generated in fuel, %	97.4
4. System pressure, nominal, psia	2,250
5. Not Used	
6. Minimum departure from nucleate boiling ratio for design transients	1.24
7. DNB correlation	WRB-2
Coolant Flow	
8. Total thermal flow rate, gpm	361,200
9. Effective flow rate for heat transfer, gpm	330,859

*All non-LOCA analyses have been performed assuming a conservatively high reactor core heat output of 3637 MWt which is intended to bound a core thermal power output of 3565 MWt plus a 2% power uncertainty, or an increased core thermal power and a corresponding power uncertainty that, when combined, do not exceed 3637 MWt reactor core heat output.

TABLE 4.1-1 (Sheet 2)

Thermal and Hydraulic Design Parameters	WCGS
Coolant Flow (Continued)	
10. Effective flow area for heat transfer, ft^2	51.1
11. Average velocity along fuel rods, ft/sec	14.4
12. Average mass velocity, 10^6 lbm/hr-ft^2	2.42
13. Nominal inlet, °F	555.8
14. Average rise in vessel, °F	65.2
15. Average rise in core, °F	70.4
16. Average in core, °F	593.2
17. Average in vessel, °F	588.4
Heat Transfer	
18. Active heat transfer, surface area, ft^2	59,742
19. Average heat flux, Btu/hr-ft^2	198,315
20. Not Used	
21. Average linear power, kW/ft	5.691

TABLE 4.1-1 (Sheet 3)

Thermal and Hydraulic Design Parameters	WCGS
Heat Transfer (Continued)	
22. Peak linear power for normal operation, kW/ft	14.23
23. Peak linear power resulting from overpower transients/operator errors, assuming a maximum overpower of 121%, kW/ft	22.4
24. Heat flux hot channel factor, F_Q	2.50[b]
25. Peak fuel control temperature at peak linear power for prevention of centerline melt, °F	4,700
Core Mechanical Design Parameters	
26. Number of fuel assemblies	193

27. Designs	RCC canless 17 X 17 LOPAR	RCC canless 17 X 17 V5H	RCC canless 17 X 17 V5H w/IFM	RCC canless 17 X 17 V5H w/IFM & PBG	RCC canless 17 x 17 V5H P+	RCC canless 17 x 17 V5H P+ Z^{+2}	RCC canless 17 x 17 RFA Z^{+2} and RFA-2 Z^{+2}
28. UO_2 rods per assembly	264	264	264	264	264	264	264
29. Rod pitch, in.	0.496	0.496	0.496	0.496	0.496	0.496	0.496
30. Overall dimensions, in.	8.426 x 8.426	8.426 x 8.426	8.426 x 8.426	8.426 x 8.426	8.426 x 8.426	8.426 x 8.426	8.426 x 8.426
31. Fuel weight, as UO_2, lb per assembly (typical)	1154	1154	1154	1149	1132	1138	1138

TABLE 4.1-1 (Sheet 4)

Core Mechanical Design Parameters

32.	Zircaloy-4, Zirlo, or Optimized ZIRLO cladding weight, lb per assembly (Approx.)	264	270	275	278	275	274	274
33.	Number of grids per assembly	See Note 1	See Note 2	See Note 3	See Note 4	See Note 5	See Note 5	See Note 5
34	Loading technique	3 Region Nonuniform	3 Region Nonuniform	3 Region Nonuniform	3 Region Nonuniform	3 Region Nonuniform	3 Region Nonuniform	3 Region Nonuniform

Note 1 8 Total Grids, 1 Inconel Top Grid, 6 Inconel Mid Grids, 1 Inconel Bottom Grid
Note 2 8 Total Grids, 1 Inconel Top Grid, 6 Zircaloy Mid Grids, 1 Inconel Bottom Grid
Note 3 11 Total Grids, 1 Inconel Top Grid, 6 Zircaloy Mid Grids, 3 Zircaloy IFM Grids, 1 Inconel Bottom Grid
Note 4 12 Total Grids, 1 Inconel Top Grid, 6 Zircaloy Mid Grids, 3 Zircaloy IFM Grids, 1 Inconel Bottom Grid, 1 Inconel Protective Bottom Grid
Note 5 12 Total, 1 Inconel Top Grid, 6 Zirlo™ Mid Grids, 3 Zirlo™ Intermediate Flow Mixing Grids, 1 Inconel Bottom Grid, 1 Inconel Protective Bottom Grid or 1 Robust Protective Bottom Grid

Fuel Rods

35.	Total Number of Fuel Rods in the core	50,952						
36.	Outside diameter, in.	0.374	0.374	0.374	0.374	0.374	0.374	0.374
37.	Diametral gap, in.	0.0065	0.0065	0.0065	0.0065	0.0065	0.0065	0.0065
38.	Clad thickness, in.	0.0225	0.0225	0.0225	0.0225	0.0225	0.0225	0.0225
39.	Clad material	Zircaloy-4	Zircaloy-4	Zircaloy-4	Zircaloy-4	Zirlo™	Zirlo™	Zirlo or Optimized ZIRLO

Fuel Pellets

40.	Material	UO_2 sintered
41.	Density % of theoretical	95
42.	Diameter, in.	0.3225

TABLE 4.1-1 (Sheet 5)

Core Mechanical Design Parameters	WCGS	
Fuel Pellets		
43. Length, in (range)	0.372 - 0.530	
44. Fuel Enrichment, Weight Percent (range)	2.1 - 5.0	
45. Deleted		
Rod Cluster Control Assemblies		
46. Number of clusters, full length / part length	53 / -	
47. Neutron absorber Full length,	Hafnium	Ag-In-Cd
48. Cladding Material	Type 304 SS-cold worked	Type 304 SS-cold worked
49. Clad thicknesses, in	0.0185	0.0185
50. Number of absorber rods per cluster	24	24

TABLE 4.1-1 (Sheet 6)

Core Mechanical Design Parameters	WCGS
Core structure	
51. Core barrel, I.D./O.D., in.	148.0/152.5
52. Thermal shield	Neutron pad design
53. Baffle thickness, in.	0.88
Structure Characteristics	
54. Core diameter, equivalent, in.	132.7
55. Core height, active fuel, in.	143.7
Reflector Thickness and Composition	
56. Top, water plus steel, in.	≈10
57. Bottom, water plus steel, in.	≈10
58. Side, water plus steel, in.	≈15
59. H_2O/U molecular ratio core, lattice, cold	2.41

Notes:
(a) Not Used.
(b) This is the value of F^Q for normal operation.
(c) Limited substitution of filler rods for fuel rods is allowed.

TABLE 4.1-2

ANALYTICAL TECHNIQUES IN CORE DESIGN

ANALYSIS	Technique	Computer Code	Section Referenced
Mechanical design of core internals, loads, deflections, and stress analysis	Static and dynamic modeling	Blowdown code, FORCE, finite element, structural analysis code, and others	3.7(N).2.1 3.9(N).2 3.9(N).3
Fuel rod design Fuel performance characteristics (temperature, internal pressure, clad stress, etc.)	Semiempirical thermal model of fuel rod with consideration of fuel density changes, heat transfer, fission gas release, etc.	Westinghouse fuel rod design model	4.2.1.1 4.2.3.2 4.2.3.3 4.3.3.1 4.4.2.11
Nuclear design (initial core design)			
1. Cross sections and group constants	Microscopic data: macroscopic constants for homogenized core regions	Modified ENDF/B Library LEOPARD CINDER type	4.3.3.2

TABLE 4.1-2 (Sheet 2)

ANALYSIS	Technique	Computer Code	Section Referenced
Nuclear Design (initial core design)			
	Group constants for control rods with self-shielding	HAMMER-AIM	4.3.3.2
2. X-Y power distributions, fuel depletion, critical boron concentrations, X-Y xenon distributions, reactivity coefficients	2-D, 2-group diffusion theory	TURTLE	4.3.3.3
3. Axial power distributions, control rod worths, and axial xenon distribution	1-D, 2-group diffusion theory	PANDA	4.3.3.3
4. Fuel rod power	Integral transport theory	LASER	4.3.3.1
5. Effective resonance temperature	Monte Carlo weighting function	REPAD	

TABLE 4.1-2 (Sheet 3)

ANALYSIS	Technique	Computer Code	Section Referenced
Nuclear Design (Continued)			
6. Criticality of reactor and fuel assemblies	2-D, 2-group diffusion theory	LEOPARD PDQ	4.3.2.6
7. Vessel irradiation	Multigroup spatial dependent transport theory	DOT	4.3.2.8
Thermal-hydraulic design (initial core design)			
1. Steady state	Subchannel analysis of local fluid conditions in rod bundles, including inertial and cross-flow resistance terms, solution progresses from core-wide to hot assembly to hot channel	THINC-IV	4.4.4.5.2
2. Transient departure from nucleate boiling analysis	Subchannel analysis of local fluid conditions in rod bundles during transients by including accumulation terms in conservation equations; solution progresses from core-wide to hot assembly to hot channel	THINC-I (THINC-III)	4.4.4.5.2

TABLE 4.1-2 (Sheet 4)

ANALYSIS	Technique	Computer Code	Section Referenced
Nuclear Design (Reload Pattern Design & Analysis)			
1. Cross section and group constants	Micro-group neutron spectrum, cell average few-group cross sections, assembly average nodal constants	NEXUS/PARAGON	4.3.3.2
2. Rod worths, Boron worths & letdown, reactivity coefficients	3-D, Diffusion Theory - based Nodal Method	ANC9	4.3.3.3
3. Nodal power distributions	3-D, Diffusion Theory - based Nodal Method	ANC9	4.3.3.3
4. Fuel Pin Powers, INCORE constants	3-D, Diffusion Theory - based Nodal Method	ANC9	4.3.3.3
Thermal-hydraulic design (Reload Pattern Design & Analysis)			
1. Steady state and transient departure from nucleate boiling analysis	Subchannel analysis of local fluid conditions in rod bundles, including inertial and cross-flow resistance terms	VIPRE-01	4.4.4.5.2

TABLE 4.1-3

DESIGN LOADING CONDITIONS FOR REACTOR CORE COMPONENTS

1. Fuel assembly weight
2. Fuel assembly spring forces
3. Internals weight
4. Control rod trip (equivalent static load)
5. Differential pressure
6. Spring preloads
7. Coolant flow forces (static)
8. Temperature gradients
9. Differences in thermal expansion
   a. Due to temperature differences
   b. Due to expansion of different materials
10. Interference between components
11. Vibration (mechanically or hydraulically induced)
12. One or more loops out of service
13. All operational transients listed in Table 3.9(N)-1
14. Pump overspeed
15. Seismic loads (Operating Basis Earthquake and Safe Shutdown Earthquake)
16. Blowdown forces (due to cold and hot leg break)

4.2 FUEL SYSTEM DESIGN

The plant design conditions are divided into four categories in accordance with their anticipated frequency of occurrence and risk to the public: Condition I - Normal Operation; Condition II - Incidents of Moderate Frequency; Condition III - Infrequent Incidents; and Condition IV - Limiting Faults. Chapter 15.0 describes bases and plant operation and events involving each condition.

The reactor is designed so that its components meet the following performance and safety criteria:

a. The mechanical design of the reactor core components and their physical arrangement, together with corrective actions of the reactor control, protection, and emergency cooling systems (when applicable) ensure that:

   1. Fuel damage* is not expected during Condition I and Condition II events. It is not possible, however, to preclude a very small number of rod failures. These are within the capability of the plant cleanup system and are consistent with plant design bases.

   2. The reactor can be brought to a safe state following a Condition III event with only a small fraction of fuel rods damaged** although sufficient fuel damage might occur to preclude immediate resumption of operation.

   3. The reactor can be brought to a safe state and the core can be kept subcritical with acceptable heat transfer geometry following transients arising from Condition IV events.

b. The fuel assemblies are designed to withstand loads induced during shipping, handling, and core loading without exceeding the criteria of Section 4.2.1.5.

c. The fuel assemblies are designed to accept control rod insertions in order to provide the required reactivity control for power operations and reactivity shutdown conditions (if in such locations).

* Fuel damage as used here is defined as penetration of the fission product barrier (i.e., the fuel rod clad).

** In any case, the fraction of fuel rods damaged must be limited so as to meet the dose guideline of 10 CFR 50.67.

d. All fuel assemblies have provisions for the insertion of incore instrumentation necessary for plant operation.

e. The reactor internals, in conjunction with the fuel assemblies and incore control components, direct reactor coolant through the core. This achieves acceptable flow distribution and restricts bypass flow so that the heat transfer performance requirements can be met for all modes of operation.

4.2.1 DESIGN BASES

The fuel rod and fuel assembly design bases are established to satisfy the general performance and safety criteria presented in this section.

Design values for the properties of the materials which comprise the fuel rod, fuel assembly, and incore control components are given in Reference 2 for Zircaloy clad fuel, Reference 20 for ZIRLO clad fuel, and Reference 28 for Optimized ZIRLO clad fuel. Other supplementary fuel design criteria/limits are given in References 21, 27 and 28.

4.2.1.1 Cladding

a. Material and Mechanical Properties

Zircaloy-4, ZIRLO cladding, and Optimized ZIRLO cladding combines neutron economy (low absorption cross-section); high corrosion resistance to coolant, fuel, and fission products; and high strength and ductility at operating temperatures. Reference 1, 20, and 29 document documents the operating experience with Zircaloy-4 Zirlo cladding, and Optimized ZIRLO cladding as a clad material. Information on the mechanical properties of the cladding is given in References 2, 20 and 28 with due consideration of temperature and irradiation effects.

b. Stress-strain limits

1. Clad stress

The von Mises criterion is used to calculate the effective stresses. The cladding stresses under Condition I and II events are less than the Zircaloy 0.2% offset yield stress, with due consideration of temperature and irradiation effects. While the cladding has some capability for accommodating plastic strain, the yield stress has been accepted as a conservative design basis.

2. Clad tensile strain

The total tensile creep strain is less than 1% from the unirradiated condition. The elastic tensile strain during a transient is less than 1% from the pretransient value. This limit is consistent with proven practice.

c. Vibration and fatigue

1. Strain fatigue

The cumulative strain fatigue cycles are less than the design strain fatigue life. This basis is consistent with proven practice. (Ref. 1).

2. Vibration

Potential fretting wear due to vibration is prevented, ensuring that the stress-strain limits are not exceeded during design life. Fretting of the clad surface can occur due to flow-induced vibration between the fuel rods and fuel assembly grid springs. Vibration and fretting forces vary during the fuel life due to clad diameter creepdown combined with grid spring relaxation.

d. Chemical properties

Chemical properties of the cladding are discussed in Reference 2 for Zircaloy, Reference 20 for ZIRLO cladding, and Reference 28 for Optimized ZIRLO cladding.

4.2.1.2 Fuel Material

a. Thermal-physical properties

The thermal-physical properties of UO_2 are described in Reference 2 with due consideration of temperature and irradiation effects.

Fuel pellet temperatures - The center temperature of the hottest pellet is below the melting temperature of the UO_2 [melting point of 5080 °F (Ref. 3) unirradiated and decreasing by 58°F per 10,000 MWD/MTU]. While a limited amount of center melting can be tolerated, the design conservatively precludes center melting. A calculated fuel centerline temperature of 4700°F has been selected as an overpower limit to ensure no fuel melting. This provides sufficient margin for uncertainties, as described in Section 4.4.2.9.

The normal design density of the fuel is 95 percent of theoretical. Additional information on fuel properties is given in Reference 2.

b. Fuel densification and fission product swelling

The design bases and models used for fuel densification and swelling are provided in Reference 18.

c. Chemical properties

Reference 2 provides the justification that no adverse chemical interactions occur between the fuel and its adjacent material.

4.2.1.3 Fuel Rod Performance

The detailed fuel rod design establishes such parameters as pellet size and density, cladding-pellet diametral gap, gas plenum size, and helium pre-pressurization level. The design also considers the effects such as fuel density changes, fission gas release, cladding creep, and other physical properties which vary with burnup. The integrity of the fuel rods is ensured by designing to prevent excessive fuel temperatures, excessive internal rod gas pressures due to fission gas releases, and excessive cladding stresses and strains. This is achieved by designing the fuel rods to satisfy the conservative design bases in the following subsections during Condition I and Condition II events over the fuel lifetime. For each design basis, the performance of the limiting fuel rod must not exceed the limits specified.

a. Fuel rod models

The basic fuel rod models and the ability to predict operating characteristics are given in References 17, 18, 27, and Section 4.2.3.

b. Mechanical design limits

Fuel rod design methodology has been introduced that reduces the densification power spike factor to 1.0 and Reference 19 demonstrates that clad flattening will not occur in Westinghouse fuel designs.

The rod internal gas pressure remains below the value which causes the fuel/clad diametral gap to increase due to outward cladding creep during steady state operation. Rod pressure is also limited so that extensive departure from nucleate boiling (DNB) propagation does not occur during normal operation and any accident event. (Reference 7).

4.2.1.4 Spacer Grids

a. Mechanical limits and material properties

The grid component strength criteria are based on experimental tests. The limit is established at the lower 95%confidence on the true mean crush strength. This limit is sufficient to ensure that under worst-case combined seismic and blowdown loads from a Condition III and IV, loss-of-coolant accident, the core will maintain a geometry amenable to cooling. As an integral part of the fuel assembly structure, the grids satisfy the applicable fuel assembly design bases and limits defined in Section 4.2.1.5.

The grid material and chemical properties are given in Reference 2 for Zircaloy-4 and Reference 20 for Zirlo™.

b. Vibration and fatigue

The grids provide sufficient fuel rod support to limit fuel rod vibration and maintain clad fretting wear to within acceptable limits (defined in Section 4.2.1.1).

4.2.1.5 Fuel Assembly

a. Structural design

Integrity of the fuel assembly structure is ensured by setting design limits on potential stresses and deformations due to various loads and by preventing the assembly structure from interfering with the functioning of other components. Three types of loads are considered.

1. Non-operational loads such as those due to shipping and handling.

2. Normal and abnormal loads which are defined for Conditions I and II.

3. Abnormal loads which are defined for Conditions III and IV.

These limits are applied to the design and evaluation of the top and bottom nozzles, guide thimbles, grids, and the thimble joints.

The design bases for evaluating the structural integrity of the fuel assemblies are:

1. Nonoperational - 4 g axial and 6 g lateral loading with dimensional stability.

2. For the normal operating and upset conditions, the fuel assembly component structural design criteria are established for the two primary material categories, namely austenitic steels and Zirconium Alloys. The stress categories and strength theory presented in the ASME Boiler and Pressure Vessel Code, Section III, are used as a general guide. The maximum shear-theory (Tresca criterion) for combined stresses is used to determine the stress intensities for the austenitic steel components. The stress intensity is defined as the numerically largest difference between the various principal stresses in a three-dimensional field. The allowable stress intensity value for austenitic steels, such as nickel-chromium-iron alloys, is given by the lowest of the following:

   (a) One-third of the specified minimum tensile strength or 2/3 of the specified minimum yield strength at room temperature;

   (b) One-third of the tensile strength or 90 percent of the yield strength at temperature but not to exceed 2/3 of the specified minimum yield strength at room temperature.

The stress limits for the austenitic steel components are given below. All stress nomenclature is per the ASME Code, Section III.

Stress Intensity Limits

Categories	Limit
General primary membrane stress intensity	Sm
Local primary membrane stress intensity	1.5 Sm
Primary membrane plus bending stress intensity	1.5 Sm
Total primary plus secondary stress intensity	3.0 Sm

The Zircaloy, Zirlo, and Optimized ZIRLO structural components, which consist of guide thimbles, fuel tubes, and mixing grids are in turn subdivided into two categories because of material differences and functional requirements. The fuel tube design criteria are covered separately in Section 4.2.1.1. The maximum shear theory is used to evaluate the guide thimble design. For conservative purposes, the Zircaloy and Zirlo™ unirradiated properties are used to define the stress limits.

(c) Abnormal loads during Condition III or IV - worst cases represented by combined seismic and blowdown loads.

1. Deflections or failures of components cannot interfere with the reactor shutdown or emergency cooling of the fuel rods.

2. The fuel assembly structural component stresses under faulted conditions are evaluated using primarily the methods outlined in Appendix F of the ASME Code, Section III. Since the current analytical methods utilize elastic analysis, the stress allowables are defined as the smaller value of 2.4 Sm or 0.70 Su for primary membrane and 3.6 Sm or 1.05 Su for primary membrane, plus primary bending. For the austenitic steel fuel assembly components, the stress intensity is defined in accordance with the rules described in the previous section for normal operating conditions. For the Zircaloy and Zirlo™ components, the stress intensity, Sm, is set as the smaller value of 2/3 of the material yield strength, Sy, or 1/3 of the ultimate strength, Su, at reactor operating temperature. This results in Zircaloy and Zirlo™ stress limits being the smaller of 1.6 Sy or 0.70 Su for primary membrane and 2.4 Sy or 1.05 Su for primary membrane plus bending. For conservative purposes, the Zircaloy and Zirlo™ unirradiated properties are used to define the stress limits.

The material and chemical properties of the fuel assembly components are given in Reference 2 for Zircaloy-4 and Reference 20 for Zirlo™.

3. Thermal-hydraulic design

This topic is discussed in Section 4.4.

4.2.1.6 Incore Control Components

The control components are subdivided into permanent and temporary devices.

The permanent type components are the rod cluster control assemblies, secondary neutron source assemblies, and thimble plug devices. The temporary components are the burnable absorber assemblies and the primary neutron source assemblies, which are normally used only in the initial core.

Materials are selected for compatibility in a pressurized water reactor environment, for adequate mechanical properties at room and operating temperature, for resistance to adverse property changes in a radioactive environment, and for compatibility with interfacing components. Material properties are given in Reference 2.

The design bases for each of the mentioned components are given in the following subsections.

a. Control (neutron absorber) rods

Design conditions which are considered under Article NB-3000 of the ASME Code, Section III are as follows:

1. External pressure equal to the reactor coolant system operating pressure with appropriate allowance for overpressure transients

2. Wear allowance equivalent to 1,000 reactor trips

3. Bending of the rod due to a misalignment in the guide tube

4. Forces imposed on the rods during rod drop

5. Loads imposed by the control rod drive mechanism

6. Radiation exposure during maximum core life

The control rod cladding is cold drawn Type 304 stainless steel tubing. The stress intensity limit, Sm, for this material is defined as 2/3 of the 0.2 percent offset yield stress.

The absorber material temperature does not exceed its melting temperature*.

7. Temperature effects at operating conditions

* The melting point basis is determined by the nominal material melting point minus uncertainty.

b. Burnable absorber rods (standard and WABA)

The cladding for burnable absorber rods is designed as a Class 1 component under Article NB-3000 of the ASME Code, Section III, 1973 for Conditions I and II. For abnormal loads during Conditions III and IV, code stresses are not considered limiting. Failures of the burnable absorber rods during conditions III and IV do not interfere with reactor shutdown or cooling of the fuel rods.

The burnable absorber material is nonstructural. The structural elements of the burnable absorber rod are designed to maintain the absorber geometry even if the absorber material is fractured. In addition, the structural elements are designed to prevent excessive slumping. The standard burnable absorber material is borosilicate glass and is designed so that the absorber material is below its softening temperature (1510 °F + 18 °F for reference 12.5 w/o boron rod). The softening temperature for borosilicate glass is defined in ASTM C 338.

The wet annular burnable absorber (WABA) material is B_4C contained in an Alumina matrix. Thermal-physical and gas release properties of Al_2O_3-B_4C are described in reference 8. The WABA rods are designed so that the absorber temperature does not exceed 1200 °F during normal operation or an overpower transient. The 1200 °F maximum temperature He gas release in a WABA rod will not exceed 30% (reference 8).

c. Neutron source rods

The neutron source rods are designed to withstand the following:

1. The external pressure equal to the reactor coolant system operating pressure with appropriate allowance for overpressure transients, and

2. An internal pressure equal to the pressure generated by released gases over the source rod life

d.Thimble plug device

The thimble plug device may be used to restrict bypass flow through those thimbles not occupied by absorber, source, or burnable absorber rods.

The thimble plug devices satisfy the following criteria:

1. Accommodate the differential thermal expansion between the fuel assembly and the core internals

2. Maintain positive contact with the fuel assembly and the core internals

3. Limit the flow through each occupied thimble to an acceptable design value

4.2.1.7 Surveillance Program

Section 4.2.4.5 and Sections 8 and 23 of Reference 9 discuss the testing and fuel surveillance operational experience program that has been and is being conducted to verify the adequacy of the fuel performance and design bases. Fuel surveillance and testing results, as they become available, are used to improve fuel rod design and manufacturing processes and ensure that the design bases and safety criteria are satisfied.

4.2.2 DESIGN DESCRIPTION

The fuel assembly, fuel rod, and incore control component design data are given in Table 4.3-1.

Each fuel assembly consists of 264 fuel rods, 24 guide thimble tubes, and one instrumentation thimble tube arranged within a supporting structure. Limited substitution of filler rods for fuel rods may be made. The instrumentation thimble is located in the center position and provides a channel for insertion of an incore neutron detector, if the fuel assembly is located in an instrumented core position. The guide thimbles provide channels for insertion of either a rod cluster control assembly, a neutron source assembly, a burnable absorber assembly, or a thimble plug device, depending on the position of the particular fuel assembly in the core. Figures 4.2-1 and 4.2-1a show a cross-section of typical fuel assembly arrays, and Figures 4.2-2, 4.2-2a, 4.2-2b, 4.2-2c, 4.2-2d, 4.2-2e and 4.2-2f show a fuel assembly full-length view. The fuel rods are loaded into the fuel assembly structure so that there is clearance between the fuel rod ends and the top and bottom nozzles.

Fuel assemblies are installed vertically in the reactor vessel and stand upright on the lower core plate, which is fitted with alignment pins to locate and orient each assembly. After all fuel assemblies are set in place, the upper support structure is installed. Alignment pins, built into the upper core plate, engage and locate the upper ends of the fuel assemblies. The upper core plate then bears downward against the holddown springs on the top nozzle of each fuel assembly to hold the fuel assemblies in place.

The V5H P+ assembly skeleton is identical to V5H except for those modifications necessary to accommodate the intended fuel operation to higher burnups. The modifications consist of the use of Zirlo™ guide thimbles and small skeleton dimensional alterations to provide additional fuel assembly and rod growth space at the extended burnup levels. The V5H P+ fuel assembly is shorter than the V5H fuel assembly. The grid centerline elevations of the V5H P+ are identical to those of the V5H fuel assembly, except for the top grid. The V5H P+ top grid has been lowered. However, since the V5H P+ fuel is intended to replace the V5H fuel, the V5H P+ exterior assembly envelope is equivalent in design dimensions, and the functional interface with the reactor internals is also equivalent to those of previous Westinghouse fuel designs. Also, the V5H P+ fuel assembly is designed to be mechanically and hydraulically compatible with the V5H fuel assembly. The same functional requirements and design criteria as previously established for the Westinghouse V5H fuel assembly remains valid for the V5H P+ fuel assembly. Figure 4.2-2c shows a full-length view of the V5H P+ fuel assembly design. A comparison between Figure 4.2-2b and Figure 4.2-2c details the small skeleton dimensional alterations mentioned above.

The V5H P+Z^{+2} assembly skeleton is similar to that previously described for V5H P+ except for those modifications necessary to accommodate the low rod internal pressure design and incorporation of a "cast" top nozzle design. The modifications consist of the use of longer Zirlo™ guide thimbles and instrument tube and repositioning of the top grid. The V5H P+Z^{+2} fuel assembly is taller than the V5H P+ fuel assembly and the same height as the V5H fuel assembly. Operational experience with the ZIRLO™ material has shown that the growth characteristics of ZIRLO™ do not require the shorter skeleton design used with the V5H P+ fuel assembly. The additional height of the V5H P+Z^{+2} fuel assembly skeleton allows the incorporation of fuel rod design modifications to accrue rod internal pressure benefits (low rod internal pressure rod design). The grid centerline elevations of the V5H P+Z^{+2} are identical to those of the V5H fuel assembly (all grids) and V5H P+ fuel assembly except for the top grid. Since the V5H P+Z^{+2} fuel is intended to replace the V5H and V5H P+ fuel, the V5H P+Z^{+2} exterior assembly envelope is equivalent in design dimensions, and the functional interface with the reactor internals is also equivalent to those of previous Westinghouse fuel designs. Also, the V5H P+Z^{+2} fuel assembly is designed to be mechanically and hydraulically compatible with the V5H and V5H P+ fuel assembly. The same functional requirements and design criteria as previously established for the Westinghouse V5H and V5H P+ fuel assemblies remains valid for the V5H P+Z^{+2} fuel assembly. Figure 4.2-2d shows a full-length view of the V5H P+Z^{+2} fuel assembly design. A comparison between Figure 4.2-2c and Figure 4.2-2d details the alterations mentioned above.

The RFA Z^{+2} assembly skeleton is similar to that previously described for the V5H P^{+} Z^{+2} except for those modifications made to accommodate a modified mixing vane LPD mid-grid, a modified mixing vane IFM grid, and thicker guide thimble and instrument tubes. The grid changes are designed to improve thermal-hydraulic performance and the addition of thicker thimble and instrument tubes reduce the potential for fuel assembly bow and subsequently incomplete rod insertion (IRI) concerns. The same functional requirements and design criteria as previously established for the Westinghouse V5H P+Z^{+2} fuel assembly design remains valid for the RFA Z^{+2} design. Figure 4.2-2d shows a full-length view of the RFA Z^{+2} fuel assembly design.

The RFA-2 Z^{+2} assembly skeleton is similar to that previously described for the RFA Z^{+2} except for the mid-grids. The differences between the RFA and RFA-2 mid-grids are the increased spring and dimple contact area with the fuel rod in the RFA-2 design. The same functional requirements and design criteria as previously established for the Westinghouse RFA Z^{+2} fuel assembly design remains valid for the RFA-2 Z^{+2} design. Figure 4.2-2d shows a full-length view of the RFA-2 Z^{+2} fuel assembly design.

The RFA-2 Z+2 assembly skeleton was modified in Cycle 21 to include a combination bottom grid and Robust Protective Grid as well as a Standardized Debris Filter Bottom Nozzle. The grid change impacts the location of the Protective Grid centerline in relation to the bottom of the fuel stack and the elevation of the Protective Grid to the bottom of the bottom nozzle. Figure 4.2-2f shows a full-length view of the RFA-2 Z^(+2) with Combo Grid and DFBN fuel assembly design.

Improper orientation of fuel assemblies within the core is prevented by the use of an indexing hole in one corner of the top nozzle top plate. The assembly is oriented with respect to the handling tool and the core by means of a pin which is inserted into this indexing hole. Visual confirmation of proper orientation is also provided by an engraved identification number on the opposite corner clamp.

4.2.2.1 Fuel Rods

Two types of fuel rod designs may be used in the V5H, V5H P+, V5H P+Z^{+2}, RFA Z^{+2} and RFA-2 Z^{+2} fuel assemblies. The fuel rod designs are referred to as Integral Fuel Burnable Absorber (IFBA) fuel rods and Non-IFBA fuel rods. The IFBA and Non-IFBA fuel rod designs are identical with the exception of the items noted in Section 4.2.2.1.2. A reference to fuel rods encompasses both designs. The fuel rod structure consists of bottom end plug, a fuel tube (clad), uranium dioxide ceramic pellets, a plenum spring and top end plug. A schematic of the fuel rod is shown in Figure 4.2-3, Figure 4.2-3a, Figure 4.2-3b, Figure 4.2-3c, and Figure 4.2-3d.

4.2.2.1.1 Non-IFBA Fuel Rods

The LOPAR and V5H fuel rods consist of uranium dioxide ceramic pellets contained in slightly cold worked Zircaloy-4 tubing, which is plugged, and seal welded at the ends to encapsulate the fuel. The fuel pellets are right circular cylinders consisting of slightly enriched uranium dioxide powder, which has been compacted by cold pressing and then sintered to the required density. The ends of each pellet are dished slightly to allow greater axial expansion at the center of the pellets.

Void volume and clearances are provided within the rods to accommodate fission gases released from the fuel, differential thermal expansion between the clad and the fuel, and fuel density changes during irradiation. Shifting of the fuel within the clad during handling or shipping prior to core loading is prevented by a stainless steel helical spring (plenum spring) which bears on top of the fuel. At assembly, the bottom plug is inserted and welded and the pellets are stacked in the clad to the required fuel height. The spring is then inserted into the top end of the fuel tube and the top end plug is pressed into the end of the tube and welded. All fuel rods are internally pressurized with helium during the top end plug welding process in order to minimize compressive clad stresses and prevent clad flattening under coolant operating pressures. A schematic of the fuel rod is shown in Figure 4.2-3.

The fuel rods are prepressurized and designed so that: 1) the internal gas pressure mechanical design limit given in Section 4.2.1.3 is not exceeded, 2) the cladding stress-strain limits (see Section 4.2.1.1) are not exceeded for Condition I and II events, and 3) clad flattening will not occur during the fuel core life.

Cycle 2 fresh fuel incorporated a small chamfer on the end of each pellet at the outer cylindrical surface and an internal gripper bottom end plug. The internal gripper feature facilitates fuel rod loading and provides appropriate lead-in for the removable top nozzle reconstitution feature.

Cycle 5 fresh fuel incorporated the high burnup short top and bottom end plug design with a slightly longer fuel tube. A schematic of the fuel rod is shown in Figure 4.2-3a.

Cycle 8 fresh fuel incorporated the Performance+ top end plug, Performance+ extended bottom end plug, and variable pitch plenum spring. The extended bottom end plug is used in conjunction with the protective bottom grid discussed in Section 4.2.2.2.4. The variable pitch plenum spring has a smaller wire diameter, coil diameter and shorter free length. The variable pitch plenum spring provides the same support as the regular V5H plenum spring but with fewer turns, which translates into less spring volume and increased void volume in the rod. A schematic of the fuel rod is shown in Figure 4.2-3b.

Cycle 10 fresh fuel incorporates the V5H P+ fuel rod. The V5H P+ fuel rod represents a modification to the V5H fuel rod intended to support extended burnup operation for the fuel clad by using Zirlo™ in place of the Zircaloy-4 clad. The Zirlo™ alloy is a zirconium alloy similar to Zircaloy-4, which has been specifically developed to enhance corrosion resistance. The V5H P+ fuel rod has the same clad wall thickness as the V5H design. The V5H P+ fuel tube is shorter to provide room for the required rod growth at extended burnups. The V5H P+ fuel rods contain, as in the V5H design, enriched uranium dioxide fuel pellets. Schematics of the V5H P+ fuel rods are shown in Figure 4.2-3c.

Cycle 10 fresh fuel (V5H P+) incorporates the use of axial blankets in the fuel rod. The axial blankets are a nominal 6 inches of unenriched fuel pellets or fully enriched annular fuel pellets at each end of the fuel rod pellet stack. Axial blankets reduce neutron leakage and improve fuel utilization. The use of fully enriched annular fuel pellets in the axial blankets also provides additional void volume. The axial blankets utilize chamfered pellets which are physically different in length from the enriched pellets used in the rest of the pellet stack to help prevent accidental mixing during manufacturing. Axial blankets continue to be utilized in subsequent fresh fuel designs.

Cycle 12 fresh fuel incorporates the low rod internal pressure fuel rod design associated with the V5H P+Z^{+2} fuel assembly design. Operational experience has shown that the ZIRLO™ material growth characteristics will accommodate a taller fuel assembly skeleton and a longer fuel rod than the V5H P+ design, while still allowing extended burnup operation. The V5H P+Z^{+2} fuel rod represents a modification to the V5H P+ fuel rod intended to provide additional rod internal void volume to achieve rod internal pressure relief. The additional void volume is created by the following configuration changes:

1) the V5H P+Z^{+2} fuel rod top end plug does not include the external gripper feature of the Performance+ top end plug, resulting in a shorter top end plug,
2) the V5H P+Z^{+2} fuel tube is longer than the V5H P+ fuel tube, and
3) the variable pitch plenum spring is longer to accommodate the increased rod length.

The V5H P+Z^{+2} fuel rods contain, as in the V5H P+ design, enriched uranium dioxide fuel pellets. Schematics of the V5H P+Z^{+2} fuel rods are shown in Figure 4.2-3d.

Cycle 13 fresh fuel, RFA Z^{+2} design, utilizes the same fuel rod design as the V5H P+Z^{+2} design.

Cycle 14 fresh fuel, RFA-2 Z^{+2} design, utilizes the same fuel rod design as the V5H P+Z^{+2} and RFA Z^{+2} design.

Cycle 16 fresh fuel incorporates the use of a fuel rod oxide coating on the RFA Z^{+2} design. The fuel rod has a very thin oxide coating at the bottom end of the fuel rod. The extra layer of oxide coating provides additional debris induced rod fretting wear protection.

Starting with cycle 23, Optimized ZIRLO cladding material will be utilized to contain the slightly enriched uranium dioxide fuel. The Optimized ZIRLO cladding material is further described in References 28 and 29.

4.2.2.1.2 Integral Fuel Burnable Absorber Fuel Rods

The Integral Fuel Burnable Absorber (IFBA) fuel rod design for the V5H, V5H P+, V5H P+Z^{+2}, RFA Z^{+2} and RFA-2 Z^{+2} designs are identical to the Non-IFBA fuel rod design for the V5H, V5H P+, V5H P+Z^{+2}, RFA Z^{+2} and RFA-2 $Z^{+}2$ designs, respectively, with the following exceptions:

a) Some of the fuel pellets are coated with a thin layer of zirconium diboride (ZrB_2) on the pellet cylindrical surface.
b) The helium back fill pressure for the IFBA fuel rod is lower than the Non-IFBA fuel rod.

The zirconium diboride coating is referred to as the Integral Fuel Burnable Absorber design or IFBA. Other than the zirconium diboride coating, the fuel pellets for an IFBA rod are identical to the enriched uranium dioxide pellets described for the Non-IFBA fuel rod. The IFBA pellets are placed in the central portion of the fuel pellet stack (up to 134 inches). The lower back fill pressure for the IFBA rod offsets the increased rod pressure at end of life due to the production and release of helium from the zirconium diboride coating on the IFBA fuel pellets.

The number and pattern of IFBA rods loaded within an assembly may vary depending on the specific application. The IFBA design provides an alternate means of reactivity control as opposed to the discrete burnable absorber designs discussed in Section 4.2.2.3. An evaluation and test program for the IFBA design features is given in section 2.5 of Reference 19. Cycle 9 fresh fuel incorporated the use of the IFBA rod design.

4.2.2.2 Fuel Assembly Structure

The fuel assembly structure consists of a bottom nozzle, thimble screws, top nozzle, guide thimbles, inserts, lock tubes, and grids, as shown in Figures 4.2-2, 4.2-2a, 4.2-2b, 4.2-2c, 4.2-2d, 4.2-2e and 4.2-2f.

4.2.2.2.1 Bottom Nozzle

The bottom nozzle serves as the bottom structural element of the fuel assembly and distributes the coolant flow to the assembly. The bottom nozzle is fabricated from Type 304 stainless steel. The standard bottom nozzle design consists of a perforated plate and four angle legs with bearing plates, as shown in Figure 4.2-2. The plate prevents accidental downward ejection of the fuel rods from the fuel assembly. The bottom nozzle is fastened to the fuel assembly guide tubes by locked thimble screws which penetrate through the nozzle and mate with a threaded plug in each guide tube.

The Cycle 5 fresh fuel design incorporated the Debris Filter Bottom Nozzle (DFBN) to reduce the possibility of fuel rod damage due to debris-induced fretting. The relatively large flow holes in a conventional nozzle are replaced with a new pattern of smaller flow holes. The holes are sized to minimize passage of debris particles large enough to cause damage while providing sufficient flow area, comparable pressure drop, and continued structural integrity of the nozzle. The Cycle 6 fresh fuel added a reinforcing skirt to the DFBN design, as shown in Figures 4.2-2a, 4.2-2b, 4.2-2c, 4.2-2d and 4.2-2e. The reinforcing skirt is located between the angle legs around the perimeter of the bottom nozzle and contains five holes on each face to allow lateral fluid flow. The legs and skirt form a plenum for the inlet coolant flow to the fuel assembly and enhance reliability during postulated adverse handling conditions while refueling. Tests to measure pressure drop and demonstrate structural integrity verified that the 304 stainless steel DFBN is totally compatible with the current design.

The Cycle 21 fresh fuel incorporates a Standardized Debris Filter Bottom Nozzle (SDFBN). The SDFBN has eliminated the side skirt communication flow holes (shown in Figure 4.2-2f) as a means of improving the debris mitigation performance of the bottom nozzle.

This nozzle has been evaluated and meets all of the applicable mechanical design criteria. In addition, there is no adverse effect on the thermal hydraulic performance of the SDFBN either with respect to the pressure drop or with respect to Departure from Nucleate Boiling (DNB).

Coolant flows from the plenum in the bottom nozzle upward through the penetrations in the plate to the channels between the fuel rods. The penetrations in the plate are positioned between the rows of the fuel rods.

Axial loads (holddown) imposed on the fuel assembly and the weight of the fuel assembly are transmitted through the bottom nozzle to the lower core plate. Indexing and positioning of the fuel assembly are provided by alignment holes in two diagonally opposite bearing plates which mate with locating pins in the lower core plate. Lateral loads on the fuel assembly are transmitted to the lower core plate through the locating pins.

4.2.2.2.2 Top Nozzle

The top nozzle functions as the upper structural element of the fuel assembly and provides a partial protective housing for the rod cluster control assembly or other components that are installed in the guide thimble tubes. The top nozzle consists of an adapter plate, enclosure, top plate, and pads. The top nozzle assembly consists of holddown springs mounted on the top nozzle as shown in Figures 4.2-2, 4.2-2a, 4.2-2b, 4.2-2c, 4.2-2d, 4.2-2e and 4.2-2f. The springs and spring screws are made of Inconel-718 and Inconel-600 respectively, whereas other components are made of Type 304 stainless steel.

The standard top nozzle adapter plate is provided with round penetrations and semicircular ended slots to permit the flow of coolant upward through the top nozzle. Other round holes are provided to accept sleeves which are welded to the adapter plate at their upper ends and mechanically attached to the thimble tubes at the lower end. The ligaments in the plate cover the tops of the fuel rods and prevent their upward ejection from the fuel assembly. The enclosure is a box-like structure which sets the distance between the adapter plate and the top plate. The top nozzle has a large square hole in the center to permit access to the thimble tubes for the control rods and provide a partial protective housing for the control rod spiders. Holddown springs are mounted on the standard top nozzle and are retained by spring screws and clamps located at two diagonally opposite corners. On the other two corners, integral pads are positioned, which contain alignment holes for locating the upper end of the fuel assembly. Figure 4.2-6 shows the top nozzle attachment to the thimble tubes for the standard top nozzle assembly.

Cycle 5 fresh fuel incorporated the reconstitutable top nozzle (RTN) design. The RTN design for the V5H and V5H P+ fuel assembly differs from the standard top nozzle design in two ways: a groove is provided in each thimble throughhole in the nozzle adapter plate to facilitate attachment and removal; and the nozzle plate thickness is reduced to provide additional axial space for fuel rod growth.

Cycle 12 fresh fuel incorporates a cast RTN design and shot-peened Inconel-600 spring screws into the top nozzle design. The top nozzle enclosure, top plate and pads are cast as a single unit and joined with the adapter plate to make the cast RTN.

Cycle 13 fresh fuel incorporates shot-peened Inconel-718 spring screws into the cast RTN top nozzle design.

Cycle 14 fresh fuel, RFA-2 Z^{+2}, utilizes the same top nozzle design as the Cycle 13 fresh fuel, RFA Z^{+2}.

In the RTN design, a stainless steel nozzle insert is mechanically connected to the top nozzle adapter plate by means of a preformed circumferential bulge near

the top of the insert. The insert engages a mating groove in the wall of the adapter plate thimble tube throughhole. The insert has four equally spaced axial slots which allow the insert to deflect inwardly at the elevation of the bulge, thus permitting the installation or removal of the top nozzle. The insert bulge is positively held in the adapter plate mating groove by placing a lock tube with a uniform ID identical to that of the thimble tube into the insert. The inserts are mechanically attached to the thimble tubes at the lower end with three bulge joints. Figure 4.2-6a shows the top nozzle attachment to the thimble tubes for the RTN assembly.

Cycle 16 fresh fuel incorporates the Westinghouse Integral Nozzle (WIN) top nozzle. The WIN design differs from the RTN design in the attachment method for the hold down springs. The WIN top nozzle includes a modified top nozzle casting that includes the spring clamps. The springs are located with pins that are welded in place but do not react to the spring force. The WIN top nozzle design eliminates the potential for the fracture of the hold down spring screws by the replacing the spring screws with the spring pins. The modification increases the fuel assembly integrity and eliminates the potential for loose parts from fractured spring screws entering the RCS during normal operations or during fuel movement during refueling outages.

To remove the top nozzle, a tool is first inserted through the lock tube and expanded radially to engage the bottom edge of the lock tube. An axial force is then exerted on the tool which overrides the local lock tube deformations and withdraws the lock tube from the insert. After the lock tubes have been withdrawn, the top nozzle is removed by raising it off the upper slotted ends of the nozzle inserts which deflect inwardly under the axial lift load. With the top nozzle removed, direct access is provided for fuel rod examination or replacement. Reconstitution is completed by the remounting of the top nozzle and the insertion of the lock tubes. The design bases and evaluation of the RTN are given in Section 2.3.2 of Reference 19.

4.2.2.2.3 Guide Thimble and Instrument Tubes

The guide thimbles are structural members which also provide channels for the neutron absorber rods, burnable absorber rods, neutron source rods, or thimble plug devices. Each thimble is fabricated from Zircaloy-4 or Zirlo™ tubing having two different diameters.

The Cycle 6 fresh fuel incorporation of the Zircaloy-4 mid grids required a concurrent incorporation of the VANTAGE 5 (V5) reduced diameter thimble tubes. The VANTAGE 5 guide thimbles are also referred to as the VANTAGE 5H (V5H) guide thimble tubes. With the exception of a reduction in the guide thimble diameter above the dashpot, the V5H and V5H P+ guide thimbles are identical to those in the LOPAR design. A 0.008 inch reduction to the guide thimble OD and ID is required due to the thicker Zircaloy/Zirlo™ grid straps. The V5H and V5H P+ guide thimble tube ID provides an adequate nominal diametral clearance of 0.061 inch for the control rods. The scram time to the dashpot for accident analyses is 2.7 seconds. The reduced V5H and V5H P+ thimble tube ID provides sufficient diametral clearance for burnable absorber rods, source rods, and any dually compatible thimble plugs. Cycle 10 fresh fuel incorporated the use of Zirlo™ material for the guide thimble and instrumentation tubes. The V5H P+ assembly design uses guide thimble and instrument tubes which are slightly shorter than those used in the V5H assembly design. Cycle 12 fresh fuel incorporated slightly longer guide thimble and instrumentation tubes as part of the V5H P+Z^{+2} fuel assembly design (same length as the V5H design).

Cycle 13 fresh fuel incorporated thicker guide thimble and instrumentation tubes with a larger outer diameter as part of the RFA Z^{+2} fuel assembly design. The RFA Z^{+2} guide thimble tube wall thickness is increased approximately 25% to improve stiffness and address incomplete rod insertion (IRI) considerations. The major and minor (dashpot) OD of the guide thimble tube are increased while maintaining the same major and minor (dashpot) ID to accommodate the increased

wall thickness. There is no change to the dashpot flow hole diameters or the dashpot transition elevation.

Cycle 14 fresh fuel, RFA-2 Z^{+2} fuel assembly design, utilizes the same guide thimble tube design included in the RFA Z^{+2} fuel assembly design.

The guide thimble diameter at the top section provides the annular area necessary to permit rapid control rod insertion during a reactor trip. The lower portion of the guide thimble reduces to a smaller diameter to produce a dashpot action near the end of the control rod travel during trip operation. The dashpot is provided with a calibrated flow port to decelerate the rod at the end of the travel. The top end of the guide thimble is fastened to an insert (RTN) or top Inconel grid sleeve (Standard Top Nozzle) by three expansion swages. When attaching to a RTN, the insert fits into and is locked into the top nozzle adapter plate using a lock tube. When attaching to a standard top nozzle, the top Inconel grid sleeve is welded to the top nozzle adapter plate. The lower end of the guide thimble is fitted with an end plug which is then fastened to the bottom nozzle by a crimp-locked thimble screw.

Fuel rod support grids are fastened to the guide thimble assemblies to create an integrated structure. Attachment of the Inconel and Zircaloy or Zirlo™ grids to the Zircaloy or Zirlo™ thimbles is performed using the mechanical fastening technique as depicted in Figures 4.2-4 and 4.2-5 except for the bottom grid which is retained by clamping between the thimble end plug and the bottom nozzle.

An expanding tool is inserted into the inner diameter of the Zircaloy or Zirlo™ thimble tube at the elevation of the grid sleeves that have been previously attached into the grid assembly. The four-lobed tool forces the thimble and sleeve outward to a predetermined diameter, thus joining the twocomponents.

When attaching to a standard top nozzle, the top inconel grid sleeve and thimble tube are joined together using three bulge joint mechanical attachments as shown in Figure 4.2-6. The sleeve is then welded to the top nozzle adapter plate. When attaching to a RTN, the thimble tube is joined together with the top nozzle insert and top Inconel grid sleeve using three bulge joint mechanical attachments as shown in Figure 4.2-6a. This bulge joint connection was mechanically tested and found to meet all applicable design criteria.

The intermediate mixing vane Zircaloy grids, incorporated with Cycle 7 fresh fuel, employ a single bulge connection to the sleeve and thimble as compared to a three bulge connection used in the top Inconel grid (Figure 4.2-5). Mechanical testing of this bulge joint connection was also found to be acceptable. Cycle 10 fresh fuel incorporated the use of Zirlo™ material for the intermediate mixing vane grids.

The bottom grid assembly is joined to the assembly by crimp lock screw, as shown in Figure 4.2-7. The stainless steel insert is spot-welded to the bottom grid and later captured between the guide thimble end plug and the bottom nozzle by means of a stainless steel thimble screw.

The described methods of grid fastening are standard and have been used successfully since the introduction of Zircaloy guide thimbles in 1969.

The central instrumentation tube of each fuel assembly is constrained by seating in a counterbore in the bottom nozzle at its lower end and is expanded at the top and mid grids in the same manner as the previously discussed expansion of the guide thimbles to the grids. This tube has a constant diameter and guides the incore neutron detectors.

The V5H, V5H P+, and V5H $P+Z^{+2}$ instrumentation tube designs have a 0.008 inch diametral decrease compared to the LOPAR assembly instrumentation tube. This

decrease still allows sufficient diametral clearance for the incore neutron detector (max. OD = 0.397 inch) to traverse the tube without binding. The RFA Z^{+2} and RFA-2 Z^{+2} instrumentation tube design includes an increased wall thickness consistant with the RFA Z^{+2} and RFA-2 Z^{+2} guide thimble tubes. The OD of the tube is increased while maintaining the same ID to accommodate the increased wall thickness.

4.2.2.2.4 Grid Assemblies

The fuel rods, as shown in Figures 4.2-2, 4.2-2a, 4.2-2b, 4.2-2c, 4.2-2d, 4.2-2e and 4.2-2f are supported at intervals along their length by grid assemblies which maintain the lateral spacing between the rods. Each fuel rod is supported within each grid by the combination of support dimples and springs. The grid assembly consists of individual slotted straps assembled and interlocked into an "egg-crate" arrangement with the straps permanently joined at their points of intersection.

The top and bottom Inconel (non-mixing vane) grids of the LOPAR, V5H, V5H P+, V5H P+Z^{+2}, RFA Z^{+2} and RFA-2 Z^{+2} assemblies are nearly identical in design. The only differences are: 1) V5H, V5H P+, V5H P+Z^{+2}, RFA Z^{+2} and RFA-2 Z^{+2} top and bottom grids have a snag-resistant design which minimizes assembly interactions during core loading/unloading, 2) V5H, V5H P+, V5H P+Z^{+2}, RFA Z^{+2} and RFA-2 Z^{+2} top and bottom grids have dimples which are rotated 90 degrees to minimize fuel rod fretting and dimple cocking, 3) V5H, V5H P+, V5H P+Z^{+2} and RFA Z^(+2) and RFA-2 Z^(+2) top and bottom grid heights have been increased to 1.522 inches, 4) the V5H, V5H P+, V5H P+Z^{+2}, RFA Z^{+2} and RFA-2 Z^{+2} top grid spring force has been reduced to minimize rod bow, and 5) the V5H, V5H P+, V5H P+Z^{+2}, RFA Z^{+2} and RFA-2 Z^{+2} top grid uses 304L stainless steel sleeves.

Cycle 4 fresh fuel incorporated the snag-resistant top and bottom grid design mentioned above into the fuel design for Wolf Creek.

The LOPAR fuel design utilizes six intermediate (mixing vane) grids made of Inconel. The snag-resistant design described for the top and bottom grid was incorporated into the six intermediate grids with Cycle 4 fresh fuel. Cycle 6 fresh fuel incorporated intermediate (mixing vane) grids made of Zircaloy material rather than Inconel. Cycle 10 fresh fuel incorporated six intermediate (mixing vane) grids made of Zirlo™ rather than Zircaloy. These Zircaloy and Zirlo™ grids (known as the V5H Zircaloy grid and V5H P+ Zirlo™ grid) are designed to give the same pressure drop as the Inconel grid. Relative to the Inconel grid, the V5H Zircaloy and V5H P+ Zirlo™ grid strap thickness and strap height are increased for structural performance. In addition to the snag-resistant design noted above, the upstream strap edges of the V5H Zircaloy grid and V5H P+ Zirlo™ grid are chamfered and a diagonal grid spring is employed to reduce pressure drop. The V5H Zircaloy grids and V5H P+ Zirlo™ grids incorporate the same grid cell support configuration as the Inconel grids (six support locations per cell: four dimples, and two springs). The Zircaloy and Zirlo™ grid interlocking strap joints and grid/sleeve joints are fabricated by laser welding, whereas the Inconel grid joints are brazed.

The V5H Zircaloy, V5H P+ Zirlo™, RFA Zirlo™ and RFA-2 Zirlo™ grid have superior dynamic structural performance relative to the Inconel grid. Structural testing was performed and analyses have shown the V5H Zircaloy grid, V5H P+ Zirlo™, RFA Zirlo™ and RFA-2 Zirlo™ seismic/LOCA grid load margin is superior to that of the Inconel grid.

The Intermediate Flow Mixer (IFM) grid in the VANTAGE 5H assembly is an adaptation of the existing VANTAGE 5 IFM grid design to a 0.374 inch OD standard fuel rod. As shown in Figures 4.2-2a, 4.2-2b, 4.2-2c, 4.2-2d, 4.2-2e and 4.2-2f. IFMs are located in the three uppermost spans between the mid-grids but are not intended to be structural members. The IFM grid envelope is slightly smaller than the mid grid. Each IFM grid cell provides four (4) point fuel rod

support. The simplified cell arrangement allows the IFM to accomplish its flow mixing objective with minimal pressure drop. Cycle 7 fresh fuel incorporated the Zircaloy Intermediate Flow Mixer grid. Cycle 10 fresh fuel incorporated the use of Zirlo™ material in the manufacture of the IFM grids.

The Protective Bottom Grid (PBG) is a partial height grid similar in configuration to the IFM Grid, but fabricated of Inconel without mixing vanes. The PBG is positioned directly above the bottom nozzle. As shown in Figures 4.2-2b, 4.2-2c, 4.2-2d, 4.2-2e, 4.2-2f and 4.2-3b, 4.2-3c, and 4.2-3d, the fuel rods are positioned close to the bottom nozzle and are modified with a slightly longer bottom end plug. The PBG provides added protection against debris induced fretting by trapping debris below this grid where it can wear against the solid end plug. In addition, the PBG provides improved resistance to grid-rod fretting by means of additional support at the bottom of the fuel rod. Cycle 8 fresh fuel incorporated the protective bottom grid.

Cycle 13 fresh fuel incorporated the RFA Z^{+2} fuel assembly design. RFA Z^{+2} changes made to the mid-grid include a modified vane pattern (which is now symmetrical), longer vane geometry, modified spring and dimple geometry, a narrower spring window cut-out, a longer intersect slot length, opposite hand spring and the incorporation of the anti-snag outer grid strap design. IFM modifications include a symmetric vane pattern, longer vane geometry, and a change to the dimple profile. The Inconel top, bottom, and protective grids are not changed in the RFA Z^{+2} design except for new insert tubing for the bottom and protective grids to accommodate the increase in thimble and instrument tube diameters.

Cycle 14 fresh fuel is the RFA-2 Z^{+2} fuel assembly design. The RFA-2 Z^{+2} design changes the mid-grid to include a modified spring and dimple geometry that increases the line-contact length of the rod-spring and rod-dimple interface. The RFA-2 Z^{+2} IFM grid design is not changed relative to the RFA Z^{+2} IFM grid design. The RFA-2 Z^{+2} Inconel top, bottom and protective grid designs are not changed relative to the RFA Z^{+2} Inconel top, bottom and protective grid designs.

The Cycle 21 fresh fuel implemented a combination bottom grid and Robust Protective Grid (RPG). Westinghouse has developed the RPG as a result of observed failures in the field as noted in Post Irradiation Exams (PIE) performed at several different plants. It was determined that observed failures were the result of two primary issues; 1) fatigue failure within the protective grid itself at the top of the end strap and 2) stress corrosion cracking (SCC) primarily within the rod support dimples. The RPG implemented design changes such as increasing the maximum nominal height of the grid, increasing te ligament length and the radii of the ligament cutouts, and the use of four additional spacers or inserts to help strengthen the grid. The nominal height of the grid was increased to allow “V-notch” window cutouts to be added to help minimize flow-induced vibration caused by vortex shedding at the trailing edge of the inner grid straps. The design changes incorporated into the RPG design helped address the issues of fatigue failures and failures due to SCC. It was determined that the above changes do not impact the thermal hydraulic performance of the RPG as there is no change to the loss coefficient. In addition, the RPG retains the original protective grid function as a debris mitigation feature.

The magnitude of the grid-restraining force on the fuel rod is set high enough to minimize possible fretting without overstressing the cladding at the points of contact between the grids and fuel rods. The grid assemblies also allow axial thermal expansion of the fuel rods without imposing restraint sufficient to develop buckling or distortion of the fuel rods.

4.2.2.2.5 Fuel Assemblies - LOPAR, V5H, and V5H P+, V5H P+Z^{+2}, RFA Z^{+2} and RFA-2 Z^{+2} designs

The initial fuel assembly design used at Wolf Creek was the Westinghouse 17x17 low-parasitic (LOPAR) fuel design. The original LOPAR fuel assembly design is shown in Figure 4.2-1, Figure 4.2-2, and Figure 4.2-3. Westinghouse developed several fuel performance enchancing features which were added to the LOPAR design over a period of several reloads. The major enhancements included:

- Chamfered pellet design
- High burnup top and bottom end plug designs
- Anti-snag grid design
- Debris Filter Bottom Nozzle (DFBN) design
- Reconstitutable Top Nozzle (RTN) design

These features were gradually added to the base LOPAR design for Cycle 2 through 5 fresh fuel. The actual point that the particular enhancement was incorporated is specified in the appropriate section of the USAR.

The Westinghouse VANTAGE 5H fuel design is a variation of the LOPAR design that includes all of the fuel performance enhancements listed above along with the following:

- VANTAGE 5H (V5H) Zircaloy-4 Mid Grid design
- VANTAGE 5 Guide Tube design

Cycle 6 fresh fuel incorporated the V5H Zircaloy mid grids and the V5 guide tube designs. This marked the point at which the fuel design for Wolf Creek became the Westinghouse VANTAGE 5H fuel design. The V5H fuel assembly design is shown in Figures 4.2-1a, 4.2-2a, 4.2-2b, 4.2-3a, and 4.2-3b. Westinghouse has continued to developed fuel performance enhancing features which were added to the base V5H design over a period of several reloads. The major enhancements include:

- Zircaloy-4 Intermediate Flow Mixer (IFM) grid design
- Inconel Protective Bottom Grid (PBG) design
- Performance+ Extended Bottom End Plug design
- Performance+ Top End Plug design
- Variable Pitch Plenum Spring design
- Integral Fuel Burnable Absorber (IFBA) design

These features were gradually added to the base V5H design for Cycle 7 through 9 fresh fuel. The actual point that the particular enhancement was incorporated is specified in the appropriate section of the USAR.

Westinghouse VANTAGE 5H with Performance+ features (V5H P+) fuel design is a variation of the V5H design that includes all of the fuel performance enhancements listed above along with the following:

- Zirlo™ Clad fuel rod design
- Zirlo™ guide thimble and instrumentation tube design
- Zirlo™ mid grid design
- Zirlo™ IFM grid design
- Zirlo™Fully enriched annular axial blankets

Cycle 10 fresh fuel incorporated the performance enhancement features listed above. This marked the point at which the fuel design became the Westinghouse VANTAGE 5H with Performance+ features (V5H P+) fuel design. The V5H P+ fuel assembly design is shown in Figures 4.2-1a, 4.2-2c and 4.2-3c.

Westinghouse VANTAGE 5H with Performance+ features, Zirlo^{+2} (V5H P+Z^{+2}) fuel design is a variation of the V5H P+ design that includes all of the fuel performance enhancements listed above along with the following:

- Low pressure fuel rod design
- Cast Reconstitutable Top Nozzle design
- Shot-peened spring screw design

To implement the low rod internal pressure fuel rod design, the following changes were required to the fuel rod and skeleton designs:

- Performance + Top End Plug design replaced by a shorter top end plug (with no external gripper) design
- Extended length Zirlo^{TM} fuel rod tube design
- Extended length Variable Pitch Plenum Spring design
- Extended length Zirlo^{TM} guide thimble tubes and instrument tubes

Cycle 12 fresh fuel incorporated the performance enhancement features listed above. This marked the point at which the fuel design became the Westinghouse VANTAGE 5H with Performance+ features, Zirlo^{+2} (V5H P+Z^{+2}) fuel design. The V5H P+Z^{+2} fuel assembly design is shown in Figures 4.2-1a, 4.2-2d and 4.2-3d.

Westinghouse Robust Fuel Assembly Zirlo^{+2} (RFA Z^{+2}) fuel design is a variation of the, V5H P+Z^{+2} design that includes the fuel performance features of the V5H P+Z^{+2} design along with the following:

- Shot-peened Inconel-718 spring screw design,
- ZIRLO^{TM} thicker thimble and instrument tube design (0.020 in. wall vs. 0.016 in.),
- Modified Zirlo^{TM} Low Pressure Drop (LPD) structural mid-grid design,
- Modified Zirlo^{TM} Intermediate Flow Mixing (IFM) grid design.

Cycle 13 fresh fuel incorporated the performance enhancement features listed above. This marked the point at which the fuel design became the Westinghouse Robust Fuel Assembly Zirlo^{+2} (RFA Z^{+2}) design. The RFA Z^{+2} fuel assembly design is shown in Figures 4.2-2d and 4.2-3d.

The Westinghouse second-generation Robust Fuel Assembly Zirlo^{+2} (RFA-2 Z^{+2}) fuel design is a variation of the RFA Z^{+2} design that includes the fuel performance features of the RFA Z^{+2} design along with the following:

- Modified Zirlo Low Pressure Drop (LPD) structural mid-grid design with increased spring and dimple contact area (RFA-2 mid-grid).

There is no change to the fuel assembly length, envelope or fuel rod design relative to the RFA Z^{+2} design.

Cycle 14 fresh fuel incorporated the performance enhancement features listed above. This marked the point at which the fuel design became the Westinghouse second-generation Robust Fuel Assembly Zirlo^{+2} (RFA-2 Z^{+2}) design. The RFA-2 Z^{+2} fuel assembly design is shown in Figures 4.2-2d and 4.2-3d.

Cycle 16 fresh fuel incorporated the performance enhancement features of the WIN top nozzle and fuel rod oxide coating. The fuel design continues to be the Westinghouse second-generation Robust Fuel Assembly Zirlo^{+2} (RFA-2 Z^{+2}) design. The RFA-2 Z^{+2} fuel assembly design with the WIN top nozzle is shown in Figures 4.2-2e and 4.2-3d.

The Cycle 21 fresh fuel incorporated a Standardized Debris Filter Bottom Nozzle (SDFBN) and a combination bottom grid and Robust Protective Grid (RPG). The fuel design continues to be the Westinghouse second-generation Robust Fuel Assembly Zirlo+2 (RFA-2 Z+2) design. The RFA-2 Z+2 fuel assembly design with the SDFBN and the RPG is shown in Figure 4.2-2f.

Table 4.3-1 provides a comparison of the LOPAR, V5H, V5H P+, V5H P+Z^{+2}, RFA Z^{+2} and RFA-2 Z^{+2} fuel assembly design parameters.

4.2.2.3 Incore Control Components

Reactivity control is provided by neutron absorbing rods and a soluble chemical neutron absorber (boric acid). The boric acid concentration is varied to control long-term reactivity changes, such as:

a. Fuel depletion and fission product buildup

b. Cold to hot, zero power reactivity change

c. Reactivity change produced by intermediate-term fission products, such as xenon and samarium

d. Burnable absorber depletion

The chemical and volume control system is discussed in Chapter 9.0.

The rod cluster control assemblies provide reactivity control for:
a. Shutdown
b. Reactivity changes resulting from coolant temperature changes in the power range
c. Reactivity changes associated with the power coefficient of reactivity
d. Reactivity changes resulting from void formation

It is desirable to have a negative moderator temperature coefficient at power levels exceeding 70% rated thermal power (RTP) throughout the entire cycle in order to reduce possible deleterious effects caused by a positive coefficient during loss-of-coolant or loss-of-flow accidents. Since soluble boron alone is insufficient to ensure a negative moderator coefficient, burnable absorber assemblies and/or IFBAs are also used. Burnable absorbers such as WABAs and IFBAs are used to achieve a better power peaking control and a flatter power distribution.

Although a negative moderator coefficient is desirable, it is acceptable and in some cases essential to have the coefficient be slightly positive in an attempt to extend cycle length. Current WCGS reload cycles are designed to have a small positive moderator temperature coefficient (<3 pcm/°F) at low thermal power (<30% RTP) during the first 25% of the cycle. The addition of excess reactivity to extend cycle length necessitates a greater amount of boric acid, which results in an increase of the moderator temperature coefficient.

The rod cluster control assemblies and their control rod drive mechanisms are the only moving parts in the reactor. Figure 4.2-8 illustrates the rod cluster control and control rod drive mechanism assembly, in addition to the arrangement of these components in the reactor, relative to the interfacing fuel assembly and guide tubes. In the following paragraphs, each reactivity control component is described in detail. The control rod drive mechanism assembly is described in Section 3.9(N).4.

The neutron source assemblies provide a means of monitoring the core during periods of low neutron level. The thimble plug may be used to limit bypass flow through those fuel assembly thimbles, which do not contain control rods, burnable absorber rods, or neutron source rods.

4.2.2.3.1 Rod Cluster Control Assembly

The rod cluster control assemblies are divided into two categories: control and shutdown. The control groups compensate for reactivity changes associated with variations in operating conditions of the reactor, i.e., power and temperature variations. Two nuclear design criteria have been employed for selection of the control group. First, the total reactivity worth must be adequate to meet the nuclear requirements of the reactor. Second in view of

the fact that these rods may be partially inserted at power operation, the total power peaking factor should be low enough to ensure that the power capability is met. The control and shutdown group provides adequate shutdown margin.

A rod cluster control assembly is composed of 24 neutron absorber rods fastened at the top end to a common spider assembly, as illustrated in Figure 4.2-9.

The absorber material used in the control rods is a solid hafnium or Silver-Indium-Cadmium (Ag-In-Cd) bar which is essentially "black" to thermal neutrons and has sufficient additional resonance absorption to significantly increase its worth. The absorber material is sealed in cold worked stainless steel tubes (see Figure 4.2-10). Sufficient diametral and end clearances are provided to accommodate relative thermal expansions.

The bottom plugs are bullet-nosed to reduce the hydraulic drag during reactor trip and to guide smoothly into the dashpot section of the fuel assembly guide thimbles.

The absorber rod end plugs are Type 308 stainless steel. The design stresses used for the Type 308 material are the same as those defined in the ASME Code, Section III, for Type 304 stainless steel. At room temperature, the yield and ultimate stresses per ASTM 580 are the same for the two alloys. In view of the similarity of the alloy composition, the temperature dependence of strength for the two materials is also assumed to be the same.

The allowable stresses used as a function of temperature are listed in Table 1-1.2 of Section III of the ASME Code. The fatigue strength for the Type 308 material is based on the S-N curve for austenitic stainless steels in Figure 1-9.2 of Section III.

The spider assembly is in the form of a central hub with radial vanes containing cylindrical fingers from which the absorber rods are suspended. Handling detents and detents for connection to the drive rod assembly are machined into the upper end of the hub. Two coil springs inside the spider body absorbs the impact energy at the end of a trip insertion. The radial vanes are joined to the hub by tack welding and brazing, and the fingers are joined to the vanes by brazing. A centerpost, which holds the spring and its retainer, is threaded into the hub within the skirt and welded to prevent loosening in service. All components of the spider assembly are made from Types 304 and 308 stainless steel except for the retainer, which is of 17-4 PH material, and the springs, which are Inconel-718 alloy.

The absorber rods are fastened securely to the spider. The rods are first threaded into the spider fingers and then pinned to maintain joint tightness, after which the pins are welded in place. The end plug below the pin position is designed with a reduced section to permit flexing of the rods to correct for small misalignments.

The overall length is such that when the assembly is withdrawn through its full travel the tips of the absorber rods remain engaged in the guide thimbles so that alignment between rods and thimbles is always maintained. Since the rods are long and slender, they are relatively free to conform to any small misalignments with the guide thimble.

4.2.2.3.2 Burnable Absorber Assembly
(Standard Borosilicate Glass and WABA)

Each burnable absorber assembly consists of burnable absorber rods attached to a holddown assembly. A burnable absorber assembly is shown in Figure 4.2-11 for the WABA rod and in Figure 4.2-11a for the borosilicate glass absorber rod. When needed for nuclear considerations, burnable absorber assemblies may be inserted into selected thimbles within fuel assemblies.

The discrete burnable absorber rods are the wet annular burnable absorber (WABA) rod design and the borosilicate glass rod design. Integral Fuel Burnable Absorber (IFBA) rods, described in Section 4.2.2.1.2, are an alternative burnable absorber that may be used. The borosilicate glass burnable absorber design was used in Cycles 1 and 2 and the WABA design was introduced in Cycle 3. Cycle 9 fresh fuel incorporated the IFBA design.

The WABA rod design consists of annular pellets of aluminum oxide-boron carbide (Al_2O_3-B_4C) burnable absorber material contained within two concentric Zircaloy tubes. These Zircaloy tubes, which form the inner and outer clad for the annular burnable absorber rod, are plugged, pressurized with helium, and seal welded at the ends to encapsulate the annular stack of absorber material. A Zircaloy spacer tube is placed at the bottom of the pellet stack to position the absorber stack within the WABA rod, and a C-shape Zircaloy spring clip is placed on top of the absorber stack to keep it in position and accommodate absorber stack growth. An annular plenum is provided within the rod to accommodate the helium gas released from the absorber material during boron depletion. The reactor coolant flows inside the inner tubing and outside the outer tubing of the annular rod. A typical WABA rod is shown in a longitudinal cross-section in Figure 4.2-12.

The borosilicate glass absorber rods consist of borosilicate glass tubes contained within Type 304 stainless steel tubular cladding which is plugged and seal welded at the ends to encapsulate the glass. The glass is also supported along the length of its inside diameter by a thin-wall tubular inner liner. The top end of the liner is open to permit the diffused helium to pass into the void volume, and the liner overhangs the glass. The liner has an outward flange at the bottom end to maintain the position of the liner with the glass. A typical borosilicate glass burnable absorber rod is shown in longitudinal and transverse cross-sections in Figure 4.2-12a.

The absorber rods in each burnable absorber assembly are grouped and attached together at the top end of the rods to a hold-down assembly by a flat perforated retaining plate which fits within the fuel assembly top nozzle and rests on the adapter plate.

The retaining plate and the absorber rods are held down and restrained against vertical motion through a spring pack which is attached to the plate and is compressed by the upper core plate when the reactor upper internals assembly is lowered into the reactor. This arrangement ensures that the absorber rods cannot be ejected from the core by flow forces. Each rod is permanently attached to the baseplate by a nut which is crimped or lock-welded into place.

The cladding of the WABA rods is Zircaloy. The cladding of the borosilicate glass rods is slightly cold worked Type 304 stainless steel. All other structural materials in the assembly are Type 304 or 308 stainless steel except for the springs, which are Inconel-718. The aluminum oxide-boron carbide pellets or the borosilicate glass tubes provide sufficient boron content to meet the criteria discussed in Section 4.3.1.

4.2.2.3.3 Neutron Source Assembly

The purpose of the neutron source assembly is to provide base neutron level to ensure that the neutron detectors are operational and responding to core multiplication neutrons. For the first core, a neutron source is placed in the reactor to provide a positive neutron count of at least 2 counts per second on the source range detectors attributable to core neutrons. The detectors, called source range detectors, are used primarily when the core is subcritical and during special subcritical modes of operations.

The source assembly permits detection of changes in the core multiplication factor during core loading and approach to criticality. This can be done since the multiplication factor is related to an inverse function of the detector count rate. Changes in the multiplication factor can be detected during addition of fuel assemblies while loading the core, changes in control rod positions, and changes in boron concentration.

The primary source rod, containing a radioactive material, spontaneously emits neutrons during initial core loading, reactor startup, and initial operation of the first core. After the primary source rod decays beyond the desired neutron flux level, neutrons are then supplied by the secondary source rod. The secondary source rod contains a stable material, which is activated during reactor operation. The activation results in the subsequent release of neutrons.

Four source assemblies were installed in the initial reactor core: two primary source assemblies and two secondary source assemblies. Subsequent cycles (2-10) utilize only the secondary source assemblies. Each primary source assembly contains one primary source rod and a number of burnable absorber rods. Each secondary source assembly contains four secondary source rods and a number of thimble plugs. A secondary source assembly is shown in Figure 4.2-14 and a primary source assembly is shown in Figure 4.2-14a.

"Double encapsulated" secondary source assemblies are available for use beginning with Cycle 11. Each of the double encapsulated secondary source assemblies contains six double encapsulated secondary source rods and a number of thimble plugs. A double encapsulated secondary source assembly is shown in Figure 4.2-14b.

Neutron source assemblies are positioned at opposite sides of the core. The source assemblies are inserted into the guide thimble tubes in fuel assemblies at selected unrodded core locations. As shown in Figure 4.2-14 and Figure 4.2-14b, the secondary source assembly contains a holddown assembly identical to that of the burnable absorber assembly. The primary and secondary source rods have the same cladding material as the absorber rods. The secondary source rods contain Sb-Be pellets stacked to a height of approximately 88 inches. A secondary source rod assembly is shown in Figure 4.2-13. The double encapsulated secondary source rods also contain Sb-Be pellets stacked to a height of approximately 88 inches. A double encapsulated secondary source rod assembly is shown in Figure 4.2-13a. The primary source rods contain capsules of californium source material and alumina spacer to position the source material within the cladding. The rods in each source assembly are permanently fastened at the top end to a holddown assembly.

The other structural members are constructed of Type 304 or Type 308 stainless steel, except for the springs. The springs exposed to the reactor coolant are Inconel-718.

4.2.2.3.4 Thimble Plug Device

Thimble plug devices may be used to limit bypass flow through the rod cluster control guide thimbles in fuel assemblies which do not contain either control rods, source rods, or burnable absorber rods. A typical thimble plug device is shown in Figures 4.2-15 and 4.2-15a.

The thimble plug devices consist of a flat baseplate with short rods suspended from the bottom surface and a spring pack assembly. The 24 short rods, called thimble plugs, project into the upper ends of the guide thimbles to reduce the bypass flow.

Each thimble plug is permanently attached to the baseplate by a nut which is crimped or lock-welded to the threaded end of the plug. Similar short rods are also used on the source assemblies and burnable absorber assemblies to plug the ends of all vacant fuel assembly guide thimbles. When in the core, the thimble plug devices interface with both the upper core plate and with the fuel assembly top nozzles by resting on the adapter plate. The spring pack is compressed by the upper core plate when the upper internals assembly is lowered into place.

All components in the thimble plug device, except for the springs, are constructed from Type 304 or Type 308 stainless steel. The springs are Inconel-718.

4.2.3 DESIGN EVALUATION

The fuel assemblies, fuel rods, and incore control components are designed to satisfy the performance and safety criteria of the introduction to Section 4.2, the mechanical design bases of Section 4.2.1, and other interfacing nuclear and thermal-hydraulic design bases specified in Sections 4.3 and 4.4.

Effects of Conditions II, III, IV or anticipated transients without trip on fuel integrity are presented in Chapter 15.0 or supporting topical reports.

The initial step in fuel rod design evaluation for a region of fuel is to determine the limiting rod(s). Limiting rods are defined as those rod(s) whose predicted performance provides the minimum margin to each of the design criteria. For a number of design criteria, the limiting rod is the highest burnup rod of a fuel region. In other instances, it may be the maximum power or the minimum burnup rod. For the most part, no single rod is limiting with respect to all design criteria.

After identifying the limiting rod(s), a worst-case performance analysis is performed which considers the effects of rod operating history, model uncertainties, and dimensional variations. To verify adherence to the design criteria, the evaluation considers the effects of postulated transient power changes during operation consistent with Conditions I and II. These transient power increases can affect both rod average and local power levels. Parameters considered include rod internal pressure, fuel temperature, clad stress, and clad strain. In fuel rod design analyses, these performance parameters provide the basis for comparison between expected fuel rod behavior and the corresponding design criteria limits.

Fuel rod and fuel assembly models used for the performance evaluations are documented and maintained under an appropriate control system. Materials properties used in the design evaluations are given in Reference 2.

4.2.3.1 Cladding

a. Vibration and wear

Fuel rod vibrations are flow induced. The effect of the vibration on the fuel assembly and individual fuel rods is minimal. The cyclic stress range associated with deflections of such small magnitude is insignificant and has no effect on the structural integrity of the fuel rod.

The reaction force on the grid supports due to rod vibration motions is also small and is much less than the spring preload. No significant wear of the clad or grid supports is expected during the life of the fuel assembly.

Clad fretting and fuel vibration have been experimentally investigated, as shown in Reference 10. Hydraulic flow test results of the RFA-2 fuel assembly are discussed in Reference 26.

b. Fuel rod internal pressure and cladding stresses

A burnup dependent fission gas release model (References 18 and 27) is used to determine the internal gas pressures as a function of irradiation time. The plenum height of the fuel rod has been designed to ensure that the maximum internal pressure of the fuel rod will not exceed the value which would cause the fuel/clad diametral gap to increase and extensive DNB propagation during steady state operation.

The clad stresses at a constant local fuel rod power are low. Compressive stresses are created by the pressure differential between the coolant pressure and the rod internal gas pressure. Because of the prepressurization with helium, the volume average effective stresses are always less than approximately 10,000 psi at the pressurization level used in this fuel rod design. Stresses due to the temperature gradient are not included in this average effective stress because thermal stresses are, in general, negative at the clad inside diameter and positive at the clad outside diameter, and their contribution to the clad volume average stress is small.

Furthermore, the thermal stress decreases with time during steady state operation due to stress relaxation. The stress due to pressure differential is highest in the minimum power rod at the beginning-of-life due to low internal gas pressure, and the thermal stress is highest in the maximum power rod due to steep temperature gradient.

Tensile stresses can occur once the clad has come into contact with the pellet. These stresses are induced by the fuel pellet swelling during irradiation. Swelling of the fuel pellet can result in small clad strains (<1 percent) for expected discharge burnups, but the associated clad stresses are very low because of clad creep (thermal and irradiation-induced creep). The 1-percent strain criterion is extremely conservative for fuel-swelling driven clad strain because the strain rate associated with solid fission products swelling is very slow. A detailed discussion on fuel rod performance is given in Section 4.2.3.3.

c. Materials and chemical evaluation

Zircaloy-4 and Zirlo clad, and Optimized ZIRLO clad has a high corrosion resistance to the coolant, fuel, and fission products. As shown in Reference 1, there is pressurized water reactor operating experience on the capability of Zircaloy and Zirlo™ as a clad material. Optimized ZIRLO cladding further enhances the corrosion resistance of ZIRLO cladding. References 28 and 29 document the material properties and operating experience for the Optimized ZIRLO cladding. Controls on fuel fabrication specify maximum moisture levels to preclude clad hydriding.

Metallographic examination of irradiated commercial fuel rods has shown occurrences of fuel/clad chemical interaction. Reaction layers of <1 mil in thickness have been observed between fuel and clad at limited points around the circumference. Metallographic data indicates that this interface layer remains very thin, even at high burnup. Thus, there is no indication of propagation of the layer and eventual clad penetration.

d. Stress Corrosion

Stress corrosion cracking is another postulated phenomenon related to fuel/clad chemical interaction. Out-of-pile tests have shown that in the presence of high cladding tensile

stresses, large concentrations of selected fission products (such as iodine) can chemically attack the Zircaloy, Zirlo, and Optimized ZIRLO tubing and can lead to eventual cladding cracking. Extensive post-irradiation examination has produced no in-pile evidence that this mechanism is operative in commercial fuel.

e. Cycling and Fatigue

A comprehensive review of the available strain fatigue models was conducted by Westinghouse as early as 1968. This review included the Langer-O'Donnell model (Reference 12), the Yao-Munse model and the Manson-Halford model. Upon completion of this review and using the results of the Westinghouse experimental programs discussed below, it was concluded that the approach defined by Langer-O'Donnell would be retained and the empirical factors of their correlation modified in order to conservatively bound the results of the Westinghouse testing program.

The Westinghouse testing program was subdivided into the following subprograms:

1. A rotating bend fatigue experiment on unirradiated Zircaloy-4 specimens at room temperature and at 725°F. Both hydrided and nonhydrided Zircaloy-4 cladding were tested.

2. A biaxial fatigue experiment in gas autoclave on unirradiated Zircaloy-4 cladding, both hydrided and unhydrided.

3. A fatigue test program on irradiated cladding from the Carolina-Virginia Tube Reactor and Yankee Core V conducted at Battelle Memorial Institute.

The results of these test programs provided information on different cladding conditions including the effects of irradiation, of hydrogen levels and of temperature.

The design equations followed the concept for the fatigue design criterion according to the ASME Boiler and Pressure Vessel Code, Section III.

It is recognized that a possible limitation to the satisfactory behavior of the fuel rods in a reactor which is subjected to daily load follow is the failure of the cladding by low cycle strain fatigue. During their normal residence time in a reactor, the fuel rods may be subjected to ~1000 cycles with typical changes in power level from 50% to 100% of their steady-state values.

The assessment of the fatigue life of the fuel rod cladding is subject to a considerable uncertainty due to the difficulty of evaluating the strain range which results from the cyclic interaction of the fuel pellets and cladding. This difficulty arises, for example, from such highly unpredictable phenomena as pellet cracking, fragmentation, and relocation. Nevertheless, since early 1968, this particular phenomenon has been investigated analytically and experimentally (Ref 12). Strain fatigue tests on irradiated and nonirradiated hydrided Zr-4 claddings were performed, which permitted a definition of a conservative fatigue life limit and recommendation on a methodology to treat the strain fatigue evaluation of the Westinghouse reference fuel rod designs.

It is believed that the final proof of the adequacy of a given fuel rod design to meet the load follow requirements can only come from

incore experiments performed on actual reactors. Experience in load follow operation dates back to early 1970 with the load follow operation of the Saxton reactor. Successful load follow operation has been performed on reactor A (>400 load follow cycles) and reactor B (>500 load follow cycles). In both cases, there was no significant coolant activity increase that could be associated with the load follow mode of operation.

f. Rod bowing

Reference 11 presents the NRC-approved model used for evaluation of fuel rod bowing. The effects of rod bowing on DNBR are described in Section 4.4.2.2.5. Also refer to item e in Section 4.2.3.3.

g. Consequences of power-coolant mismatch

This subject is discussed in Chapter 15.0.

h. Irradiation stability of the cladding

As shown in References 1, 20, and 29, there is considerable PWR operating experience to date on the capabilities of Zircaloy-4, ZIRLO, and Optimized ZIRLO alloy as cladding materials. Extensive experience with irradiated Zircaloy-4 is summarized in Reference 2, Appendices A through E in Reference 20 for ZIRLO cladding, and Reference 29 for Optimized ZIRLO cladding.

i. Creep collapse and creepdown

This subject and the associated irradiation stability of cladding have been evaluated, using the models described in Reference 19.

4.2.3.2 Fuel Materials Considerations

Sintered, high density uranium dioxide fuel reacts only slightly with the clad at core operating temperatures and pressures. In the event of clad defects, the high resistance of uranium dioxide to attack by water protects against fuel deterioration, although limited fuel erosion can occur. As has been shown by operating experience and extensive experimental work, the thermal design parameters conservatively account for changes in the thermal performance of the fuel elements due to pellet fracture which may occur during power operation. The consequences of defects in the clad are greatly reduced by the ability of uranium dioxide to retain fission products, including those which are gaseous or highly volatile. Observations from several operating Westinghouse pressurized water reactors (Ref. 9) have shown that fuel pellets can densify under irradiation to a density higher than the manufactured values. Fuel densification and subsequent settling of the fuel pellets can result in local and distributed gaps in the fuel rods. Fuel densification has been minimized by improvements in the fuel manufacturing process and by specifying a nominal 95-percent initial fuel density.

The evaluation of fuel densification effects and their consideration in fuel design are described in References 18 and 27. The treatment of fuel swelling and fission gas release are described in Reference 18.

The effects of waterlogging on fuel behavior are discussed in Section 4.2.3.3.

4.2.3.3 Fuel Rod Performance

In the calculation of the steady state performance of a nuclear fuel rod, the following interacting factors must be considered.

a. Clad creep and elastic deflection

b. Pellet density changes, thermal expansion, gas release, and thermal properties as a function of temperature and fuel burnup

c. Internal pressure as a function of fission gas release, rod geometry, and temperature distribution

These effects are evaluated using fuel rod design models (References 18 and 27) which include appropriate models for time-dependent fuel densification. With the above interacting factors considered, the model determines the fuel rod performance characteristics for a given rod geometry, power history, and axial power shape. In particular, internal gas pressure, fuel and clad temperatures, and clad deflections are calculated. The fuel rod is divided into several axial sections and radially into a number of annular zones. Fuel density changes are calculated separately for each segment. The effects are integrated to obtain the internal rod pressure.

The initial rod internal pressure is selected to delay fuel/clad mechanical interaction and to avoid the potential for flattened rod formation. It is limited, however, by the design criteria for the rod internal pressure (see Section 4.2.1.3).

The gap conductance between the pellet surface and the clad inner diameter is calculated as a function of the composition, temperature, and pressure of the gas mixture and the gap size or contact pressure between clad and pellet. After computing the fuel temperature for each pellet annular zone, the fractional fission gas release is assessed, using an empirical model derived from experimental data (References 18 and 27). The total amount of gas released is based on the average fractional release within each axial and radial zone and the gas generation rate which, in turn, is a function of burnup. Finally, the gas released is summed over all zones, and the pressure is calculated.

The model shows good agreement with a variety of published and proprietary data on fission gas release, fuel temperatures, and clad deflections (References 18 and 27). These data include variations in power, time, fuel density, and geometry.

a. Fuel/cladding mechanical interaction

One factor in fuel element duty is potential mechanical interaction of fuel and clad. This fuel/clad interaction produces cyclic stresses and strains in the clad, and these, in turn, consume clad fatigue life. The reduction of fuel/clad interaction is therefore a goal of design. The technology of using prepressurized fuel rods has been developed to further this objective.

The gap between the fuel and clad is initially sufficient to prevent hard contact between the two. However, during power operation a gradual compressive creep of the clad onto the fuel pellet occurs due to the external pressure exerted on the rod by the coolant. Clad compressive creep eventually results in fuel/clad contact. Once fuel/clad contact occurs, changes in power level result in changes in clad stresses and strains. By using prepressurized fuel rods to partially offset the effect of the coolant external pressure, the rate of clad creep toward the surface of the fuel is reduced. Fuel rod prepressurization delays the time at which fuel/clad contact occurs and hence significantly reduces the extent of cyclic stresses and strains experienced by the clad

both before and after fuel/clad contact. These factors result in an increase in the fatigue life margin of the clad and lead to greater clad reliability. If gaps should form in the fuel stacks, clad flattening will be prevented by the rod prepressurization so that the flattening time will be greater than the fuel core life.

A two-dimensional (r,Θ) finite element model has been developed to investigate the effects of radial pellet cracks on stress concentrations in the clad. Stress concentration, herein, is defined as the difference between the maximum clad stress in the Θ-direction and the mean clad stress. The first case has the fuel and clad in mechanical equilibrium and, as a result, the stress in the clad is close to zero. In subsequent cases, the pellet power is increased in steps, and the resultant fuel thermal expansion imposes tensile stress in the clad. In addition to uniform clad stresses, stress concentrations develop in the clad adjacent to radial cracks in the pellet. These radial cracks have a tendency to open during a power increase but the frictional forces between fuel and clad oppose the opening of these cracks and result in localized increases in clad stress. As the power is further increased, large tensile stresses exceed the ultimate tensile strength of UO_2, and additional cracks in the fuel are created which limits the magnitude of the stress concentration in the clad.

As part of the standard fuel rod design analysis, the maximum stress concentration evaluated from finite element calculations is added to the volume-averaged effective stress in the clad, as determined from one-dimensional stress/strain calculations. The resultant clad stress is then compared to the temperature-dependent Zircaloy/Zirlo/Optimized ZIRLO yield stress in order to assure that the stress/strain criteria are satisfied.

Transient Evaluation Method

Pellet thermal expansion due to power increases is considered the only mechanism by which significant stresses and strains can be imposed on the clad. Such increases are a consequence of fuel shuffling , reactor power escalation following extended reduced power operation, and full-length control rod movement. In the mechanical design model, lead rod burnup values are obtained using best estimate power histories, as determined by core physics calculations. During burnup, the amount of diametral gap closure is evaluated, based upon the pellet expansion cracking model, clad creep model, and fuel swelling model. At various times during the depletion, the power is increased locally on the rod to the burnup-dependent attainable power density, as determined by core physics calculations. The radial, tangential, and axial clad stresses resulting from the power increase are combined into a volume average effective clad stress.

The Von Mises criterion is used to determine if the clad yield stress has been exceeded. This criterion states that an isotropic material in multiaxial stress will

begin to yield plastically when the effective stress exceeds the yield stress, as determined by an axial tensile test. The yield stress correlation is that for irradiated cladding, fuel/clad interaction occurs at high burnup. In applying this criterion, the effective stress is increased by an allowance which accounts for stress concentrations in the clad adjacent to radial cracks in the pellet, prior to the comparison with the yield stress. This allowance was evaluated using a two-dimensional (r, Θ) finite element model.

Slow transient power increases can result in large clad strains without exceeding the clad yield stress because of clad creep and stress relaxation. Therefore, in addition to the yield stress criterion, a criterion on allowable clad strain is necessary. Based upon high strain rate burst and tensile test data on irradiated tubing, 1-percent strain was determined to be a conservative lower limit on irradiated clad deformation and was thus adopted as a design criterion.

A comprehensive review of the available strain-fatigue models was conducted by Westinghouse as early as 1968. This included the Langer-O'Donnell model (Ref. 12), the Yao-Munse model, and the Manson-Halford model. Upon completion of this review and using the results of the Westinghouse experimental programs discussed below, it was concluded that the approach defined by Langer-O'Donnell would be retained and the empirical factors of their correlation modified in order to conservatively bound the results of the Westinghouse testing program.

The Langer-O'Donnell empirical correlation has the following form:

$$S_a = \frac{E}{4\sqrt{N_f}} \ln\left(\frac{100}{(100 - RA)}\right) + S_e$$

where:

S_a = $1/2\ E\ \Delta\varepsilon_t$ = pseudo-stress amplitude which causes failure in N_f cycles (lb/in.^{2})

$\Delta\varepsilon_t$ = total strain range (in./in.)

E = Young's Modulus (lb/in.^{2})

N_f = number of cycles to failure

RA = reduction in area at fracture in a uniaxial tensile test (%)

S_e = endurance limit (lb/in.^{2})

Both RA and S_e are empirical constants which depend on the type of material, the temperature, and irradiation.

The Westinghouse testing program is described in section 4.2.3.1.e.

The design equations followed the concept for the fatigue design criterion according to the ASME Code, Section III. Namely,

1. The calculated pseudo-stress amplitude (S_a) has to be multiplied by a factor of 2 in order to obtain the allowable number of cycles (N_f)

2. The allowable cycles for a given S_a is 5 percent of N_f, maintaining a safety factor of 20 on cycles.

The lesser of the two allowable number of cycles is selected. The cumulative fatigue life fraction is then computed as:

$$\sum_{1}^{k} \frac{n_k}{N_{fk}} \leq 1$$

where:

n_k = number of diurnal cycles of mode k

N_{fk} = number of allowable cycles

It is recognized that a possible limitation to the satisfactory behavior of the fuel rods in a reactor which is subjected to daily load follow is the failure of the clad by low-cycle strain fatigue. During their normal residence time in the reactor, the fuel rods may be subjected to 1,000 cycles or more with typical changes in power level from 50 to 100 percent of their steady state values.

The assessment of the fatigue life of the fuel rod clad is subject to a considerable uncertainty due to the difficulty of evaluating the strain range which results from the cyclic interaction of the fuel pellets and clad. This difficulty arises, for example, from such highly unpredictable phenomena as pellet cracking, fragmentation, and relocation. Nevertheless, since early 1968, this particular phenomenon has been investigated analytically and experimentally (Ref. 12). Strain fatigue tests on irradiated and nonirradiated hydrided Zircaloy-4 claddings were performed which permitted a definition of a conservative fatigue life limit and recommendation on a methodology to treat the strain fatigue evaluation of the Westinghouse reference fuel rod designs.

It is believed that the final proof of the adequacy of a given fuel rod design to meet the load follow requirements can come only from incore experiments performed on actual reactors. Experience in load follow operation dates back to early 1970 with the load follow operation of the Saxton reactor. Successful load follow operation has been performed on reactor A (~400 load follow cycles) and reactor B (~500 load follow cycles). In both cases, there was no significant coolant activity increase that could be associated with the load follow mode of operation.

b. Irradiation experience

Westinghouse fuel operational experience is presented in Reference 1. Additional test assembly and test rod experiences are given in Sections 8 and 23 of Reference 9.

c. Fuel and cladding temperature

The methods used for evaluation of fuel rod temperatures are presented in Section 4.4.2.11.

d. Waterlogging

Local cladding deformations typical for waterlogging* bursts have never been observed in commercial Westinghouse fuel. Experience has shown that the small number of rods which have acquired clad defects, regardless of primary mechanism, remain intact and do not progressively distort or restrict coolant flow. In fact, such small defects are normally observed through reductions in coolant activity to be progressively closed upon further operation due to the buildup of zirconium oxide and other substances. Secondary failures which have been observed in defected rods are attributed to hydrogen embrittlement of the cladding. Post-irradiation examinations point to the hydriding failure mechanism rather than a waterlogging mechanism; the secondary failures occur as axial cracks in the cladding and are similar regardless of the primary failure mechanism. Such cracks do not result in flow blockage or increase the effects of any postulated transients.

More information is provided in References 15 and 16.

e. Potentially damaging temperature effects during transients

The fuel rod experiences many operational transients (intentional maneuvers) during its residence in the core. A number of thermal effects must be considered when analyzing the fuel rod performance.

The clad can be in contact with the fuel pellet at some time in the fuel lifetime. Clad/pellet interaction occurs if the fuel pellet temperature is increased after the clad is in contact with the pellet. Clad/pellet interaction is discussed earlier in the section.

* Waterlogging damage of a previously defected fuel rod has occasionally been postulated as a mechanism for subsequent rupture of the cladding. Such damage has been postulated as a consequence of a power increase on a rod after water has entered such a rod through a clad defect of appropriate size. Rupture is postulated upon power increase if the rod internal pressure increase is excessive due to insufficient venting of water to the reactor coolant.

The potential effects of operation with waterlogged fuel discussed above concluded that waterlogging is not a concern during operational transients.

Clad flattening, as shown in Reference 6 and 19, has been observed in some operating power reactors. Thermal expansion (axial) of the fuel rod stack against a flattened section of the clad could cause failure of the clad. This is no longer a concern because clad flattening is precluded during the fuel residence in the core (see Section 4.2.3.1).

Potential differential thermal expansion between the fuel rods and the guide thimbles during a transient is considered in the design. Excessive bowing of the fuel rods is precluded because the grid assemblies allow axial movement of the fuel rods relative to the grids. Specifically, thermal expansion of the fuel rods is considered in the grid design so that axial loads imposed on the fuel rods during a thermal transient will not result in excessively bowed fuel rods.

f. Fuel element burnout and potential energy release

As discussed in Section 4.4.2.2, the core is protected from DNB over the full range of possible operating conditions. In the extremely unlikely event that DNB should occur, the clad temperature will rise due to the steam blanketing at the rod surface and the consequent degradation in heat transfer. During this time, there is a potential for chemical reaction between the cladding and the coolant. However, because of the relatively good film boiling heat transfer following DNB, the energy release resulting from this reaction is insignificant compared to the power produced by the fuel.

g. Coolant flow blockage effects on fuel rods

This evaluation is presented in Section 4.4.4.6.

4.2.3.4 Spacer Grids

The coolant flow channels are established and maintained by the structure composed of grids and guide thimbles. The lateral spacing between fuel rods is provided and controlled by the support dimples of adjacent grid cells. Contact of the fuel rods on the dimples is maintained through the clamping force of the grid springs. Lateral motion of the fuel rods is opposed by the spring force and the internal moments generated between the spring and the support dimples. Grid testing is discussed in Reference 13 (LOPAR), Reference 22 (V5H), References 20 and 23 (V5H P+), and References 24 and 25 (RFA and RFA-2).

As shown in Reference 13 (LOPAR), Reference 22 (V5H), and References 20 and 23 (V5H P+), and References 24 and 25 (RFA and RFA-2) grid crushing tests and seismic and loss-of-coolant accident evaluations demonstrate that the grids will maintain a geometry that is capable of being cooled under the worst-case accident Condition III & IV event.

4.2.3.5 Fuel Assembly

4.2.3.5.1 Stresses and Deflections

The fuel assembly component stress levels are limited by the design. For example, stresses in the fuel rod due to axial thermal expansion and Zircaloy, ZIRLO clad, or Optimized ZIRLO clad irradiation growth are limited by the relative motion of the rod as it slips over the grid spring and dimple surfaces. Clearances between the fuel rod ends and nozzles are provided so that Zircaloy, ZIRLO clad, or Optimized ZIRLO clad irradiation growth does not result in rod end interferences. Stresses in the fuel assembly caused by tripping of the rod cluster control assembly have little influence on fatigue because of the small number of events during the life of an assembly. Assembly components and prototype fuel assemblies made from production parts have been subjected to structural tests to verify that the design bases requirements are met.

The fuel assembly design loads for shipping have been established at 4 g axial and 6 g lateral directions. Accelerometers are permanently placed into the shipping cask to monitor and detect fuel assembly accelerations that would exceed the criteria. Past history and experience have indicated that loads which exceed the allowable limits rarely occur. Exceeding the limits requires reinspection of the fuel assembly for damage. Tests on various fuel assembly components, such as the grid assembly, sleeves, inserts, and structure joints, have been performed to assure that the shipping design limits do not result in impairment of fuel assembly function. Seismic analysis of the fuel assembly is presented in Reference 13 (LOPAR), Reference 22 (V5H), References 20 and 23 (V5H P+), and Reference 24 (RFA). Since the RFA-2 mid-grid change has no impact on the seismic/LOCA analysis, the conclusion for the RFA Z^{+2} design in Reference 24 remains valid for the RFA-2 Z^{+2} design.

4.2.3.5.2 Dimensional Stability

A prototype fuel assembly has been subjected to column loads in excess of those expected in normal service and faulted conditions (Ref. 13).

No interference between control rods and thimble tubes will occur during insertion of the rods following a postulated loss-of-coolant accident transient due to fuel rod swelling, thermal expansion, or bowing. In the early phase of the transient following the coolant break, the high axial loads, which could be generated by the difference in thermal expansion between fuel clad and thimbles, are relieved by slippage of the fuel rods through the grids. The relatively low drag force restraint on the fuel rods will induce only minor thermal bowing, which is insufficient to close the fuel rod-to-thimble tube gap.

Reference 13 (LOPAR), Reference 22 (V5H), References 20 and 23 (V5H P+), and Reference 24 (RFA) shows that the fuel assemblies will maintain a geometry amenable to cooling during a combined seismic and double-ended loss-of-coolant accident. Reference 25 shows that the grid crush strength and seismic factor $P/K^{1/2}$ improved with the RFA-2 design relative to the RFA design. Since the contact length change has no impact on the fuel assembly models used in the seismic and LOCA evaluation, the seismic and LOCA evaluation for the RFA design is applicable for the RFA-2 design.

4.2.3.6 Reactivity Control Assembly and Burnable Absorber Rods

a. Internal pressure and cladding stresses during normal, transient and accident conditions

The designs of the standard burnable absorber, WABA, and source rods provide a sufficient cold void volume to accommodate the internal pressure increase during operation. This is not a concern for the standard absorber rod because no gas is released by the absorber material.

For the standard absorber rod, the use of glass in tubular form provides a central void volume along the length of the rods (see Figure 4.2-12a). For the WABA rods, an annular plenum is provided within the rod to accommodate the helium gas released from the absorber material during boron depletion (see Figure 4.2-12). For the source rods, a void volume is provided within the rod in order to limit the internal pressure increase until end of life (see Figures 4.2-13 and 4.2-13a).

The stress analysis of the standard absorber and source rods assumes 100-percent gas release to the rod void volume, in addition to the initial pressure within the rod. The stress analysis of the WABA rods assumes a helium release rate of 30% due to the design of the rod.

During normal transient and accident conditions the void volume limits the internal pressures to values which satisfy the criteria in Section 4.2.1.6. These limits are established not only to ensure that peak stresses do not reach unacceptable values, but also to limit the amplitude of the oscillatory stress component in consideration of the fatigue characteristics of the materials.

Rod, guide thimble, and dashpot flow analyses indicate that the flow is sufficient to prevent coolant boiling within the guide thimble. Therefore, clad temperatures at which the clad material has adequate strength to resist coolant operating pressures and rod internal pressures are maintained.

b. Thermal stability of the absorber material, including phase changes and thermal expansion

The radial and axial temperature profiles within the source and burnable absorber rods have been determined by considering gap conductance, thermal expansion, neutron or gamma heating of the contained material as well as gamma heating of the clad.

The maximum temperature of the silver-indium-cadmium alloy or hafnium control rod absorber material was calculated and found to be significantly less than the material melting point, and occurs axially at only the highest flux region. The thermal expansion properties of the absorber material and the phase changes are discussed in Reference 3.

The maximum temperature of the borosilicate glass was calculated to be about 1300^{o}F and takes place following the initial rise to power. As the operating cycle proceeds, the glass temperature decreases for the following reasons: 1) reduction in power generation due to boron-10 depletion, 2) better gap conductance as the helium produced diffuses to the gap, and 3) external gap reduction due to borosilicate glass creep.

The maximum temperature of the aluminum oxide-boron carbide burnable absorber pellet is calculated to be less than 1200^{o}F which takes place following the initial rise to power. As the operating cycle proceeds, the burnable absorber pellet temperature decreases for the following reasons: (1) reduction in heat generation due to B_{10} depletion, (2) better gap conductance as the helium produced diffuses to the gap.

Sufficient diametral and end clearances have been provided in the neutron absorber, burnable absorber, and source rods to accommodate the relative thermal expansions between the enclosed material and the surrounding clad and end plug.

c. Irradiation stability of the absorber material, taking into consideration gas release and swelling

The irradiation stability of the absorber material is discussed in Reference 3 for the Ag-In-Cd and hafnium material. Irradiation produces no deleterious effects in the absorber material.

Gas release is not a concern for the control rod material because no gas is released by the absorber material. Sufficient diametral and end clearances are provided to accommodate swelling of the absorber material.

Based on experience with borosilicate glass and on nuclear and thermal calculations, gross swelling or cracking of the glass tubing is not expected during operation. Some minor creep of the glass at the hot spot, on the inner surface of the tube, could occur but would continue only until the glass came in contact with the inner liner. The wall thickness of the inner liner is sized to provide adequate support in the event of slumping and to collapse locally before rupture of the exterior cladding if unexpected large volume changes, due to swelling or cracking, should occur. The ends of the inner liner are open to allow helium, which diffuses out of the glass, to occupy the central void.

The Al_2O_3-B_4C WABA pellets are designed such that gross swelling or crumbling of the pellets is not expected during reactor operation. Although some minor cracking of the pellets may occur due to temperature cycles during startup and shutdown, this cracking should not affect the overall absorber stack integrity.

d. Potential for chemical interaction, including possible waterlogging rupture

The structural materials selected have good resistance to irradiation damage and are compatible with the reactor environment.

Corrosion of the materials exposed to the coolant is quite low, and proper control of chloride and oxygen in the coolant will prevent the occurrence of stress corrosion. The potential for the interference with rod cluster control movement due to possible corrosion phenomena is very low.

Waterlogging rupture is not a failure mechanism associated with Westinghouse-designed control rods. However, a breach of the cladding for any postulated reason does not result in serious consequences. The Ag-In-Cd and hafnium absorber material are relatively inert and would still remain remote from high coolant velocity regions. Rapid loss of material resulting in significant loss of reactivity control material would not occur. There is extensive U.S. Naval reactor experience with unclad hafnium as an absorber material, and its corrosion resistance has been excellent, in fact it has been reported to be superior to Zircaloy-2, with respect to corrosion resistance (Ref. 3).

4.2.4 TESTING AND INSPECTION PLAN

4.2.4.1 Quality Assurance Program

The quality assurance program plan of the Westinghouse Nuclear Fuel Division is summarized in Reference 14.

The program provides for control over all activities affecting product quality, commencing with design and development and continuing through procurement, materials handling, fabrication, testing and inspection, storage, and transportation. The program also provides for the indoctrination and training of personnel and for the auditing of activities affecting product quality through a formal auditing program.

Westinghouse drawings and product, process, and material specifications identify the inspections to be performed.

4.2.4.2 Quality Control

Quality control philosophy is generally based on the following inspections being performed to a 95-percent confidence that at least 95 percent of the product meets specification, unless otherwise noted.

a. Fuel system components and parts

   The characteristics inspected depend upon the component parts and includes dimensional, visual check, audits of test reports, material certification and nondestructive examination such as X-ray and ultrasonic.

   All material used in this core is accepted and released by Quality Control.

b. Pellets

Inspection is performed for dimensional characteristics such as diameter, density, length, and squareness of ends. Additional visual inspections are performed for cracks, chips, and surface conditions, according to approved standards.

Density is determined in terms of weight per unit length and is plotted on zone charts used in controlling the process. Chemical analyses are taken on a specified sample basis throughout pellet production.

c. Rod inspection

Fuel rod, control rod, burnable absorber, and source rod inspections consist of the following nondestructive examination techniques and methods, as applicable.

1. Leak testing

Each fuel, WABA, and secondary source rod is tested, using a calibrated mass spectrometer, with helium being the detectable gas.

2. Enclosure welds

All weld enclosures are nondestructively examined by a qualified volumetric nondestructive examination method (e.g., per ASME 142, x-ray or ultrasonics) in accordance with Westinghouse specifications.

3. Dimensional

All rods are dimensionally inspected prior to final release. The requirements include such items as length, camber, and visual appearance.

4. Plenum dimensions

All of the fuel rods and burnable absorber rods are inspected by X-ray, gamma scanning, or other approved methods to ensure proper plenum dimensions.

5. Pellet-to-pellet gaps

All of the fuel rods are inspected by gamma scanning or other methods to ensure that no significant gaps exist between pellets.

6. Enrichment Deviation

All of the fuel rods are gamma scanned to verify enrichment control prior to acceptance for assembly loading.

7. Traceability

   Traceability of rods and associated rod components is established by Quality Control.

d. Assemblies

   Each fuel, control, burnable absorber and source rod assembly is inspected for compliance with drawing and/or specification requirements. Other incore control component inspection and specification requirements are given in Section 4.2.4.3.

e. Other inspections

   The following inspections are performed as part of the routine inspection operation:

   1. Tool and gage inspection and control, including standardization to primary and/or secondary working standards. Tool inspection is performed at prescribed intervals on all serialized tools. Complete records of calibration and conditions of tools are kept.

   2. Audits of inspection activities and records are performed to ensure that prescribed methods are followed and that records are correct and properly maintained.

   3. Surveillance inspection, where appropriate, and audits of outside contractors are performed to ensure conformance with specified requirements.

f. Process control

   To prevent the possibility of mixing enrichments during fuel manufacture and assembly, strict enrichment segregation and other process controls are exercised.

   The UO_2 powder is kept in sealed containers. The contents are fully identified both by descriptive tagging and preselected color coding. A Westinghouse identification tag completely describing the contents is affixed to the containers before transfer to powder storage. Isotopic content is confirmed by analysis.

   Powder withdrawal from storage can be made by only one authorized group, which directs the powder to the correct pellet production line. All pellet production lines are physically separated from each other, and pellets of only a single nominal enrichment and density are produced in a given production line at any given time.

Finished pellets are placed on trays and transferred to segregated storage racks within the confines of the pelleting area. Samples from each pellet lot are tested for isotopic content and impurity levels prior to acceptance by Quality Control. Physical barriers prevent mixing of pellets of different enrichments in this storage area. Unused powder and substandard pellets are returned to storage in the original color-coded containers.

Loading of pellets into the clad is performed in isolated production lines, and again only one enrichment is loaded on a line at a time.

A serialized traceability code is laser marked on each fuel tube, which identifies the contract and enrichment. The end plugs are inserted and the end plugs are then inert welded to seal the tube. The code provides a reference to the fuel contained in the fuel rods.

At the time of installation into an assembly, the rod codes are placed into a matrix to identify each rod in its position within a given assembly. Before a fuel assembly is Quality Control released, the traceability codes on the described matrix are checked to ensure that the fuel rods in the assembly are from the correct region. Traceability of all fuel assembly components in an assembly are permanently maintained and identified with a unique identification number engraved on the fuel assembly top nozzle.

Similar traceability is provided for burnable absorber rods, source rods, and control rods, as required.

4.2.4.3 Incore Control Component Testing and Inspection

Tests and inspections are performed on each reactivity control component to verify the mechanical characteristics. In the case of the rod cluster control assembly, prototype testing has been conducted, and both manufacturing tests/inspections and functional testing at the plant site are performed.

During the component manufacturing phase, the following requirements apply to the reactivity control components to ensure proper functioning during reactor operation:

a. All materials are procured to specifications to attain the desired standard of quality.

b. All spider assemblies are proof tested by applying a load to the spider body so that a specified load with a given tolerance is applied to each vane. This proof load applied to each vane provides a bending moment at the spider body greater than the load caused by the acceleration imposed by the control rod drive mechanism.

c. All rods are checked for integrity by the methods described in Section 4.2.4.2, item c.

d. To ensure proper fitup with the fuel assembly, the rod cluster control, burnable absorber, and source assemblies are installed in the fuel assembly without restriction or binding in the dry condition. In addition, each rod assembly must meet a straightness requirement over the entire inserted length of each rod assembly. Following core loading, but prior to initial criticality, the rod cluster control assemblies were tested to demonstrate reliable operation in accordance with Regulatory Guide 1.68, Appendix A, Section 2.b. This testing is further discussed in Section 14.2.12.3.27.

In order to demonstrate continuous free movement of the RCCAs and to ensure acceptable core power distributions during operations, partial movement checks are performed on every rod cluster control assembly, as required by the technical specifications. In addition, periodic drop tests of the rod cluster control assemblies are performed at each refueling shutdown to demonstrate continued ability to meet trip time requirements.

If a RCCA cannot be moved by its mechanism, adjustments in the boron concentration ensure that adequate shutdown margin would be achieved following a trip. Thus inability to move one rod cluster control assembly can be tolerated. More than one inoperable rod cluster control assembly could be tolerated, but would impose additional demands on the plant operator. Therefore, the number of inoperable rod cluster control assemblies has been limited to one.

4.2.4.4 Tests and Inspections by Others

If any tests and inspections are to be performed on behalf of Westinghouse, Westinghouse will review and approve the quality control procedures, inspection plans, etc. to be utilized to ensure that they are equivalent to the description provided in Sections 4.2.4.1 through 4.2.4.3 and are performed to meet all Westinghouse requirements.

4.2.4.5 Inservice Surveillance

Westinghouse has conducted a program to examine detailed aspects of the 17 x 17 fuel assembly. This program is described in Section 23 of Reference 9. Reference 1 is periodically updated in order to provide recent results of operating experience with Westinghouse fuel and incore control components.

4.2.4.6 Onsite Inspection

Written procedures are used by the station staff for the post-shipment inspection of all new fuel and associated components, such as control rods, plugs, and inserts. Fuel handling procedures specify the sequence in which handling and inspection take place.

Loaded fuel containers, when received onsite, are externally inspected to ensure that labels and markings are intact and seals are unbroken. After the containers are opened, the shock indicators attached to the suspended internals are inspected to determine if movement during transit exceeded design limitations.

Following removal of the fuel assembly from the container in accordance with detailed procedures, the fuel assembly plastic wrapper is examined for evidence of damage. The polyethylene wrapper is then removed, and a visual inspection of the entire bundle is performed.

Control rod, source and burnable absorber assemblies usually are shipped in fuel assemblies and are inspected after removal of the fuel assembly from the container. The control rod assembly is withdrawn a few inches from the fuel assembly to ensure free and unrestricted movement, and the exposed section is visually inspected for mechanical integrity, replaced in the fuel assembly and stored with the fuel assembly. Control rod, source or burnable poison assemblies may be stored separately or within fuel assemblies.

4.2.5 REFERENCES

1. Slagle, W.H., "Operational Experience with Westinghouse Cores," WCAP-8183 (latest revision).

2. Beaumont, M. D., et al., "Properties of Fuel and Core Component Materials," WCAP-9179, Revision 1 (Proprietary) and WCAP-9224 (Non-Proprietary), July 1978.

3. Beaumont, M. D., et al., "Properties of Fuel and Core Component Materials", WCAP-9179, Revision 1 (Proprietary) and WCAP-9224 (Non-Proprietary) Appendix A, "Hafnium", October 1980.

4. Deleted

5. Deleted

6. George, R. A., Lee, Y. C., and Eng, G. H., "Revised Clad Flattening Model," WCAP-8377 (Proprietary) and WCAP-8381 (Non-Proprietary), July 1974.

7. Risher, D. H., et al., "Safety Analysis for the Revised Fuel Rod Internal Pressure Design Basis," WCAP-8963 (Proprietary), November 1976 and WCAP-8964 (Non-Proprietary), August 1977.

8. Skarita, J., et al., "Westinghouse Wet Annular Burnable Absorber Evaluation Report", WCAP-10021-P-A, Revision 1 (Proprietary), October, 1983.

9. Eggleston, F. T., "Safety-Related Research and Development for Westinghouse Pressurized Water Reactors, Program Summaries - Winter 1977 - Summer 1978," WCAP-8768, Revision 2, October 1978.

10. Demario, E. E., "Hydraulic Flow Test of the 17 x 17 Fuel Assembly," WCAP-8278 (Proprietary) and WCAP-8279 Non-Proprietary), February 1974.

11. Skaritka, J. (Ed.), "Fuel Rod Bow Evaluation," WCAP-8691, Rev. 1 (Proprietary) and WCAP-8692, Rev. 1 (Non-Proprietary), July 1979.

12. O'Donnell, W. J. and Langer, B. F., "Fatigue Design Basis for Zircaloy Components," Nuclear Science and Engineering, 20, 1-12, 1964.

13. Gesinski, L. and Chiang, D., "Safety Analysis of the 17 x 17 Fuel Assembly for Combined Seismic and Loss-of-Coolant Accident," WCAP-8236 (Proprietary) and WCAP-8288 (Non-Proprietary), December 1973 and Addendum 1 (Proprietary) March 1974.

14. "Quality Management System," Revision 2.1

15. Stephan, L. A., "The Effects of Cladding Material and Heat Treatment on the Response of Waterlogged UO2 Fuel Rods to Power Bursts," IN-ITR-111, January 1970.

16. Western New York Nuclear Research Center Correspondence With the U.S. Atomic Energy Commission on February 11 and August 27, 1971, Docket No. 50-57.

17. Davidson, S.L., et.al., "Extended Burnup Evaluation of Westinghouse Fuel," WCAP-10125-P-A (Proprietary) and WCAP-10126-A (Non-Proprietary), December 1985.

18. Weiner, R.A., et.al., "Improved Fuel Performance Models for Westinghouse Fuel Rod Design and Safety Evaluations," WCAP-10851-P-A (Proprietary) and WCAP-11873-A (Non-Proprietary), August 1988.

19. Kersting, P.J., et.al., "Assessment of Clad Flattening and Densification Power Spike Factor Elimination in Westinghouse Nuclear Fuel", WCAP-13589-A (Proprietary), March 1995.

20. Davidson, S.L., Nuhfer, D.L. (Eds.) "VANTAGE + Fuel Assembly Reference Core Report", WCAP-12610-A and Appendices A through D, June 1990.

21. Davidson, S.L., "Westinghouse Fuel Criteria Evaluation Process", WCAP-12488-A, October 1994.

22. Davidson, S.L., (Ed.), "Reference Core Report - VANTAGE 5 Fuel Assembly", WCAP-10444-P-A, September 1985 and Addendum 2A, February 1989.

23. Letter from Slater, J.L., Westinghouse, to Norton, W.B., WCNOC, dated May 5, 1994, "Safety Evaluations For Region 10 (SAHF) Fuel Changes", Westinghouse letter number 94SAP-G-0027 (WCNOC letter number 94-00490) and Attachment A, SECL-92-305, "Performance + Fuel Features".

24. Kitchen, T. J., "17 x 17 Standard Robust Fuel Assembly (17 x 17 STD RFA)", Safety Evaluation Check List, SECL-98-056, September 1998.

25. Seel, D. D. (Ed.), "17x17" Robust Fuel Assembly with RFA-2 Mid-Grid Final Design Review Package", DR-01-5 (Proprietary), October 2001.

26. H. A. Sepp, "Fuel Criterion Evaluation Process (FCEP) Notification of the RFA-2 Design (Proprietary", LTR-NRC-01-44, December 19, 2001.

27. Foster, J. P. and Sidener, S., "Westinghouse Improved Performance Analysis and Design Model (PAD 4.0)", WCAP-15063-P-A, Revision 1 with Errata, July 2000.

28. Shah, H. H., "Optimized ZIRLO™," WCAP-12610-P-A & CENPD-404-P-A Addendum 1-A, July 2006

29. Gresham, J.A., "SER Compliance of WCAP-12610-P-A & CENPD-404-P-A Addendum 1-A, 'Optimized ZIRLO™' (Proprietary/Non-Proprietary)," Westinghouse Letter LTR-NRC-13-6 (ADAMS Accession Number ML 13070A189), February 2013.

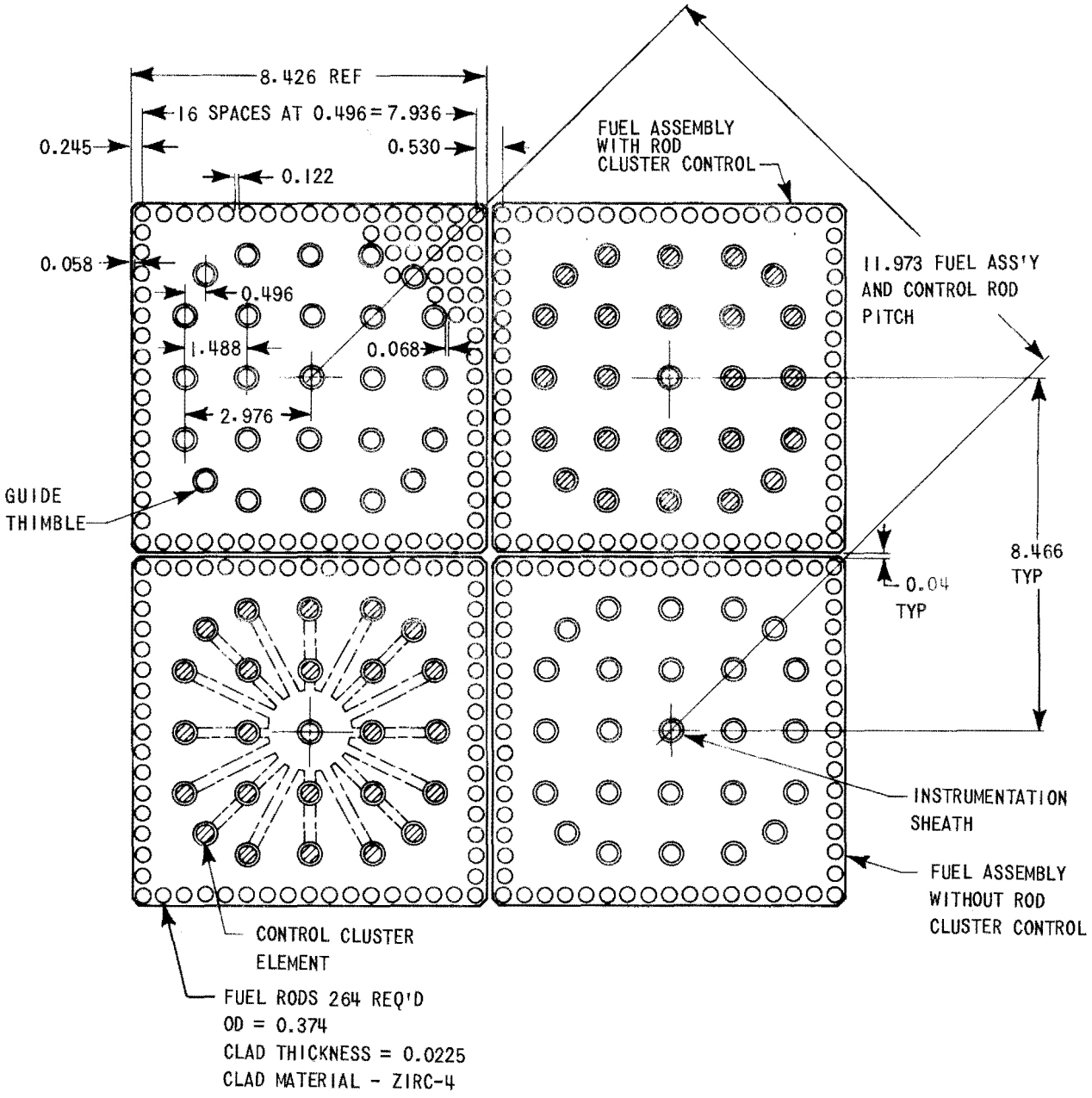

Rev. 11

WOLF CREEK
UPDATED SAFETY ANALYSIS REPORT

FIGURE 4.2-1

FUEL ASSEMBLY CROSS SECTION
17 X 17

LOPAR

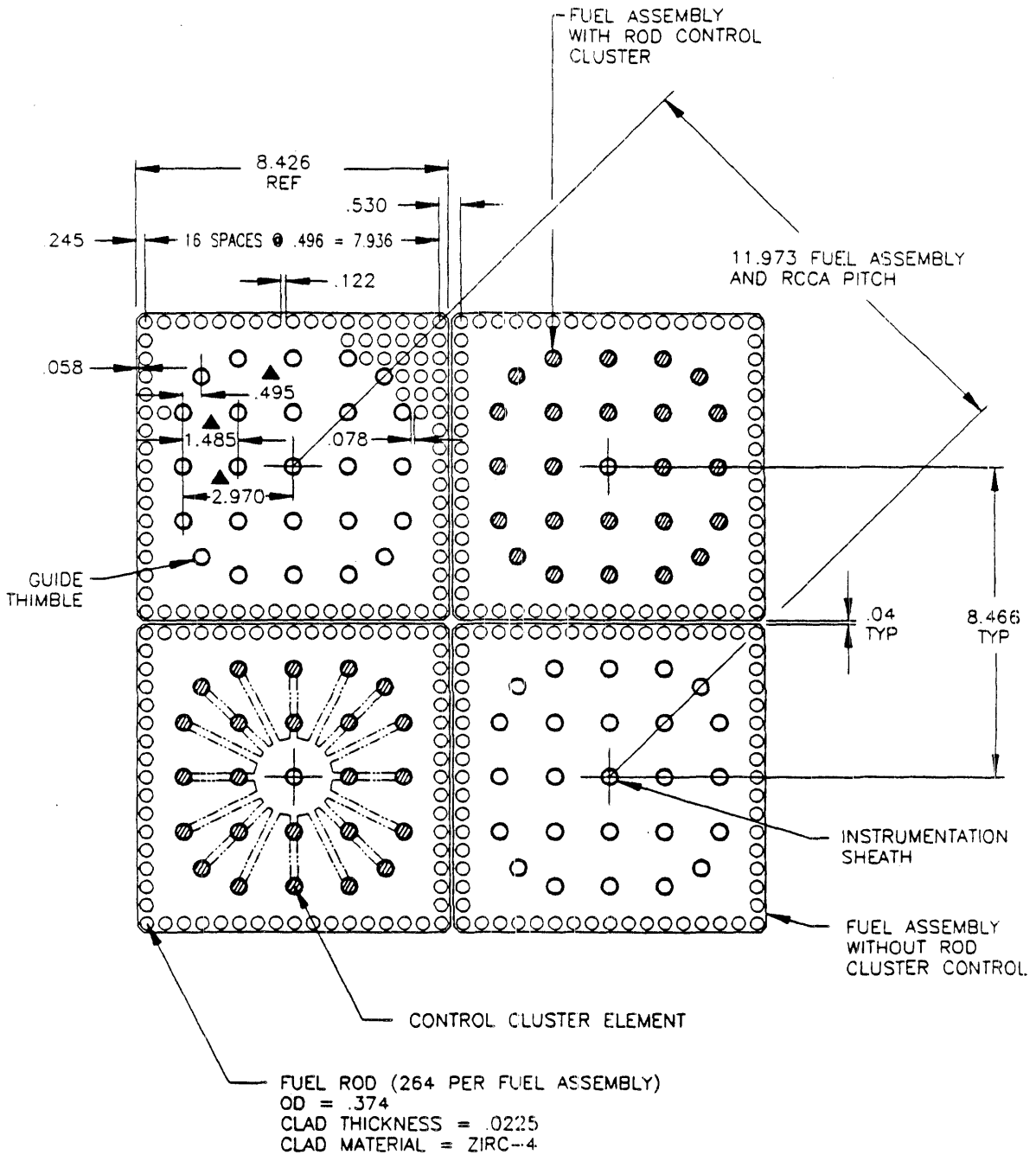

▲ GUIDE THIMBLE DIMENSIONS
AT TOP NOZZLE ADAPTOR PLATE

Rev. 11

DIMENSIONS ARE IN INCHES (NOMINAL)

WOLF CREEK
UPDATED SAFETY ANALYSIS REPORT

FIGURE 4.2-1A

FUEL ASSEMBLY CROSS SECTION
17 x 17 VANTAGE 5H

14023

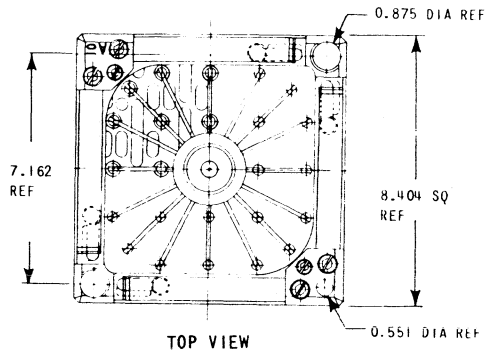

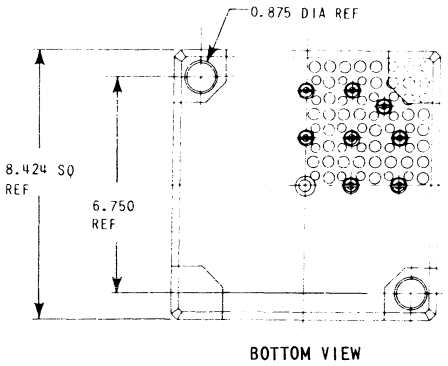

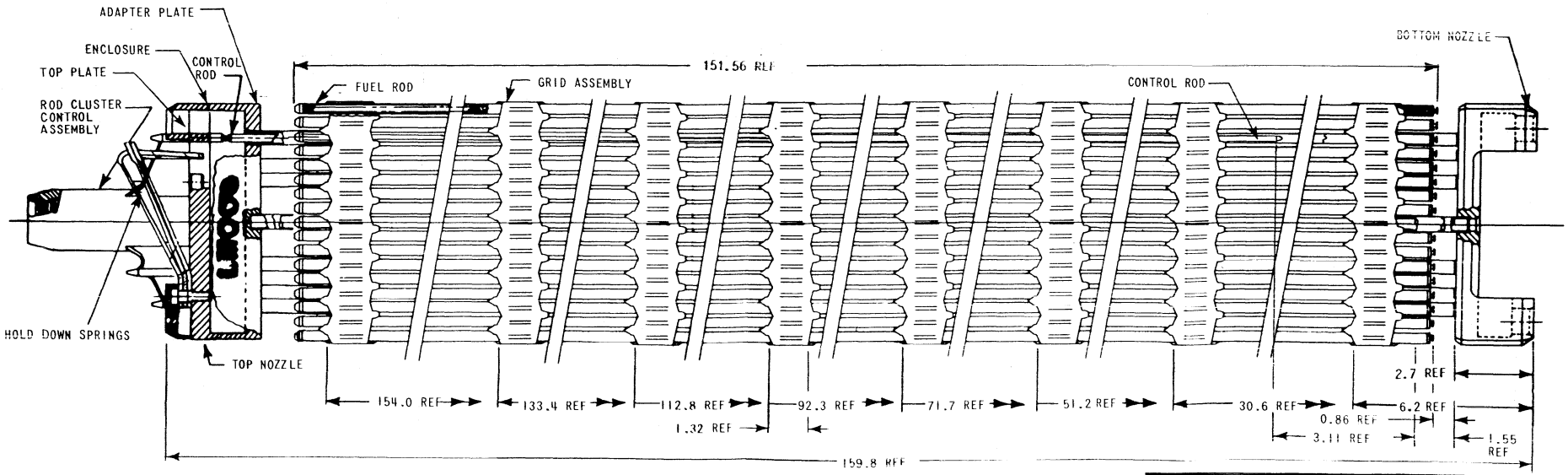

Rev. 0

WOLF CREEK
UPDATED SAFETY ANALYSIS REPORT

FIGURE 4.2-2

TYPICAL FUEL ASSEMBLY
OUTLINE 17 x 17

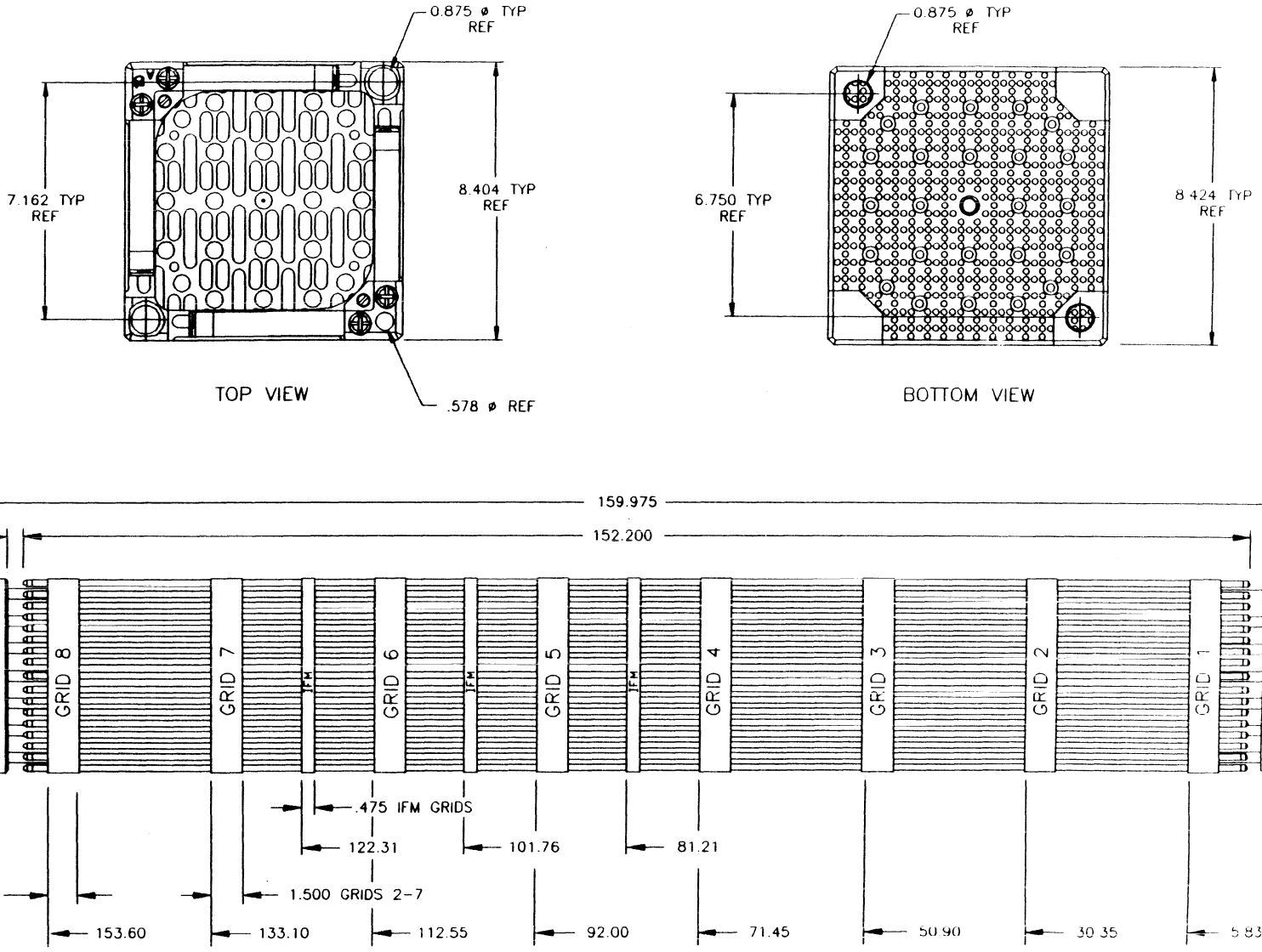

Rev. 11

WOLF CREEK
UPDATED SAFETY ANALYSIS REPORT

FIGURE 4.2-2A

FUEL ASSEMBLY OUTLINE
17 X 17 VANTAGE 5H WITH IFM GRIDS

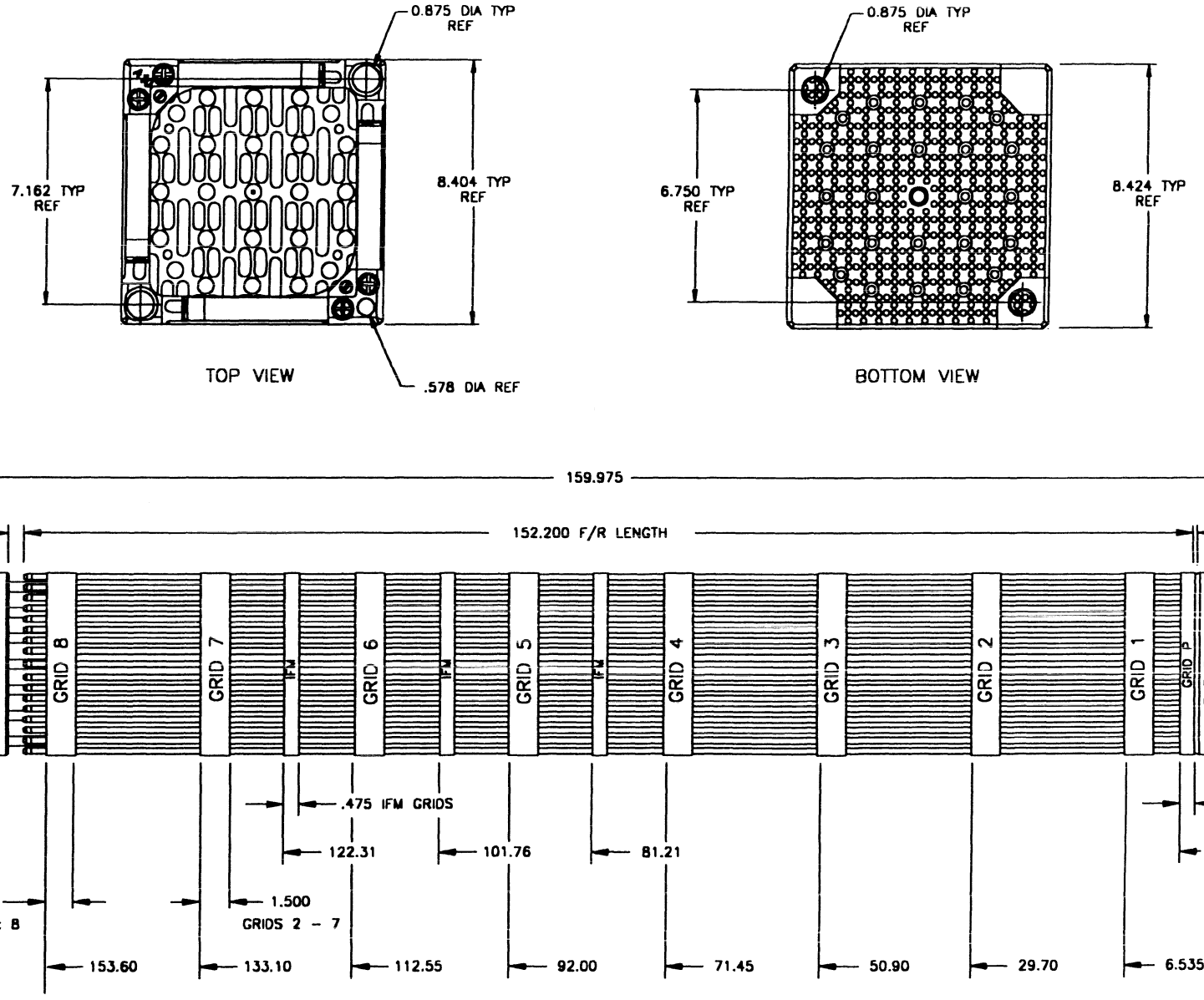

Rev. 11

WOLF CREEK FIGURE 4.2-2B
FUEL ASSEMBLY OUTLINE 17x17 VANTAGE 5H with IFMs & PBG

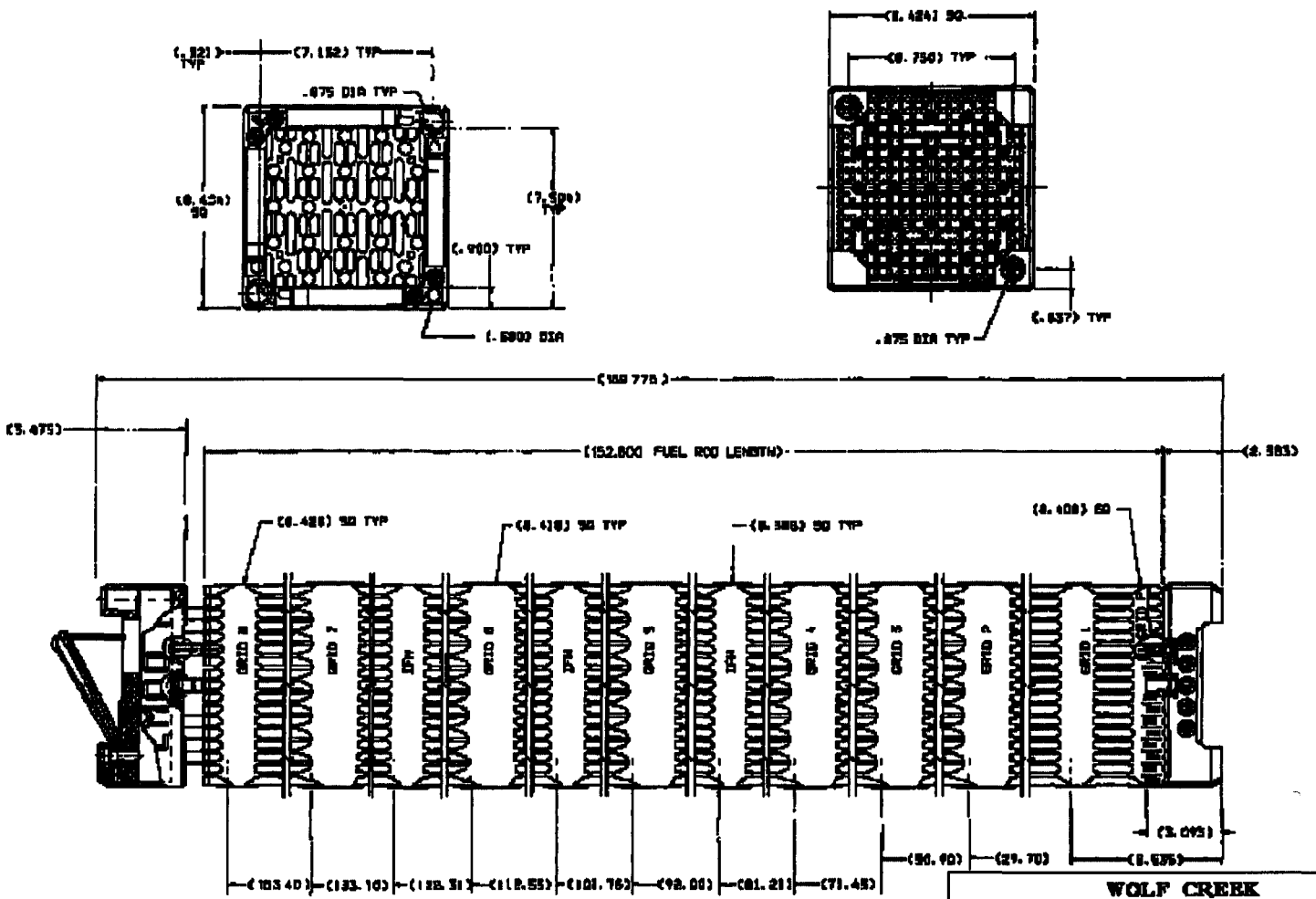

WOLF CREEK
UPDATED SAFETY ANALYSIS REPORT

FIGURE 4.2-2C

FUEL ASSEMBLY OUTLINE
17x17 VANTAGE 5H WITH
PERFORMANCE+ FEATURES (V5H P+)

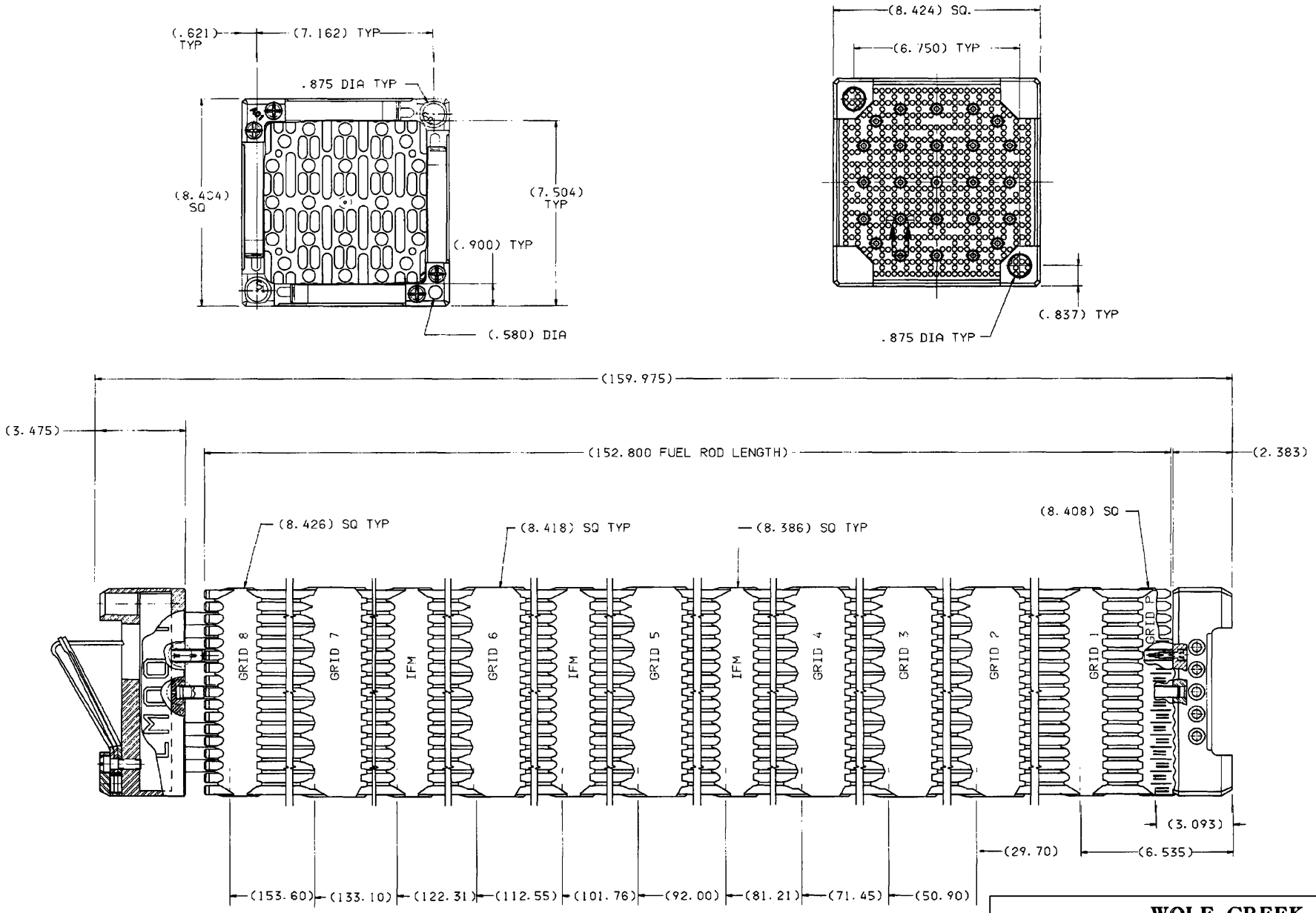

REV.18

WOLF CREEK
UPDATED SAFETY ANALYSIS REPORT

FIGURE 4.2-2D

FUEL ASSEMBLY OUTLINE 17x17
VANTAGE 5H WITH PERFORMANCE+
FEATURES, ZIRLO•2 (V5H P+Z•2)
RFA Z•2 AND RFA-2 Z•2

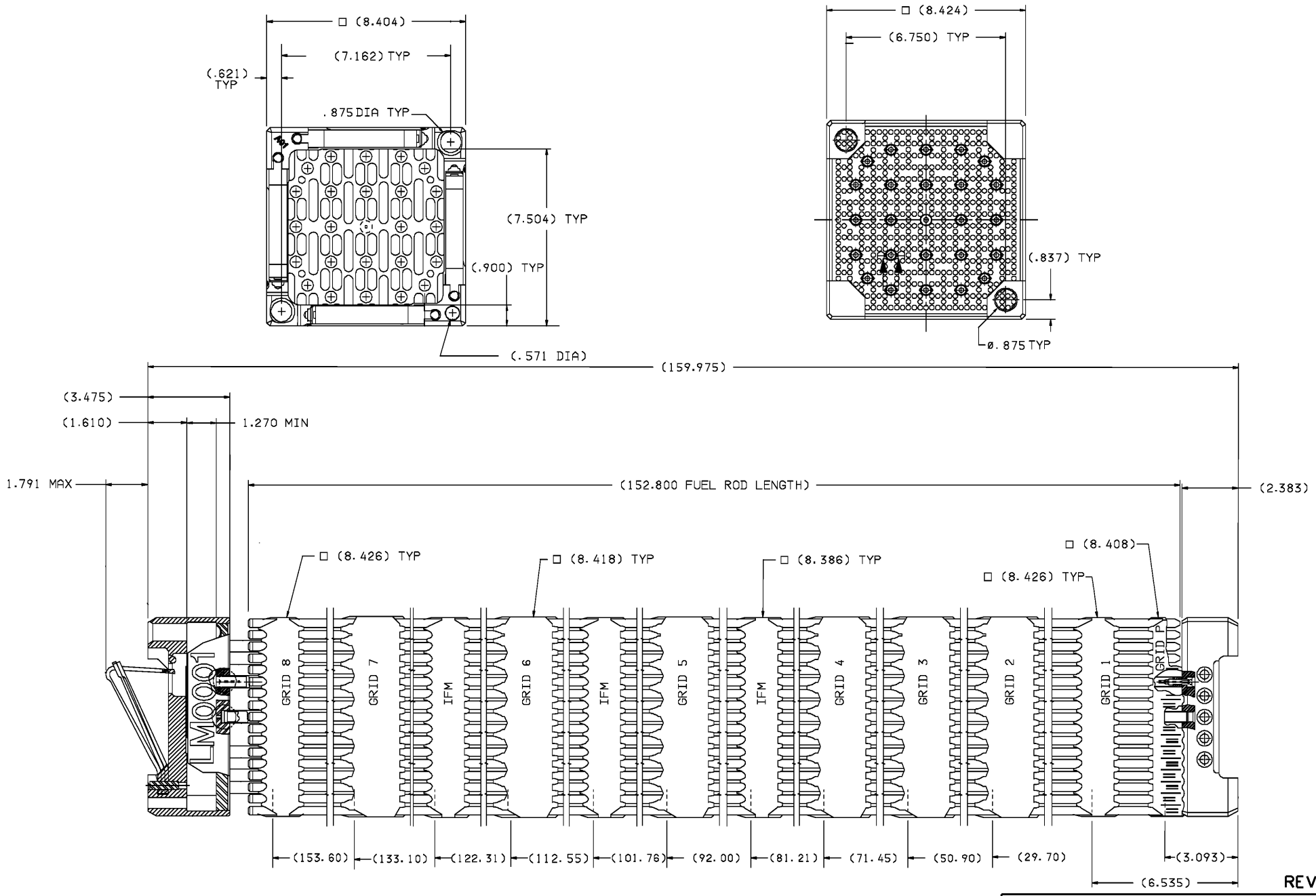

REV. 21

WOLF CREEK
UPDATED SAFETY ANALYSIS REPORT

FIGURE 4.2-2E

FUEL ASSEMBLY OUTLINE 17x17
STANDARD, PERFORMANCE+ FEATURES
Zirlo™, RFA, RFA-2, WIN

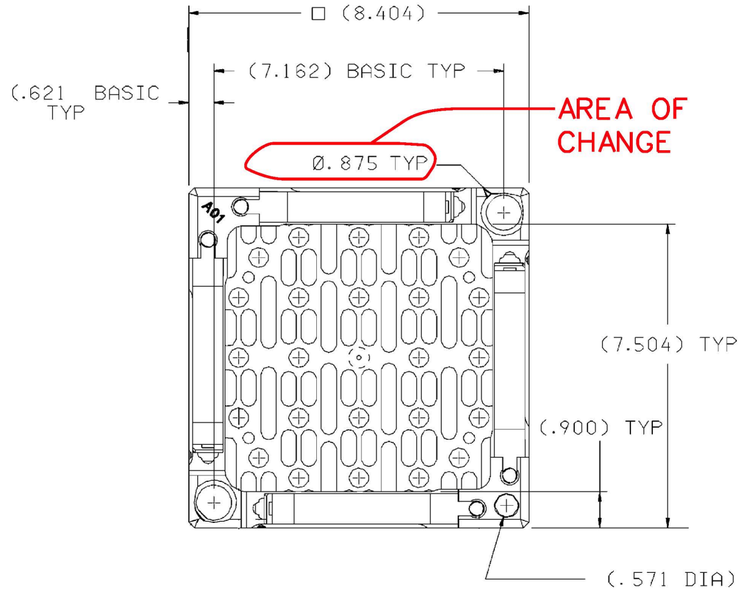

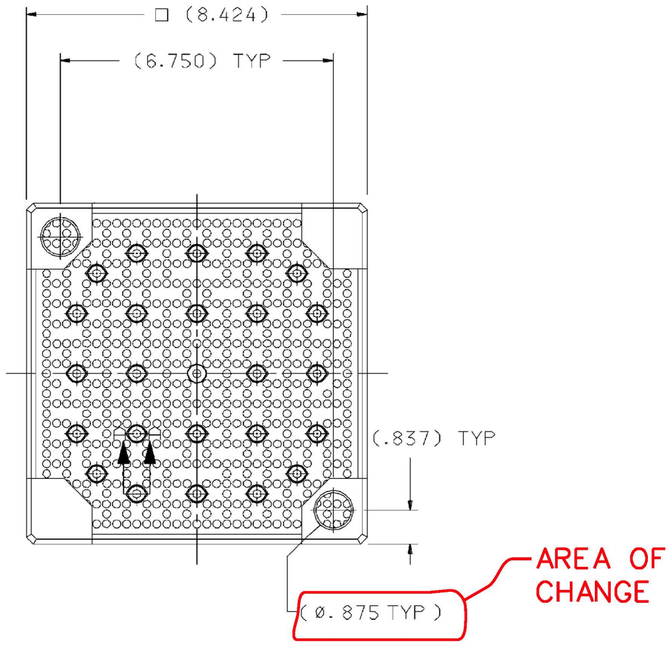

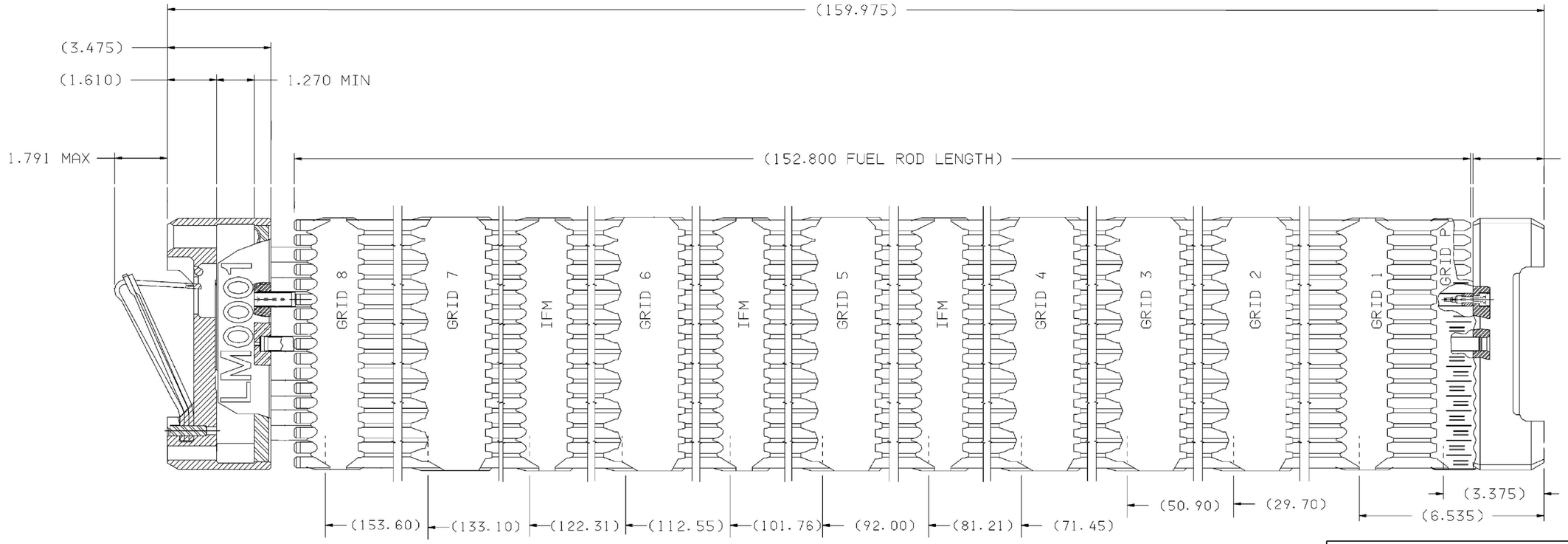

REV. 32

WOLF CREEK
UPDATED SAFETY ANALYSIS REPORT

FIGURE 4.2-2F
TOP AND BOTTOM RECONSTITUTABLE
17 STD WIN P+ Z+2 (WITH ZIRLO/
OPTIMIZED ZIRLO CLADDING) RFA
F/A OUTLINE (COMBO GRID AND SDFBN)

AREA OF CHANGE

17X22 C SIZE

WOLF CREEK

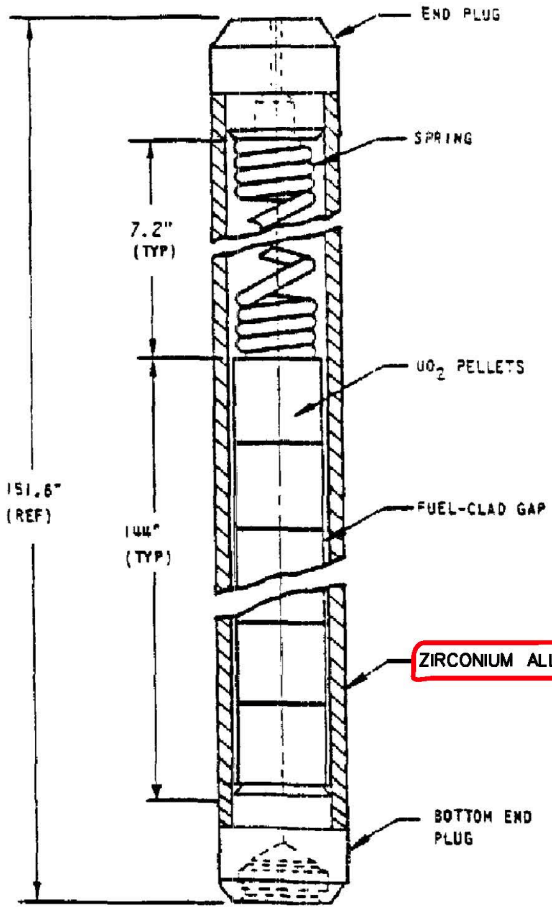

SPECIFIED DIMENSION DEPEND ON DESIGN VARIABLES SUCH AS PRE-PRESSURIZATION, POWER HISTORY, AND DISCHARGE BURNUP.

REV.32

WOLF CREEK
UPDATED SAFETY ANALYSIS REPORT

FIGURE 4.2-3

FUEL ROD SCHEMATIC
STANDARD ROD

8 1/2X11 A SIZE

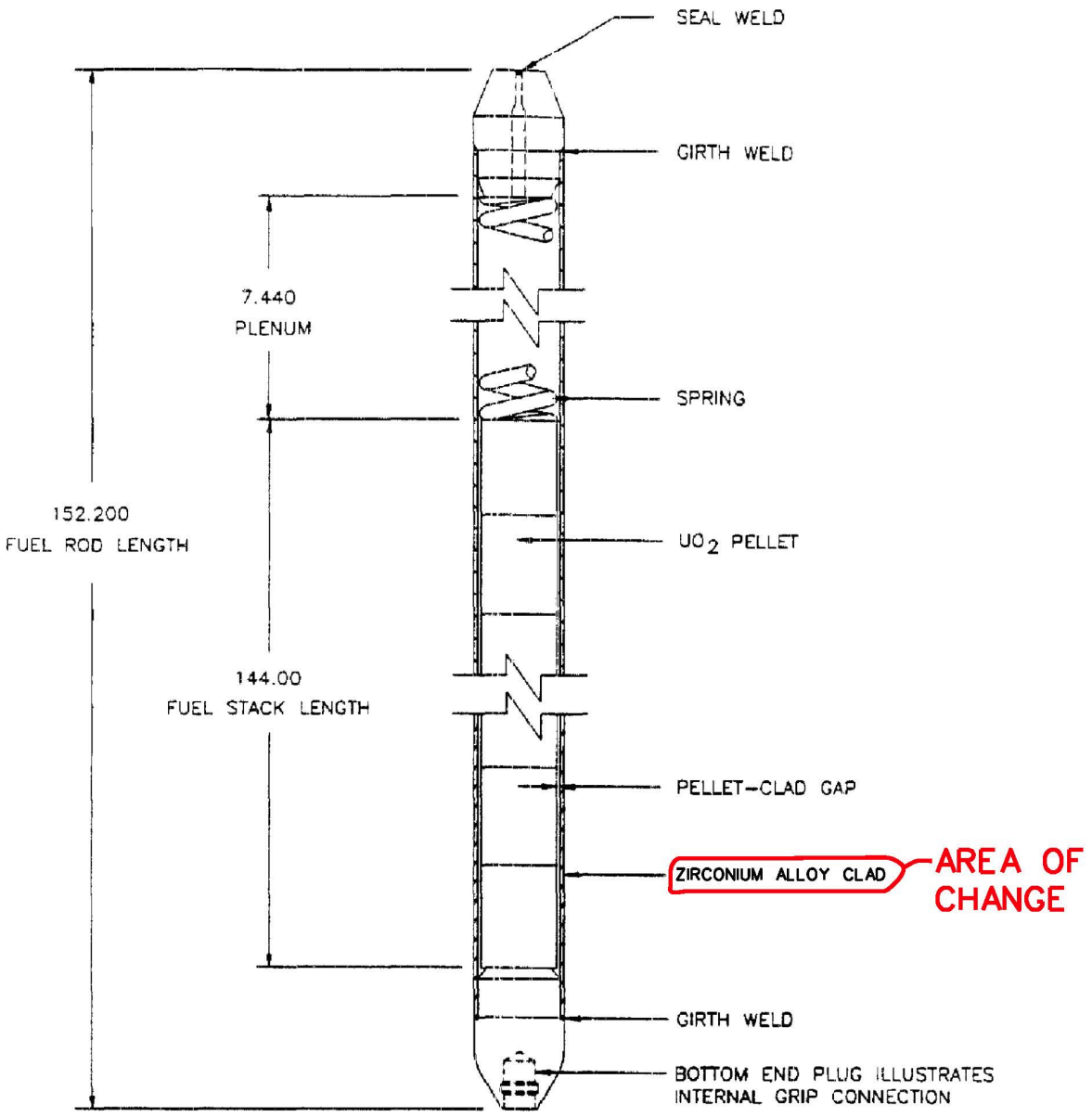

SPECIFIED DIMENSION DEPEND ON DESIGN VARIABLES SUCH AS PRE-PRESSURIZATION, POWER HISTORY, AND DISCHARGE BURNUP.

REV.32

DIMENSIONS ARE IN INCHES (NOMINAL)

WOLF CREEK
UPDATED SAFETY ANALYSIS REPORT

FIGURE 4.2-3A

FUEL ROD SCHEMATIC
HIGH BURNUP ROD

8 1/2X11 A SIZE

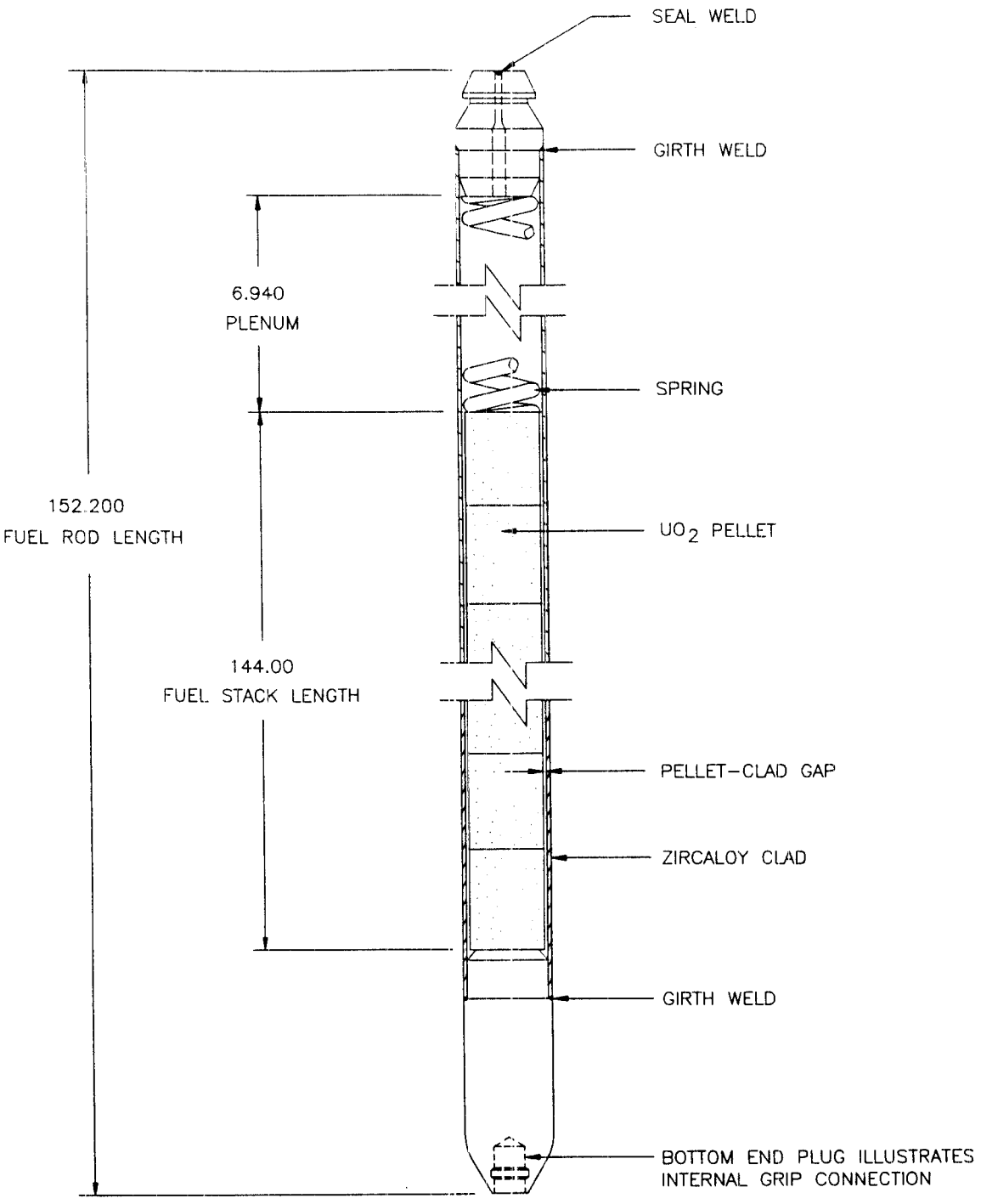

SPECIFIC DIMENSIONS DEPEND ON DESIGN VARIABLES SUCH AS
PREPRESSURIZATION, POWER HISTORY, AND DISCHARGE BURNUP

Rev. 11

WOLF CREEK FIGURE 4.2–3B
FUEL ROD SCHEMATIC PERFORMANCE + ZIRC-4

DIMENSIONS ARE IN INCHES (NOMINAL)

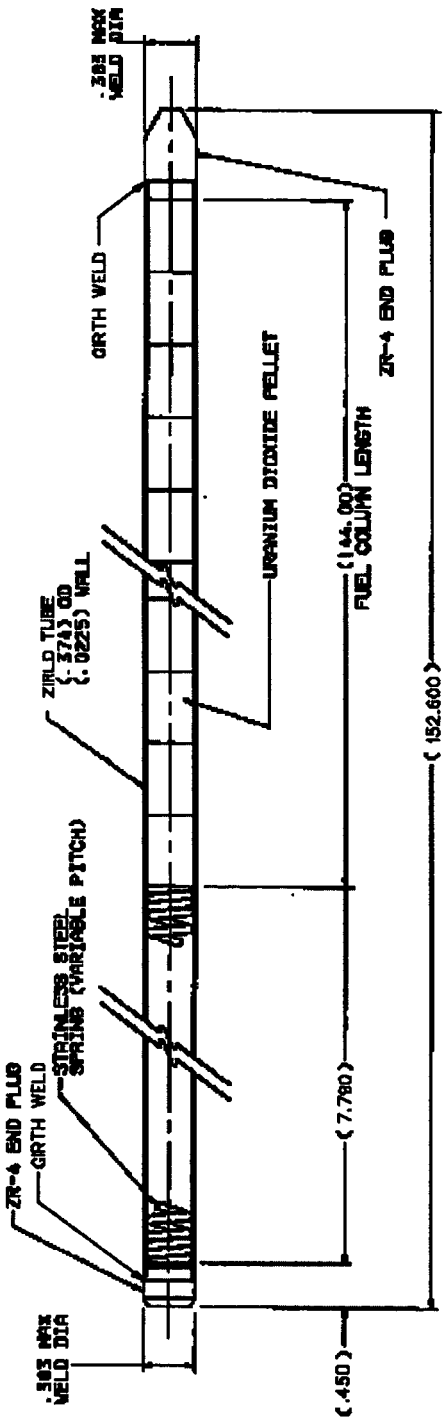

REV 18

WOLF CREEK UPDATED SAFETY ANALYSIS REPORT
FIGURE 4.2-3C FUEL ROD SCHEMATIC PERFORMANCE+, ZIRLO

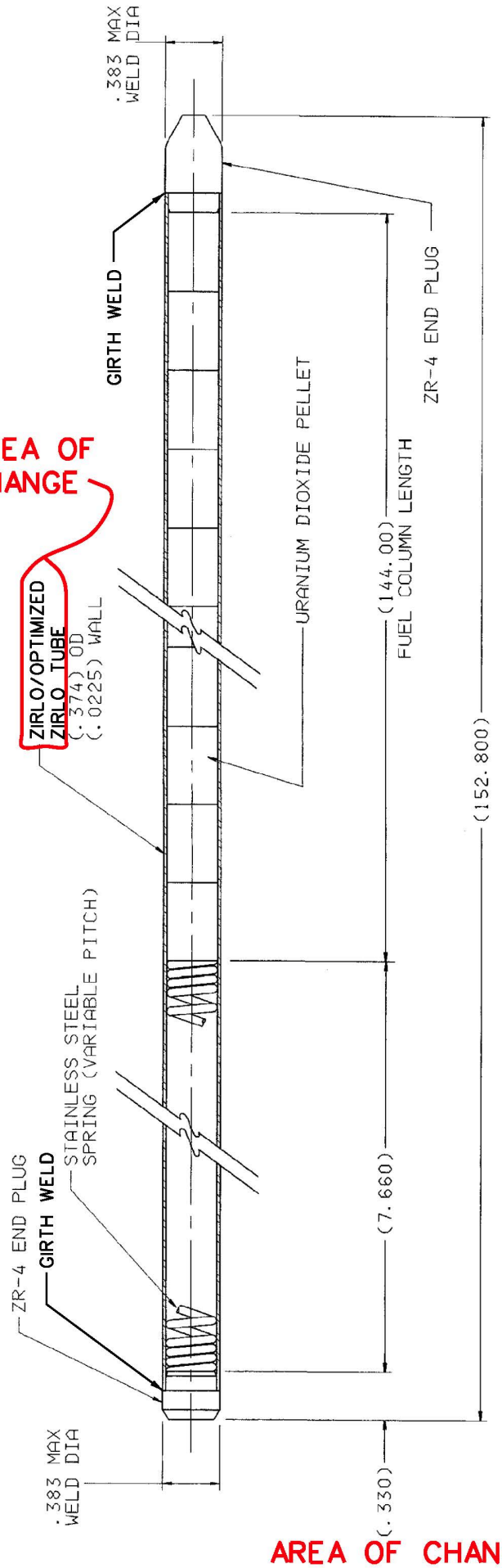

REV.32

WOLF CREEK
UPDATED SAFETY ANALYSIS REPORT

FIGURE 4.2-3D

FUEL ROD SCHEMATIC
PERFORMANCE+, Z^{+2} (WITH
ZIRLO/OPTIMIZED ZIRLO CLADDING)

8 1/2X11 A SIZE

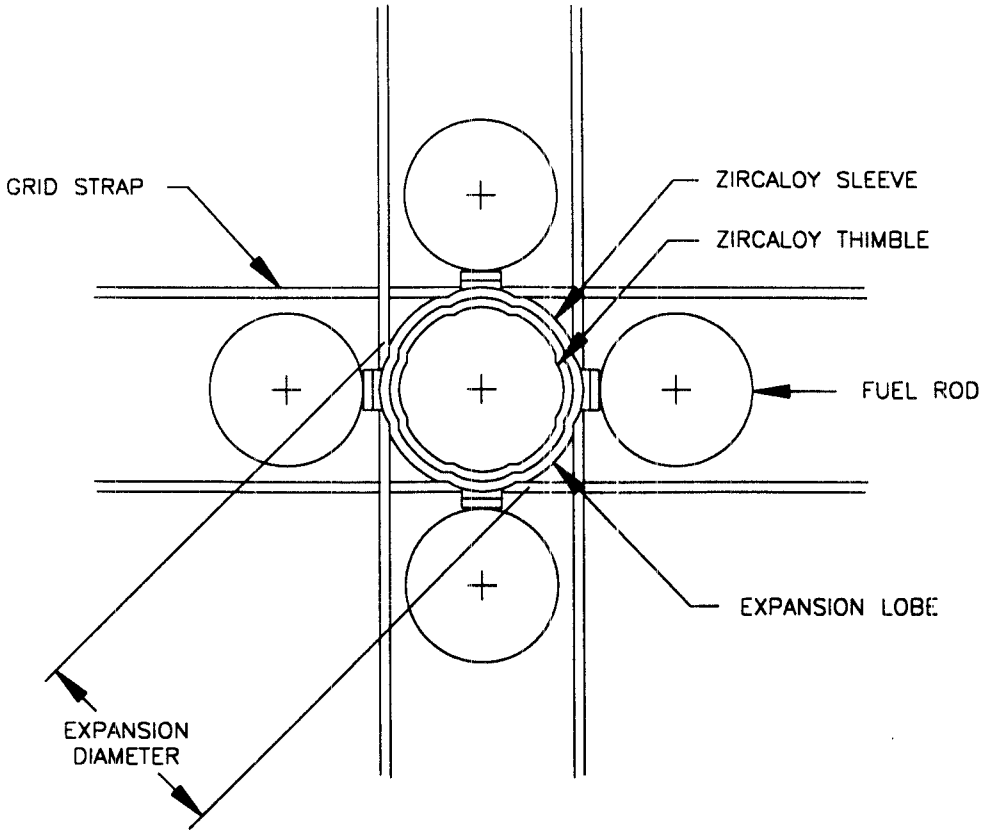

MID GRID EXPANSION JOINT DESIGN

Rev. 9

WOLF CREEK FIGURE 4.2-4
MID GRID EXPANSION JOINT PLAN VIEW

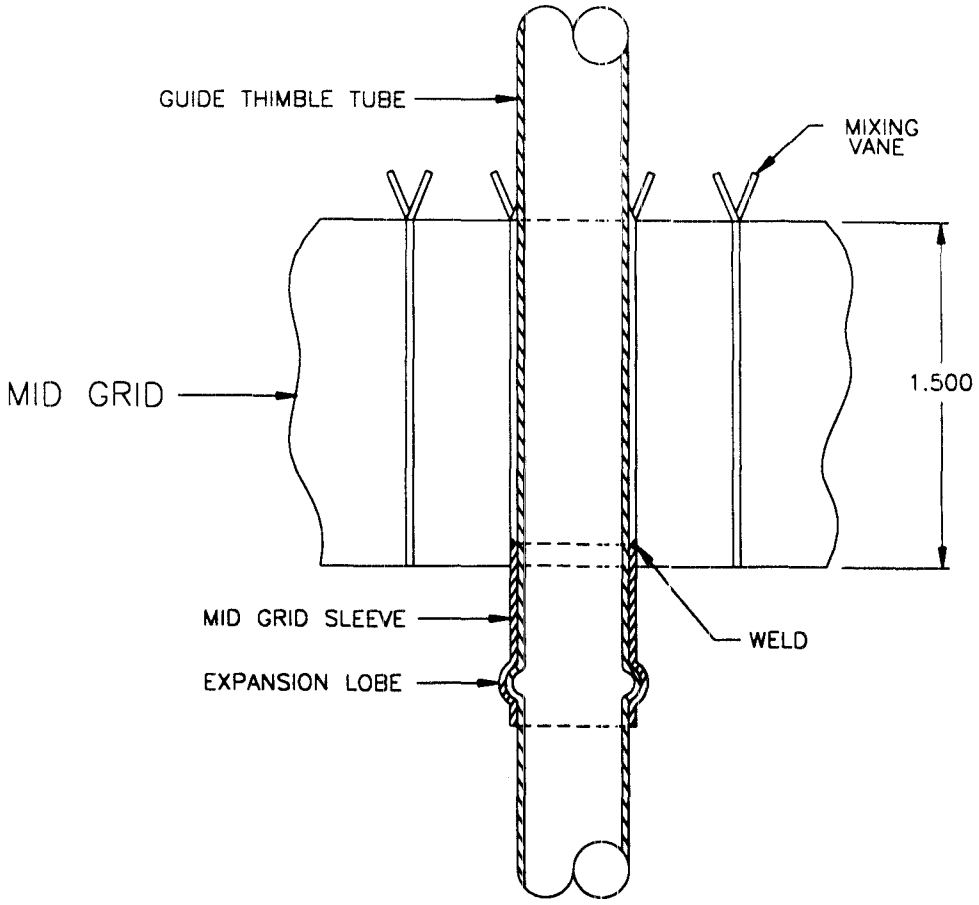

DIMENSIONS ARE IN INCHES (NOMINAL)

Rev. 9

WOLF CREEK FIGURE 4.2-5
MID GRID EXPANSION JOINT ELEVATION VIEW

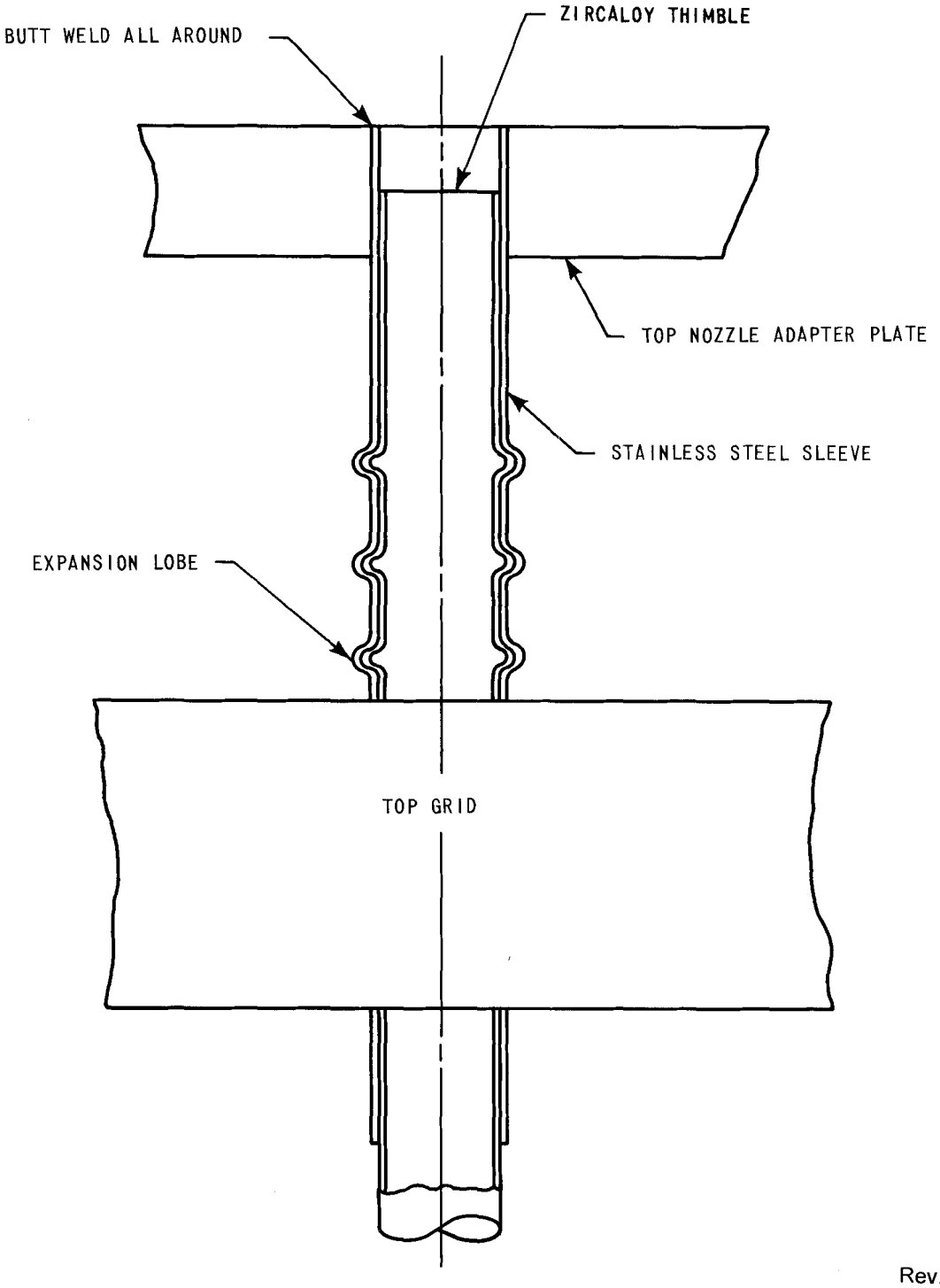

Rev. 11

WOLF CREEK
UPDATED SAFETY ANALYSIS REPORT

FIGURE 4.2-6

TOP GRID TO NOZZLE ATTACHMENT

STANDARD

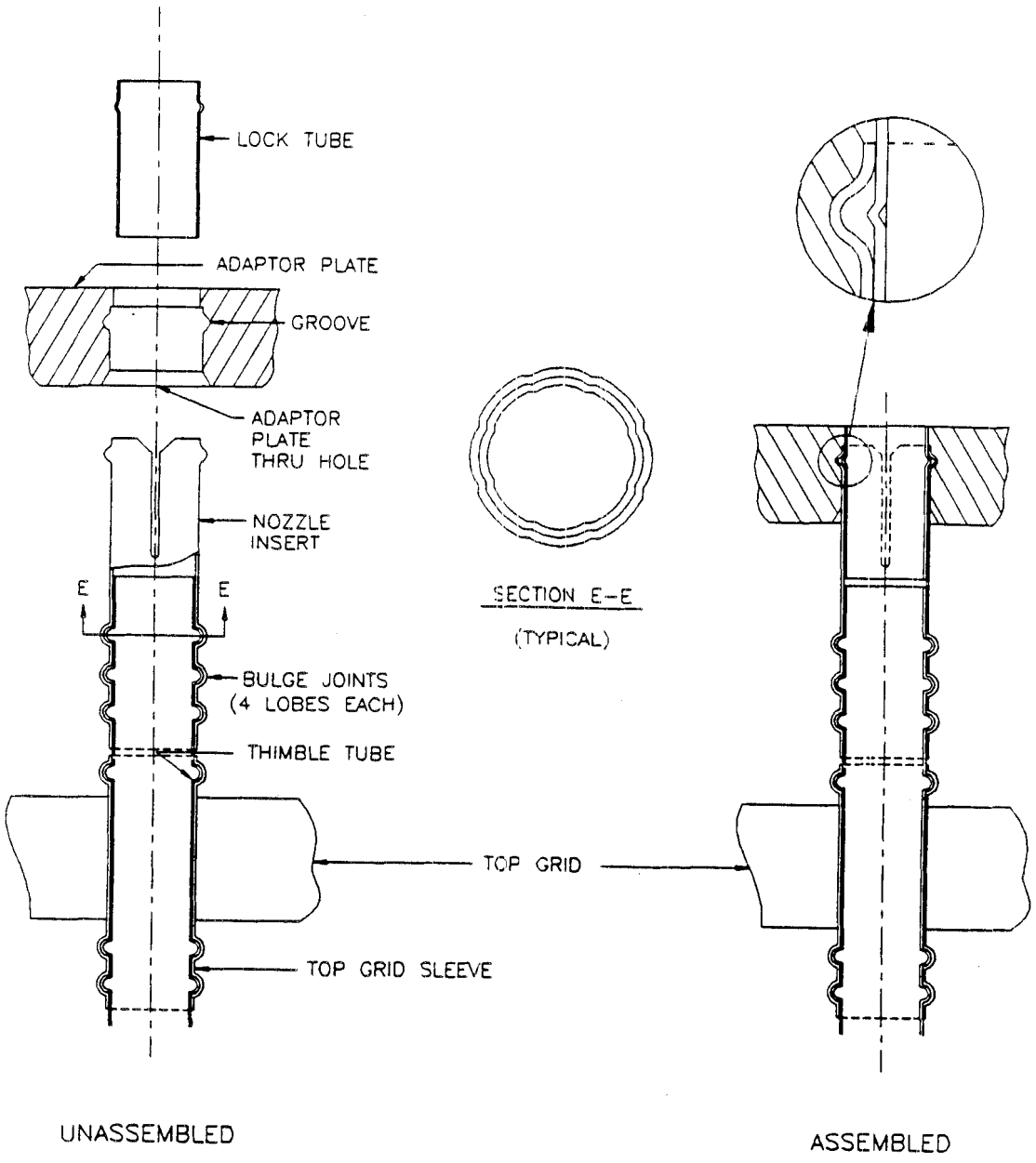

Rev. 11

WOLF CREEK
UPDATED SAFETY ANALYSIS REPORT

FIGURE 4.2-6A
THIMBLE / INSERT / TOP GRID SLEEVE
BULGE JOINT GEOMETRY

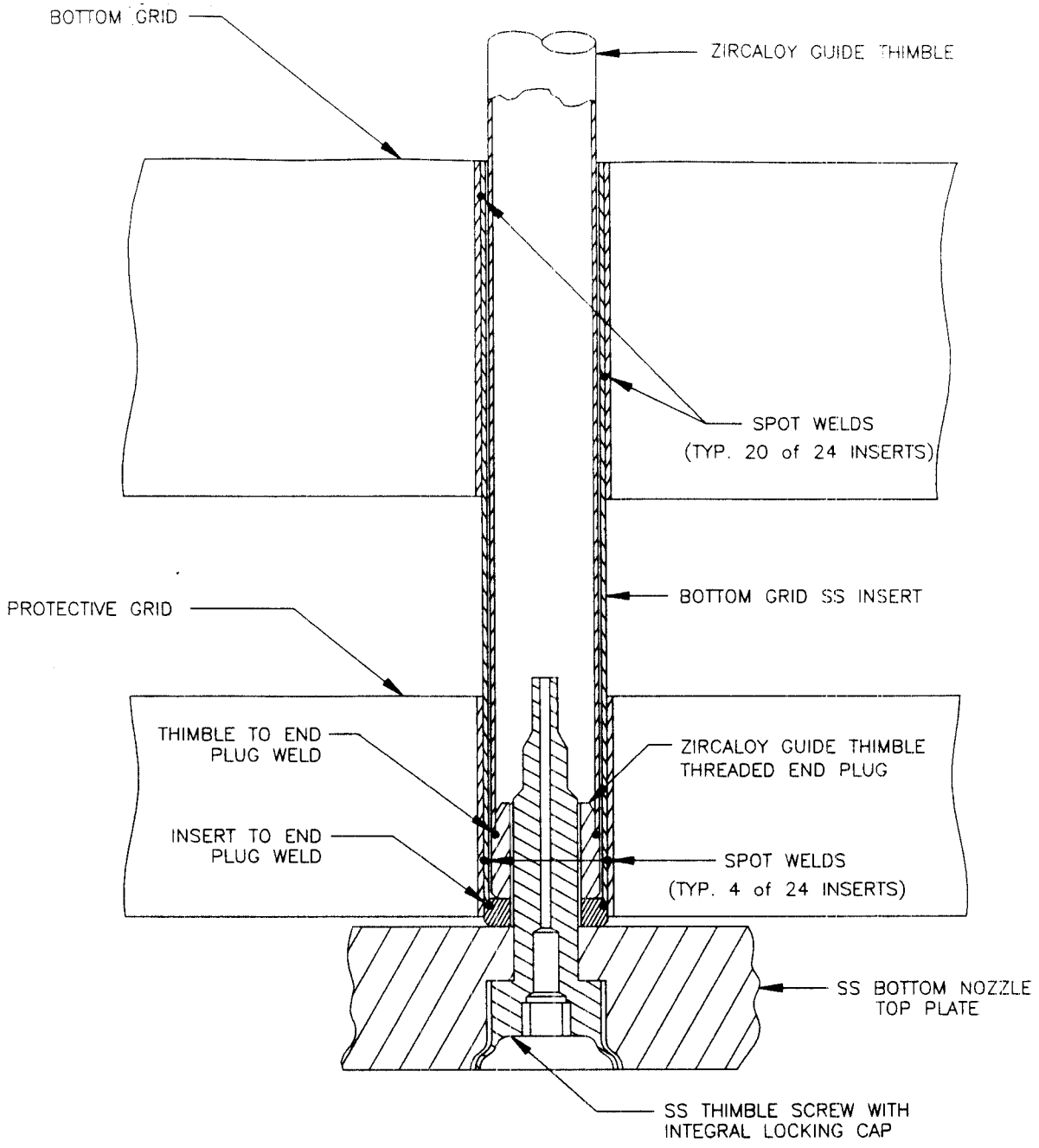

Rev. 9

WOLF CREEK FIGURE 4.2–7
GUIDE THIMBLE TO BOTTOM NOZZLE JOINT

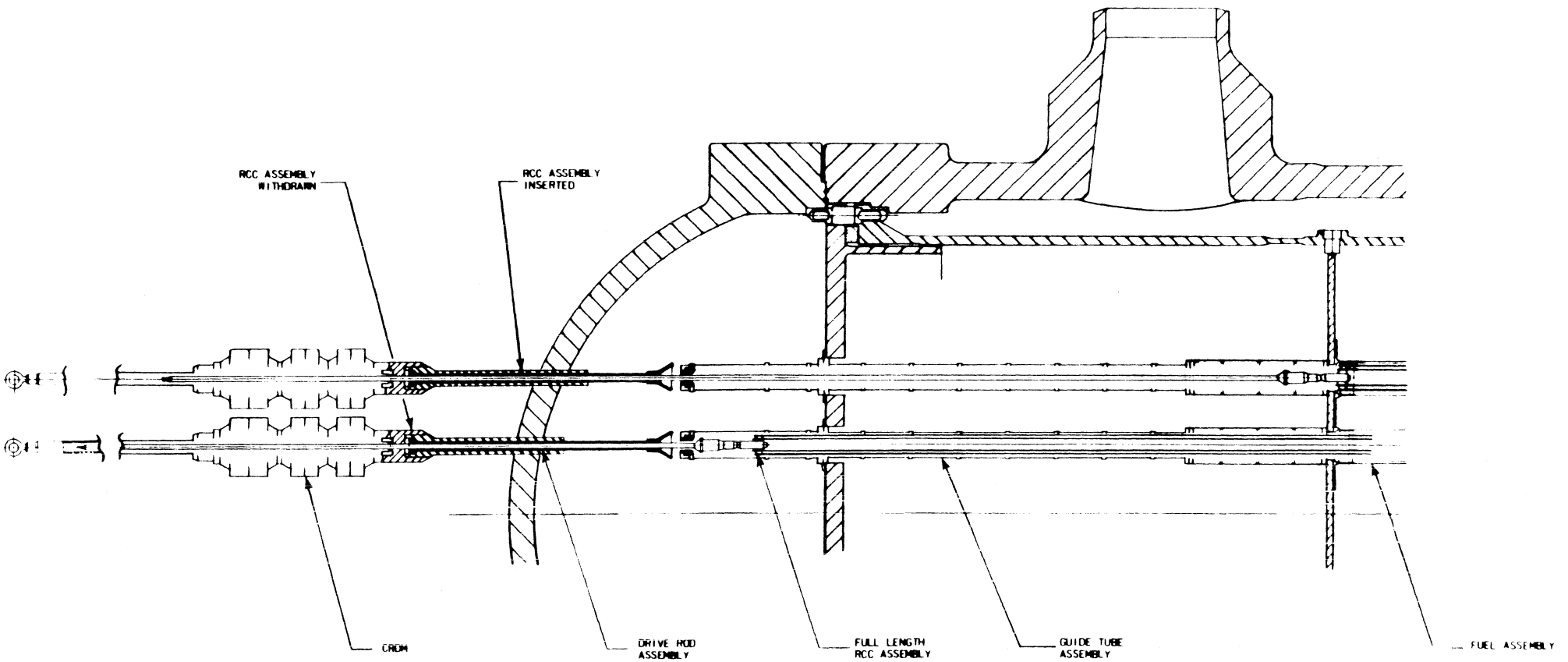

Rev. 6

WOLF CREEK
UPDATED SAFETY ANALYSIS REPORT

FIGURE 4.2-8
ROD CLUSTER CONTROL AND DRIVE ROD ASSEMBLY WITH INTERFACING COMPONENTS

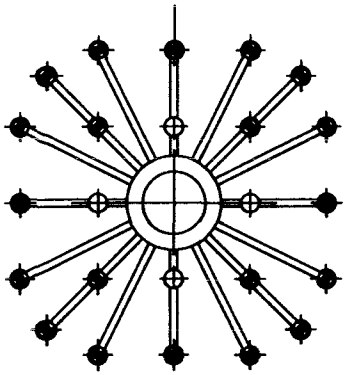

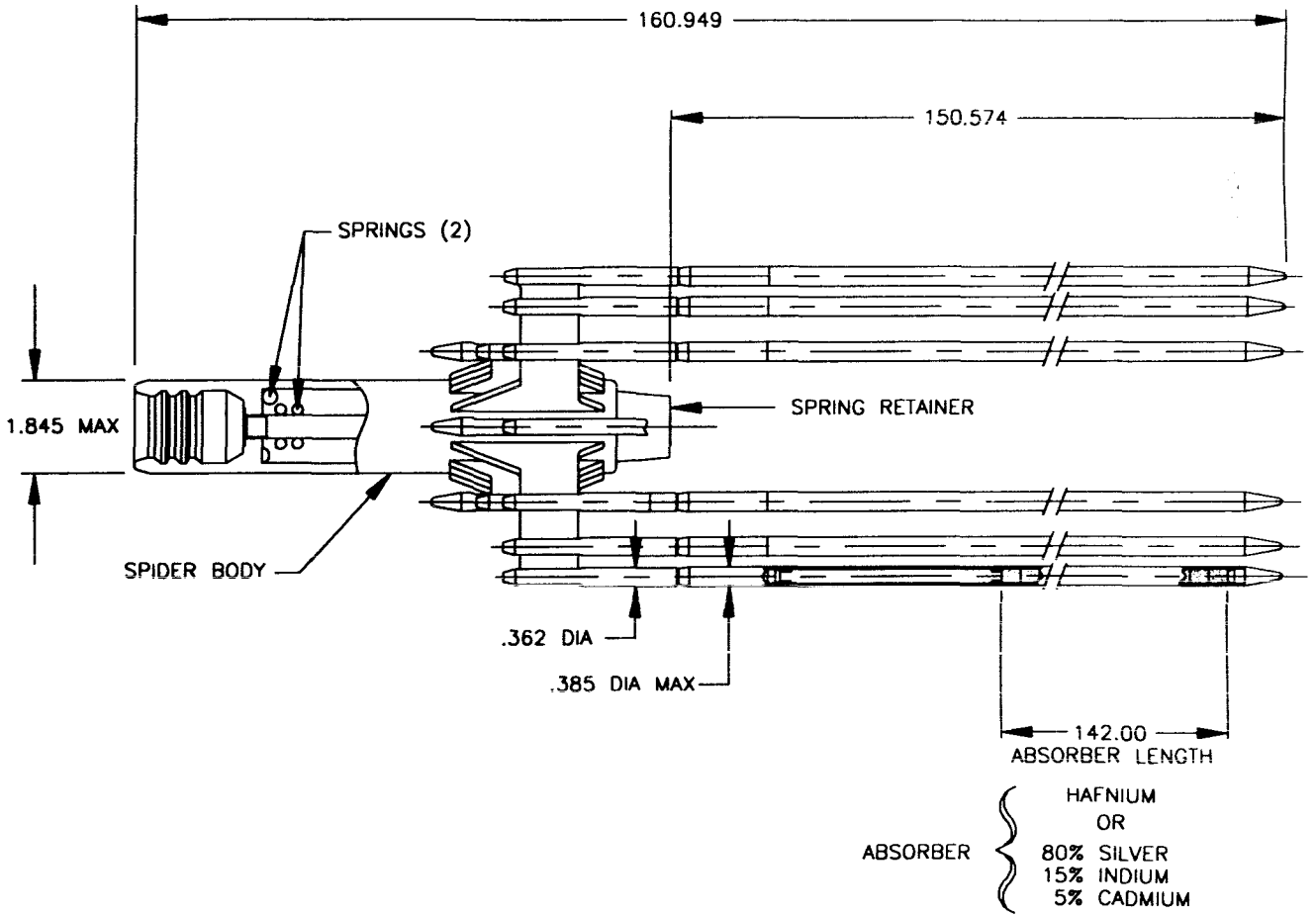

Rev. 9

WOLF CREEK
FIGURE 4.2-9

ROD CLUSTER CONTROL ASSEMBLY
OUTLINE

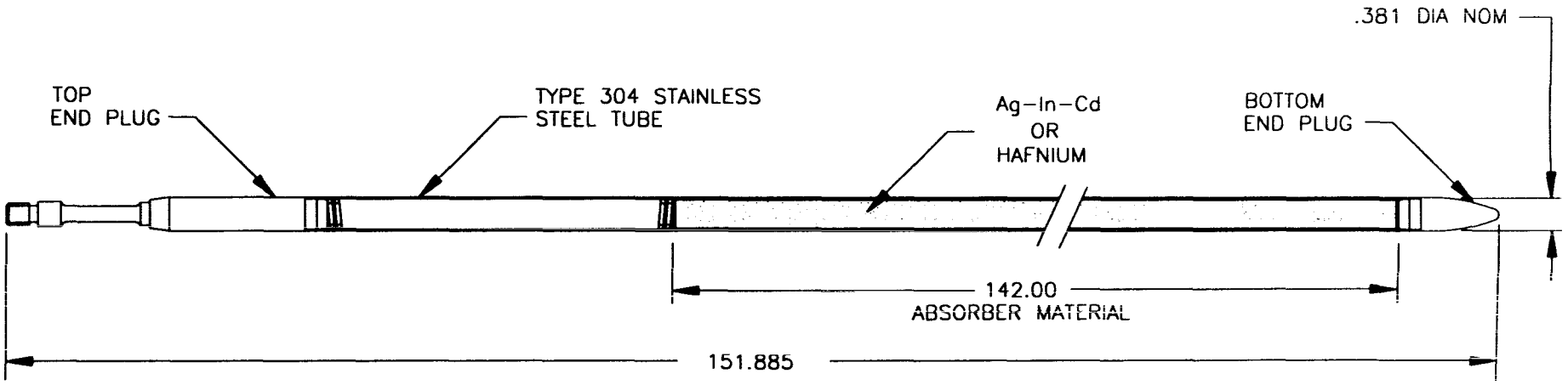

Rev. 9

WOLF CREEK
FIGURE 4.2-10

ABSORBER ROD

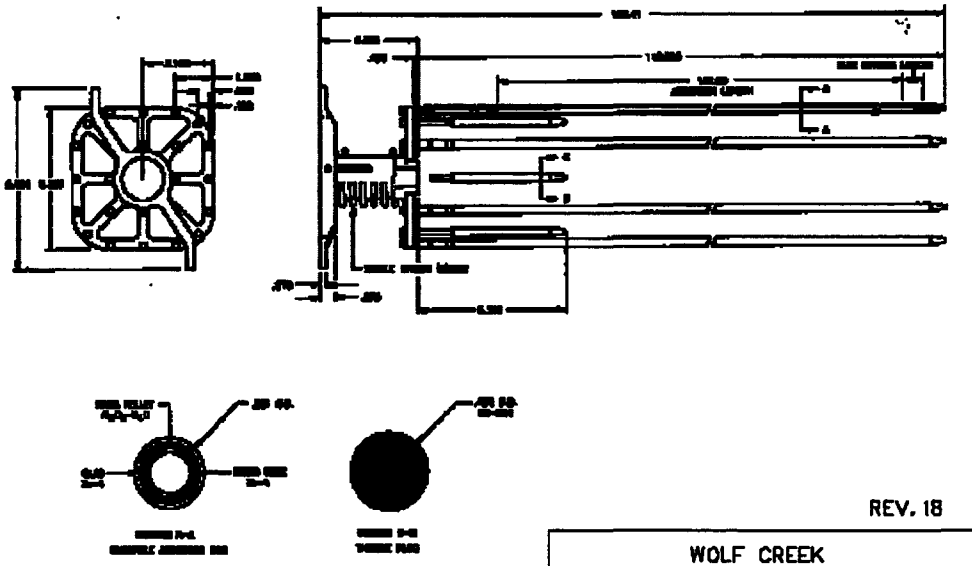

REV. 18

WOLF CREEK
UPDATED SAFETY ANALYSIS REPORT

FIGURE 4 2-11

WET ANNULAR
BURNABLE ABSORBER ASSEMBLY

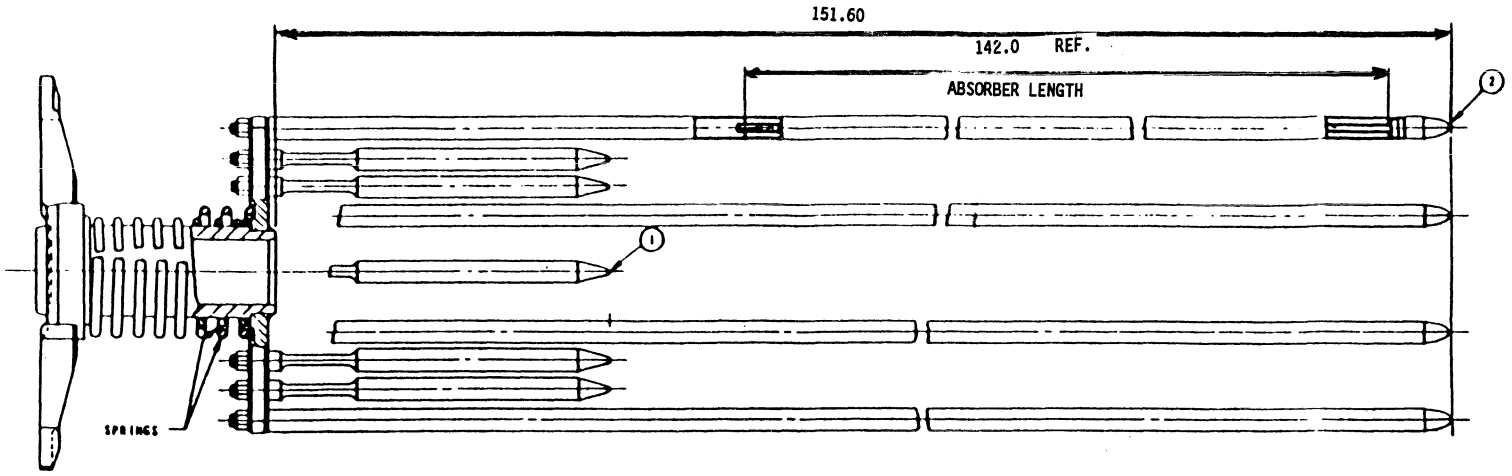

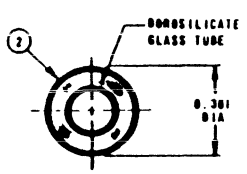

BURNABLE
ABSORBER ROD

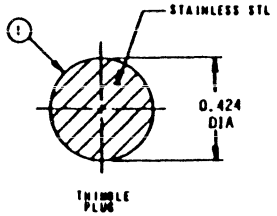

THIMBLE
PLUG

Rev. 11

WOLF CREEK
UPDATED SAFETY ANALYSIS REPORT

FIGURE 4.2-11a

TYPICAL BOROSILICATE GLASS
BURNABLE ABSORBER
ROD ASSEMBLY

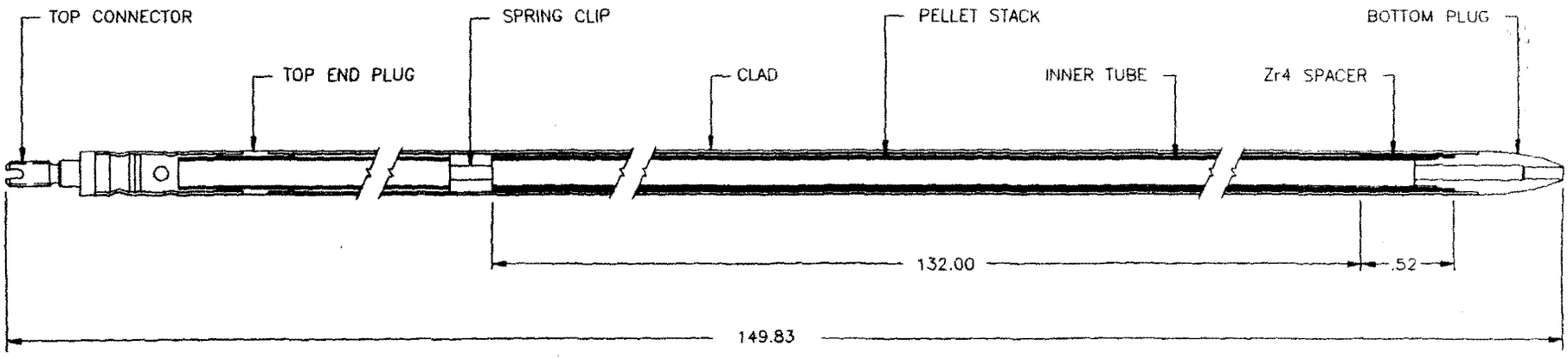

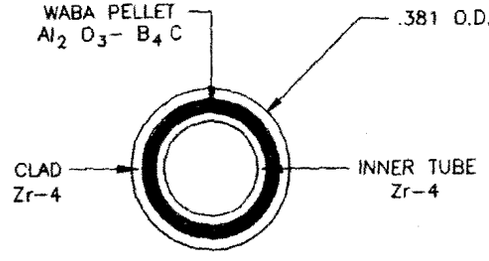

SECTION A-A

BURNABLE ABSORBER ROD

Rev. 9

WOLF CREEK FIGURE 4.2-12
WET ANNULAR BURNABLE ABSORBER ROD ASSEMBLY

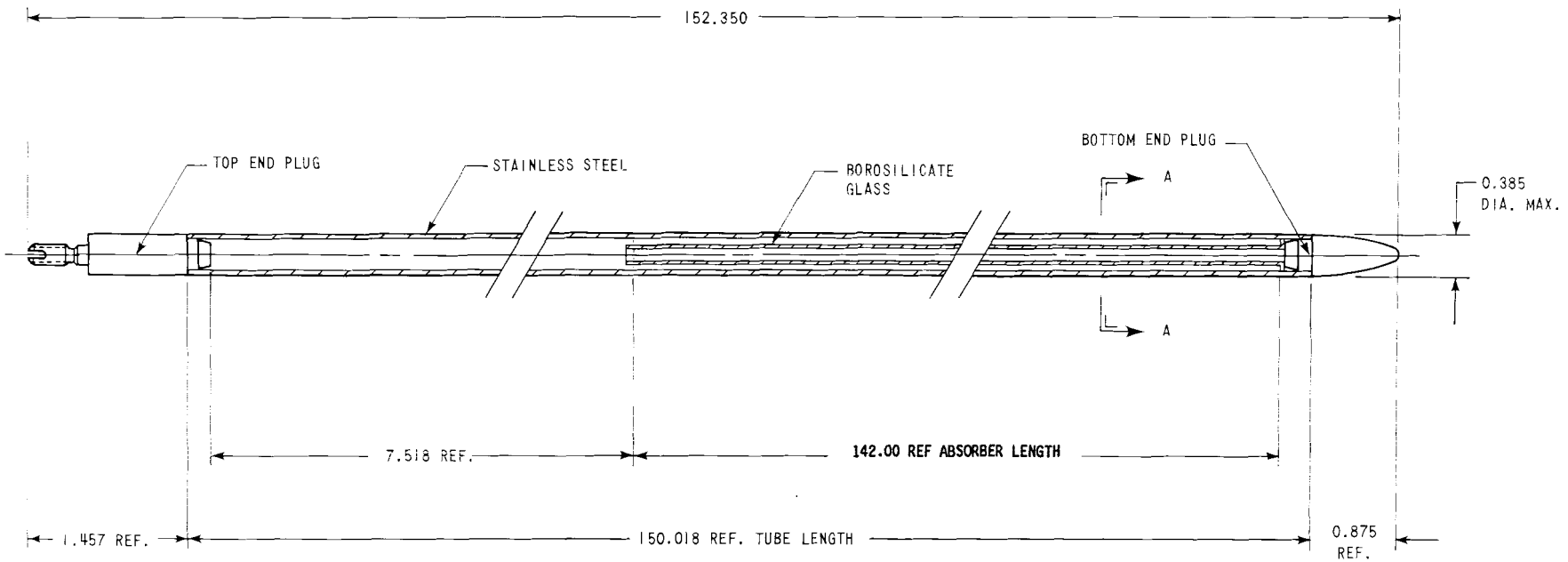

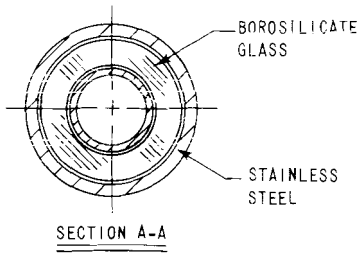

SECTION A-A IS SHOWN IN FIGURE 4.2-12c

Rev. 11

WOLF CREEK
UPDATED SAFETY ANALYSIS REPORT

FIGURE 4.2-12a

BOROSILICATE GLASS
BURNABLE ABSORBER ROD

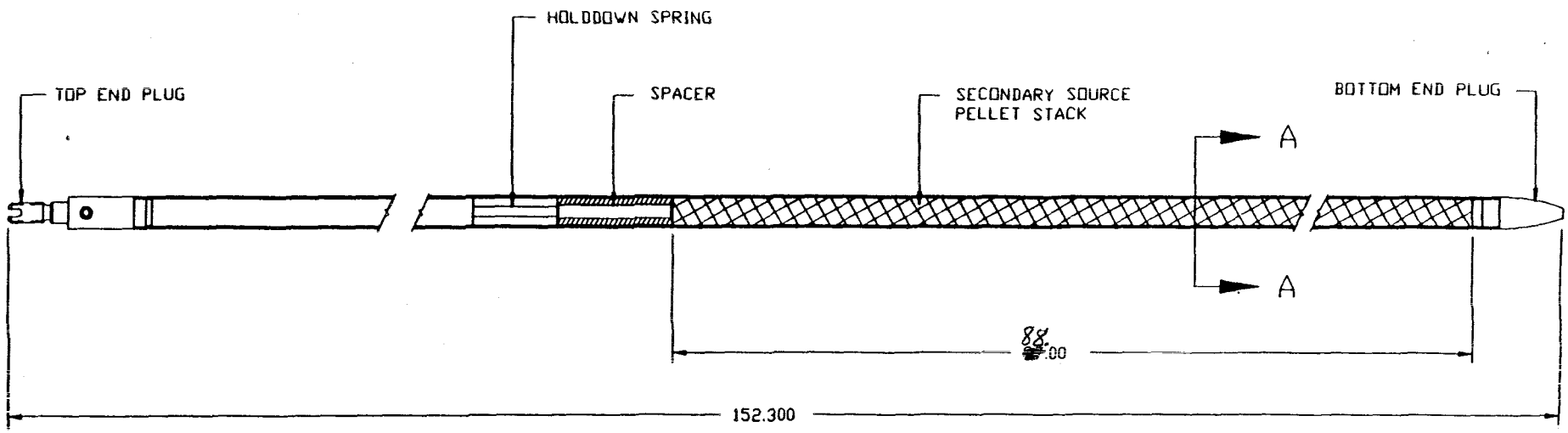

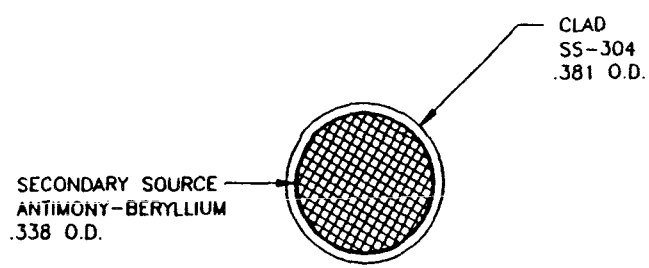

SECTION A-A

SECONDARY SOURCE

Rev. 11

WOLF CREEK
UPDATED SAFETY ANALYSIS REPORT

FIGURE 4.2-13
SECONDARY SOURCE ROD ASSEMBLY

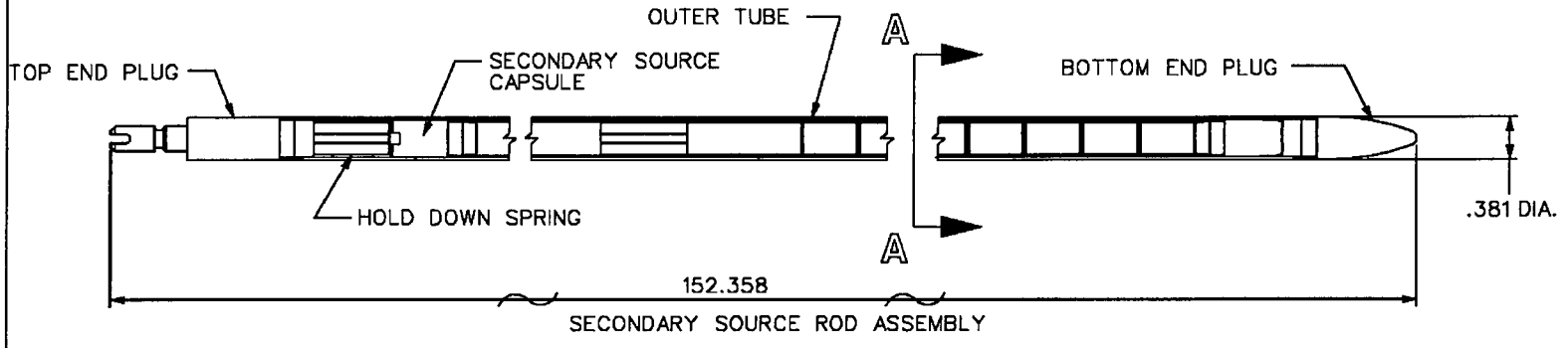

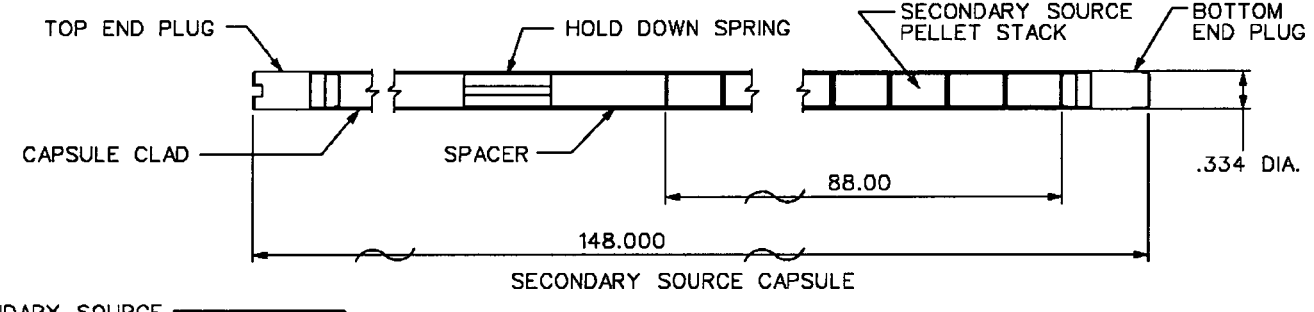

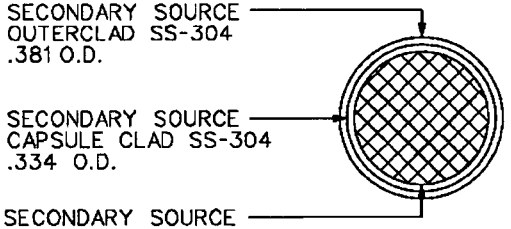

SECTION "A-A"

SCALE 8:1

DOUBLE ENCAPSULATED SECONDARY SOURCE ROD

WOLF CREEK
UPDATED SAFETY ANALYSIS REPORT

Figure 4.2-13A, REV. 13
DOUBLE ENCAPSULATED SECONDARY SOURCE ROD ASSEMBLY

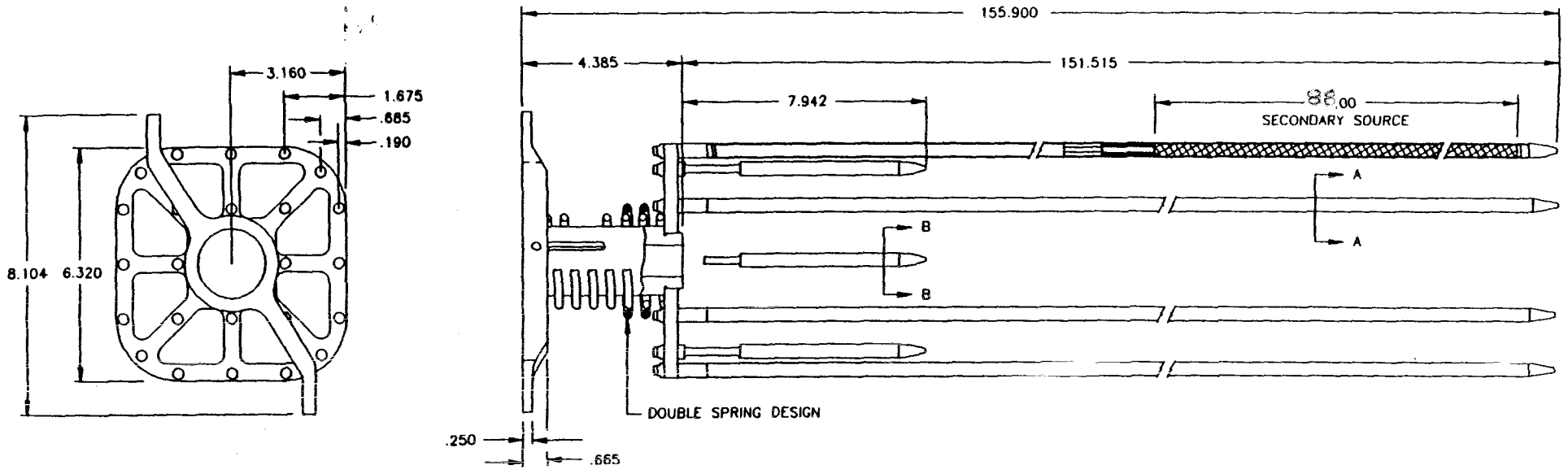

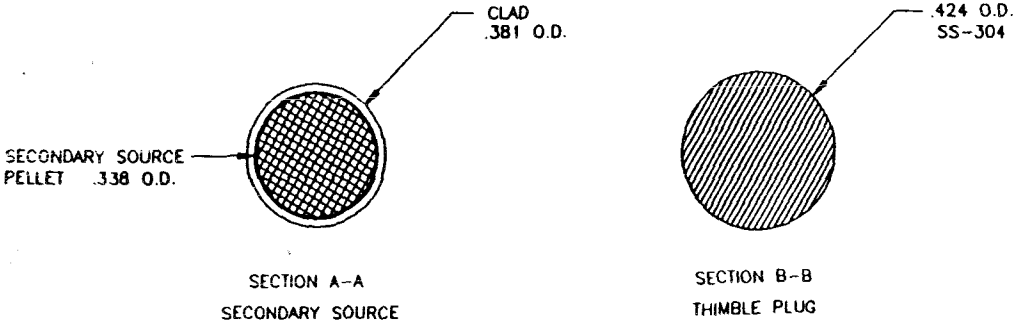

Rev. 11

WOLF CREEK
UPDATED SAFETY ANALYSIS REPORT

FIGURE 4.2-14
SECONDARY SOURCE ASSEMBLY

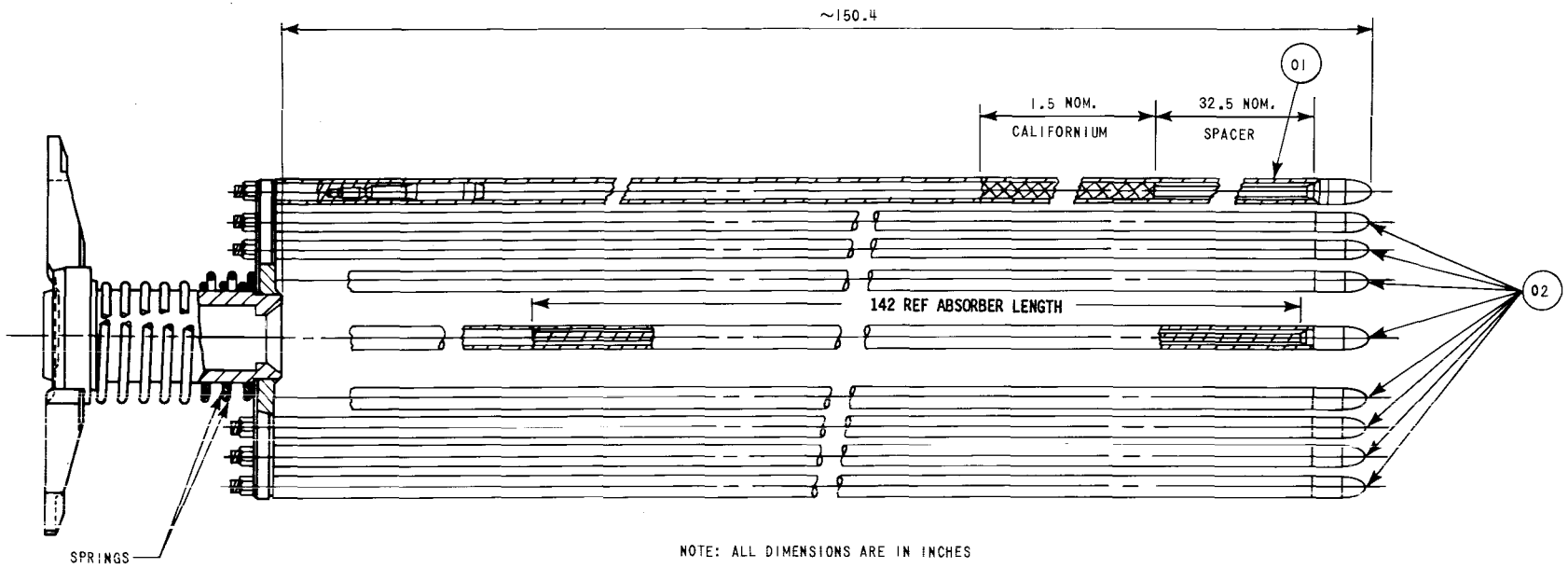

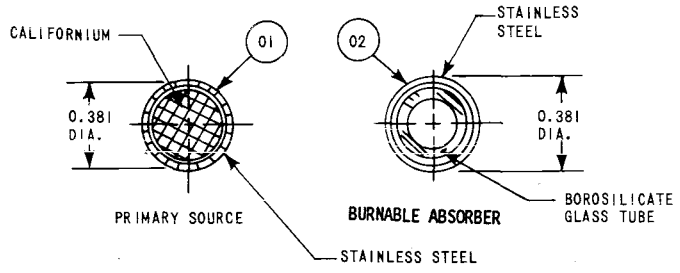

Rev. 11

WOLF CREEK
UPDATED SAFETY ANALYSIS REPORT

FIGURE 4.2-14A

TYPICAL PRIMARY SOURCE ASSEMBLY

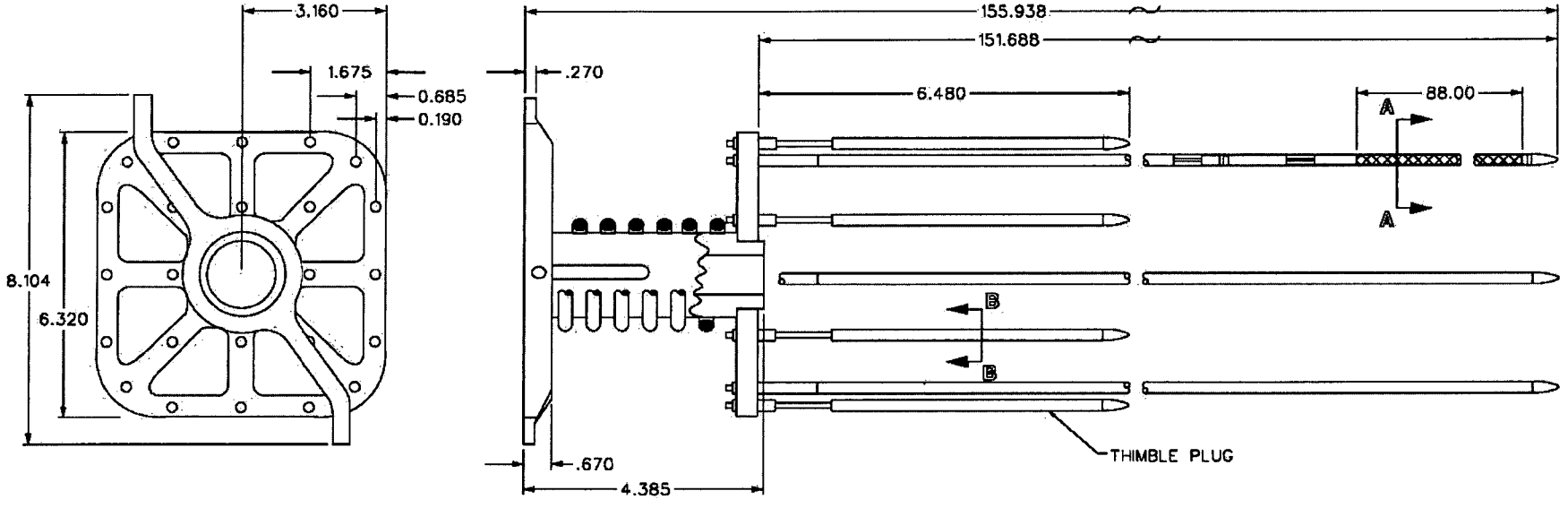

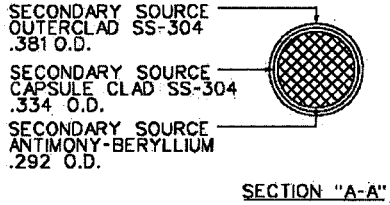

SECTION "A-A"
SCALE 8:1

DOUBLE ENCAPSULATED
SECONDARY SOURCE ROD

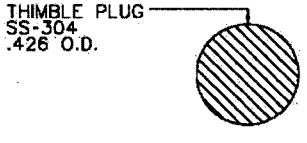

SECTION "B-B"
SCALE 8:1

THIMBLE PLUG

WOLF CREEK
UPDATED SAFETY ANALYSIS REPORT

Figure 4.2-14B, REV. 13

DOUBLE ENCAPSULATED
SECONDARY SOURCE ASSEMBLY

Wolf Creek

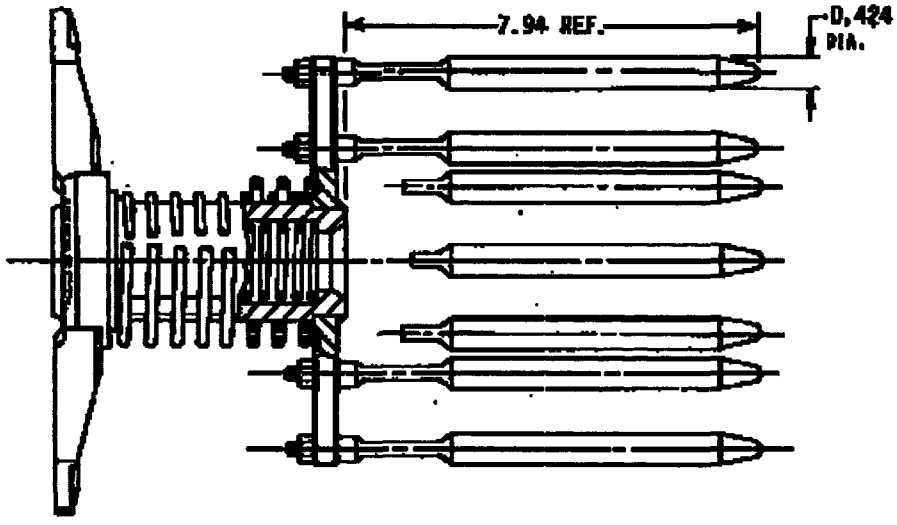

REV. 18

WOLF CREEK
UPDATED SAFETY ANALYSIS REPORT

FIGURE 4.2-15

TYPICAL DOUBLE SPRING THIMBLE
PLUG DEVICE

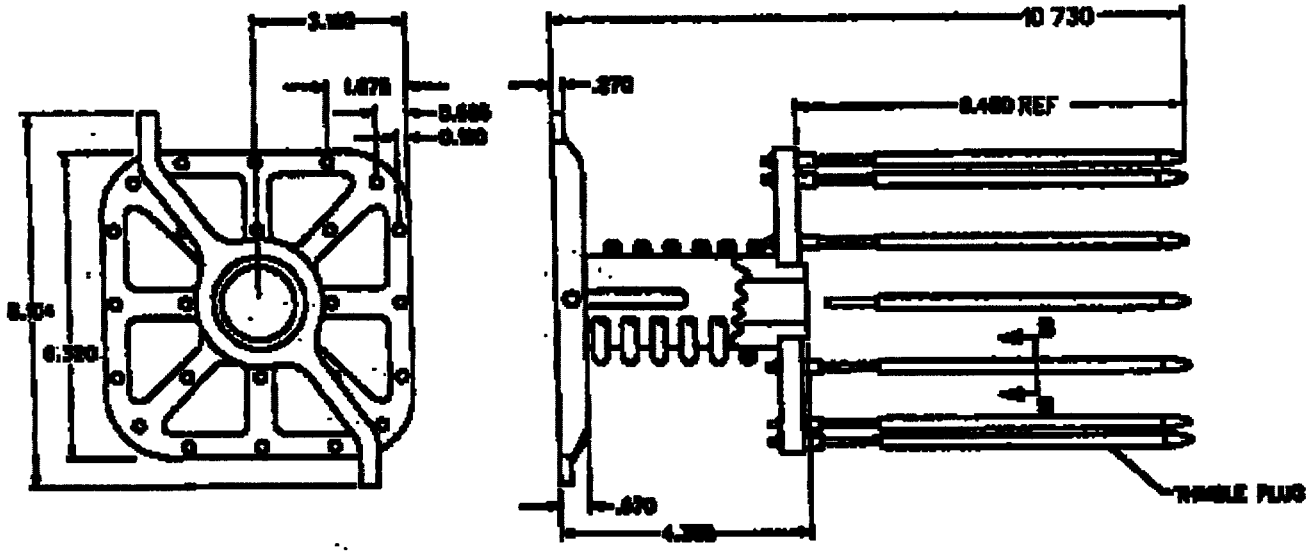

REV. 18

WOLF CREEK
UPDATED SAFETY ANALYSIS REPORT

FIGURE 4.2-15A

TYPICAL SINGLE SPRING THIMBLE PLUG DEVICE

4.3 NUCLEAR DESIGN

4.3.1 DESIGN BASES

This section describes the design bases and functional requirements used in the nuclear design of the fuel and reactivity control system and relates these design bases to the General Design Criteria (GDC) presented in 10 CFR 50, Appendix A. Where applicable, supplemental criteria such as the "Final Acceptance Criteria for Emergency Core Cooling Systems" are addressed. But, before discussing the nuclear design bases, it is appropriate to briefly review the four major categories ascribed to conditions of plant operation.

The full spectrum of plant conditions is divided into four categories, in accordance with the anticipated frequency of occurrence and risk to the public:

a. Condition I - Normal Operation
b. Condition II - Incidents of Moderate Frequency
c. Condition III - Infrequent Faults
d. Condition IV - Limiting Faults

In general, the Condition I occurrences are accommodated with margin between any plant parameter and the value of that parameter which would require either automatic or manual protective action. Condition II incidents are accommodated with, at most, a shutdown of the reactor with the plant capable of returning to operation after corrective action. Fuel damage (fuel damage as used here is defined as penetration of the fission product barrier, i.e., the fuel rod clad) is not expected during Condition I and Condition II events. It is not possible, however, to preclude a very small number of rod failures. These are within the capability of the chemical and volume control system (CVCS) and are consistent with the plant design basis.

Condition III incidents do not cause more than a small fraction of the fuel elements in the reactor to be damaged, although sufficient fuel element damage might occur to preclude immediate resumption of operation. The release of radioactive material due to Condition III incidents is not sufficient to interrupt or restrict public use of those areas beyond the exclusion radius. Furthermore, a Condition III incident does not by itself generate a Condition IV fault or result in a consequential loss of function of the reactor coolant or reactor containment barriers.

Condition IV occurrences are faults that are not expected to occur but are defined as limiting faults which must be designed against. Condition IV faults do not cause a release of radioactive material that results in exceeding the limits of 10 CFR 50.67.

The core design power distribution limits related to fuel integrity are met for Condition I occurrences through conservative design and maintained by the action of the control system. The requirements for Condition II occurrences are met by providing an adequate protection system which monitors reactor parameters. The control and protection systems are described in Chapter 7.0, and the consequences of Condition II, III, and IV occurrences are given in Chapter 15.0.

4.3.1.1 Fuel Burnup

Basis

A limitation on initial installed excess reactivity or average discharge burnup is not required other than as is quantified in terms of other design bases, such as core negative reactivity feedback and shutdown margin discussed below.

Discussion

Fuel burnup is a measure of fuel depletion which represents the integrated energy output of the fuel (MWD/MTU) and is a convenient means for quantifying fuel exposure criteria.

The core design lifetime or design discharge burnup is achieved by installing sufficient initial excess reactivity in each fuel region and by following a fuel replacement program (such as that described in Section 4.3.2) that meets all safety-related criteria in each cycle of operation.

Initial excess reactivity installed in the fuel, although not a design basis, must be sufficient to maintain core criticality at full power operating conditions throughout cycle life with equilibrium xenon, samarium, and other fission products present. The end of design cycle life is defined to occur when the chemical shim concentration is essentially zero with control rods present to the degree necessary for operational requirements (e.g., the controlling bank at the "bite" position). In terms of chemical shim boron concentration, this represents approximately 10 ppm with no control rod insertion.

4.3.1.2 Negative Reactivity Feedbacks (Reactivity Coefficient)

Basis

The fuel temperature coefficient will be negative, and the moderator temperature coefficient of reactivity will be nonpositive for full-power operating conditions, thereby providing negative reactivity feedback characteristics. The design basis meets GDC-11.

Discussion

When compensation for a rapid increase in reactivity is considered, there are two major effects. These are the resonance absorption effects (Doppler) associated with changing fuel temperature and the neutron spectrum and reactor composition change effects resulting from changing moderator density. These basic physics characteristics are often identified by reactivity coefficients. The use of slightly enriched uranium ensures that the Doppler coefficient of reactivity is negative. This coefficient provides the most rapid reactivity compensation. The core is also designed to have an overall non-positive moderator temperature coefficient of reactivity during full power operation so that average coolant temperature or void content provides another, slower compensatory effect. Full power operation is permitted only in a range of overall non-positive moderator temperature coefficient. The desired moderator temperature coefficient can be achieved through use of fixed burnable absorber and/or control rods by limiting the reactivity held down by soluble boron.

Restrictions on burnable absorber content (quantity and distribution) are not applied as a design basis other than as they relate to accomplishment of the desired moderator temperature coefficient at power operating conditions discussed above.

4.3.1.3 Control of Power Distribution

Basis

The nuclear design basis is that, with at least a 95 percent confidence level:

a. The fuel will not be operated at greater than 14.48 kW/ft under normal operating conditions, including an allowance of 2 percent for calorimetric error and not including power spike factor due to densification.

b. Under abnormal conditions, including the maximum over-power condition, the fuel peak power will not cause melting, as defined in Section 4.4.1.2.

c. There is at least a 95% probability that the fuel will not operate with a power distribution that violates the departure from nucleate boiling (DNB) design basis discussed in Section 4.4.1 under Condition I and II events including the maximum overpower condition.

d. Fuel management will be such as to produce values of fuel rod power and burnup consistent with the assumptions in the fuel rod mechanical integrity analysis of Section 4.2.

The above basis meets GDC-10.

Discussion

Calculation of extreme power shapes which affect fuel design limits is performed with proven methods and verified frequently with measurements from operating reactors. The conditions under which limiting power shapes are assumed to occur are chosen conservatively with regard to any permissible operating state.

Even though there is good agreement between calculated peak power and measurements, a nuclear uncertainty (see Section 4.3.2.2.1) is applied to calculated peak local power. Such a margin is provided both for the analysis for normal operating states and for anticipated transients.

4.3.1.4 Maximum Controlled Reactivity Insertion Rate

Basis

The maximum reactivity insertion rate due to withdrawal of rod cluster control assemblies at power or by boron dilution is limited. A maximum reactivity change rate for accidental withdrawal of control banks is set such that peak heat generation rate and DNBR do not exceed the maximum allowable at over-power conditions. This satisfies GDC-25.

The maximum reactivity worth of control rods and the maximum rates of reactivity insertion employing control rods are limited so as to preclude rupture of the coolant pressure boundary or disruption of the core internals to a degree which would impair core cooling capacity due to a rod withdrawal or ejection accident (see Chapter 15.0).

Following any Condition IV event (rod ejection, steam line break, etc.) the reactor can be brought to the shutdown condition, and the core will maintain acceptable heat transfer geometry. This satisfies GDC-28.

Discussion

Reactivity addition associated with an accidental withdrawal of a control bank (or banks) is limited by the maximum rod speed (or travel rate) and by the worth of the bank(s). For this reactor, the maximum control rod speed is 45 inches per minute.

The reactivity change rates are conservatively calculated assuming unfavorable axial power and xenon distributions. The peak xenon burnout rate is significantly lower than the maximum reactivity addition rate for normal operation and for accidental withdrawal of two banks.

4.3.1.5 Shutdown Margins

Basis

Minimum shutdown margin as specified in the Core Operating Limits Report (COLR) is required at any power operating condition, in the hot standby condition, hot shutdown condition, and in the cold shutdown condition.

In all analyses involving reactor trip, the single, highest worth rod cluster control assembly is postulated to remain untripped in its full out position (stuck rod criterion). This satisfies GDC-26.

Discussion

Two independent reactivity control systems are provided: control rods and soluble boron in the coolant. The control rod system can compensate for the reactivity effects of the fuel and water temperature changes accompanying power level changes over the range from full-load to no-load. In addition, the control rod system provides the minimum shutdown margin under Condition I events and is capable of making the core subcritical rapidly enough to prevent exceeding acceptable fuel damage limits (very small number of rod failures), assuming that the highest worth control rod is stuck out upon trip.

The boron system can compensate for all xenon burnout reactivity changes and will maintain the reactor in the cold shutdown condition. Thus, backup and emergency shutdown provisions are provided by a mechanical and a chemical shim control system which satisfies GDC-26.

Basis

When fuel assemblies are in the pressure vessel and the vessel head is not in place, k_{eff} will be maintained at or below 0.95 with control rods and soluble boron. Further, the fuel will be maintained sufficiently subcritical that removal of all rod cluster control assemblies will not result in criticality.

Discussion

ANSI Standard N18.2 specifies a k_{eff} not to exceed 0.95 in spent fuel storage racks and transfer equipment flooded with pure water and a k_{eff} not to exceed 0.98 in normally dry new fuel storage racks, assuming optimum moderation. No criterion is given for the refueling operation. However, a 5-percent margin, which is consistent with spent fuel storage and transfer and the new fuel storage, is adequate for the controlled and continuously monitored operations involved.

The boron concentration required to meet the refueling shutdown criteria is specified in the COLR. Verification that this shutdown criteria is met, including uncertainties, is achieved based on calculations performed with the ANC computer code (Reference 31). The subcriticality of the core is continuously monitored, as described in the Technical Specifications.

4.3.1.6 Stability

Basis

The core will be inherently stable to power oscillations at the fundamental mode. This satisfies GDC-12.

Spatial power oscillations within the core with a constant core power output, should they occur, can be reliably and readily detected and suppressed.

Discussion

Oscillations of the total power output of the core, from whatever cause, are readily detected by the loop temperature sensors and by the nuclear instrumentation. The core is protected by these systems, and a reactor trip would occur if power increased unacceptably, preserving the design margins to fuel design limits. The stability of the turbine/steam generator/ core systems and the reactor control system is such that total core power oscillations are not normally possible. The redundancy of the protection circuits ensures an extremely low probability of exceeding design power levels.

The core is designed so that diametral and azimuthal oscillations due to spatial xenon effects are self-damping, and no operator action or control action is required to suppress them. The stability to diametral oscillations is so great that this excitation is highly improbable. Convergent azimuthal oscillations can be excited by prohibited motion of individual control rods. Such oscillations are readily observable and alarmed, using the excore long ion chambers. Indications are also continuously available from incore thermocouples and loop temperature measurements. Movable incore detectors can be activated to provide more detailed information. In all proposed cores, these horizontal plane oscillations are self-damping by virtue of reactivity feedback effects designed into the core.

However, axial xenon spatial power oscillations may occur late in core life. The control bank and excore detectors are provided for control and monitoring of axial power distributions.

Assurance that fuel design limits are not exceeded is provided by reactor Overpower ΔT and Overtemperature ΔT trip functions which use the measured axial power imbalance as an input. Detection and suppression of xenon oscillations are discussed in Section 4.3.2.7.

4.3.1.7 Anticipated Transients Without SCRAM

The effects of anticipated transients with failure to trip are not considered in the design bases of the plant. Analysis has shown that the likelihood of such a hypothetical event is negligibly small. Furthermore, generic analyses of the consequences of a hypothetical failure to trip following anticipated transients has shown that no significant core damage would result, system peak pressures would be limited to acceptable values, and no failure of the reactor coolant system would result (Ref. 1 and 3). Nevertheless, in accordance with the final USNRC ATWS rule; 10CFR50.62(b) “Requirements for Reduction of Risk from Anticipated Transients Without Scram (ATWS) Events for Light-Water-Cooled Nuclear Power Plants,” ATWS Mitigation System Actuation Circuitry (AMSAC) has been installed at Wolf Creek (see Section 15.8). The AMSAC system initiates a turbine trip and actuates auxiliary feedwater independent of the reactor trip system. The AMSAC equipment is described in Section 7.7.1.11.

4.3.2 DESCRIPTION

4.3.2.1 Nuclear Design Description

The reactor core consists of a specified number of fuel rods which are held in bundles by spacer grids and top and bottom fittings. The fuel rods are constructed of Zircaloy, ZIRLO, or Optimized ZIRLO cylindrical tubes containing UO_2 fuel pellets. The bundles, known as fuel assemblies, are arranged in a pattern which approximates a right circular cylinder.

Each fuel assembly normally contains a 17 x 17 rod array composed of 264 fuel rods, 24 rod cluster control thimbles, and an incore instrumentation thimble. Figure 4.2-1 shows a cross-sectional view of a 17 x 17 fuel assembly and the related rod cluster control locations. Further details of the fuel assembly are given in Section 4.2.

Fuel assemblies of different enrichments are used in the WCGS core loadings to establish a favorable radial power distribution. A typical checker-board loading pattern is shown in Figure 4.3-1. The exact reloading pattern, initial and final positions of fuel assemblies, and the number of fresh fuel assemblies and their placement are dependent on the energy requirement for each cycle, and burnup and power histories of previous cycles.

The core average enrichment is determined by the amount of fissionable material required to provide the desired core life-time and energy requirements. The physics of the burnout process is such that operation of the reactor depletes the amount of fuel available due to the absorption of neutrons by the U-235 atoms and their subsequent fission. In addition, the fission process results in the formation of fission products, some of which readily absorb neutrons. These effects, depletion and the buildup of fission products, are partially offset by the buildup of plutonium shown in Figure 4.3-2 for a typical 17 x 17 fuel assembly, which occurs due to the nonfission absorption of neutrons in U-238. Therefore, at the beginning of any cycle a reactivity reserve equal to the depletion of the fissionable fuel and the buildup of fission product poisons over the specified cycle life must be "built" into the reactor. This excess reactivity is controlled by removable neutron absorbing material in the form of boron dissolved in the primary coolant and burnable absorber rods or IFBAs.

The concentration of the soluble neutron absorber is varied to compensate for reactivity changes due to fuel burnup, fission product poisoning including xenon and samarium, burnable absorber depletion, and the cold-to-operating moderator temperature change. Figure 4.3-46 shows a typical boron letdown curve. Using its normal makeup path, the CVCS is capable of inserting negative reactivity at a rate of approximately 30 pcm/min when the reactor coolant boron concentration is 1,000 ppm and approximately 35 pcm/min when the reactor coolant boron concentration is 100 ppm. If the emergency boration path is used, the CVCS is capable of inserting negative reactivity at a rate of approximately 65 pcm/min when the reactor coolant concentration is 1,000 ppm and approximately 75 pcm/min when the reactor coolant boron concentration is 100 ppm. The peak burn-out rate for xenon is 25 pcm/min (Section 9.3.4 discusses the capability of the CVCS to counteract xenon decay). Rapid transient reactivity requirements and safety shutdown requirements are met with control rods.

During operation, the absorber content in burnable absorber rods or IFBAs is depleted, thus adding positive reactivity to offset some of the negative reactivity from fuel depletion and fission product buildup. The depletion rate of the burnable absorber rods or IFBAs is not critical since chemical shim is always available and flexible enough to cover any possible deviations in the expected burnable absorber depletion rate. Figure 4.3-3 is a plot of typical core depletions with and without burnable absorber rods. Note that even at end-of-life conditions some residual absorber remains in the burnable absorber rods, resulting in a net decrease during the cycle lifetime.

In addition to reactivity control, the burnable absorber rods are strategically located to provide a favorable radial power distribution. Figure 4.3-4 shows the burnable absorber distributions within a fuel assembly for several IFBA patterns used in a 17 x 17 array for WCGS. A typical core loading pattern with IFBA for WCGS is shown in Figure 4.3-5.

Tables 4.3-2 through 4.3-4 contain a summary of the reactor core design parameters for WCGS Cycle 3, including reactivity coefficients, delayed neutron fraction, and neutron lifetimes. Sufficient information is included to permit an independent calculation of the nuclear performance characteristics of the core.

4.3.2.2 Power Distributions

The accuracy of power distribution calculations has been confirmed through approximately 1,000 flux maps during some 20 years of operation under conditions very similar to those expected. Details of this confirmation are given in Reference 2 and in Section 4.3.2.2.7.

4.3.2.2.1 Definitions

Power distributions are quantified in terms of hot channel factors. These factors are a measure of the peak pellet power within the reactor core and the total energy produced in a coolant channel, relative to the total reactor power output, and are expressed in terms of quantities related to the nuclear or thermal design, namely:

Power density is the thermal power produced per unit volume of the core (kW/liter).

Linear power density is the thermal power produced per unit length of active fuel (kW/ft). Since fuel assembly geometry is standardized, this is the unit of power density most commonly used. For all practical purposes, it differs from kW/liter by a constant factor which includes geometry and the fraction of the total thermal power which is generated in the fuel rod.

Average linear power density is the total thermal power produced in the fuel rods divided by the total active fuel length of all rods in the core.

Local heat flux is the heat flux at the surface of the cladding ($Btu\text{-}ft^{-2}\text{-}hr^{-1}$). For nominal rod parameters, this differs from linear power density by a constant factor.

Rod power or rod integral power is the length integrated linear power density in one rod (kW).

Average rod power is the total thermal power produced in the fuel rods divided by the number of fuel rods (assuming all rods have equal length).

The hot channel factors used in the discussion of power distributions in this section are defined as follows:

F_Q, heat flux hot channel factor, is defined as the maximum local heat flux on the surface of a fuel rod divided by the average fuel rod heat flux, allowing for manufacturing tolerances on fuel pellets and rods.

F_Q^N, nuclear heat flux hot channel factor, is defined as the maximum local fuel rod linear power density divided by the average fuel rod linear power density, assuming nominal fuel pellet and rod parameters.

F_Q^E, engineering heat flux hot channel factor, is the allowance on heat flux required for manufacturing tolerances. The engineering factor allows for local variations in enrichment, pellet density and diameter, surface area of the fuel rod, and eccentricity of the gap between pellet and clad. Combined statistically, the net effect is a factor of 1.03 to be applied to fuel rod surface heat flux.

F_{DH}^E, nuclear enthalpy rise hot channel factor, is defined as the ratio of the integral of linear power along the rod with the highest integrated power to the average rod power.

Manufacturing tolerances, hot channel power distribution, and surrounding channel power distributions are treated explicitly in the calculation of the DNBR described in Section 4.4.

It is convenient for the purposes of discussion to define subfactors of F_Q. However, design limits are set in terms of the total peaking factor.

F_Q = Total peaking factor or heat flux hot channel factor

$$= \frac{\text{Maximum kW/ft}}{\text{Average kW/ft}}$$

$$F_Q = F_Q^N \times F_Q^E$$

$$F_Q = \max F_{XY}^N(Z) \times P(Z) \times F_U^N \times F_Q^E$$

where:

F_Q^N and F_Q^E are defined above

F_U^N = factor for conservatism, assumed to be 1.05

$F_{XY}^N(Z)$ = ratio of peak power density to average power density in the horizontal plane of peak local power

P(Z) = ratio of the power per unit core height in the horizontal plane at height Z to the average value of power per unit core height

4.3.2.2.2 Radial Power Distributions

The power shape in horizontal sections of the core at full power is a function of the fuel assembly and burnable absorber loading patterns, the control rod pattern, and the fuel burnup distribution. Thus, at any time in the cycle, a horizontal section of the core can be characterized as unrodded or with group D control rods. These two situations combined with burnup effects determine the radial power shapes which can exist in the core at full power. Typical values of radial factor F_{XY}^N are given in Table 4.3-2. The effect on radial power shapes of power level, xenon, samarium, and moderator density effects are considered also but these are quite small. The effect of nonuniform flow distribution is negligible. While radial power distributions in various planes of the core are often illustrated, the core radial enthalpy rise distribution, as determined by the integral of power up each channel, is of greater interest.

Since the position of the hot channel varies from time to time, a single reference radial design power distribution is selected for DNB calculations. This reference power distribution is chosen conservatively to concentrate power in one area of the core, minimizing the benefits of flow redistribution. Assembly powers are normalized to core average power. The radial power distribution within a fuel rod and its variation with burnup as utilized in thermal calculations and fuel rod design is discussed in Section 4.4.

4.3.2.2.3 Assembly Power Distributions

For the purpose of illustration, typical assembly power distributions from the BOL and EOL conditions are given for the same assembly in Figures 4.3-12 and 4.3-13, respectively.

Since the detailed power distribution surrounding the hot channel varies from time to time, a conservatively flat radial assembly power distribution is assumed in the DNB analysis, described in Section 4.4, with the rod of maximum integrated power artificially raised to the design value of F^N_{DH}. Care is taken in the nuclear design of all fuel cycles and all operating conditions to ensure that a flatter assembly power distribution does not occur with limiting values of F^N_{DH}.

4.3.2.2.4 Axial Power Distributions

The shape of the power profile in the axial or vertical direction is largely under the control of the operator through either the manual operation of the control rods or automatic motion of rods responding to manual operation of the CVCS. Nuclear effects which cause variations in the axial power shape include moderator density, Doppler effect on resonance absorption, spatial distribution of xenon, and burnup. Automatically controlled variations in total power output and full length rod motion are also important in determining the axial power shape at any time. Signals are available to the operator from the excore ion chambers, which are long ion chambers outside the reactor vessel running parallel to the axis of the core. Separate signals are taken from the top and bottom halves of the chambers. The difference between top and bottom signals from each of four pairs of detectors is displayed on the control panel and called the flux difference, DI. Calculations of core average peaking factor for many plants and measurements from operating plants under many operating situations are associated with either DI or axial offset in such a way that an upper bound can be placed on the peaking factor. For these correlations, axial offset is defined as:

$$\text{axial offset} = \frac{f_t - f_b}{f_t + f_b}$$

and f_t and f_b are the top and bottom detector readings.

Representative axial power shapes for BOL, MOL, and EOL conditions are shown in Figures 4.3-14 through 4.3-16. These figures cover a wide range of axial offset, including values not permitted at full power.

The radial power distributions involving the partial insertion of control rods represent a synthesis of power shapes from the rodded and unrodded planes. The applicability of the separability assumption upon which this procedure is based is assured through extensive three-dimensional calculations of possible rodded conditions. As an example, Figure 4.3-17 compares the axial power distribution for several assemblies at different distances from inserted control rods with the core average distribution.

The only significant difference from the average occurs in the low power peripheral assemblies, thus confirming the validity of the separability assumption.

4.3.2.2.5 Local Power Peaking

In January 1993 Westinghouse submitted topical report WCAP-13589 (Reference 35) to the NRC; NRC approval of the report was received in January 1995. WCAP-13589 evaluated the densification power spike factor and the clad flattening design criterion based on fuel examination data. This data showed that, for the then current Westinghouse nuclear fuel designs, pellet gaps did not occur which were large enough to permit cladding collapse. The report concluded that a densification power spike factor S(Z) (where Z is axial location in the core) of 1.0 was appropriate for current Westinghouse nuclear fuel designs. Later fuel designs, not covered by the data in WCAP-13589, were evaluated as outlined in Reference 36 to assure that the conclusions of WCAP-13589 applied to those designs as well. The reduced power spike factor of 1.0 is appropriate for use with all Westinghouse fuel in the WCGS core.

4.3.2.2.6 Limiting Power Distributions

According to the ANSI classification of plant conditions (see Chapter 15.0), Condition I occurrences are those which are expected frequently or regularly in the course of power operation, maintenance, or maneuvering of the plant. As such, Condition I occurrences are accommodated with margin between any plant parameter and the value of that parameter which would require either automatic or manual protective action. Inasmuch as Condition I occurrences occur frequently or regularly, they must be considered from the point of view of affecting the consequences of fault conditions (Conditions II, III and IV). In this regard, analysis of each fault condition described is generally based on a conservative set of initial conditions corresponding to the most adverse set of conditions which can occur during Condition I operation.

The list of steady state and shutdown conditions, permissible deviations (such as one coolant loop out of service), and operational transients is given in Chapter 15.0. Implicit in the definition of normal operation is proper and timely action by the reactor operator. That is, the operator follows recommended operating procedures for maintaining appropriate power distributions and takes any necessary remedial actions when alerted to do so by the plant instrumentation. Thus, as stated above, the worst or limiting power distribution which can occur during normal operation is to be considered as the starting point for analysis of Conditions II, III, and IV events.

Improper procedural actions or errors by the operator are assumed in the design as occurrences of moderate frequency (Condition II). Some of the consequences which might result are discussed in Chapter 15.0. Therefore, the limiting power shapes which result from such Condition II events are those power shapes which deviate from the normal operating condition at the recommended axial offset band, e.g., during a xenon transient following a change in power level brought about by control rod motion. Power shapes which fall in this category are used for determination of the reactor protection system setpoints so as to maintain margin to overpower or DNB limits.

The means for maintaining power distributions within the required hot channel factor limits are described in the Technical Specifications. A complete discussion of power distribution control in Westinghouse pressurized water reactors is included in Reference 6. Detailed background information on the following design constraints on local power density in a Westinghouse pressurized water reactor, the defined operating procedures, and on the measures taken to preclude exceeding design limits is presented in the Westinghouse topical report on power distribution control and load following procedures (Ref. 7). The following paragraphs summarize these reports and describe the calculations used to establish the upper bound on peaking factors.

The calculations used to establish the upper bound on peaking factors, F_Q and F^N_{DH}, include all of the nuclear effects which influence the radial and/or axial power distributions throughout core life for various modes of operation, including load follow, reduced power operation, and axial xenon transients.

Radial power distributions are calculated including fuel and moderator temperature feedback effects. The steady state nuclear design calculations are done for normal flow with the same mass flow in each channel and flow redistribution effects are neglected. The effect of flow redistribution is calculated explicitly where it is important in the DNB analysis of accidents. The effect of xenon on radial power distribution is small but is included as part of the normal design process. Radial power distributions are relatively fixed and easily bounded with upper limits.

The core average axial profile, however, can experience significant changes which can occur rapidly as a result of rod motion and load changes and more slowly due to xenon distribution. For the study of points of closest approach to axial power distribution limits, several thousand cases are examined. Since the properties of the nuclear design dictate what axial shapes can occur, boundaries on the limits of interest can be set in terms of the parameters which are readily observed on the plant. Specifically, the nuclear design parameters which are significant to the axial power distribution analysis are:

a. Core power level

b. Core height

c. Coolant temperature and flow

d. Coolant temperature program as a function of reactor power

e. Fuel cycle lifetimes

f. Rod bank worths

g. Rod bank overlaps

Normal operation of the plant assumes compliance with the following conditions:

a. Control rods in a single bank move together with no individual rod insertion differing by more than 13 steps (indicated) from the bank demand position.

b. Control banks are sequenced with overlapping banks.

c. The control full length bank insertion limits are not violated.

d. Axial power distribution control procedures, which are given in terms of flux difference control and control bank position, are observed.

The axial power distribution procedures referred to above are part of the required operating procedures which are followed in normal operation. Briefly they require control of the axial offset (flux difference divided by fractional power) at all power levels within a permissible operating band of a target value corresponding to the equilibrium full power value. This minimizes xenon transient effects on the axial power distribution, since the procedures essentially keep the xenon distribution in phase with the power distribution.

Calculations are performed for normal operation of the reactor, including load following maneuvers. Beginning, peak reactivity, middle, and end-of-cycle conditions are included in the calculations. Different histories of operation are assumed prior to calculating the effect of load follow transients on the axial power distribution. A finite number of maneuvers each cycle are analyzed to determine the general behavior of the local power density as a function of core elevation.

These cases represent many possible reactor states in the life of one fuel cycle, and they have been chosen as sufficiently definitive of the cycle by comparison with much more exhaustive studies performed on some 20 or 30 different, but typical, plant and fuel cycle combinations. The cases are described in detail in Reference 7, and they are considered to be necessary and sufficient to generate a local power density limit which, when increased by 5 percent for conservatism, will not be exceeded with a 95-percent confidence level. Many of the points do not approach the limiting envelope. However, they are part of the time histories which lead to the hundreds of shapes which do define the envelope. They also serve as a check that the reactor studied is typical of those studied more exhaustively.

Thus it is not possible to single out any transient or steady state condition which defines the most limiting case. It is not even possible to separate out a small number which form an adequate analysis. The process of generating a myriad of shapes is essential to the philosophy that leads to the required level of confidence. A maneuver which provides a limiting case for one reactor fuel cycle (defined as approaching the line of Figure 4.3-21) is not necessarily a limiting case for another reactor or fuel cycle with different control bank worths, enrichments, burnup, coefficient, etc. Each shape depends on the detailed history of operation up to that time and on the manner in which the operator conditioned xenon in the days immediately prior to the time at which the power distribution is calculated.

The calculated points are synthesized from axial calculations combined with radial factors appropriate for rodded and unrodded planes. In these calculations, the effects on the unrodded radial peak of xenon redistribution that occurs following the withdrawal of a control bank (or banks) from a rodded region is obtained. A detailed discussion of this effect may be found in Reference 7. The calculated values have been increased by a factor of 1.05 for conservatism and a factor of 1.03 for the engineering factor F_Q^E.

The envelope drawn over the calculated [max (F_Q . Power)] points in Figure 4.3-21 represents an upper bound envelope on local power density versus elevation in the core. It should be emphasized that this envelope is a conservative representation of the bounding values of local power density. Expected values are considerably smaller and, in fact, less conservative bounding values may be justified with additional analysis or surveillance requirements. For example, Figure 4.3-21 bounds both BOL and EOL conditions but without consideration of radial power distribution flattening with burnup, i.e., both BOL and EOL points presume the same radial peaking factor. Inclusion of the burnup flattening effect would reduce the local power densities corresponding to EOL conditions which may be limiting at the higher core elevations.

Finally, as previously discussed, this upper bound envelope is based on procedures of load follow which require operation within an allowed deviation from a target equilibrium value of axial offset. These procedures are detailed in the Technical Specifications and are followed by relying only upon excore surveillance supplemented by the normal monthly full core map requirement and by computer-based alarms on deviation and time of deviation from the allowed flux difference band.

Allowing for fuel densification effects the average linear power at 3565 MWt is 5.68 kW/ft. From Figure 4.3-21, the conservative upper bound value of normalized local power density, including uncertainty allowances, is 2.50, corresponding to a peak linear power of 14.48 kW/ft at 102 percent power.

To determine reactor protection system setpoints, with respect to power distributions, three categories of events are considered, namely rod control equipment malfunctions, operator errors of commission, and operator errors of omission. In evaluating these three categories of events, the core is assumed to be operating within the four constraints described above.

The first category comprises uncontrolled rod withdrawal (with rods moving in the normal bank sequence) for full length banks. Also included are motions of the full-length banks below their insertion limits, which could be caused, for example, by uncontrolled dilution or primary coolant cooldown. Power distributions were calculated throughout these occurrences, assuming short term corrective action. That is, no transient xenon effects were considered to result from the malfunction. The event was assumed to occur from typical normal operating situations, which include normal xenon transients. It was further assumed in determining the power distributions that total core power level would be limited by reactor trip to below 118 percent. Since the study is to determine protection limits with respect to power and axial offset, no credit was taken for trip setpoint reduction due to flux difference. The peak power density which can occur in such events, assuming reactor trip at or below 118 percent, is less than that required for center-line melt, including uncertainties and densification effects.

The second category assumes that the operator mispositions the full-length rod bank in violation of the insertion limits and creates short-term conditions not included in normal operating conditions.

The third category assumes that the operator fails to take action to correct a flux difference violation. The results for F_Q are multiplied by a factor to include an allowance for calorimetric error. The peak linear power does not exceed the centerline fuel melt kW/ft limit.

Since the peak kW/ft is below the centerline fuel melt limit, no flux difference penalties are required for overpower protection. It should be noted that a reactor overpower accident is not assumed to occur coincident with an independent operator error. Additional detailed discussion of these analyses is presented in Reference 7.

Analyses of possible operating power shapes show that the appropriate hot channel factors F_Q and $F^N_{\Delta H}$ for peak local power density and for DNB analysis at full power are the values given in Table 4.3-2 and addressed in the Technical Specifications.

The maximum allowable F_Q can be increased with decreasing power, as shown in the Core Operating Limits Report (COLR). Increasing $F^N_{\Delta H}$ with decreasing power is permitted by the DNB protection setpoints points and allows radial power shape changes with rod insertion to the insertion limits, as described in Section 4.4.4.3. The allowance for increased $F^N_{\Delta H}$ permitted is $F^N_{\Delta H} = 1.65\ [1 + 0.3\ (1-P)]$. This becomes a design basis criterion which is used for establishing acceptable control rod patterns and control bank sequencing. Likewise, fuel loading patterns for each cycle are selected with consideration of this design criterion. The worst values of $F^N_{\Delta H}$ for possible rod configurations occurring in normal operation are used in verifying that this criterion is met. The worst values generally occur when the rods are assumed to be at their insertion limits. Maintenance of constant axial offset control establishes rod positions which are above the allowed rod insertion limits, thus providing increasing margin to the $F^N_{\Delta H}$ criterion. As discussed in Section 3.2 of Reference 8, it has been determined that the COLR limits are met, provided the above conditions a and b are observed. These limits are taken as input to the thermal-hydraulic design basis, as described in Section 4.4.4.3.1.

When a situation is possible in normal operation which could result in local power densities in excess of those assumed as the precondition for a subsequent hypothetical accident, but which would not itself cause fuel failure, administrative controls and alarms are provided for returning the core to a safe condition. These alarms are described in detail in Chapter 7.0.

4.3.2.2.7 Experimental Verification of Power Distribution Analysis

This subject is discussed in depth in Reference 2. A summary of this report is given below. It should be noted that power-distribution-related measurements are incorporated into the evaluation of calculated power distribution information, using an incore instrumentation processing code described in Reference 9. The measured versus calculational comparison is normally performed periodically throughout the cycle lifetime of the reactor, as required by Technical Specifications.

In a measurement of the heat flux hot channel factor, F_Q, with the movable detector system described in Sections 7.7.1 and 4.4.6, the following uncertainties have to be considered:

a. Reproducibility of the measured signal

b. Errors in the calculated relationship between detector current and local flux

c. Errors in the calculated relationship between detector flux and peak rod power some distance from the measurement thimble

The appropriate allowance for category a above has been quantified by repetitive measurements made with several inter-calibrated detectors by using the common thimble features of the incore detector system. The WCGS system allows more than one detector to access any thimble. Errors in category b above are quantified to the extent possible, by using the detector current measured at one thimble location to predict fluxes at another location, which is also measured. Local power distribution predictions are verified in critical experiments on arrays of rods with simulated guide thimbles, control rods, burnable absorbers, etc. These critical experiments provide quantification of errors of categories a and c above.

Reference 2 describes critical experiments performed at the Westinghouse Reactor Evaluation Center and measurements taken on two Westinghouse plants with incore systems of the same type as used in the WCGS plant. The report concludes that the uncertainty associated with F_Q (heat flux) is 4.58 percent at the 95-percent confidence level with only 5 percent of the measurements greater than the inferred value. This is the equivalent of a 1.645σ limit on a normal distribution and is the uncertainty to be associated with a full core flux map with movable detectors reduced with a reasonable set of input data incorporating the influence of burnup on the radial power distribution. The uncertainty is usually rounded up to 5 percent.

In comparing measured power distributions (or detector currents) with calculations for the same operating conditions, it is not possible to isolate out the detector reproducibility. Thus a comparison between measured and predicted power distributions has to include some measurement error. Such a comparison is given in Figure 4.3-24 for one of the maps used in Reference 2. Since the first publication of Reference 2, hundreds of maps have been taken on these and other reactors. The results confirm the adequacy of the 5-percent uncertainty allowance on the calculated F_Q.

A similar analysis for the uncertainty in $F^N_{\Delta H}$ (rod integral power) measurements results in an allowance of 3.65 percent at the equivalent of a 1.645σ confidence level. For historical reasons, an 8 percent uncertainty factor is allowed in the nuclear design calculational basis; that is, the predicted rod integrals at full power must not exceed the design $F^N_{\Delta H}$ less 8 percent. This 8 percent may be reduced in final design to 4 percent to allow a wider range of acceptable axial power distributions in the DNB analysis and still meet the design bases of Section 4.3.1.3.

A measurement in the second cycle of a 121 assembly, 12 foot, core is compared with a simplified one-dimensional core average axial calculation in Figure 4.3-25. This calculation does not give explicit representation to the fuel grids.

The accumulated data on power distributions in actual operation is basically of three types:

a. Much of the data is obtained in steady state operation at constant power in the normal operating configuration.

b. Data with unusual values of axial offset are obtained as part of the excore detector calibration exercise which is performed monthly.

c. Special tests have been performed in load follow and other transient xenon conditions which have yielded useful information on power distributions.

These data are presented in detail in Reference 8. Figure 4.3-26 contains a summary of measured values of FQ as a function of axial offset for five plants from that report.

4.3.2.2.8 Testing

An extensive series of physics tests was performed on the first core. These tests and the criteria for satisfactory results are described in Chapter 14.0. Since not all limiting situations can be created at BOL, the main purpose of the tests was to provide a check on the calculational methods used in the predictions for the conditions of the test. Tests performed at the beginning of each reload cycle are limited to verification of the selected safety-related parameters of the reload design.

4.3.2.2.9 Monitoring Instrumentation

The adequacy of instrument numbers, spatial deployment, required correlations between readings and peaking factors, calibration, and errors are described in References 2, 6, and 8. The relevant conclusions are summarized in Sections 4.3.2.2.7 and 4.4.6.

Provided the limitations given in Section 4.3.2.2.6 on rod insertion and flux difference are observed, the excore detector system provides adequate on-line monitoring of power distributions. Further details of specific limits on the observed rod positions and flux difference are given in the Technical Specifications, together with a discussion of their bases.

Limits for alarms, reactor trip, etc. are given in the Technical Specifications. Descriptions of the systems provided are given in Section 7.7.

4.3.2.3 Reactivity Coefficients

The kinetic characteristics of the reactor core determine the response of the core to changing plant conditions or to operator adjustments made during normal operation, as well as the core response during abnormal or accidental transients. These kinetic characteristics are quantified in reactivity coefficients. The reactivity coefficients reflect the changes in the neutron multiplication due to varying plant conditions, such as power, moderator or fuel temperatures, or pressure or void conditions, although the latter are relatively unimportant in the WCGS reactor. Since reactivity coefficients change during the life of the core, ranges of coefficients are employed in transient analysis to determine the response of the plant throughout life. The results of such simulations and the reactivity coefficients used are presented in Chapter 15.0. The reactivity coefficients are calculated on a corewise basis by radial and axial diffusion theory methods. The effect of radial and axial power distribution on core average reactivity coefficients is implicit in those calculations and is not significant under normal operating conditions. For example, a skewed xenon distribution which results in changing axial offset by 5 percent changes the moderator and Doppler temperature coefficients by less than 0.01 pcm/F and 0.03 pcm/F, respectively. An artificially skewed xenon distribution which results in changing the radial $F^N_{\Delta H}$ by 3 percent changes the moderator and Doppler temperature coefficients by less than 0.03 pcm/F and 0.001 pcm/F, respectively. The spatial effects are accentuated in some transient conditions, for example, in postulated rupture of the main steam line break and rupture of a rod cluster control assembly mechanism housing described in Sections 15.1.5 and 15.4.8, and are included in these analyses.

The analytical methods and calculational models used in calculating the reactivity coefficients are given in Section 4.3.3. Quantitative information for calculated reactivity coefficients, including fuel-Doppler coefficient, moderator coefficients (density, temperature, pressure, and void) and power coefficient is given in the following sections.

4.3.2.3.1 Fuel Temperature (Doppler Power) Coefficient

The fuel temperature (Doppler Power) coefficient (DPC) is defined as the change in reactivity per degree change in effective fuel temperature and is primarily a measure of the Doppler broadening of U-238 and Pu-240 resonance absorption peaks. Doppler broadening of other isotopes is also considered but their contribution to the Doppler effect is small. An increase in fuel temperature increases the effective resonance absorption cross-sections of the fuel and produces a corresponding reduction in reactivity.

The DPC is calculated by performing three-dimensional calculations using the ANC computer code (Ref. 31).

The Doppler coefficient becomes more negative as a function of life as the Pu-240 content increases, thus increasing the Pu-240 resonance absorption, but the overall value becomes less negative since the fuel temperature changes with burnup, as described in Section 4.3.3.1. The upper and lower limits of Doppler coefficient used in accident analyses are given in Chapter 15.0.

4.3.2.3.2 Moderator Coefficients

The moderator coefficient is a measure of the change in reactivity due to a change in specific coolant parameters, such as density, temperature, pressure, or void. The coefficients so obtained are moderator density, temperature, pressure, and void coefficients.

Moderator Density and Temperature Coefficients

The moderator temperature (density) coefficient is defined as the change in reactivity per degree change in the moderator temperature. Generally, the effects of the changes in moderator density as well as the temperature are considered together.

The soluble boron used in the reactor as a means of reactivity control also has an effect on moderator density coefficient, since the soluble boron poison density as well as the water density is decreased when the coolant temperature rises. A decrease in the soluble poison density introduces a positive component in the moderator coefficient. If the concentration of soluble poison is large enough, the net value of the coefficient may be positive.

With the burnable absorber rods present, however, the initial hot boron concentration is sufficiently low that the moderator temperature coefficient may be negative at operating temperatures. The effect of control rods is to make the moderator coefficient more negative since the thermal neutron mean free path, and hence the volume affected by the control rods, increases with an increase in temperature.

With burnup, the moderator coefficient becomes more negative, primarily as a result of boric acid dilution, but also to a significant extent from the effects of the buildup of plutonium and fission products.

The moderator coefficient is calculated for a range of plant conditions by performing ANC calculations, in which the moderator temperature (and density) is varied. Typical values for MTC are shown in Table 4.3-6 as a function of core average temperature, boron concentration, and burnup. Figure 4.3-6 shows MTC plotted as a function of burnup for conditions of hot full power and just critical boron concentration.

The moderator coefficients presented here are calculated on a corewide basis, since they are used to describe the core behavior in normal and accident situations when the moderator temperature changes can be considered to affect the entire core.

Moderator Pressure Coefficient

The moderator pressure coefficient relates the change in moderator density, resulting from a reactor coolant pressure change, to the corresponding effect on neutron production. This coefficient is of much less significance in comparison with the moderator temperature coefficient. A change of 50 psi in pressure has approximately the same effect on reactivity as a 1/2-degree change in moderator temperature. This coefficient can be determined from the moderator temperature coefficient by relating change in pressure to the corresponding change in density. The moderator pressure coefficient is negative over a portion of the moderator temperature range at BOL but is always positive at operating conditions and becomes more positive during life.

Moderator Void Coefficient

The moderator void coefficient relates the change in neutron multiplication to the presence of voids in the moderator. In a pressurized water reactor, this coefficient is not very significant because of the low void content in the coolant. The core void content is less than 1/2 of 1 percent and is due to local or statistical boiling. The void coefficient varies from 50 pcm/percent void at BOL and at low temperatures to -250 pcm/percent void at EOL and at operating temperatures. The void coefficient at operating temperature becomes more negative with fuel burnup.

4.3.2.3.3 Power Coefficient

The combined effect of moderator temperature and fuel temperature change as the core power level changes is called the total power coefficient and is expressed in terms of reactivity change per percent power change. It becomes more negative with burnup reflecting the combined effect of moderator and fuel temperature coefficients with burnup.

4.3.2.3.4 Comparison of Calculated and Experimental Reactivity Coefficients

Section 4.3.3 describes the comparison of calculated and experimental reactivity coefficients in detail.

Experimental evaluation of the reactivity coefficients will be performed during the physics startup tests described in Chapter 14.0.

4.3.2.3.5 Reactivity Coefficients Used in Transient Analysis

Table 4.3-2 gives the limiting values as well for the reactivity coefficients. The limiting value is used as design limits in the transient analysis. The exact values of the coefficient used in the analysis depend on whether the transient of interest is examined at the BOL or EOL, whether most negative or the most positive (least negative) coefficients are appropriate, and whether spatial nonuniformity must be considered in the analysis. Conservative values of coefficients, considering various aspects of analysis, are used in the transient analysis. This is described in Chapter 15.0.

The limiting values shown in Table 4.3-2 are chosen to encompass the best estimate reactivity coefficients, including the uncertainties given in Section 4.3.3.3 over appropriate operating conditions calculated for this cycle and the expected values for the subsequent cycles. The most positive, as well as the most negative, values are selected to form the design basis range used in the transient analysis. A direct comparison of the best estimate and design limit values can be misleading since, in many instances, the most conservative combination of reactivity coefficients is used in the transient analysis even though the extreme coefficients assumed may not simultaneously occur at the conditions of lifetime, power level, temperature, and boron concentration assumed in the analysis. The need for a reevaluation of any accident in a subsequent cycle is contingent upon whether or not the coefficients for that cycle fall within the identified range used in the analysis presented in Chapter 15.0 with due allowance for the calculational uncertainties given in Section 4.3.3.3. Control rod requirements are given in Table 4.3-3 for the core described and for an equilibrium cycle, since these are markedly different. These latter numbers are provided for information only since refueling specifications for subsequent cycles have not yet been established.

4.3.2.4 Control Requirements

To ensure the shutdown margin stated in the COLR under conditions where a cooldown to ambient temperature is required, concentrated soluble boron is added to the coolant. Boron concentrations for several core conditions are listed in Table 4.3-2; these values were calculated with ANC (Reference 31) for Cycle 9. For all core conditions including refueling, the boron concentration is well below the solubility limit. The rod cluster control assemblies are employed to bring the reactor to the hot shutdown condition. The minimum required shutdown margin is given in the COLR.

The ability to accomplish the shutdown for hot conditions is demonstrated in Table 4.3-3 by comparing the difference between the rod cluster control assembly reactivity available with an allowance for the worst stuck rod with that required for control and protection purposes. The shutdown margin includes an allowance of 10 percent for analytic uncertainties (see Section 4.3.2.4.9). The largest reactivity control requirement appears at the EOL when the moderator temperature coefficient reaches its peak negative value as reflected in the larger power defect.

The control rods are required to provide sufficient reactivity to account for the power defect from full power to zero power and to provide the required shutdown margin. The reactivity addition resulting from power reduction consists of contributions from Doppler, moderator temperature, flux redistribution, and reduction in void content as discussed below.

4.3.2.4.1 Doppler

The Doppler effect arises from the broadening of U-238 and Pu-240 resonance cross-sections with an increase in effective pellet temperature. This effect is most noticeable over the range of zero power to full power due to the large pellet temperature increase with power generation.

4.3.2.4.2 Variable Average Moderator Temperature

When the core is shut down to the hot, zero power condition, the average moderator temperature changes from the equilibrium full-load value determined by the steam generator and turbine characteristics (steam pressure, heat transfer, tube fouling, etc.) to the equilibrium no-load value, which is based on the steam generator shell side design pressure. The design change in temperature is conservatively increased to account for the control dead band and measurement errors.

Since the moderator coefficient at full-load temperature is negative, there is a reactivity addition with power reduction. The moderator coefficient becomes more negative as the fuel depletes because the boron concentration is reduced. This effect is the major contributor to the increased control requirement at EOL.

4.3.2.4.3 Redistribution

During full power operation, the coolant density decreases with core height, and this, together with partial insertion of control rods, results in less fuel depletion near the top of the core. Under steady state conditions, the relative power distribution will be slightly asymmetric toward the bottom of the core. On the other hand, at hot zero power conditions, the coolant density is uniform up the core, and there is no flattening due to Doppler. The result will be a flux distribution which at zero power can be skewed toward the top of the core. The reactivity insertion due to the skewed distribution is calculated with an allowance for effects of xenon distribution.

4.3.2.4.4 Void Content

A small void content in the core is due to nucleate boiling at full power. The void collapse coincident with power reduction makes a small reactivity contribution.

4.3.2.4.5 Rod Insertion Allowance

At full power, the control bank is operated within a prescribed band of travel to compensate for small changes in boron concentration, changes in temperature, and very small changes in the xenon concentration not compensated for by a change in boron concentration. When the control bank reaches either limit of this band, a change in boron concentration is required to compensate for additional reactivity changes. Since the insertion limit is set by a rod travel limit, a conservatively high calculation of the inserted worth is made which exceeds the normally inserted reactivity.

4.3.2.4.6 Burnup

The reactor core is composed of an array of fuel assemblies that are similar in mechanical design, but different in fuel enrichment. Within each fuel assembly, all rods are of the same enrichment. Three different enrichments were employed in the first core. Other enrichments are employed in reload fuel. The enrichments for cycle 1 at Wolf Creek were 2.10 (Region 1), 2.60 (Region 2), and 3.10 (Region 3) weight percent. The average enrichment has increased in each successive cycle load in order to achieve an eighteen month cycle. This began in Cycle 2 and Cycle 4 was the first eighteen month cycle. For a 12 month cycle, excess reactivity of approximately 10 percent $\Delta\rho$ (hot) is installed at the beginning of the cycle to provide sufficient reactivity to compensate for fuel depletion and fission product buildup throughout the cycle. Excess reactivity is installed at the beginning of each cycle to provide sufficient reactivity to compensate for fuel depletion and fission product buildup throughout the cycle. This reactivity is controlled by the addition of soluble boron to the coolant and by burnable absorber. The soluble boron concentrations for several core configurations are given in Table 4.3-2; these values were calculated with ANC for Cycle 9. Since the excess reactivity for burnup is controlled by soluble boron and/or burnable absorber, it is not included in control rod requirements.

4.3.2.4.7 Xenon and Samarium Poisoning

Changes in xenon and samarium concentrations in the core occur at a sufficiently slow rate, even following rapid power level changes, that the resulting reactivity change can be controlled by changing the soluble boron concentration (also see Section 4.3.2.4.16).

4.3.2.4.8 pH Effects

Changes in reactivity due to a change in coolant pH, if any, are sufficiently small in magnitude and occur slowly enough to be controlled by the boron system. Further details are provided in Reference 11.

4.3.2.4.9 Experimental Confirmation

Following a normal shutdown, the total core reactivity change during cooldown with a stuck rod has been measured on a 121 assembly, 10-foot-high core, and 121 assembly, 12-foot-high core. In each case, the core was allowed to cool down until it reached criticality simulating the steam line break accident. For the 10-foot core, the total reactivity change associated with the cooldown is overpredicted by about 0.3 percent with respect to the measured result. This represents an error of about 5 percent in the total reactivity change and is about half the uncertainty allowance for this quantity. For the 12-foot core, the difference between the measured and predicted reactivity change was an even smaller 0.2 percent. These measurements and others demonstrate the ability of the methods described in Section 4.3.3.

4.3.2.4.10 Control

Core reactivity is controlled by means of a chemical poison dissolved in the coolant, rod cluster control assemblies, and burnable absorber rods, as described below.

4.3.2.4.11 Chemical Poison

Boron in solution as boric acid is used to control relatively slow reactivity changes associated with:

a. The moderator temperature defect in going from cold shutdown at ambient temperature to the hot operating temperature at zero power

b. The transient xenon and samarium poisoning, such as that following power changes or changes in rod cluster control position

c. The reactivity effects of fissile inventory depletion and buildup of long-life fission products

d. The burnable absorber depletion

The boron concentrations for various core conditions are presented in Table 4.3-2; these values were calculated with ANC for Cycle 9.

4.3.2.4.12 Rod Cluster Control Assemblies

The number of rod cluster control assemblies is shown in Table 4.3-1. The rod cluster control assemblies are used for shutdown and control purposes to offset fast reactivity changes associated with:

a. The required shutdown margin in the hot zero power, stuck rods condition

b. The reactivity compensation as a result of an increase in power above hot zero power (power defect, including Doppler, and moderator reactivity changes)

c. Unprogrammed fluctuations in boron concentration, coolant temperature, or xenon concentration (with rods not exceeding the allowable rod insertion limits)

d. Reactivity ramp rates resulting from load changes

The allowed control bank reactivity insertion is limited at full power to maintain shutdown capability. As the power level is reduced, control rod reactivity requirements are also reduced, and more rod insertion is allowed. The control bank position is monitored, and the operator is notified by an alarm if the limit is approached. The determination of the insertion limit uses conservative xenon distributions and axial power shapes. In addition, the rod cluster control assembly withdrawal pattern determined from these analyses is used in determining power distribution factors and in determining the maximum worth of an inserted rod cluster control assembly ejection accident. For further discussion, refer to the COLR on rod insertion limits.

Power distribution, rod ejection, and rod misalignment analyses are based on the arrangement of the shutdown and control groups of the rod cluster control assemblies shown in Figure 4.3-36. All shutdown rod cluster control assemblies are withdrawn before withdrawal of the control banks is initiated. In going from zero to 100-percent power, control banks A, B, C, and D are withdrawn sequentially. The limits of rod positions and further discussion on the basis for rod insertion limits are provided in the COLR.

4.3.2.4.13 Reactor Coolant Temperature

Reactor coolant (or moderator) temperature control has added flexibility in reactivity control of the Westinghouse pressurized water reactor. This feature takes advantage of the negative moderator temperature coefficient inherent in a pressurized water reactor to:

a. Maximize return to power capabilities

b. Provide $\pm$5 percent power load regulation capabilities without requiring control rod compensation

c. Extend the time in cycle life to which daily load follow operations can be accomplished

Reactor coolant temperature control supplements the dilution capability of the plant by lowering the reactor coolant temperature to supply positive reactivity through the negative moderator coefficient of the reactor. After the transient is over, the system returns the reactor coolant temperature to the programmed value.

Moderator temperature control of reactivity, like soluble boron control, has the advantage of not significantly affecting the core power distribution. However, unlike boron control, temperature control can be rapid enough to achieve reactor power change rates of 5 percent/minute.

4.3.2.4.14 Burnable Absorber Rods

The standard burnable absorber of WABA rods provide partial control of the excess reactivity available during the first fuel cycle. In doing so, these rods prevent the moderator temperature coefficient from being positive at normal operating conditions. They perform this function by reducing the requirement for soluble poison in the moderator at the beginning of the first fuel cycle, as described previously. For purposes of illustration, a typical burnable absorber rod pattern in the core together with the number of rods per assembly are shown in Figure 4.3-5, while the arrangements within an assembly are displayed in Figure 4.3-4. The reactivity worth of these rods is shown in Table 4.3-1. The boron in the rods is depleted with burnup but at a sufficiently slow rate so that the resulting critical concentration of soluble boron is such that the moderator temperature coefficient remains below the safety analysis limit at all times for power operating conditions in the first cycle.

4.3.2.4.15 Peak Xenon Startup

Compensation for the peak xenon buildup is accomplished, using the boron control system. Startup from the peak xenon condition is accomplished with a combination of rod motion and boron dilution. The boron dilution may be made at any time, including during the shutdown period, provided the shutdown margin is maintained.

4.3.2.4.16 Load Follow Control and Xenon Control

During load follow maneuvers, power changes are accomplished using control rod motion and dilution or boration by the boron system as required. Control rod motion is limited by the control rod insertion limits on full-length rods, as provided in the COLR and discussed in Sections 4.3.2.4.12 and 4.3.2.4.13. The power distribution is maintained within acceptable limits through location of the full-length rod bank. Reactivity changes due to the changing xenon concentration can be controlled by rod motion and/or changes in the soluble boron concentration.

Late in cycle life, extended load follow capability is obtained by augmenting the limited boron dilution capability at low soluble boron concentrations by temporary moderator temperature reductions.

Rapid power increases (5 percent/min) from part power during load follow operation are accomplished with a combination of rod motion, moderator temperature reduction, and boron dilution. The rapid power increase is accomplished initially by a combination of rod withdrawal and moderator temperature reduction. As the slower boron dilution takes effect after the initial rapid power increase, the moderator temperature is returned to the programmed value.

4.3.2.4.17 Burnup

Control of the excess reactivity for burnup is accomplished, using soluble boron and/or burnable absorber. Sufficient burnable absorber is installed at the beginning of a cycle to give the desired cycle lifetime, without exceeding the boron concentration limit. The practical minimum boron concentration is in the range of 0 to 10 ppm.

4.3.2.5 Control Rod Patterns and Reactivity Worth

The rod cluster control assemblies are designated by function as the control groups and the shutdown groups. The terms "group" and "bank" are used synonymously throughout this report to describe a particular grouping of control assemblies. The rod cluster assembly pattern is displayed in Figure 4.3-36, which is not expected to change during the life of the plant. The control banks are labeled A, B, C, and D and the shutdown banks are labeled SA, SB, SC, SD, and SE. Each bank, although operated and controlled as a unit, is composed of two subgroups. The axial position of the control rod banks may be controlled manually or automatically, while the shutdown banks are only controlled manually. The rod cluster control assemblies are all dropped into the core following actuation of reactor trip signals.

Two criteria have been employed for selection of the control groups. First the total reactivity worth must be adequate to meet the requirements specified in Table 4.3-3. Second, in view of the fact that these rods may be partially inserted at power operation, the total power peaking factor should be low enough to ensure that the power capability requirements are met. Analyses indicate that the first requirement can be met either by a single group or by two or more banks whose total worth equals at least the required amount. The axial power shape would be more peaked, following movement of a single group of rods worth 3 to 4 percent. Therefore, four banks (described as A, B, C, and D in Figure 4.3-36) have been selected. Typical control bank worths are shown in Table 4.3-2.

The position of control banks for criticality under any reactor condition is determined by the concentration of boron in the coolant. On an approach to criticality, boron is adjusted to ensure that criticality will be achieved with control rods above the insertion limit set by shutdown and other considerations (see the COLR).

Ejected rod worths are given in Section 15.4.8 for several different conditions.

Allowable deviations due to misaligned control rods are discussed in the Technical Specifications.

A representative calculation for three banks of control rods withdrawn simultaneously (rod withdrawal accident) is given in Figure 4.3-37.

Calculation of control rod reactivity worth versus time following reactor trip involves both control rod velocity and differential reactivity worth. The rod position versus time of travel after rod release assumed is given in Figure 4.3-38. For nuclear design purposes, the reactivity worth versus rod position is calculated by a series of steady state calculations at various control rod positions, assuming all rods out of the core as the initial position in order to minimize the initial reactivity insertion rate. Also, to be conservative, the rod of highest worth is assumed stuck out of the core, and the flux distribution (and thus reactivity importance) is assumed to be skewed to the bottom of the core. The result of these calculations is shown on Figure 4.3-39.

The shutdown groups provide additional negative reactivity to assure an adequate shutdown margin. Shutdown margin is defined as the amount by which the core would be subcritical at hot shutdown if all rod cluster control assemblies are tripped, but assuming that the highest worth assembly remains fully withdrawn and no changes in xenon or boron take place. The loss of control rod worth due to the material irradiation is negligible, since only bank D may be in the core under normal operating conditions (near full power).

The values given in Table 4.3-3 show that the available reactivity in withdrawn rod cluster control assemblies provides the design bases minimum shutdown margin, allowing for the highest worth cluster to be at its fully withdrawn position. An allowance for the uncertainty in the calculated worth of N-1 rods is made before determination of the shutdown margin.

4.3.2.6 Criticality of the Reactor During Refueling and Criticality of Fuel Assemblies

The basis for maintaining the reactor subcritical during refueling is presented in Section 4.3.1.5, and a discussion of how control requirements are met is given in Sections 4.3.2.4 and 4.3.2.5.

Criticality of fuel assemblies outside the reactor is precluded by adequate design of fuel transfer and fuel storage facilities and by administrative control procedures. Sections 9.1.1 and 9.1.2 identify those criteria important to criticality safety analyses.

4.3.2.7 Stability

4.3.2.7.1 Introduction

The stability of the pressurized water reactor cores against xenon-induced spatial oscillations and the control of such transients are discussed extensively in References 6, 14, 15, and 16. A summary of these reports is given in the following discussion, and the design bases are given in Section 4.3.1.6.

In a large reactor core, xenon-induced oscillations can take place with no corresponding change in the total power of the core. The oscillation may be caused by a power shift in the core, which occurs rapidly by comparison with the xenon-iodine time constants. Such a power shift occurs in the axial direction when a plant load change is made by control rod motion and results in a change in the moderator density and fuel temperature distributions. Such a power shift could occur in the diametral plane of the core as a result of abnormal control action.

Due to the negative power coefficient of reactivity, pressurized water reactor cores are inherently stable to oscillations in total power. Protection against total power instabilities is provided by the control and protection system, as described in Section 7.7. Hence, the discussion on the core stability will be limited here to xenon-induced spatial oscillations.

4.3.2.7.2 Stability Index

Power distributions, either in the axial direction or in the X-Y plane, can undergo oscillations due to perturbations introduced in the equilibrium distributions without changing the total core power. The overtones in the current pressurized water reactors and the stability of the core against xenon-induced oscillations can be determined in terms of the eigenvalues of the first flux overtones. Writing the eigenvalue ξ of the first flux harmonic as:

$$\xi = b + ic \qquad [4.3\text{-}1]$$

then b is defined as the stability index and $T = 2\pi/c$ as the oscillation period of the first harmonic. The time-dependence of the first harmonic $\delta\phi$ in the power distribution can now be represented as:

$$\delta\phi(t) = A\, e^{\xi t} = a e^{bt} \cos ct \qquad [4.3\text{-}2]$$

where A and a are constants. The stability index can also be obtained approximately by:

$$b = \frac{1}{T} \ln \frac{A_{n+1}}{A_n} \qquad [4.3\text{-}3]$$

where A_n and A_{n+1} are the successive peak amplitudes of the oscillation and T is the time period between the successive peaks.

4.3.2.7.3 Prediction of the Core Stability

The stability of the core described herein (i.e., with 17 x 17 fuel assemblies) against xenon-induced spatial oscillations is expected to be equal to or better than that of earlier designs for cores of similar size. The prediction is based on a comparison of the parameters which are significant in determining the stability of the core against the xenon-induced oscillations, namely: 1) the overall core size is unchanged and spatial power distributions will be similar, 2) the moderator temperature coefficient is expected to be similar to or slightly more negative, and 3) the Doppler coefficient of reactivity is expected to be equal to or slightly more negative at full power.

Analysis of both the axial and X-Y xenon transient tests, discussed in Section 4.3.2.7.5, shows that the calculational model is adequate for the prediction of core stability.

4.3.2.7.4 Stability Measurements

a. Axial measurements

Two axial xenon transient tests conducted in a pressurized water reactor with a core height of 12 feet and 121 fuel assemblies is reported in Reference 17 and will be briefly discussed here. The tests were performed at approximately 10 percent and 50 percent of cycle life.

Both a free-running oscillation test and a controlled test were performed during the first test. The second test at mid-cycle consisted of a free-running oscillation test only. In each of the free-running oscillation tests, a perturbation was introduced to the equilibrium power distribution through an impulse motion of the control bank D and the subsequent oscillation period. In the controlled test conducted early in the cycle, the part-length rods were used to follow the oscillations to maintain an axial offset within the prescribed limits. The axial offset of power was obtained from the excore ion chamber readings (which had been calibrated against the incore flux maps) as a function of time for both free-running tests, as shown in Figure 4.3-40.

The total core power was maintained constant during these spatial xenon tests, and the stability index and the oscillation period were obtained from a least squares fit of the axial offset data in the form of Equation [4.3-2]. The axial offset of power is the quantity that properly represents the axial stability in the sense that it essentially eliminates any contribution from even-order harmonics, including the fundamental mode. The conclusions of the tests are:

1. The core was stable against induced axial xenon transients, both at the core average burnups of 1550 MWD/MTU and 7700 MWD/MTU. The measured stability indices are -0.041 hr^{-1} for the first test (Curve 1 of Figure 4.3-40) and -0.014 hr^{-1} for the second test (Curve 2 of Figure 4.3-40). The corresponding oscillation periods are 32.4 and 27.2 hours, respectively.

2. The reactor core becomes less stable as fuel burnup progresses and the axial stability index was essentially zero at 12,000 MWD/MTU. However, the movable control rod system can control axial oscillations, as described in Section 4.3.2.7.

b. Measurements in the X-Y plane

Two X-Y xenon oscillation tests were performed at a pressurized water reactor plant with a core height of 12 feet and 157 fuel assemblies. The first test was conducted at a core average burnup of 1540 MWD/MTU and the second at a core average burnup of 12,900 MWD/MTU. Both of the X-Y xenon tests show that the core was stable in the X-Y plane at both burnups. The second test shows that the core became more stable as the fuel burnup increased, and all Westinghouse pressurized water reactors with 121 and 157 assemblies are expected to be stable throughout their burnup cycles.

In each of the two X-Y tests, a perturbation was introduced to the equilibrium power distribution through an impulse motion of one rod cluster control unit located along the diagonal axis. Following the perturbation, the uncontrolled oscillation was monitored, using the movable detector and thermocouple system and the excore power range detectors. The quadrant tilt difference (QTD) is the quantity that properly represents the diametral oscillation in the X-Y plane of the reactor core in that the differences of the quadrant average powers over two symmetrically opposite quadrants essentially eliminates the contribution to the oscillation from the azimuthal mode. The QTD data were fitted in the form of Equation [4.3-2] through a least squares method. A stability index of -0.076 hr^{-1} with a period of 29.6 hours was obtained from the thermocouple data shown in Figure 4.3-41.

It was observed in the second X-Y xenon test that the pressurized water reactor core with 157 fuel assemblies had become more stable due to an increased fuel depletion, and the stability index was not determined.

4.3.2.7.5 Comparison of Calculations with Measurements

The analysis of the axial xenon transient tests was performed in an axial slab geometry, using a flux synthesis technique. The direct simulation of the axial offset data was carried out using the PANDA Code (Ref. 18). The analysis of the X-Y xenon transient tests was performed on an X-Y geometry, using a modified TURTLE Code (Ref. 10) concurring with the Advanced Nodal Code (ANC)(Ref. 31). The PANDA, TURTLE, and ANC codes solve the two-group time-dependent neutron diffusion equation with time-dependent xenon and iodine concentrations. The fuel temperature and moderator density feedback is limited to a steady state model. All the X-Y calculations were performed in an average enthalpy plane.

The basic nuclear cross-sections used in this study were generated from a unit cell depletion program which has evolved from the code ARK(C) which is essentially a combination of the codes LEOPARD (Ref. 19) and CINDER (Ref. 20). The detailed experimental data during the tests, including the reactor power level, enthalpy rise, and the impulse motion of the control rod assembly, as well as the plant follow burnup data, were closely simulated in the study.

The results of the stability calculation for the axial tests are compared with the experimental data in Table 4.3-5. The calculations show conservative results for both of the axial tests with a margin of approximately -0.01 hr-1 in the stability index.

An analytical simulation of the first X-Y xenon oscillation test shows a calculated stability index of $-0.081\ hr^{-1}$, in good agreement with the measured value of $-0.076\ hr^{-1}$. As indicated earlier, the second X-Y xenon test showed that the core had become more stable compared to the first test, and no evaluation of the stability index was attempted. This increase in the core stability in the X-Y plane due to increased fuel burnup is due mainly to the increased magnitude of the negative moderator temperature coefficient.

Previous studies of the physics of xenon oscillations, including three-dimensional analysis, are reported in the series of topical reports, References 14, 15 and 16. A more detailed description of the experimental results and analysis of the axial and X-Y xenon transient tests is presented in Reference 17 and Section 1 of Reference 21.

4.3.2.7.6 Stability Control and Protection

The excore detector system is utilized to provide indications of xenon-induced spatial oscillations. The readings from the excore detectors are available to the operator and also form part of the protection system.

a. Axial power distribution

   For maintenance of proper axial power distributions, the operator is instructed to maintain an axial offset within a prescribed operating band, based on the excore detector readings. Should the axial offset be permitted to move far enough outside this band, the protection limit will be reached, and the power will be automatically reduced.

Twelve-foot pressurized water reactor cores become less stable to axial xenon oscillations as fuel burnup progresses. However, free xenon oscillations are not allowed to occur, except for special tests. The full-length control rod banks are sufficient to dampen and control any axial xenon oscillations present. Should the axial offset be inadvertently permitted to move far enough outside the control band due to an axial xenon oscillation, or any other reason, the protection limit on axial offset will be reached and the power will be automatically reduced.

b. Radial power distribution

The core described herein is calculated to be stable against X-Y xenon-induced oscillations at all times in life.

The X-Y stability of large pressurized water reactors has been further verified as part of the startup physics test program for pressurized water reactor cores with 193 fuel assemblies. The measured X-Y stability of the cores with 157 and 193 assemblies was in good agreement with the calculated stability, as discussed in Sections 4.3.2.7.4 and 4.3.2.7.5. In the unlikely event that X-Y oscillations occur, backup actions are possible and would be implemented, if necessary, to increase the natural stability of the core. This is based on the fact that several actions could be taken to make the moderator temperature coefficient more negative, which will increase the stability of the core in the X-Y plane.

Provisions for protection against nonsymmetric perturbations in the X-Y power distribution that could result from equipment malfunctions are made in the protection system design. This includes control rod drop, rod misalignment, and asymmetric loss-of-coolant flow.

A more detailed discussion of the power distribution control in pressurized water reactor cores is presented in References 6 and 7.

4.3.2.8 Vessel Irradiation

A brief review of the methods and analyses used in the determination of neutron and gamma ray flux attenuation between the core and the pressure vessel is given below. A more complete discussion on the pressure vessel irradiation and surveillance program is given in Section 5.3.

The materials that serve to attenuate neutrons originating in the core and gamma rays from both the core and structural components consist of the core baffle, core barrel, neutron pads, and associated water annuli, all of which are within the region between the core and the pressure vessel.

In general, few group neutron diffusion theory codes are used to determine fission power density distributions within the active core, and the accuracy of these analyses is verified by incore measurements on operating reactors. Region and rodwise power-sharing information from the core calculations is then used as source information in two-dimensional S_n transport calculations (DOT code) which compute the flux distributions throughout the reactor.

The neutron flux distribution and spectrum in the various structural components varies significantly from the core to the pressure vessel.

As discussed in Section 5.3, the irradiation surveillance program utilizes actual test samples to verify the accuracy of the calculated fluxes at the vessel.

4.3.3 ANALYTICAL METHODS

Calculations required in nuclear design consist of three distinct types, which are performed in sequence:

a. Determination of effective fuel temperatures

b. Generation of macroscopic few-group parameters

c. Space-dependent, few-group diffusion calculations

These calculations are carried out by computer codes which can be executed individually. However, at Westinghouse most of the codes required have been linked to form an automated design sequence which minimizes design time, avoids errors in transcription of data, and standardizes the design methods.

4.3.3.1 Fuel Temperature (Doppler) Calculations

Temperatures vary radially within the fuel rod, depending on the heat generation rate in the pellet, the conductivity of the materials in the pellet, gap, and clad, and the temperature of the coolant.

The fuel temperatures for use in most nuclear design Doppler calculations are obtained from a simplified version of the Westinghouse fuel rod design model described in Section 4.2.1.3 which considers the effect of radial variation of pellet conductivity, expansion-coefficient and heat generation rate, elastic deflection of the clad, and a gap conductance which depends on the initial fill gap, the hot open gap dimension, and the fraction of the pellet over which the gap is closed. The fraction of the gap assumed closed represents an empirical adjustment used to produce good agreement with observed reactivity data at BOL. Further gap closure occurs with burnup and accounts for the decrease in Doppler defect with burnup which has been observed in operating plants. For detailed calculations of the Doppler coefficient, such as for use in xenon stability calculations, a more sophisticated temperature model is used which accounts for the effects of fuel swelling, fission gas release, and plastic clad deformation.

Radial power distributions in the pellet as a function of burnup were obtained from LASER (Ref. 22) calculations.

The effective U-238 temperature for resonance absorption was obtained from the radial temperature distribution by applying a radially dependent weighting function. The weighting function was determined from REPAD (Ref. 23) Monte Carlo calculations of resonance escape probabilities in several steady state and transient temperature distributions. In each case, a flat pellet temperature was determined which produced the same resonance escape probability as the actual distribution. The weighting function was empirically determined from these results.

The effective Pu-240 temperature for resonance absorption was determined by a convolution of the radial distribution of Pu-240 densities from LASER burnup calculations and the radial weighting function. The resulting temperature was burnup dependent, but the difference between U-238 and Pu-240 temperatures, in terms of reactivity effects, was small.

The effective pellet temperature for pellet dimensional change was that value which produce the same outer pellet radius in a virgin pellet as that obtained from the temperature model. The effective clad temperature for dimensional change was its average value.

The temperature calculational model was validated by plant Doppler defect data, as shown in Table 4.3-7, and Doppler coefficient data, as shown in Figure 4.3-42. Stability index measurements also provided a sensitive measure of the Doppler coefficient near full power (see Section 4.3.2.7). It can be seen that Doppler defect data was typically within 0.2 percent of prediction.

4.3.3.2 Macroscopic Group Constants

Macroscopic group constants for use in the spatial few group diffusion codes were generated for the initial core with a linked version of LEOPARD (Reference 19) and CINDER (Reference 20) codes. Cross sections for reloads were previously generated using the PHOENIX-P code (Reference 32). Starting in reload Cycle 21, cross section calculations are done using the PARAGON/NEXUS (References 4 and 5) code package. A description of each code follows.

Macroscopic few-group constants and consistent microscopic cross-sections (needed for feedback and microscopic depletion calculations) are generated for fuel cells by a version of the LEOPARD (Ref. 19) and CINDER (Ref. 20) codes, which are linked internally and provide burnup-dependent cross-sections. Normally, a simplified approximation of the main fuel chains is used. However, where needed, a complete solution for all the significant isotopes in the fuel chains, from Th-232 to Cm-244, is available (Ref. 24). Fast and thermal cross-section library tapes contain microscopic cross-sections taken for the most part from the ENDF/B (Ref. 25) library, with a few exceptions where other data provided better agreement with critical experiments, isotopic measurements, and plant critical boron values. The effect on the unit fuel cell of nonlattice components in the fuel assembly is obtained by supplying an appropriate volume fraction of these materials in an extra region which is homogenized with the unit cell in the fast (MUFT) and thermal (SOFOCATE) flux calculations. In the thermal calculation, the fuel rod, clad, and moderator are homogenized by energy-dependent disadvantage factors derived from an analytical fit to integral transport theory results.

Group constants for burnable absorber cells, guide thimbles, instrument thimbles, and interassembly gaps are generated in a manner analogous to the fuel cell calculation. Reflector group constants are taken from infinite medium LEOPARD calculations.

Baffle group constants are calculated from an average of core and radial reflector microscopic group constants for stainless steel.

Group constants for control rods are calculated in a linked version of the HAMMER (Ref. 26) and AIM (Ref.27) codes to provide a better treatment of self-shielding in the broad resonance structure of the isotopes at epithermal energies than is available in LEOPARD. The Doppler broadened cross-sections of the control rod materials are represented as smooth cross-sections in the 54-group LEOPARD fast group structure and in 30 thermal groups. The four group constants in the rod cell and appropriate extra region are generated in the coupled space-energy transport HAMMER calculation. A corresponding AIM calculation of the homogenized rod cell with extra region is used to adjust the absorption cross-sections of the rod cell to match the reaction rates in HAMMER. These transport-equivalent group constants are reduced to two-group constants for use in space-dependent diffusion calculations. In discrete X-Y calculations, only one mesh interval per cell is used, and the rod group constants are further adjusted for use in this standard mesh by reaction rate matching the standard mesh unit assembly to a fine mesh unit assembly calculation.

Validation of the cross-section method is based on analysis of critical experiments, as shown in Table 4.3-4, isotopic data, as shown in Table 4.3-8, plant critical boron (C_B) values at HZP, BOL, as shown in Table 4.3-9, and at HFP as a function of burnup, as shown in Figures 4.3-43 through 4.3-46. Control rod worth measurements are shown in Table 4.3-10.

Confirmatory critical experiments on burnable poisons are described in Reference 28.

The PHOENIX-P computer code is a two-dimensional, multigroup, transport based lattice code and capable of providing all necessary data for PWR analysis. Being a dimensional lattice code, PHOENIX-P does not rely on pre-determined spatial/spectral interaction assumption for a heterogeneous fuel lattice, hence, will provide a more accurate multi-group flux solution than versions of LEOPARD/CINDER. The PHOENIX-P computer code is approved by the USNRC as the lattice code for generating macroscopic and microscopic few group cross sections for PWR analysis (Reference 32).

The solution for the detailed spatial flux and energy distribution is divided into two major steps in PHOENIX-P (Reference 32). In the first step, a two-dimensional fine energy group nodal solution is obtained which couples individual subcell regions (pellet, clad and moderator) as well as surrounding pins. PHOENIX-P uses a method based on the Carlvik's collision probability approach and heterogeneous response fluxes which preserves the heterogeneity of the pin cells and their surroundings. The nodal solution provides accurate and detailed local flux distribution which is then used to spatially homogenize the pin cells to fewer groups.

The second step in the solution process solves for the angular flux distribution using a standard S4 discrete ordinates calculation. This step is based on the group-collapsed and homogenized cross sections obtained from the first step of the solution. The S4 fluxes are then used to normalize the detailed spatial and energy nodal fluxes. The normalized nodal fluxes are used to compute reaction rates, power distribution and to deplete the fuel and burnable absorbers. A standard B1 calculation is employed to evaluate the fundamental mode critical spectrum and to provide an improved fast diffusion coefficient for the core spatial codes.

The PHOENIX-P code originally employed a 42 energy group library which had been derived mainly from the ENDF/B-V files. Starting in Cycle 11, the PHOENIX code was upgraded to a 70 group library, which was derived from the ENDF/B-VI files.

The PHOENIX-P cross sections library was designed to properly capture integral properties of the multi-group data during group collapse, and enabling proper modeling of important resonance parameters. The library contains all neutronic data necessary for modeling fuel, fission produces, cladding and structural, coolant and control/burnable absorber materials present in Light Water Reactor cores.

Group constants for burnable absorber cells, guide thimbles, instrument thimbles, control rod cells and other non-fuel cells can be obtained directly from PHOENIX-P without any adjustments such as those required in the cell or 1-dimensional lattice codes.

PARAGON has been approved by the NRC as the new generation of Westinghouse lattice code (Reference 4). PARAGON is a replacement for PHOENIX-P and its primary use will be to provide the same types of input data that PHOENIX-P generates for use in three dimensional core simulator codes. This includes macroscopic cross sections, microscopic cross sections for feedback adjustments to the macroscopic cross sections, pin factors for pin power reconstruction calculations, discontinuity factors for a nodal method solution, and other data needed for safety analysis or other downstream applications.

PARAGON is based on collision probability – interface current cell coupling methods. PARAGON provides flexibility in modeling that was not available in PHOENIX-P including exact cell geometry representation instead of cylinderization, multiple rings and regions within the fuel pin and moderator cell geometry, and variable cell pitch. The solution method permits flexibility in choosing the quality of the calculation through both increasing the number of regions modeled within the cell and the number of angular current directions tracked at the cell interfaces.

The calculation scheme in PARAGON is based on the conventional lattice modules: resonance calculation, flux solution, leakage correction and depletion. The detailed theory of these modules is described in Reference 4. The cross-section resonance calculation module is based on the space dependent Dancoff method (Reference 4); it is a generalization of the PHOENIX-P methodology that permits to subdivide the fuel pin into many rings and therefore generates space dependent self-shielded isotopic cross-sections. The flux solution module uses the interface current collision probability method and permits a detailed representation of the fuel cells (Reference 4). The other two modules (leakage and depletion) are similar to the ones used in PHOENIX-P.

The current PARAGON cross section library is a 70-group library, based on the ENDF/B basic nuclear data, with the same group structure as the library currently used with PHOENIX-P. The PARAGON qualification library has been improved through the addition of more explicit fission products and fission product chains (Reference 4). PARAGON is however designed to employ any number of energy groups.

The new NEXUS cross-section generation system uses PARAGON as the lattice code (Reference 5).

4.3.3.3 Spatial Few-Group Diffusion Calculations

For the initial core, spatial few-group diffusion calculations primarily consisted of two-group X-Y calculations using an updated version of the TURTLE code, and two-group axial calculations were performed using an updated version of the PANDA code. Spatial few-group diffusion calculations for reload cores are performed with the ANC code (Advanced Nodal Code) (Reference 31). The three dimensional nature of ANC provides both the radial and axial power distributions.

For the initial core, validation of TURTLE reactivity calculations was associated with the validation of the group constants themselves, as discussed in Section 4.3.3.2. Validation of the Doppler calculations was associated with the fuel temperature validation discussed in Section 4.3.3.1. Validation of the moderator coefficient calculations was obtained by comparison with plant measurements at hot zero power conditions, as shown in Table 4.3-11.

Axial calculations are used to determine differential control rod worth curves (reactivity versus rod insertion) and axial power shapes during steady state and transient xenon conditions (flyspeck curve). Group constants and the radial buckling used in the axial calculation were obtained from the PANDA radial calculation, in which group constants in annular rings representing the various material regions in the X-Y plane are homogenized by flux-volume weighting.

For reload cores, nodal three dimensional calculations are carried out to determine the critical boron concentrations and power distributions. The moderator coefficient is evaluated by varying the inlet temperature in the same calculations used for power distribution and reactivity predictions.

ANC is used in two-dimensional and three-dimensional calculations. ANC can be used for safety analyses and to calculate critical boron concentrations, control rod worth, reactivity coefficients, etc.

For reload cores, nodal three dimensional calculations are carried out to determine the critical boron concentrations and power distributions. The moderator coefficient is evaluated by varying the inlet temperature in the same calculations used for power distribution and reactivity predictions.

ANC is used in two-dimensional and three-dimensional calculations. ANC can be used for safety analyses and to calculate critical boron concentrations, control rod worth, reactivity coefficients, etc.

Validation of the spatial codes for calculating power distributions involves the use of incore and excore detectors and is discussed in Section 4.3.2.2.7.

4.3.4 REFERENCES

1. "Westinghouse Anticipated Transients Without Reactor Trip Analysis," WCAP-8330, August 1974.

2. Langford, F. L. and Nath, R. J., "Evaluation of Nuclear Hot Channel Factor Uncertainties," WCAP-7308-L (Proprietary), April 1969 and WCAP-7810 (Non-Proprietary), December 1971.

3. Letter from T. M. Anderson (Westinghouse) to S. H. Hanauer (USNRC), "ATWS Submittal," NS-TMA-2182, December 1979.

4. Ouisolumen, M. et al., "Qualification of the Two-Dimensional Transport Code PARAGON" WCAP-16045-P-16045-P-A, August 2004.

5. Zhang, B. et al., "Qualification of the NEXUS Nuclear Data Methodology", WCAP-16045-P-A, Addendum 1, November 2005.

6. "Power Distribution Control of Westinghouse Pressurized Water Reactors," WCAP-7811, December 1971.

7. Morita, T., et al., "Power Distribution Control and Load Following Procedures," WCAP-8385 (Proprietary) and WCAP-8403 (Non-Proprietary), September 1974.

8. McFarlane, A. F., "Power Peaking Factors," WCAP-7912-P-A (Proprietary) and WCAP-7912-A (Non-Proprietary), January 1975.

9. Meyer, C. E. and Stover, R. L., "Incore Power Distribution Determination in Westinghouse Pressurized Water Reactors," WCAP-8498, July 1975.

10. Barry, R. F. and Altomare, S., "The TURTLE 24.0 Diffusion Depletion Code," WCAP-7213-P-A (Proprietary) and WCAP-7758-A (Non-Proprietary), February 1975.

11. Cermak, J. 0., et al., "Pressurized Water Reactor pH - Reactivity Effect Final Report," WCAP-3696-8 (EURAEC-2074), October 1968.

12. Strawbridge, L. E. and Barry, R. F., "Criticality Calculation for Uniform Water-Moderated Lattices," Nucl. Sci. and Eng. 23, 58 (1965).

13. Dominick, I. E. and Orr, W. L., "Experimental Verification of Wet Fuel Storage Criticality Analyses," WCAP-8682 (Proprietary) and WCAP-8683 (Non-Proprietary), December 1975.

14. Poncelet, C. G. and Christie, A. M., "Xenon-Induced Spatial Instabilities in Large Pressurized Water Reactors," WCAP-3680-20 (EURAEC-1974), March 1968.

15. Skogen, F. B. and McFarlane, A. F., "Control Procedures for Xenon-Induced X-Y Instabilities in Large Pressurized Water Reactors," WCAP-3680-21 (EURAEC-2111), February 1969.

16. Skogen, F. B. and McFarlane, A. F., "Xenon-Induced Spatial Instabilities in Three-Dimensions," WCAP-3680-22 (EURAC-2116), September 1969.

17. Lee, J. C., et al., "Axial Xenon Transient Tests at the Rochester Gas and Electric Reactor," WCAP-7964, June 1971.

18. Barry, R. F. and Minton, G., "The PANDA Code," WCAP-7048-P-A (Proprietary) and WCAP-7757-A (Non-Proprietary), February 1975.

19. Barry, R. F., "LEOPARD - A Spectrum Dependent Non-Spatial Depletion Code for the IBM-7094," WCAP-3269-26, September 1963.

20. England, T. R., "CINDER - A One-Point Depletion and Fission Product Program," WAPD-TM-334, August 1962.

21. Eggleston, F. T., "Safety-Related Research and Development for Westinghouse Pressurized Water Reactors, Program Summaries - Winter 1977 - Summer 1978," WCAP-8768, Revision 2, October 1978.

22. Poncelet, C. G., "LASER - A Depletion Program for Lattice Calculations Based on MUFT and THERMOS," WCAP-6073, April 1966.

23. Olhoeft, J. E., "The Doppler Effect for a Non-Uniform Temperature Distribution in Reactor Fuel Elements," WCAP-2048, July 1962.

24. Nodvik, R. J., "Supplementary Report on Evaluation of Mass Spectrometric and Radiochemical Analyses of Yankee Core I Spent Fuel, Including Isotopes of Elements Thorium Through Curium," WCAP-6086, August 1969.

25. Drake, M. K. (Ed.), "Data Formats and Procedure for the ENDF/B Neutron Cross Section Library," BNL-50274, ENDF-102, Vol. 1, 1970.

26. Suich, J. E. and Honek, H. C., "The HAMMER System, Heterogeneous Analysis by Multigroup Methods of Exponentials and Reactors," DP-1064, January 1967.

27. Flatt, H. P. and Buller, D. C., "AIM-5, A Multigroup, One Dimensional Diffusion Equation Code," NAA-SR-4694, March 1960.

28. "Nuclear Design of Westinghouse Pressurized Water Reactors with Burnable Poison Rods," WCAP-7806, December 1971.

29. Nodvik, R. J., "Saxton Core II Fuel Performance Evaluation," WCAP-3385-56, Part II, "Evaluation of Mass Spectrometric and Radiochemical Materials Analyses of Irradiated Saxton Plutonium Fuel," July 1970.

30. Leamer, R. D., et al., "PuO2-UO2 Fueled Critical Experiments," WCAP-3726-1, July 1967.

31. Liu, Y. S., et al., "ANC: A Westinghouse Advanced Nodal Computer Code," WCAP-10965, December 1985.

32. Nguyen, T.Q., et.al., "Qualification of the PHOENIX-P/ANC Nuclear Design System for Pressurized Water Reactor Cores," WCAP-11596-P-A, June, 1988.

33. Not Used.

34. Jackson, E.W., et.al., "Qualification of Steady State Core Physics Methodology for Wolf Creek Design and Analysis", TR-91-0018 W01, December 1991.

35. Kersting P.J., et.al., "Assessment of Clad Flattening and Densification Power Spike Factor Elimination in Westinghouse Nuclear Fuel", WCAP-13589-A (Proprietary), March 1995.

36. Letter, N.J. Liparulo (W) to R.C. Jones (NRC), Subject: Response to Second Request for Additional Information on WCAP-13589, "Assessment of Clad Flattening and Densification Power Spike Factor Elimination in Westinghouse Nuclear Fuel," AW-94-751, dated November 7, 1994.

TABLE 4.3-1

REACTOR CORE DESCRIPTION

Active Core

Equivalent diameter, in.	132.7
Active fuel height, in.	143.7
Height-to-diameter ratio	1.08
Total cross section area, ft^2	96.06
H_2O/U molecular ratio, lattice, cold	2.41

Reflector Thickness and Composition

Top - water plus steel, in.	~10
Bottom - water plus steel, in.	~10
Side - water plus steel, in.	~15

Fuel Assemblies

Total Number in the Core	193						
Fuel Assembly Type	LOPAR (Standard)	V5H	V5H w/IFM	V5H w/IFM & PBG	V5H P+	V5H P+Z^{+2}	RFA Z^{+2} and RFA-2 Z^{+2}
Rod Array	17x17	17x17	17x17	17x17	17x17	17x17	17 x 17
Rods per assembly	264	264	264	264	264	264	264
Rod pitch, in.	0.496	0.496	0.496	0.496	0.496	0.496	0.496
Overall transverse dimensions, in.	8.426 x 8.426	8.426 x 8.426	8.426 x 8.426	8.426 x 8.426	8.426x 8.426	8.426x 8.426	8.426x 8.426
Fuel weight, as UO_2, lb. per assembly (Approximate)	1154	1154	1154	1149	1132	1138	1138
Zircaloy/ZIRLO/Optimized ZIRLO weight, lb. per assembly (Approximate)	264	270	275	278	275	274	274
Number of grids per assembly	8 - Type R	8	11	12	12	12	12
Composition of grids	Inconel-718	(see note 1)	(see note 2)	(see note 3)	(see note 4)	(see note 4)	(see note 4)
Weight of Zircaloy/ZIRLO grids in active core region, lb. per assembly (Approximate)	N/A	11.70	14.61	14.61	14.65	14.65	14.65
Weight of Inconel grids in active core region, lb. per assembly (Approximate)	12.04	2.22	2.22	2.22	2.22	2.22	2.22
Number of guide thimbles per assembly	24	24	24	24	24	24	24
Composition of guide thimbles	Zircaloy-4	Zircaloy-4	Zircaloy-4	Zircaloy-4	ZIRLO	ZIRLO	ZIRLO
Number of Instrument guide thimbles per assembly	1	1	1	1	1	1	1
Composition of Instrument tube	Zircaloy-4	Zircaloy-4	Zircaloy-4	Zircaloy-4	ZIRLO	ZIRLO	ZIRLO
Diameter of guide thimbles, upper part (above dashpot), in.	0.450 I.D. x 0.482 O.D.	0.442 I.D. x 0.474 O.D.	0.442 I.D. x 0.474 O.D.	0.442 I.D. x 0.474 O.D.	0.442 I.D. x 0.474 O.D.	0.442 I.D. x 0.474 O.D.	0.442 I.D. x 0.482 O.D
Diameter of guide thimbles, lower part (below dashpot), in.	0.397 I.D. x 0.429 O.D.	0.397 I.D. x 0.430 O.D.	0.397 I.D. x 0.430 O.D.	0.397 I.D. x 0.430 O.D.	0.397 I.D. x 0.430 O.D.	0.397 I.D. x 0.430 O.D.	0.397 I.D. x 0.439 O.D.
Diameter of Instrument guide thimbles, full length, in.	0.448 I.D. x 0.484 O.D.	0.440 I.D. x 0.476 O.D.	0.440 I.D. x 0.476 O.D.	0.440 I.D. x 0.476 O.D.	0.440 I.D. x 0.476 O.D.	0.440 I.D. x 0.476 O.D.	0.442 I.D. x 0.482 O.D.

Note (1) Eight total grids - 1 Inconel Top Grid, 1 Inconel Bottom Grid, 6 Zircaloy Mid Grids

Note (2) Eleven total grids - 1 Inconel Top Grid, 1 Inconel Bottom Grid, 6 Zircaloy Mid Grids, 3 Zircaloy IFM Grids

Note (3) Twelve total grids - 1 Inconel Top Grid, 1 Inconel Bottom Grid, 6 Zircaloy Mid Grids, 3 Zircaloy IFM Grids, 1 Inconel Protective Bottom Grid

Note (4) Twelve total grids - 1 Inconel Top Grid, 1 Inconel Bottom Grid, 6 ZIRLO Mid Grids, 3 ZIRLO IFM Grids, 1 Inconel Protective Bottom Grid

TABLE 4.3-1 (Sheet 2)

Fuel Rods			
Total Number fuel rods in the core		50,952	
Fuel Rod Type (applicable Fuel Assembly Type)		Standard (LOPAR and V5H)	Performance + (V5H P+, V5H P+Z^{+2}, RFA Z^{+2}, and RFA-2 Z^{+2})
Outside diameter, in.		0.374	0.374
Diameter gap, in.		0.0065	0.0065
Clad thickness, in.		0.0225	0.0225
Clad material		Zircaloy-4	ZIRLO or Optimized ZIRLO
Fuel Pellets			
Material		UO_2 sintered	
Density (percent of theoretical)		95	
Fuel enrichments (weight percent range)		2.1-5.0	
Diameter, in. (Typical)		0.3225	
Length, in. (Typical)		0.387	
Mass of UO_2 per foot of fuel rod, lb/ft		0.363	
Rod Cluster Control Assemblies			
Number of clusters, full length, in the core	53		
Neutron Absorber Material		Hafnium	Silver-Indium-Cadnium
Diameter, in.		0.341	0.341
Density, $lb/in.^3$		0.454	0.367
Cladding material		Type 304, cold worked stainless steel	Type 304, cold worked stainless steel
Clad thickness, in.		0.0185	0.0185
Number of absorber rods per cluster		24	24
Excess Reactivity (Initial Core)			
Maximum fuel assembly $K\infty$ (cold, clean unborated water)	1.39		
Maximum core reactivity (cold, zero power, beginning of cycle, zero soluble boron)	1.222		

TABLE 4.3-1 (Sheet 3)

Deleted Table

TABLE 4.3-2

NUCLEAR DESIGN PARAMETERS

Core average linear power, including densification effects, kW/ft	5.68
Total Heat flux hot channel factor, F_Q	2.50
Nuclear enthalpy rise hot channel factor, $F^N_{\Delta H}$	1.65

Reactivity Coefficients[a]	Design Limits (Sheet 1 Only)
Doppler-only power coefficients, see Figure 15.0-2	
(pcm/%power)[b]	
Upper curve	-19.4 to -12.7
Lower curve	-10.1 to -6.7
Doppler temperature coefficient (pcm/F)[b]	-3.5 to -1.0
Boron coefficient (pcm/ppm)[b]	-16 to -5
Moderator temperature coefficient (pcm/F)[b]	+6 to -50
Rodded moderator density (pcm/gm/cc)[b]	<47,000
Boron coefficient for boron dilution (pcm/ppm)[b]	
Modes 1, 2, and 3	-12.5
Modes 4 and 5	-14.0

TABLE 4.3-2 (Sheet 2)

Delayed Neutron Fraction and Prompt NeutronLifetime		
β_{eff} Limits: maximum at BOL, (minimum at EOL)		0.0075 (0.0044)
1* microsecond (Typical reload)		12.7 (BOL)
Control Rods		
Rod requirements		See Table 4.3-3
Maximum bank worth, pcm		<2000
Maximum ejected rod worth		See Chapter 15.0
Bank worth, HZP no overlap (pcm) (b)	BOL, Xe free (Reload)	EOL, Xe = Equ. (Reload)
Bank D	606	571
Bank C	645	999
Bank B	445	716
Bank A	396	5351
Typical Radial Factor (BOL to EOL)		
Unrodded		1.37 to 1.28
D bank		1.50 to 1.45
D + C banks		1.60 to 1.45
D + C + B banks		1.80 to 1.55

TABLE 4.3-2 (Sheet 3)

Boron Concentrations	
Zero power, k_{eff} = 0.99, cold[e] Typical Reload, all RCCA out, No Xenon, 3000 MWD/T	2050
Zero power, k_{eff} = 0.99, hot[f] Typical Reload, all RCCA out, No Xenon, 3000 MWD/T	2310
Design basis refueling boron concentration	See COLR
Zero power, k_{eff} < 0.95, cold[e] Typical Reload, all RCCA out, No Xenon, 3000 MWD/T	1960
Zero power, k_{eff} = 1.00, hot[e] Typical Reload, all RCCA out, No Xenon, 3000 MWD/T	2150
Full power, k_{eff} = 1.0 Typical Reload, all RCCA out, No Xenon, 3000 MWD/T	1950
Full power, k_{eff} = 1.0, Typical Reload, all RCCA out, No Xenon, 3000 MWD/T	1550
Reduction with fuel burnup	
First cycle (ppm/GWD/MTU)[c]	See Figure 4.3-3
Reload cycle (ppm/GWD/MTU)	~ 100

TABLE 4.3-2 (Sheet 4)

NOTES:

(a) Uncertainties are given in Section 4.3.3.3.

(b) 1 pcm = (percent mille) 10^{-5} $\Delta\rho$ where $\Delta\rho$ is calculated from two statepoint values of k_{eff} by In (k_1/k_2).

(c) Gigawatt day (GWD) = 1000 megawatt day (1,000 MWD). During the first cycle, fixed burnable poison rods are present which significantly reduce the boron letdown rate compared to reload cycles.

(d) Deleted

(e) Cold means 68°F, 1 atm.

(f) Hot means 557°F, 2250 psia.

TABLE 4.3-3

REACTIVITY REQUIREMENTS FOR ROD CLUSTER CONTROL ASSEMBLIES

Reactivity Effects (percent)	Beginning-of-Life (First Cycle)	End-of-Life (First Cycle)	End-of-Life (Typical Reload Cycle)
1. Control requirements			
Fuel temperature, Doppler (%Δρ)	1.37	1.21	
Moderator temperature (%Δρ)[a]	0.15	1.15	
Redistribution (%Δρ)	0.50	0.85	
Rod insertion allowance (%Δρ)	0.50	0.50	
2. Total control (%Δρ)	2.52	3.71	3.29
3. Estimated rod cluster control assembly worth (53 rods)			
a. All full length assemblies inserted (%Δρ)	7.54	7.42	Not Required
b. All but one (highest worth) assemblies inserted (%Δρ)	6.46	6.39	5.74

Rev. 13

TABLE 4.3-3 (Sheet 2)

Reactivity Effects (percent)	Beginning-of-Life (First Cycle)	End-of-Life (First Cycle)	End-of-Life (Typical Reload Cycle)
4. Estimated rod cluster control assembly credit with 10 percent adjustment to accomodate uncertainties, 3b - 10 precent (%$\Delta\rho$)	5.82	5.75	5.17
5. Shutdown margin available 4-2 (%$\Delta\rho$)	3.30	2.04	1.88 (b)

NOTES:

(a) Includes void effects.

(b) The design basis minimum shutdown is 1.3 percent.

TABLE 4.3-4

BENCHMARK CRITICAL EXPERIMENTS

Description of Experiments*	Number of Experiments	LEOPARD k_{eff} Using Experimental Bucklings
UO_2		
Al clad	14	1.0012
SS clad	19	0.9963
Borated H_2O	7	0.9989
Subtotal	40	0.9985
U-Metal		
Al clad	41	0.9995
Unclad	20	0.9990
Subtotal	61	0.9993
Total	101	0.9990

* Reported in Reference 12.

TABLE 4.3-5

AXIAL STABILITY INDEX PRESSURIZED WATER
REACTOR CORE WITH A 12-FOOT HEIGHT

Burnup (MWD/MTU)	F_Z	C_B (ppm)	Stability Index (hr^{-1}) Exp	Calc
1550	1.34	1065	-0.041	-0.032
7700	1.27	700	-0.014	-0.006
5090*			-0.0325	-0.0255

RADIAL STABILITY INDEX

2250**			-0.068	-0.07

* 4-loop plant, 12-foot core in Cycle 1, axial stability test.
** 4-loop plant, 12-foot core in Cycle 1, radial (X-Y) stability test.

Table 4.3-6

ARO Moderator Temperature Coefficients versus Average Moderator Temperature and Burnup

			Average Moderator Temperature (Deg. F)				
		Power:	0	25%	50%	75%	100%
		Core Avg Temp.:	557	565.3	573.4	581.4	589.1
GWD/T	PPM	RCS Avg Temp.:	557	564.3	571.6	579.1	586.5
0.150	2500		4.86	3.89	2.72	1.39	-0.22
0.150	2000		1.20	0.04	-1.35	-2.90	-4.74
0.150	1500		-2.90	-4.28	-5.87	-7.66	-9.72
3	2500		5.60	4.55	3.28	1.82	0.04
3	2000		1.79	0.53	-0.97	-2.66	-4.67
3	1500		-2.50	-3.97	-5.70	-7.61	-9.84
10	1500		-4.83	-6.68	-8.81	-11.15	-13.86
10	1000		-9.74	-11.80	-14.13	-16.67	-19.52
10	500		-15.21	-17.49	-20.02	-22.76	-25.78
21.4	1000		-12.28	-14.72	-17.51	-20.64	-24.08
21.4	500		-17.85	-20.51	-23.52	-26.78	-30.22
21.4	0		-24.22	-27.12	-30.32	-33.65	-37.15

ARO, HFP Equilibrium Xenon

TABLE 4.3-7

COMPARISON OF MEASURED AND CALCULATED DOPPLER DEFECTS

Plant	Fuel Type	Core Burnup (MWD/MTU)	Measured (pcm)*	Calculated (pcm)
1	Air-filled	1800	1700	1710
2	Air-filled	7700	1300	1440
3	Air and helium-filled	8460	1200	1210

* pcm = 10^5 x ln (k_1/k_2)

TABLE 4.3-8

SAXTON CORE II ISOTOPICS
ROD MY, AXIAL ZONE 6

Atom Ratio	Measured (a)	2σ Precision (%)	LEOPARD Calculation
U-234/U	4.65×10^{-5}	±29	4.60×10^{-5}
U-235/U	5.74×10^{-3}	±0.9	5.73×10^{-3}
U-236/U	3.55×10^{-4}	±5.6	3.74×10^{-4}
U-238/U	0.99386	±0.01	0.99385
Pu-238/Pu	1.32×10^{-3}	±2.3	1.222×10^{-3}
Pu-239/Pu	0.73971	±0.03	0.74497
Pu-240/Pu	0.19302	±0.2	0.19102
Pu-241/Pu	6.014×10^{-2}	±0.3	5.74×10^{-2}
Pu-242/Pu	5.81×10^{-3}	±0 9	5.38×10^{-3}
Pu/U (b)	5.938 x 10-2	±0.7	5.970×10^{-2}
Np-237/U-238	1.14×10^{-4}	±15	0.86×10^{-4}
Am-241/Pu-239	1.23×10^{-2}	±15	1.08×10^{-2}
Cm-242/Pu-239	1.05×10^{-4}	±10	1.11×10^{-4}
Cm-244/Pu-239	1.09×10^{-4}	±20	0.98×10^{-4}

NOTES:
(a) Reported in Reference 29.
(b) Weight ratio.

TABLE 4.3-9

CRITICAL BORON CONCENTRATIONS, HZP, BOL

Plant Type	Measured	Calculated
2-loop, 121 assemblies 10-foot core	1583	1589
2-loop, 121 assemblies 12-foot core	1625	1624
2-loop, 121 assemblies 12-foot core	1517	1517
3-loop, 157 assemblies 12-foot core	1169	1161

TABLE 4.3-10

COMPARISON OF MEASURED AND CALCULATED ROD WORTH

2-Loop Plant, 121 Assemblies, 10-Foot Core	Measured (pcm)	Calculated (pcm)
Group B	1885	1893
Group A	1530	1649
Shutdown group	3050	2917
ESADA Critical*, 0.69" Pitch, 2 w/o PuO_2, 8% Pu-240, 9 Control Rods		
6.21" rod separation	2250	2250
2.07" rod separation	4220	4160
1.38" rod separation	4100	4019

* Reported in Reference 30.

TABLE 4.3-11

COMPARISON OF MEASURED AND CALCULATED MODERATOR COEFFICIENTS AT HZP, BOL

Plant Type/ Control Bank Configuration	Measured γ_{iso}* (pcm/F)	Calculated γ_{iso} (pcm/F)
3-loop, 157 assemblies, 12-foot core		
D at 160 steps	-0.50	-0.50
D in, C at 190 steps	-3.01	-2.75
D in, C at 28 steps	-7.67	-7.02
B, C, and D in	-5.16	-4.45
2-loop, 121 assemblies, 12-foot core		
D at 180 steps	+0.85	+1.02
D in, C at 180 steps	-2.40	-1.90
C and D in, B at 165 steps	-4.40	-5.58
B, C, and D in, A at 174 steps	-8.70	-8.12
4-loop, 193 assemblies, 12-foot core		
ARO	-0.52	-1.2
D in	-4.35	-5.7
D and C in	-8.59	-10.0
D, C, and B in	-10.14	-10.55
D, C, B, and A in	-14.63	-14.45

* Isothermal coefficients, which include the Doppler effect in the fuel.

$$\gamma_{iso} = 10^5 \ln\frac{k_2}{k_1}/\Delta T°F$$

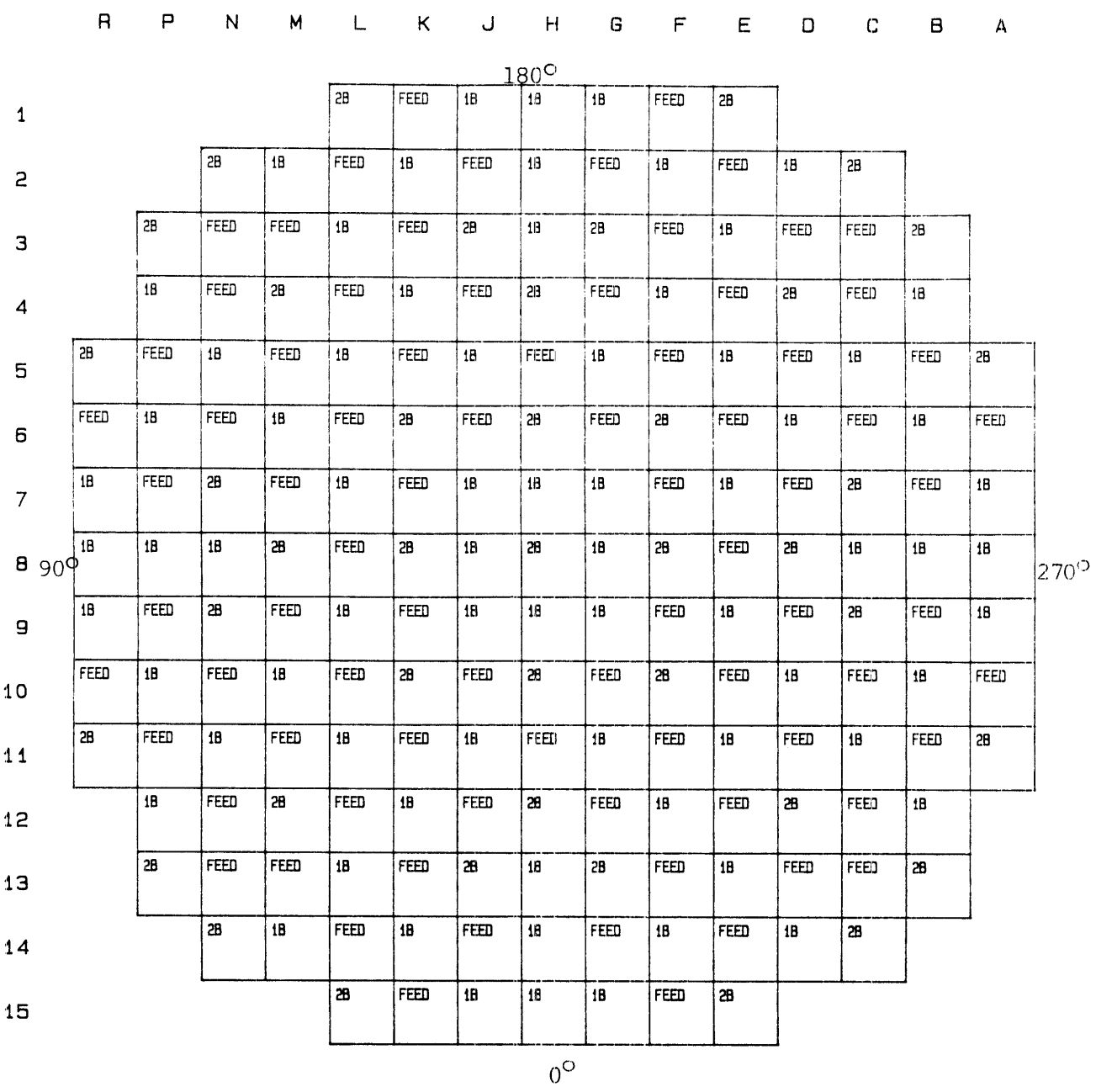

1B = Once Burnt
2B = Twice Burnt

Rev. 4

WOLF CREEK
UPDATED SAFETY ANALYSIS REPORT

FIGURE 4.3-1

TYPICAL CORE LOADING PATTERN

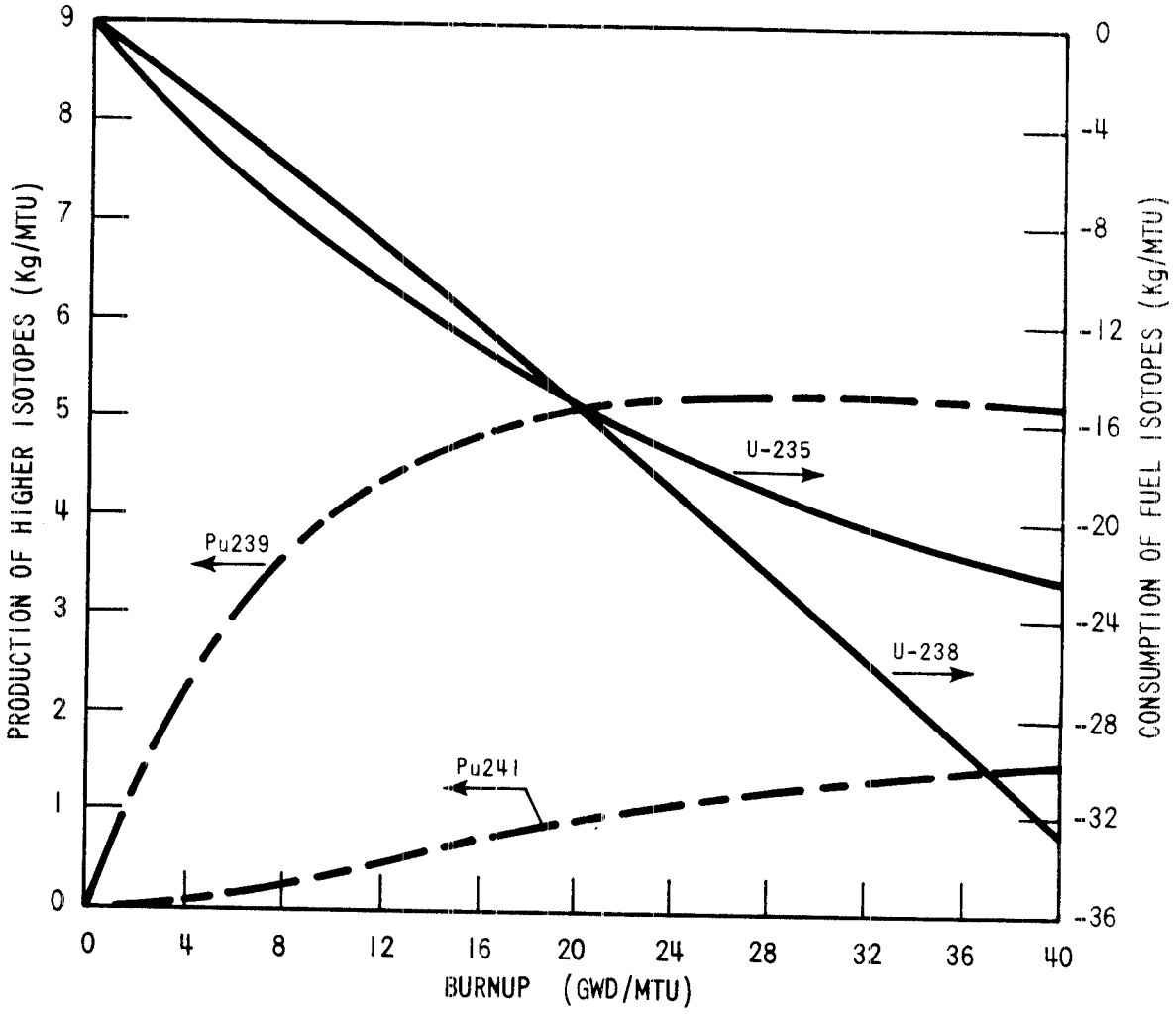

Rev. 0

WOLF CREEK
UPDATED SAFETY ANALYSIS REPORT

FIGURE 4.3-2

PRODUCTION AND CONSUMPTION OF HIGHER ISOTOPES

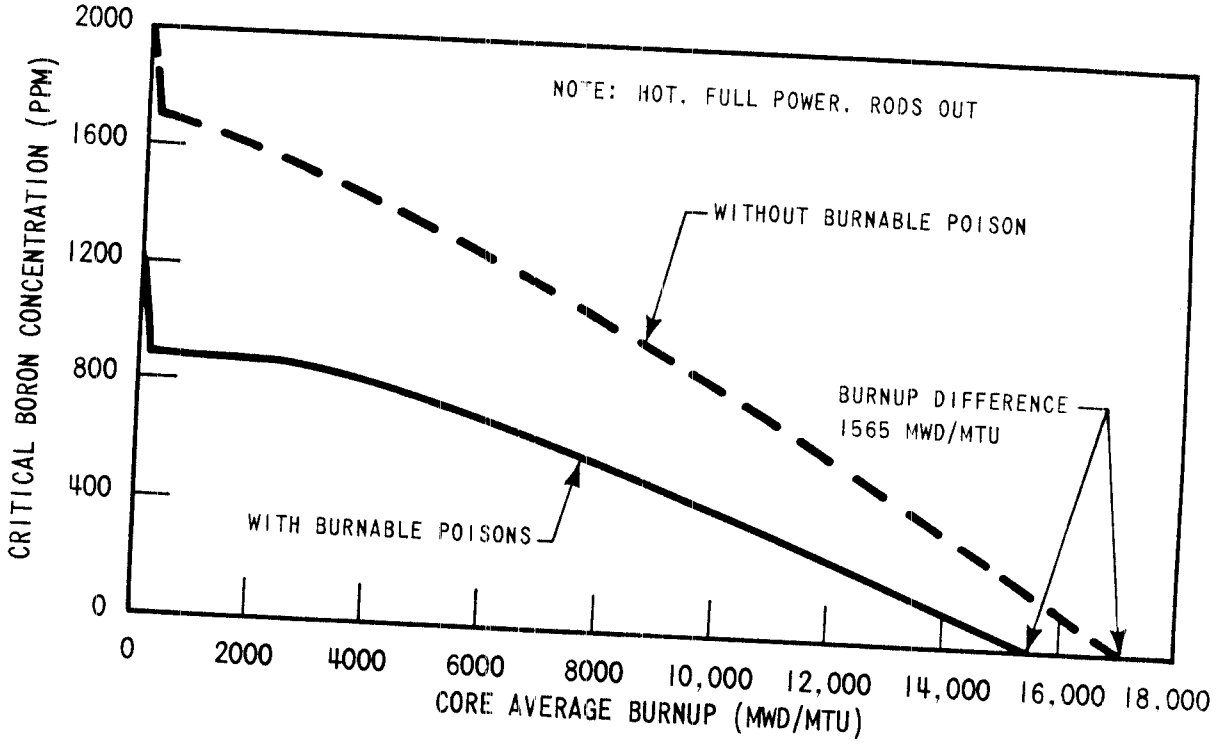

Rev. 0

WOLF CREEK
UPDATED SAFETY ANALYSIS REPORT

FIGURE 4.3-3

BORON CONCENTRATION VERSUS FIRST CYCLE BURNUP WITH AND WITHOUT BURNABLE POISON RODS

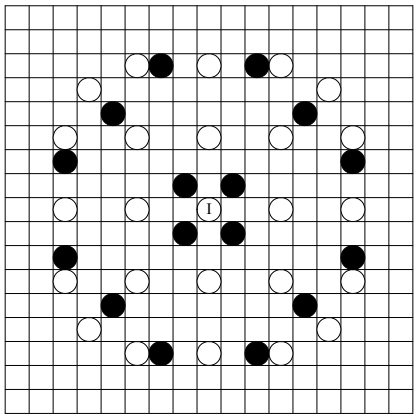

16 IFBA Pattern

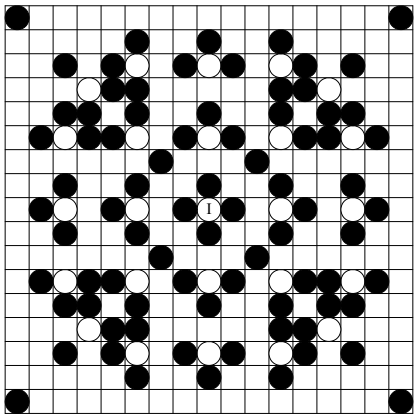

80 IFBA Pattern

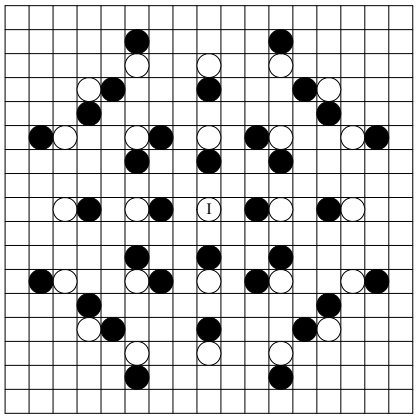

32 IFBA Pattern

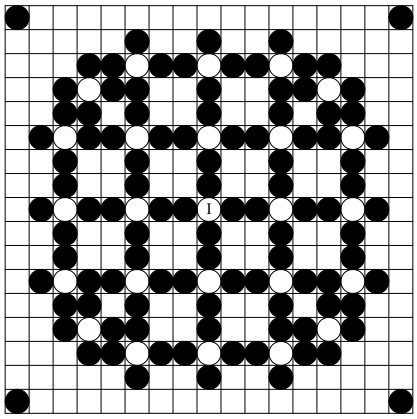

104 IFBA Pattern

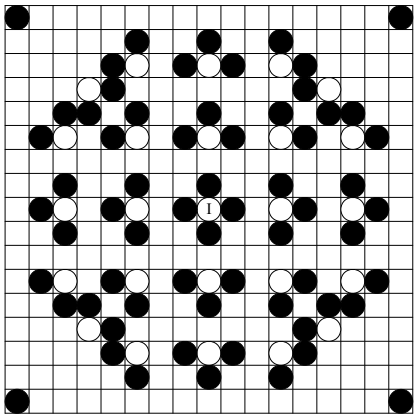

64 IFBA Pattern

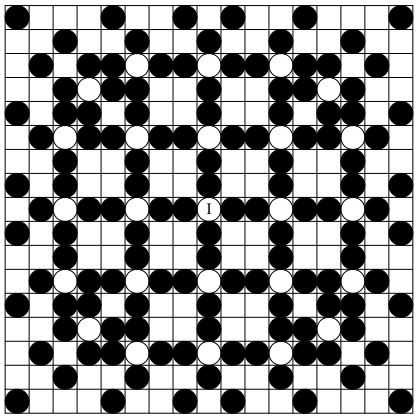

128 IFBA Pattern

- GUIDE TUBE
- I - INST. TUBE
- IFBA

Rev. 16

WOLF CREEK UPDATED SAFETY ANALYSIS REPORT
FIGURE 4.3-4 TYPICAL INTEGRAL FUEL BURNABLE ABSORBER ROD ARRANGEMENT WITHIN AN ASSEMBLY

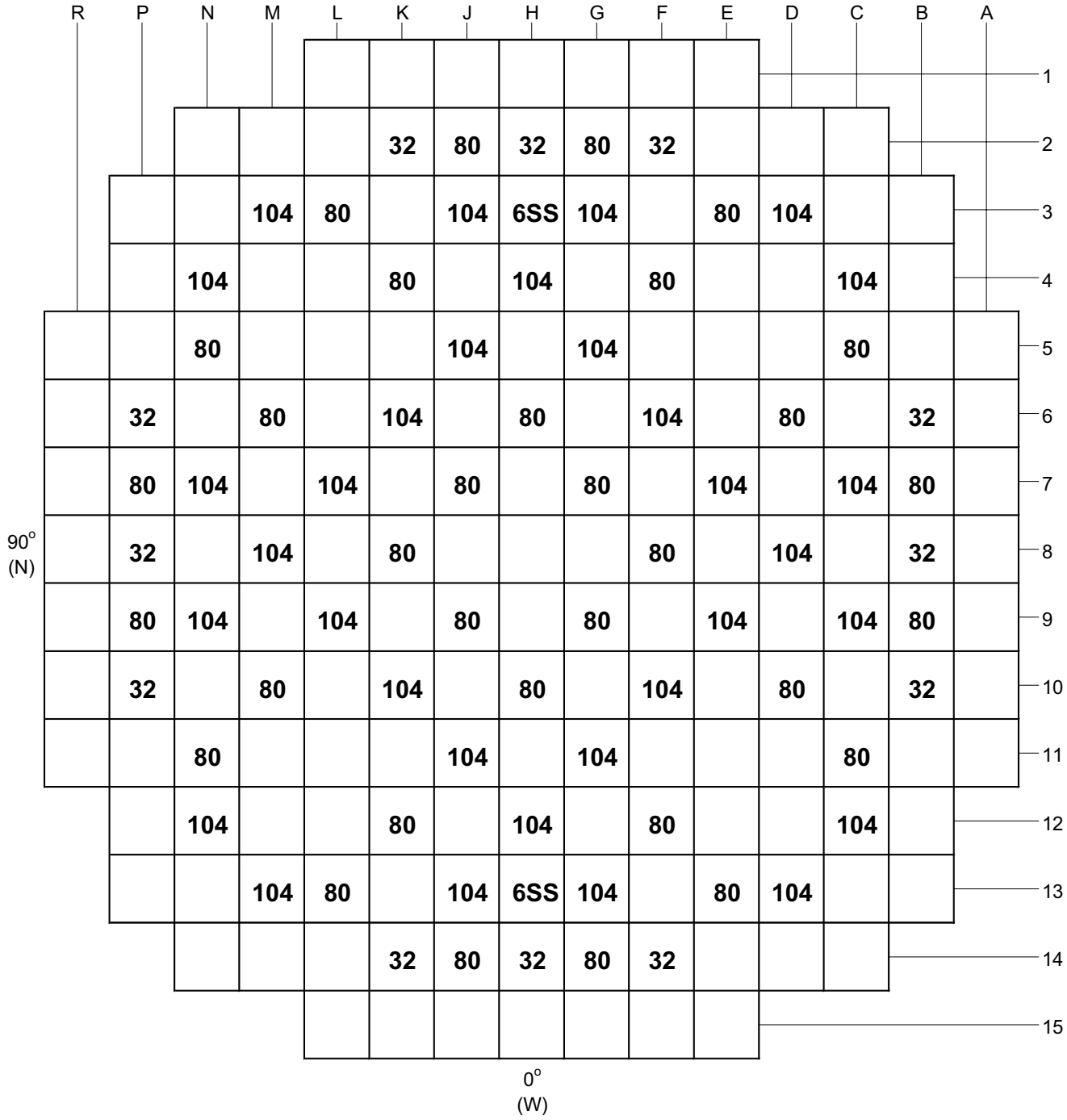

Rev. 13

WOLF CREEK
UPDATED SAFETY ANALYSIS REPORT

FIGURE 4.3-5

TYPICAL INTEGRAL FUEL BURNABLE ABSORBER AND

SOURCE ASSEMBLY LOCATIONS

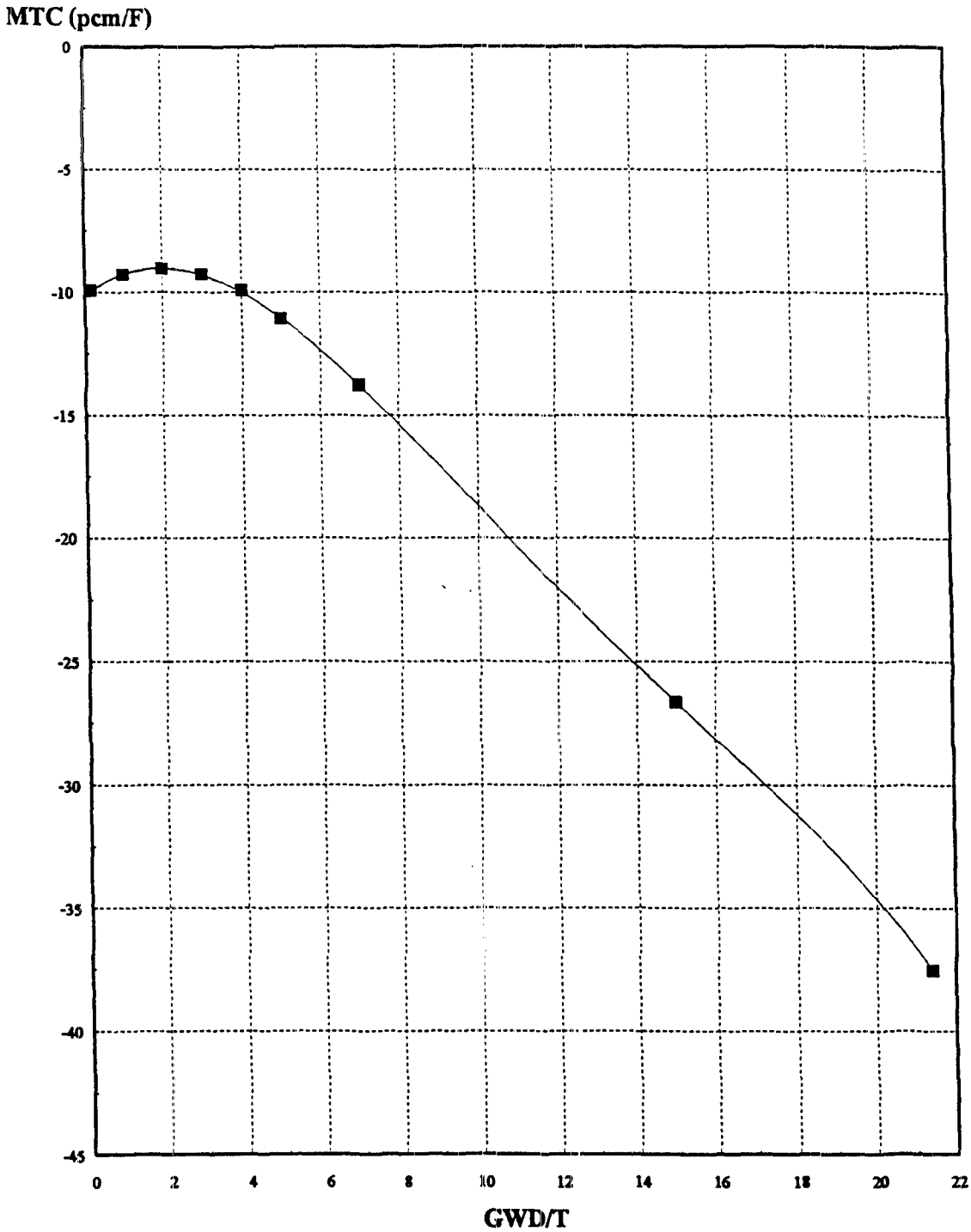

Rev. 11

WOLF CREEK UPDATED SAFETY ANALYSIS REPORT
FIGURE 4.3-6 MTC VS BURNUP at HFP, ARO CRITICAL CONDITIONS (TYPICAL)

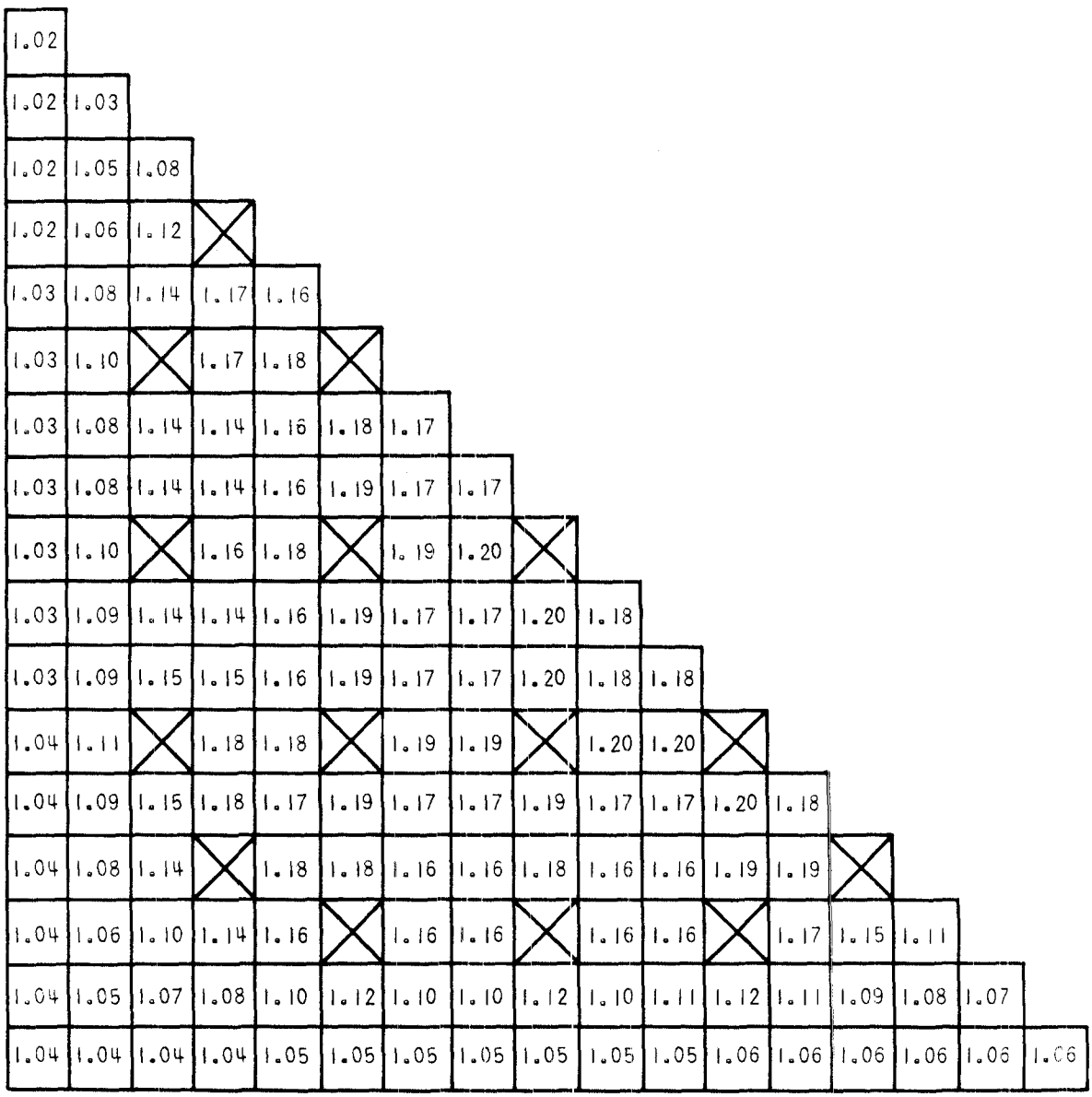

Rev. 0

WOLF CREEK
UPDATED SAFETY ANALYSIS REPORT

FIGURE 4.3-12

RODWISE POWER DISTRIBUTION IN A TYPICAL ASSEMBLY NEAR BEGINNING-OF-LIFE, HOT FULL POWER, EQUILIBRIUM XENON, UNRODDED CORE

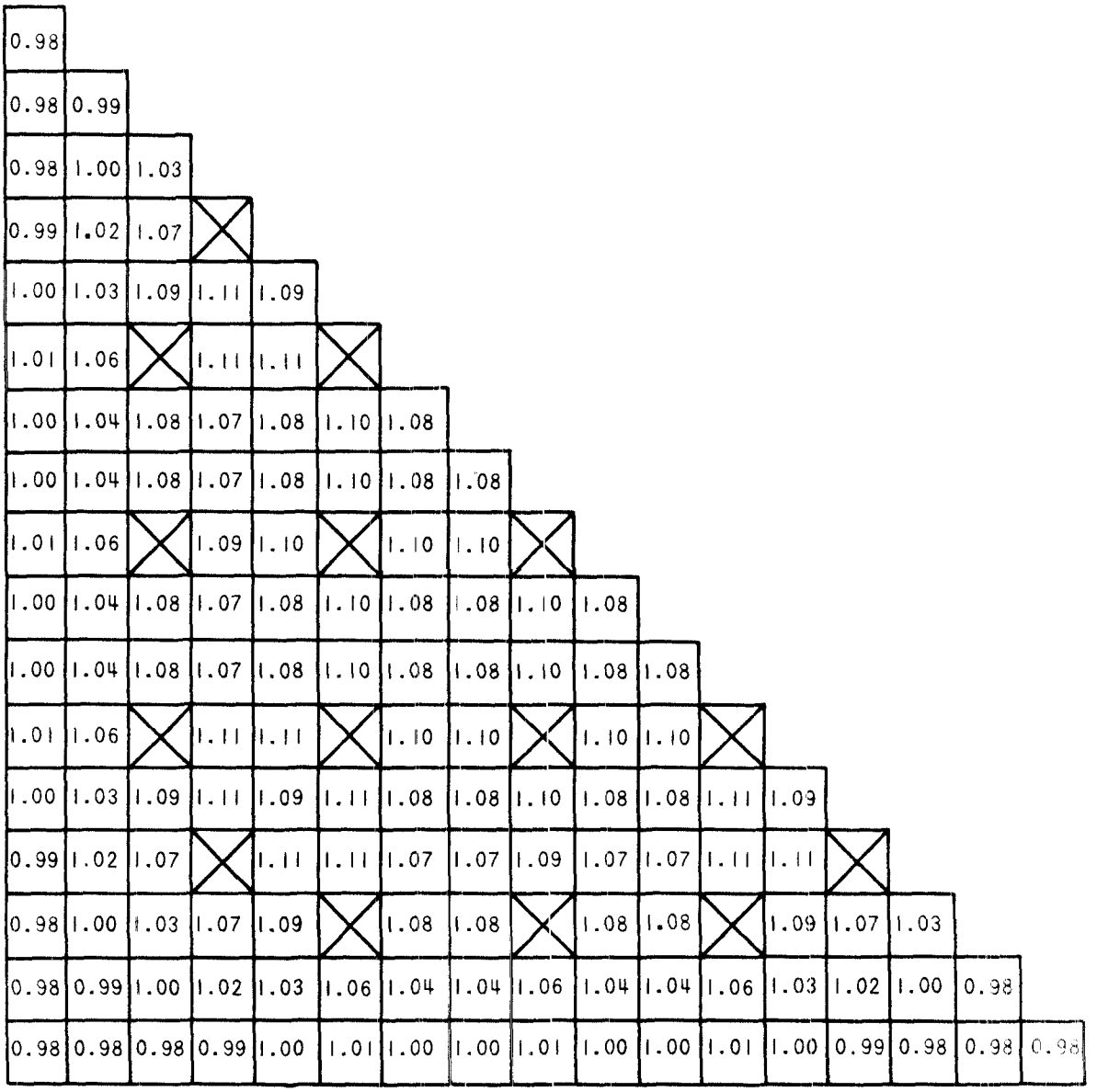

Rev. 0

WOLF CREEK
UPDATED SAFETY ANALYSIS REPORT

FIGURE 4.3-13

RODWISE POWER DISTRIBUTION IN A TYPICAL ASSEMBLY NEAR END-OF-LIFE, HOT FULL POWER, EQUILIBRIUM XENON, UNRODDED CORE

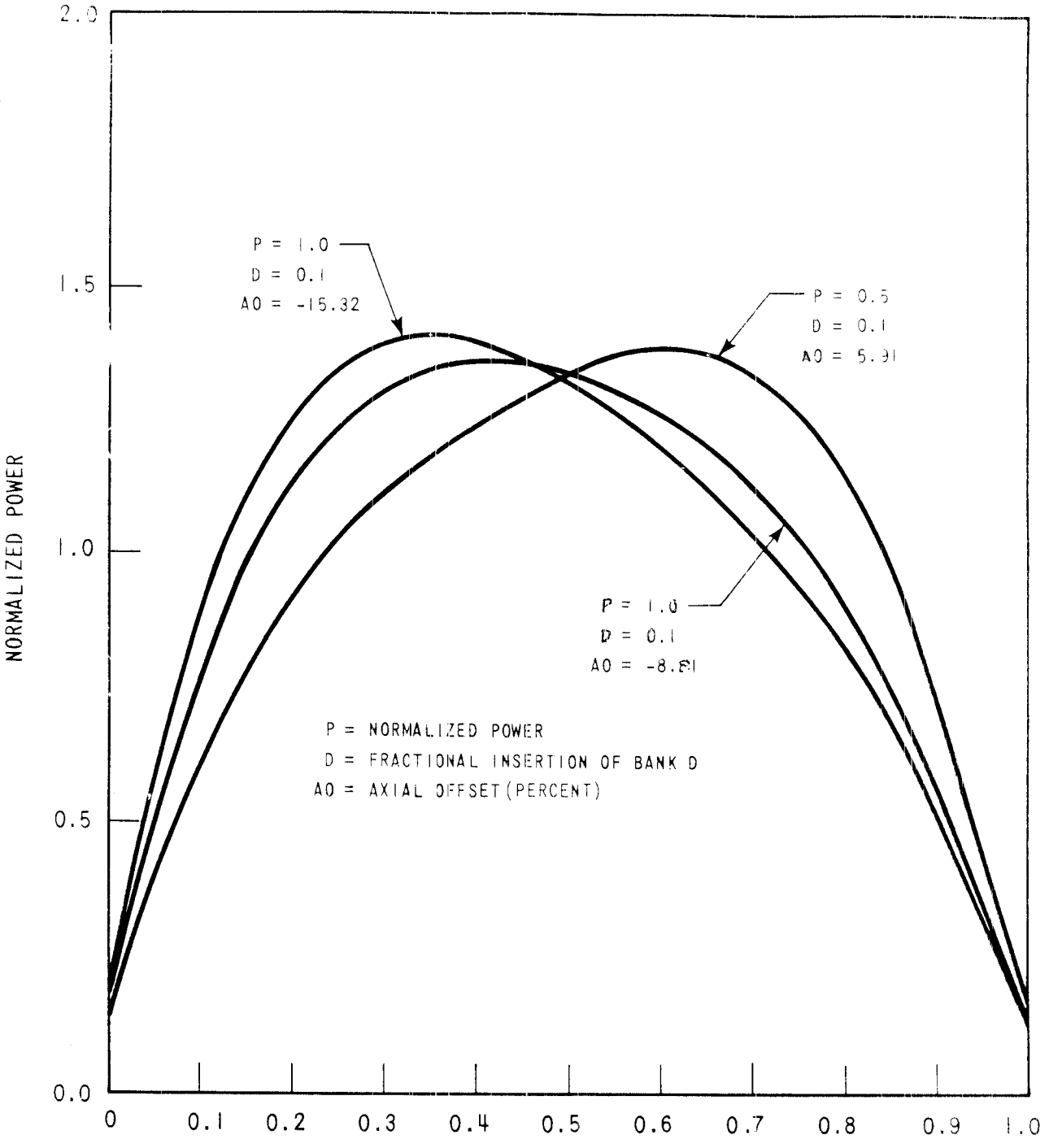

Rev. 0

WOLF CREEK
UPDATED SAFETY ANALYSIS REPORT

FIGURE 4.3-14

TYPICAL AXIAL POWER SHAPES
OCCURRING AT BEGINNING-OF-LIFE

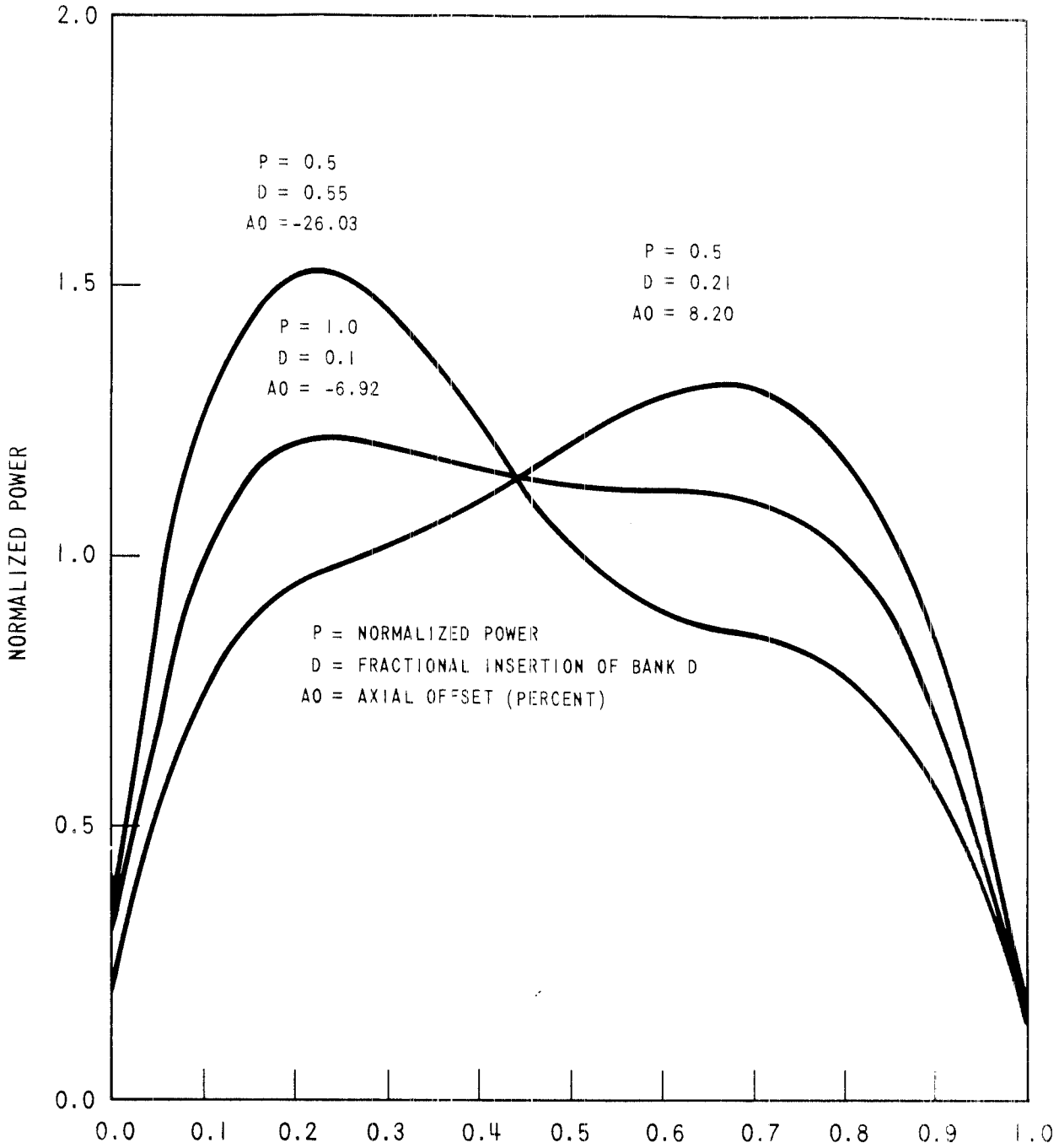

Rev. 0

WOLF CREEK
UPDATED SAFETY ANALYSIS REPORT

FIGURE 4.3-15

TYPICAL AXIAL POWER SHAPES
OCCURRING AT MIDDLE-OF-LIFE

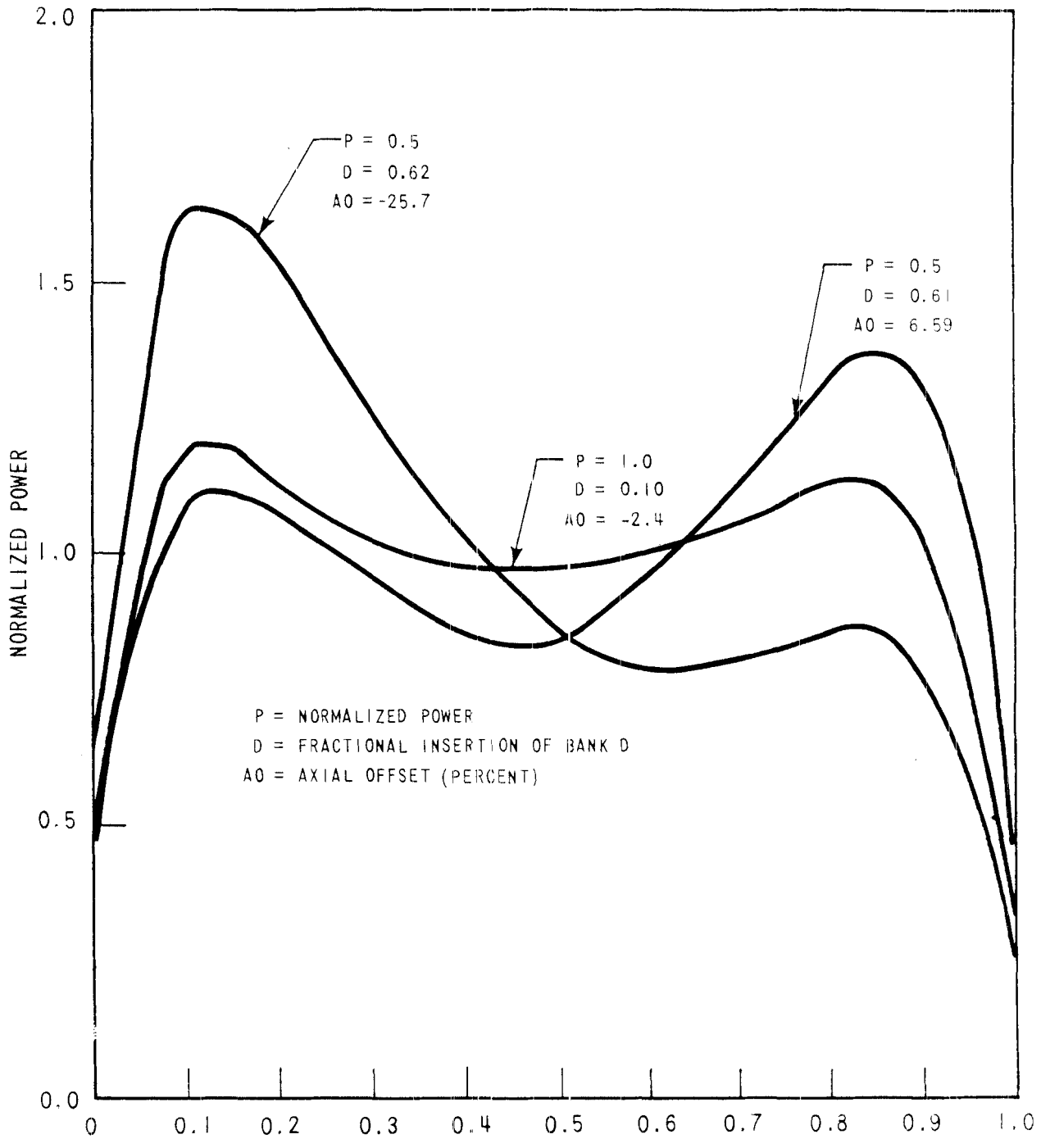

Rev. 0

WOLF CREEK
UPDATED SAFETY ANALYSIS REPORT

FIGURE 4.3-16

TYPICAL AXIAL POWER SHAPES
OCCURRING AT END-OF-LIFE

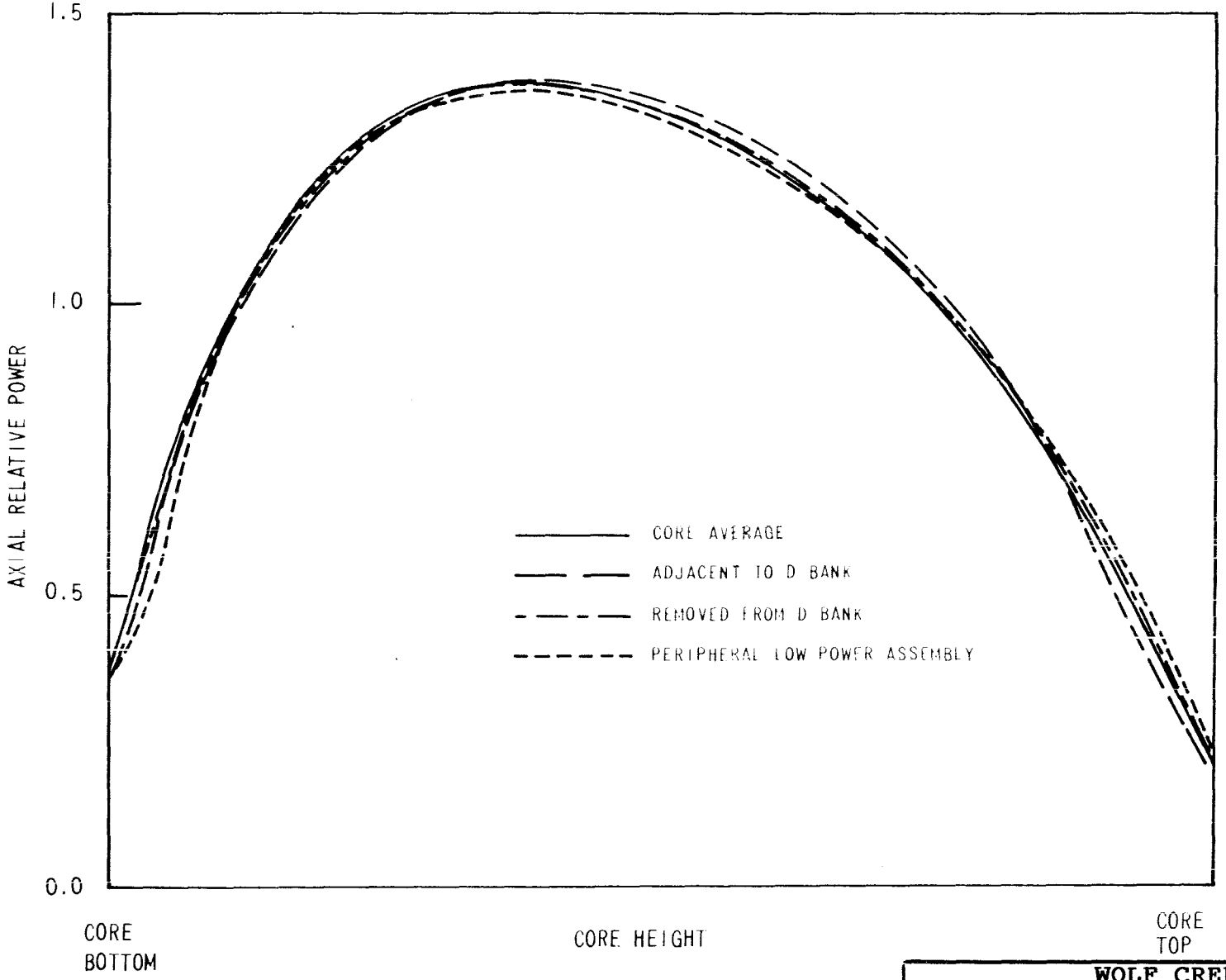

WOLF CREEK
UPDATED SAFETY ANALYSIS REPORT

FIGURE 4.3-17

COMPARISON OF A TYPICAL ASSEMBLY AXIAL POWER DISTRIBUTION WITH CORE AVERAGE AXIAL DISTRIBUTION BANK D SLIGHTLY INSERTED

K(Z)-NORMALIZED PEAKING FACTOR VS. CORE HEIGHT

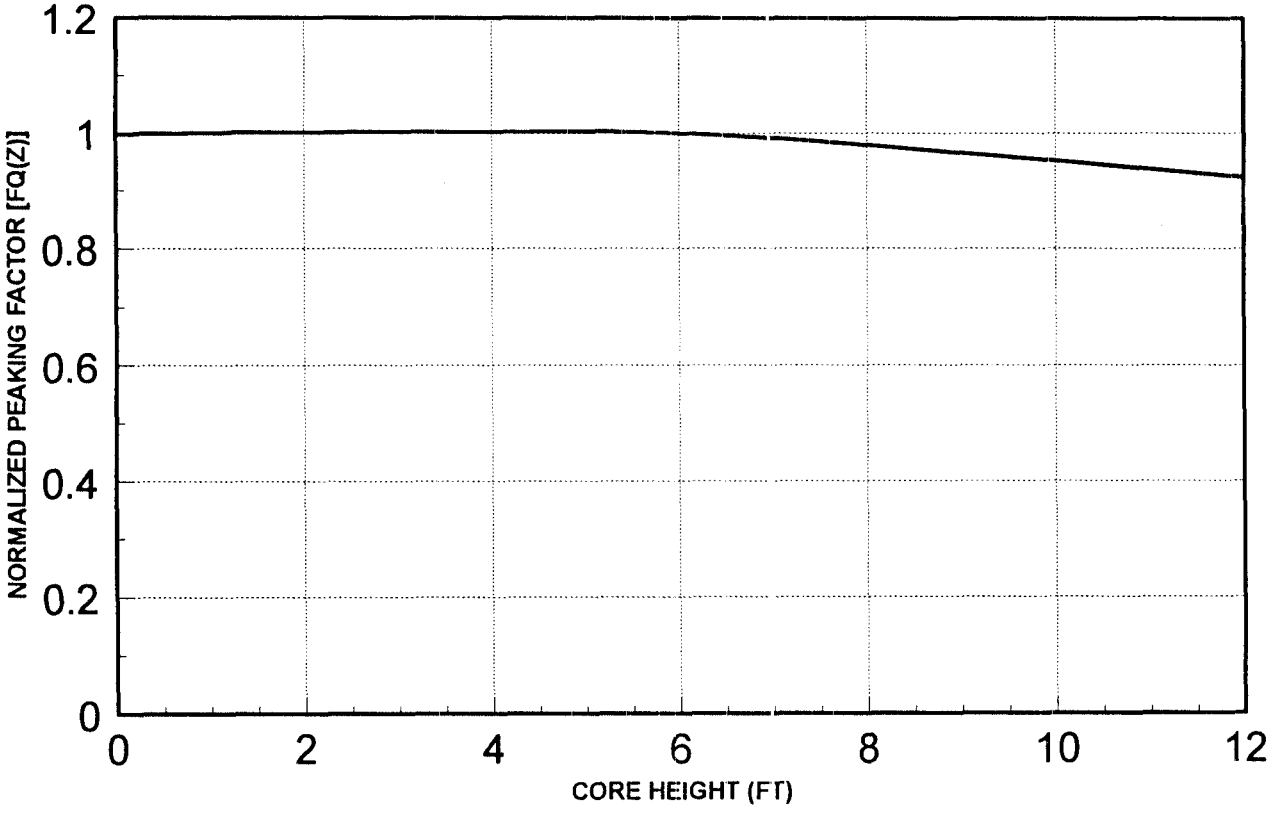

FQT=2.50	
Elevation (ft)	k(z)
0.0	1.0
6.0	1.0
12.0	0.925

Rev. 7

WOLF CREEK
UPDATED SAFETY ANALYSIS REPORT

FIGURE 4.3-21
MAXIMUM FQX POWER VERSUS AXIAL
HEIGHT DURING NORMAL OPERATION

WOLF CREEK

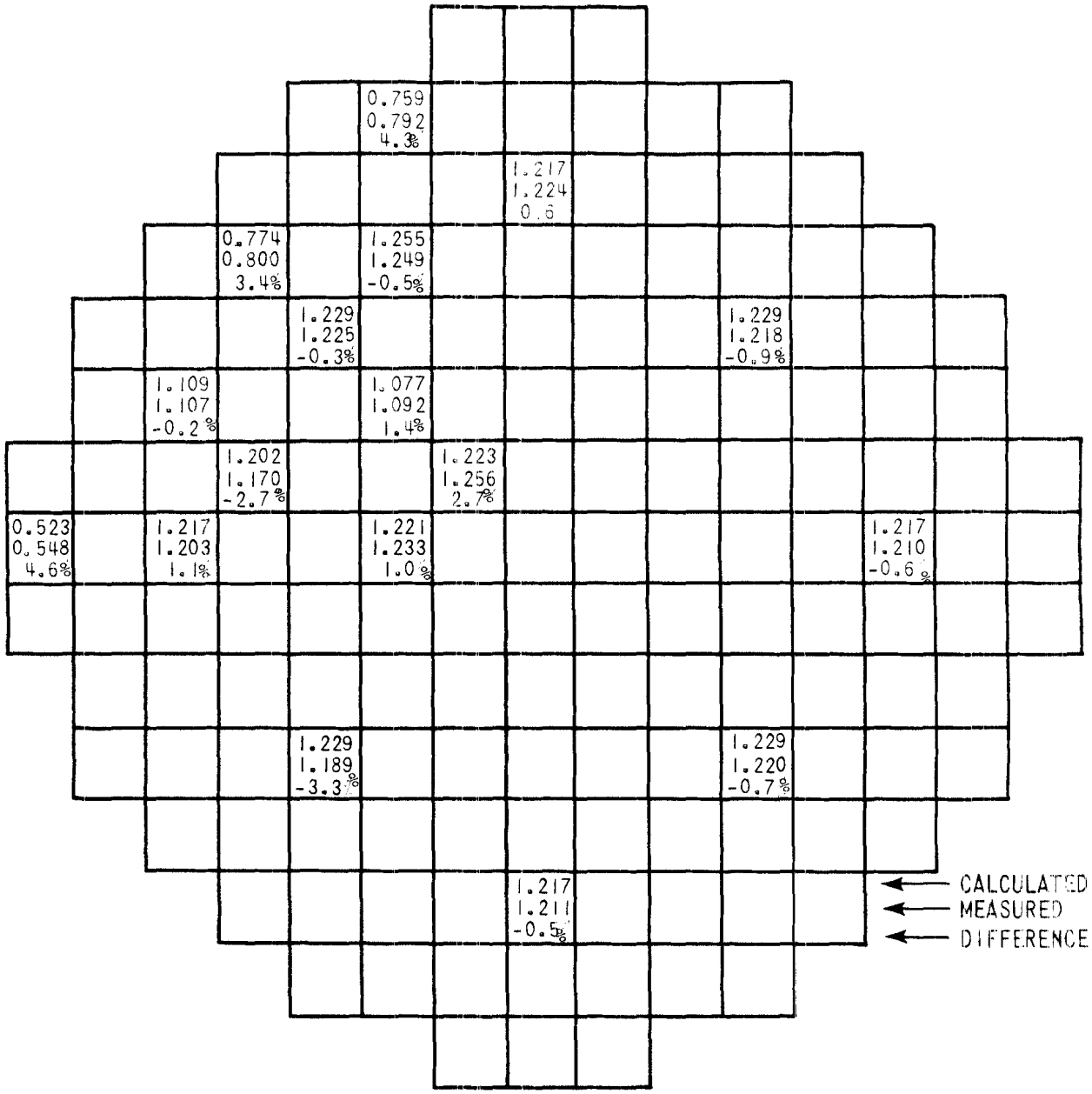

PEAKING FACTORS

$\bar{F}_z$ = 1.5

$F^N_{\Delta H}$ = 1.357

F^N_Q = 2.07

Rev. 0

WOLF CREEK
UPDATED SAFETY ANALYSIS REPORT

FIGURE 4.3-24

COMPARISON BETWEEN CALCULATED AND MEASURED RELATIVE FUEL ASSEMBLY POWER DISTRIBUTION

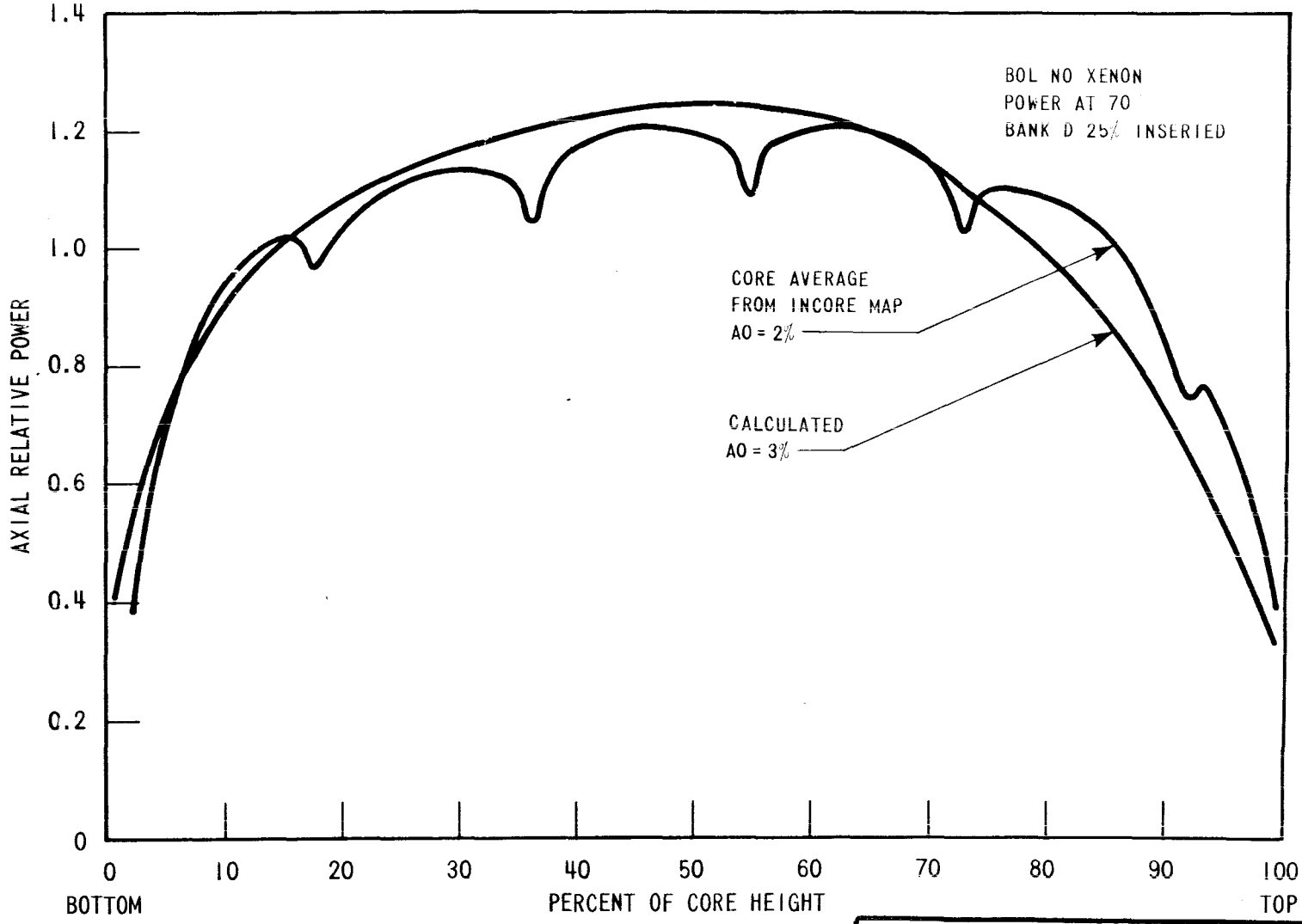

Rev. 0

WOLF CREEK
UPDATED SAFETY ANALYSIS REPORT

FIGURE 4.3-25

COMPARISON OF TYPICAL CALCULATED AND MEASURED AXIAL SHAPES

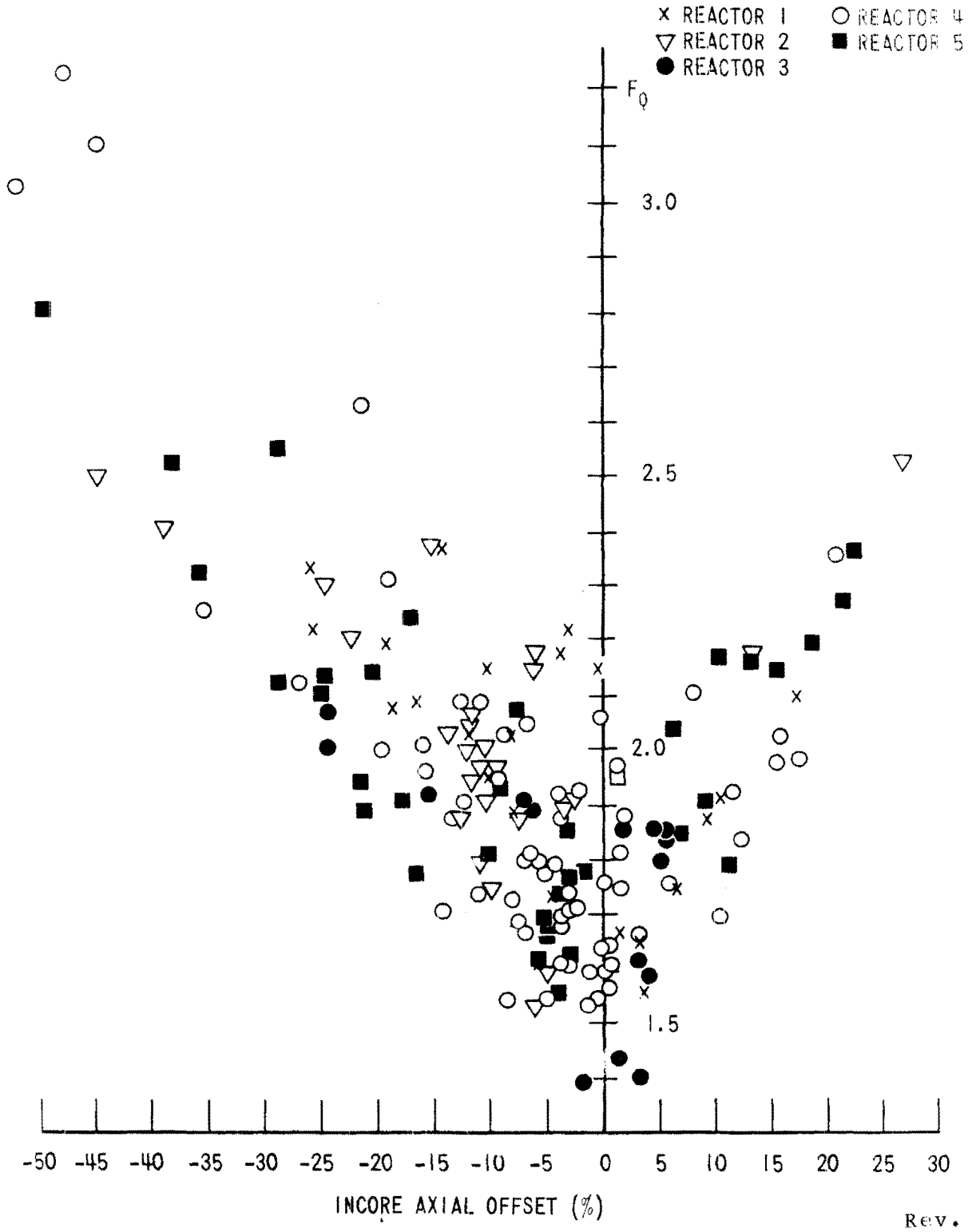

Rev. 0

WOLF CREEK
UPDATED SAFETY ANALYSIS REPORT

FIGURE 4.3-26

MEASURED VALUES OF F_Q FOR FULL POWER ROD CONFIGURATIONS

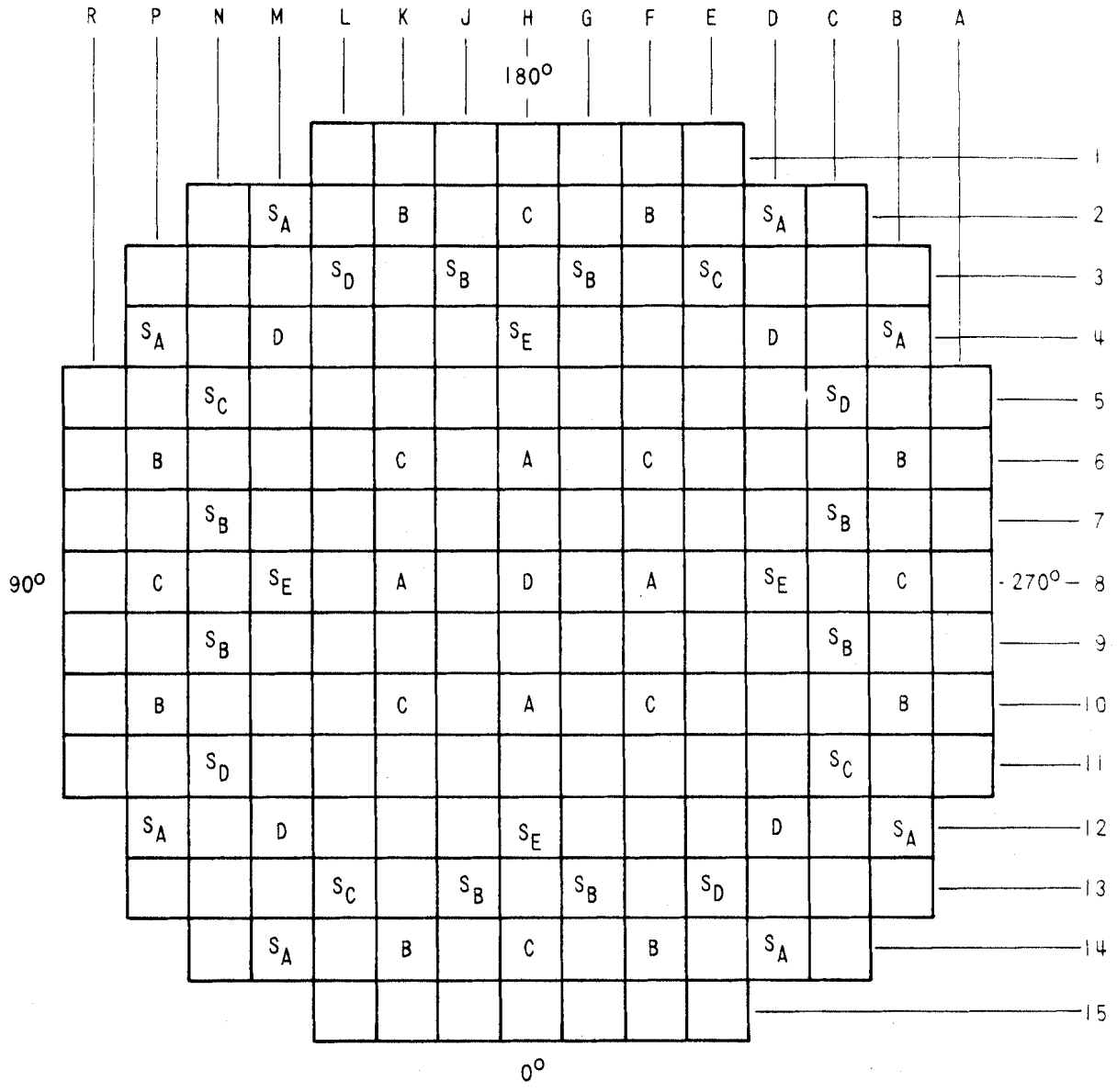

CONTROL BANK	NUMBER OF RODS
A	4
B	8
C	8
D	5
TOTAL	25

SHUTDOWN BANK	NUMBER OF RODS
S_A	8
S_B	8
S_C	4
S_D	4
S_E	4
TOTAL	28

Rev. 0

WOLF CREEK
UPDATED SAFETY ANALYSIS REPORT

FIGURE 4.3-36

ROD CLUSTER CONTROL ASSEMBLY PATTERN

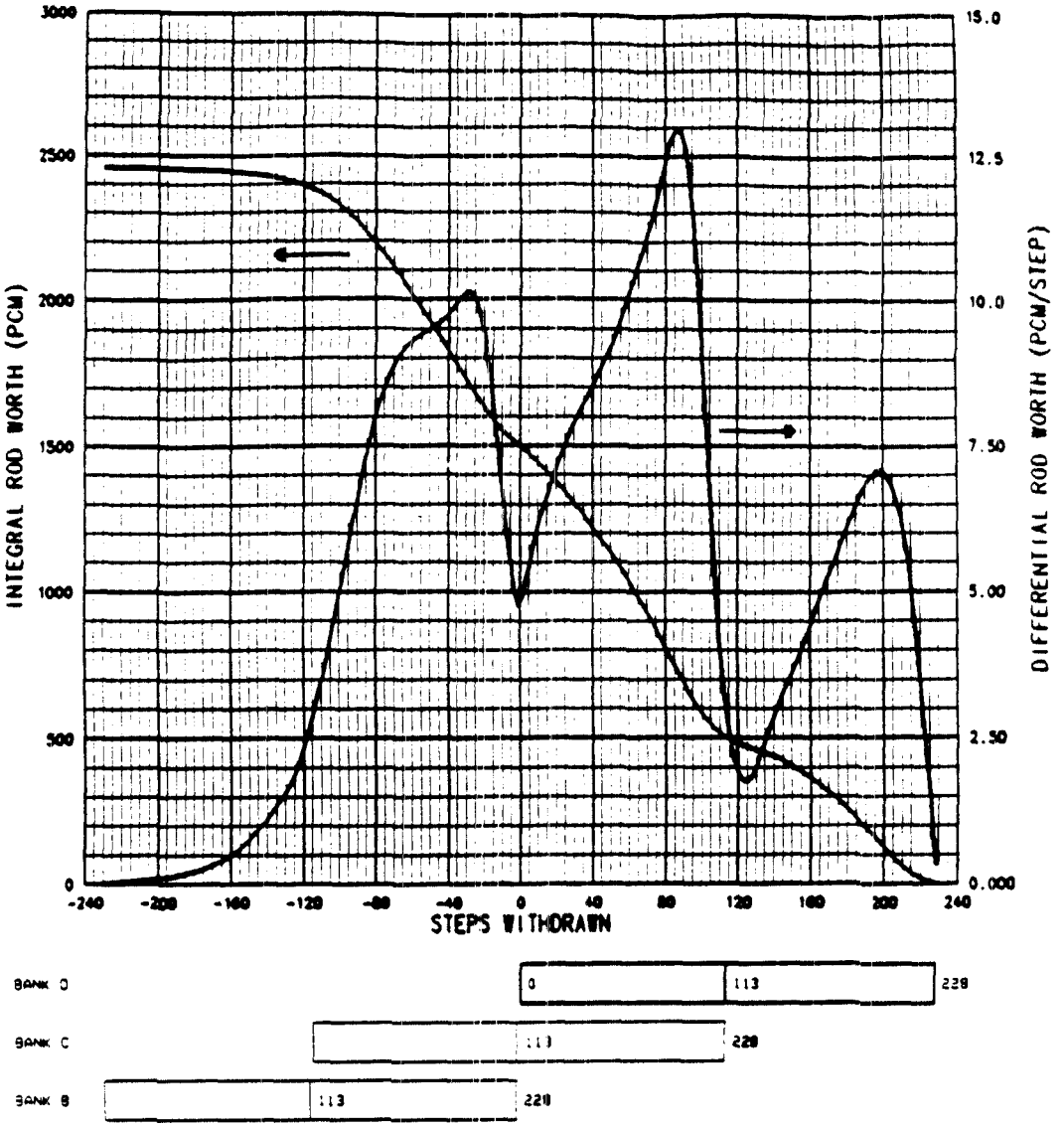

DIFFERENTIAL AND INTEGRAL ROD WORTH VERSUS STEPS WITHDRAWN AT EOL, HZP, HFP EQ XENON, BANKS D, C, AND B MOVING WITH 113 STEP OVERLAP

Rev. 4

WOLF CREEK UPDATED SAFETY ANALYSIS REPORT
FIGURE 4.3-37 EXAMPLE DIFFERENTIAL AND INTEGRAL ROD WORTH VERSUS STEPS WITHDRAWN AT MOL, HZP, HFP, EQ XENON BANKS, D, C, AND B MOVING WITH 113 STEP OVERLAP

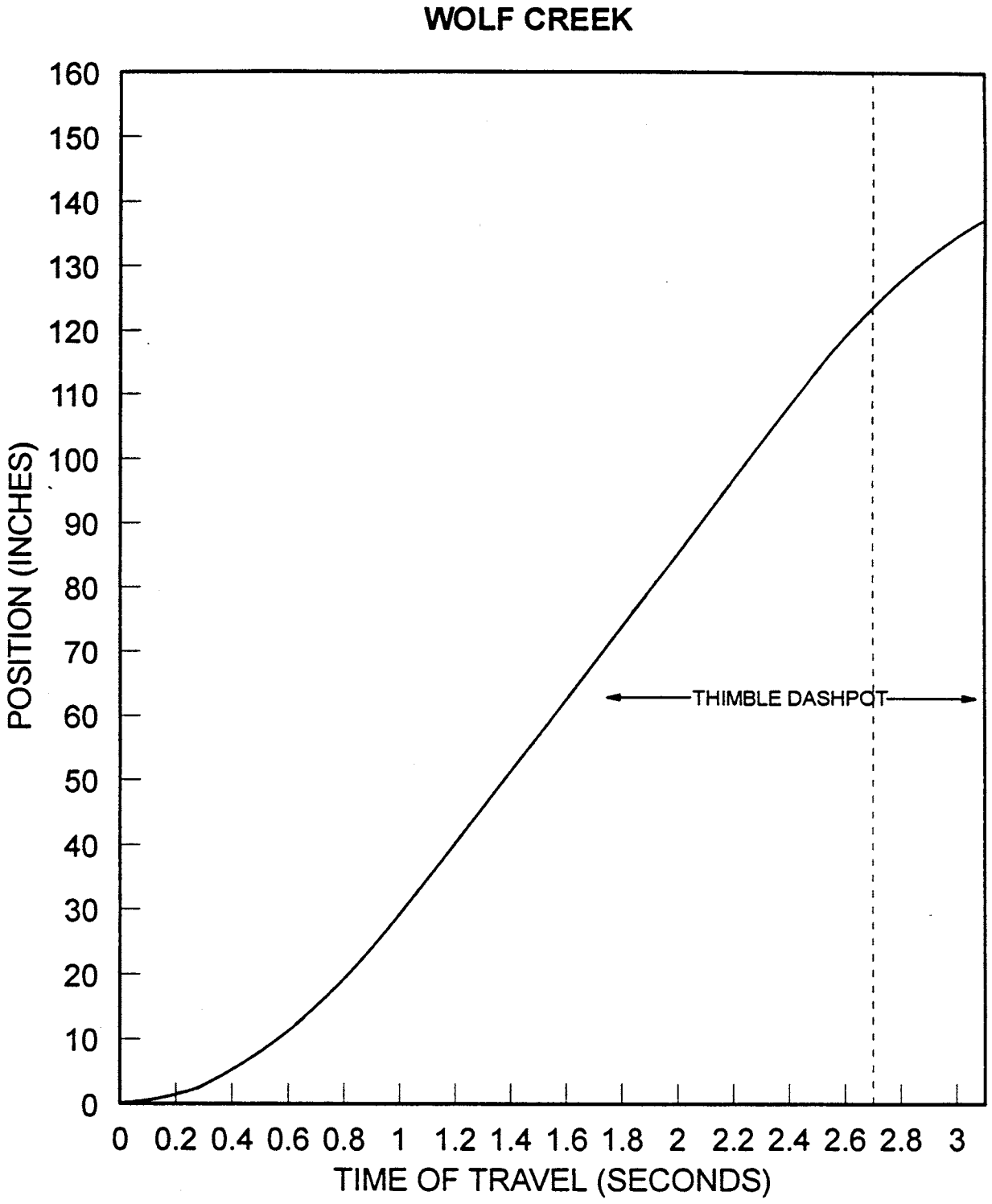

Rev. 7

WOLF CREEK UPDATED SAFETY ANALYSIS REPORT
FIGURE 4.3-38 DESIGN TRIP CURVE

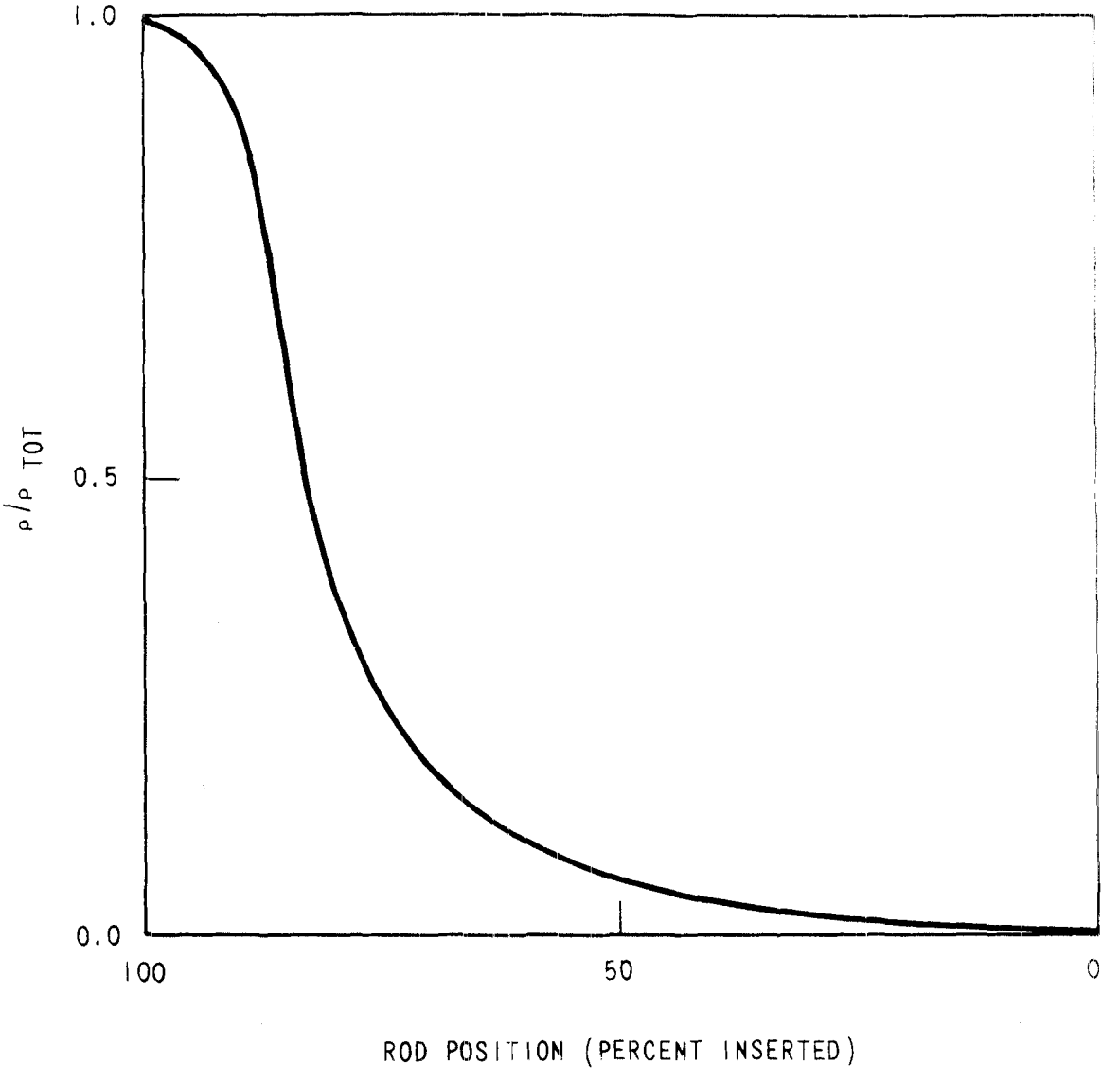

Rev. 0

WOLF CREEK
UPDATED SAFETY ANALYSIS REPORT

FIGURE 4.3-39

TYPICAL NORMALIZED ROD WORTH VERSUS PERCENT INSERTION, ALL RODS OUT BUT ONE

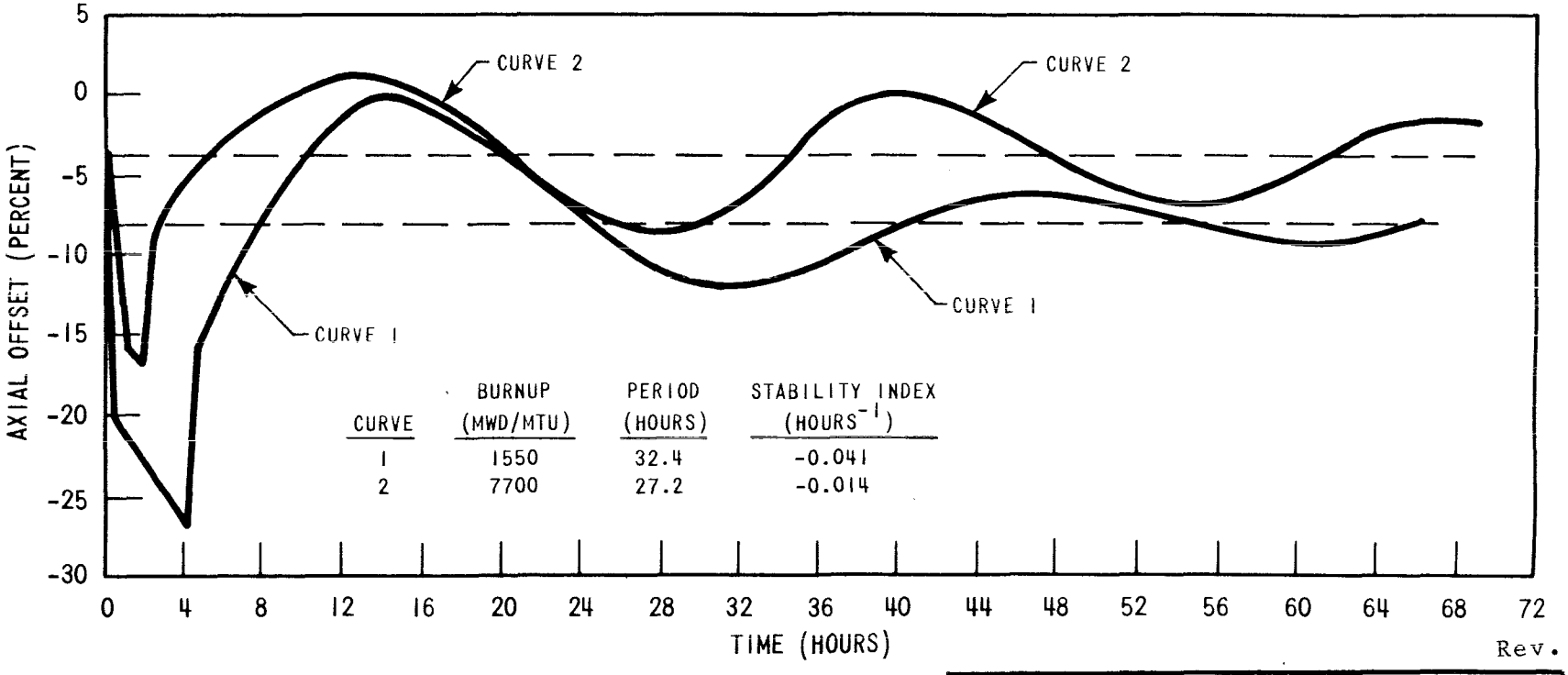

Rev. 0

WOLF CREEK
UPDATED SAFETY ANALYSIS REPORT

FIGURE 4.3-40

AXIAL OFFSET VERSUS TIME, PWR CORE WITH A 12 FOOT HEIGHT AND 121 ASSEMBLIES

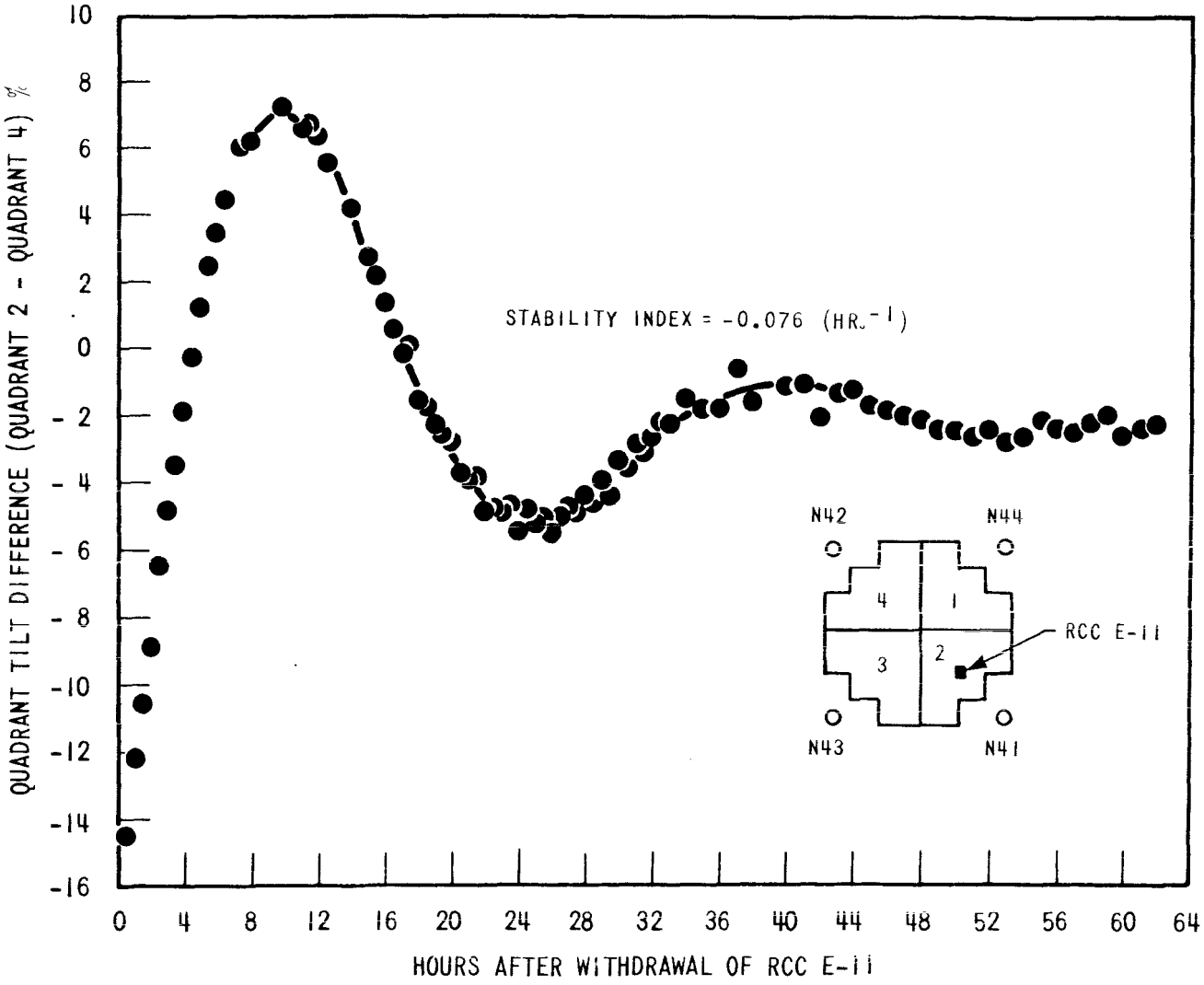

Rev. 0

WOLF CREEK
UPDATED SAFETY ANALYSIS REPORT

FIGURE 4.3-41

X-Y XENON TEST THERMOCOUPLE
RESPONSE QUADRANT TILT DIFFERENCE
VERSUS TIME

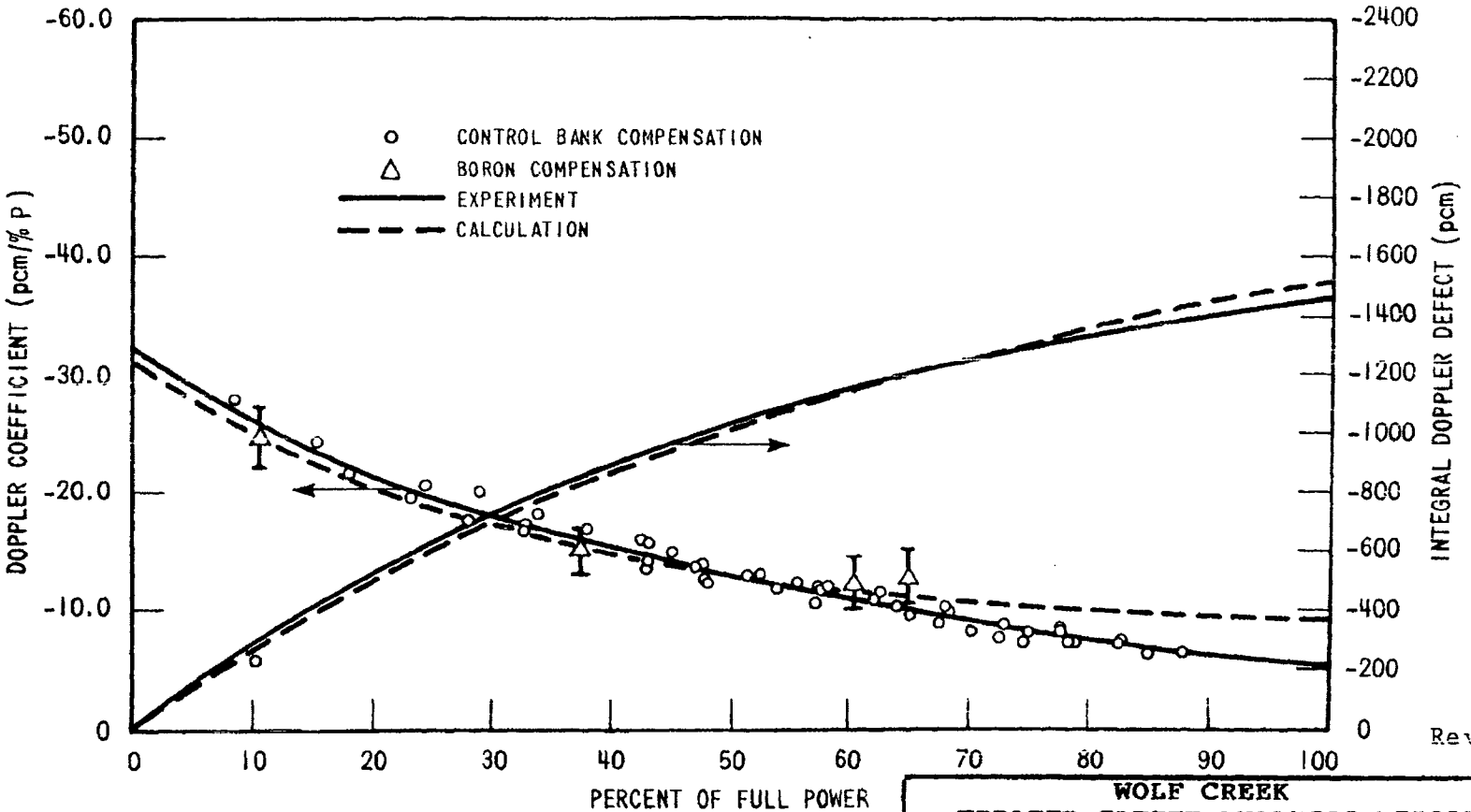

Rev. 0

WOLF CREEK
UPDATED SAFETY ANALYSIS REPORT

FIGURE 4.3-42

CALCULATED AND MEASURED DOPPLER DEFECT AND COEFFICIENTS AT BOL, 2-LOOP PLANT, 121 ASSEMBLIES, 12 FOOT CORE

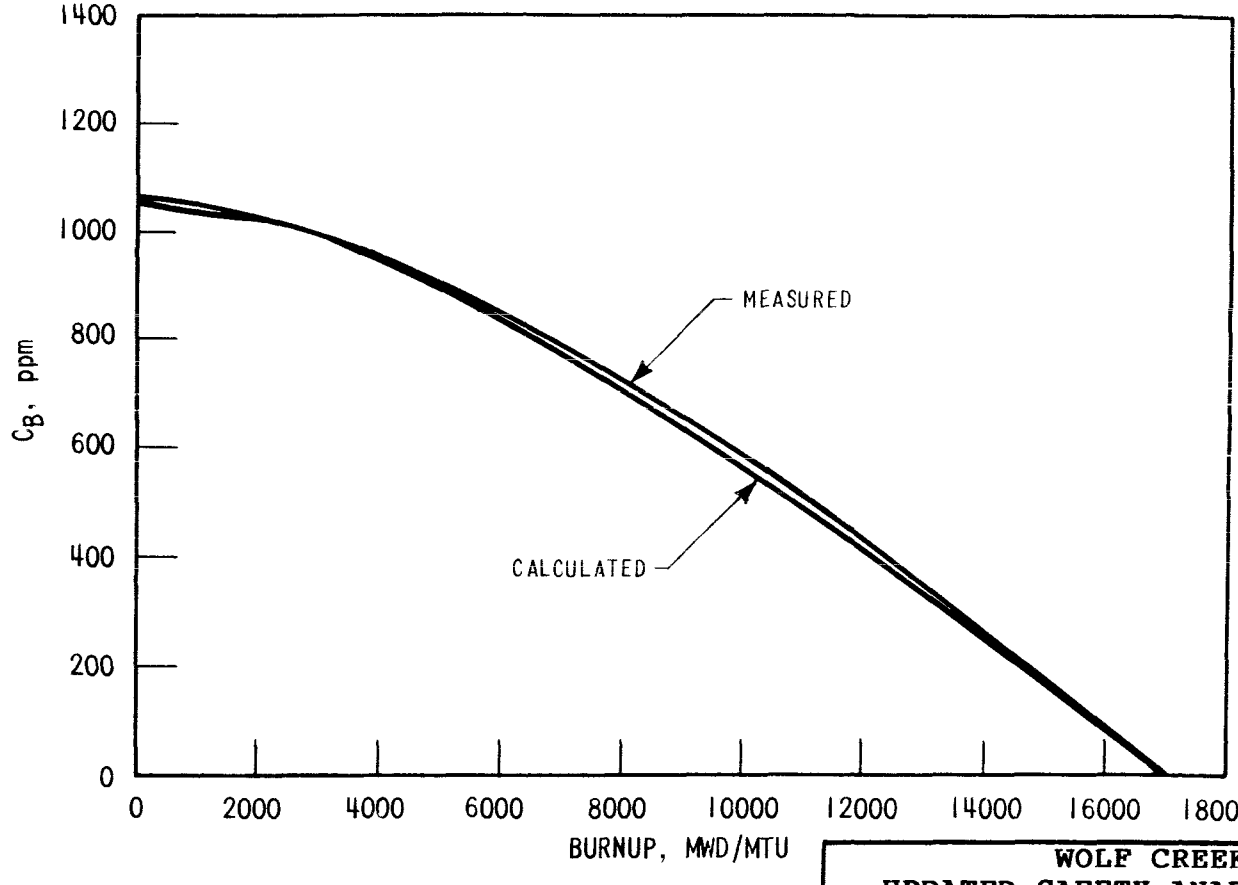

Rev. 0

WOLF CREEK
UPDATED SAFETY ANALYSIS REPORT

FIGURE 4.3-43

COMPARISON OF CALCULATED AND MEASURED BORON CONCENTRATION 2-LOOP PLANT, 121 ASSEMBLIES, 12 FOOT CORE

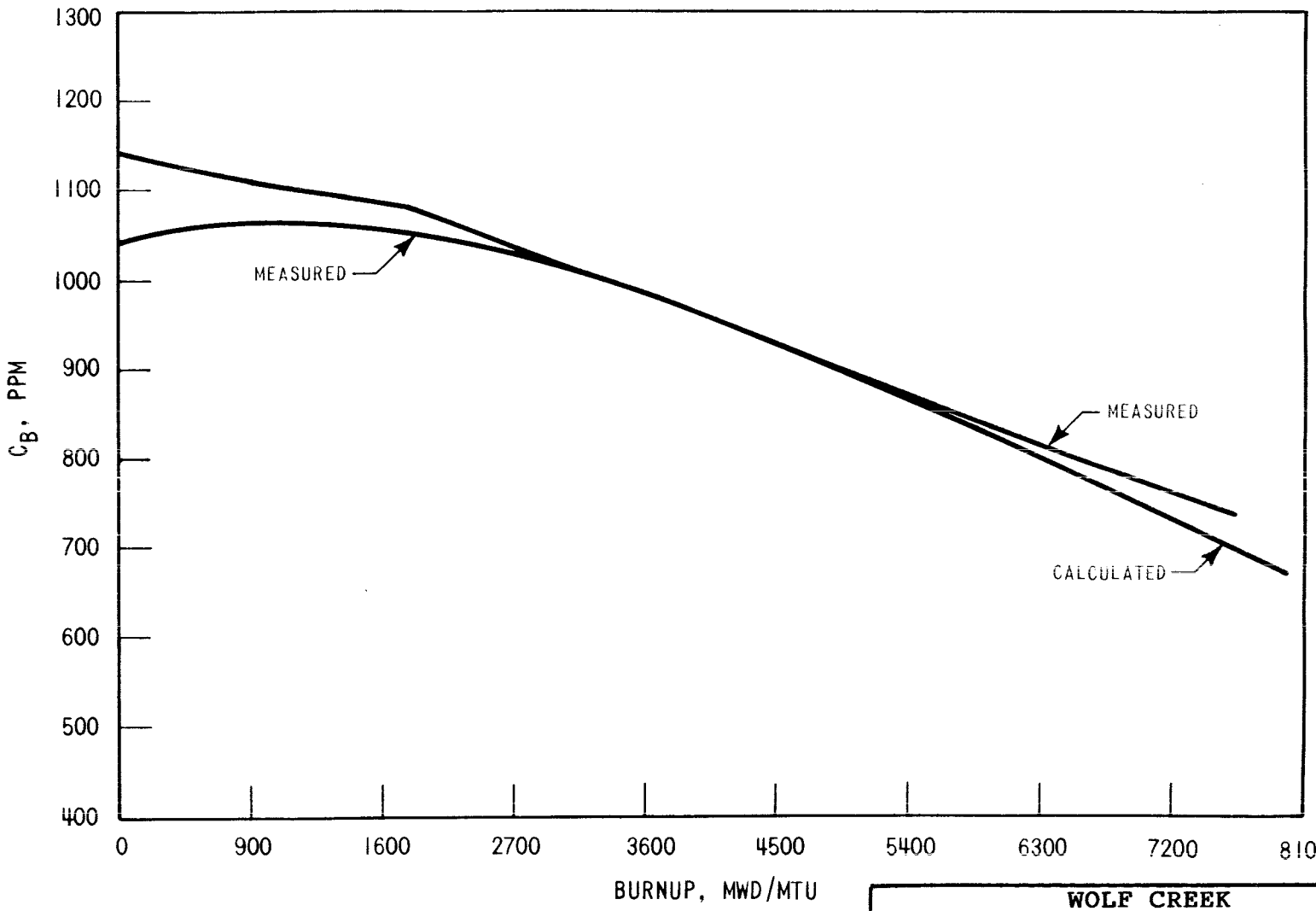

Rev. 0

WOLF CREEK
UPDATED SAFETY ANALYSIS REPORT

FIGURE 4.3-44

COMPARISON OF CALCULATED AND MEASURED C_B, 2-LOOP PLANT. 121 ASSEMBLIES, 12 FOOT CORE

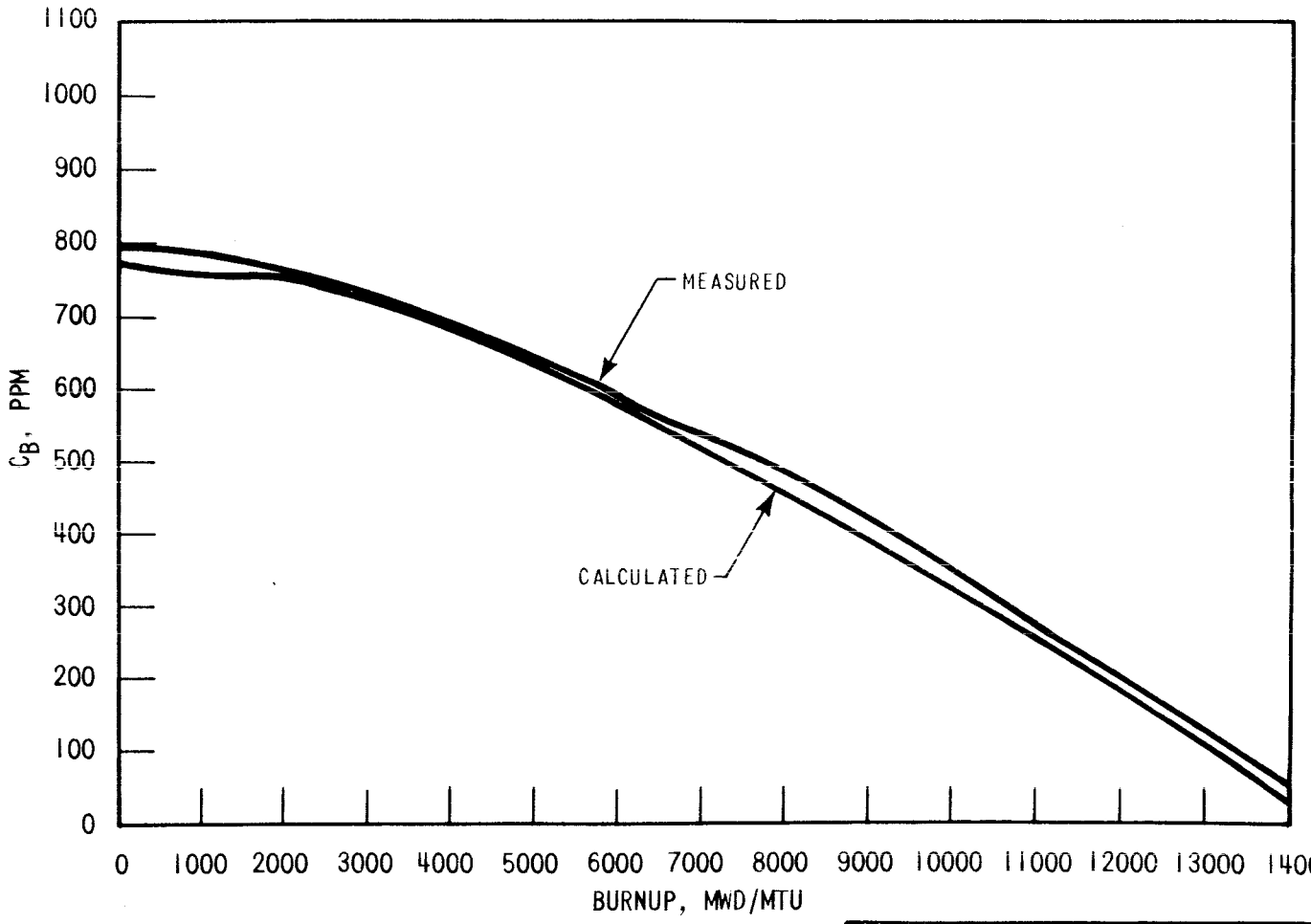

Rev. 0

WOLF CREEK
UPDATED SAFETY ANALYSIS REPORT

FIGURE 4.3-45

COMPARISON OF CALCULATED AND MEASURED C_B, 3-LOOP PLANT, 157 ASSEMBLIES, 12 FOOT CORE

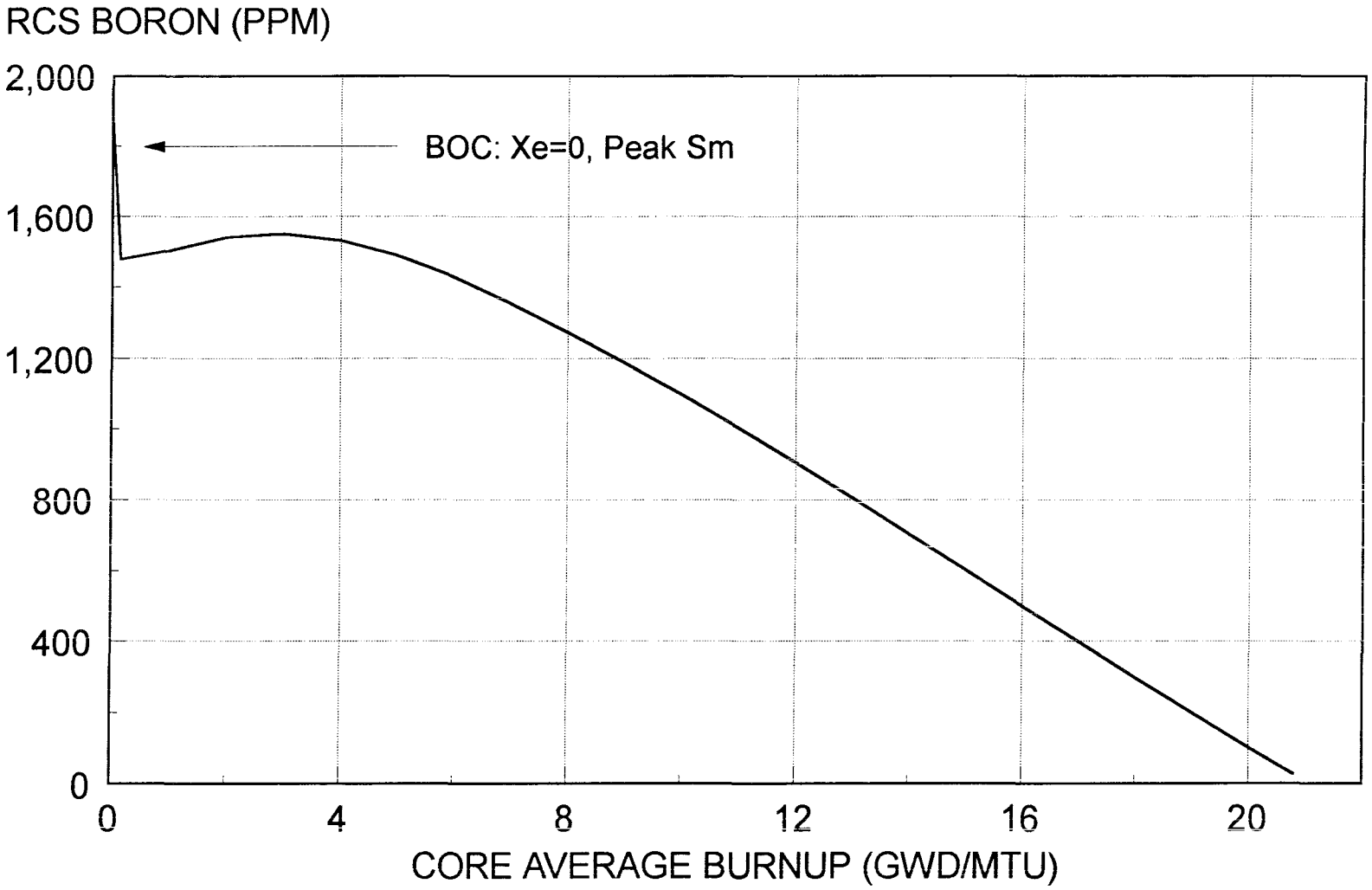

Rev. 11

WOLF CREEK
UPDATED SAFETY ANALYSIS REPORT

FIGURE 4.3-46

TYPICAL BORON LETDOWN CURVE

4.4 THERMAL AND HYDRAULIC DESIGN

4.4.1 DESIGN BASES

The overall objective of the thermal and hydraulic design of the reactor core is to provide adequate heat transfer which is compatible with the heat generation distribution in the core such that heat removal by the reactor coolant system or the emergency core cooling system (when applicable) assures that the following performances and safety criteria requirements are met:

a. Fuel damage (defined as penetration of the fission product barrier, i.e., the fuel rod clad) is not expected during normal operation and operational transients (Condition I) or any transient conditions arising from faults of moderate frequency (Condition II). It is not possible, however, to preclude a very small number of rod failures. These will be within the capability of the plant cleanup system and are consistent with the plant design bases.

b. The reactor can be brought to a safe state following a Condition III event with only a small fraction of fuel rods damaged (see above definition) although sufficient fuel damage might occur to preclude resumption of operation without considerable outage time.

c. The reactor can be brought to a safe state and the core can be kept subcritical with acceptable heat transfer geometry following transients arising from Condition IV events.

In order to satisfy the above criteria, the following design bases have been established for the thermal and hydraulic design of the reactor core.

4.4.1.1 Departure from Nucleate Boiling Design Basis

Basis

There will be at least a 95% probability that departure from nucleate boiling (DNB) will not occur on the limiting fuel rods during normal operation and operational transients and any transient conditions arising from faults of moderate frequency (Condition I and II events) at 95% confidence level.

Discussion

The design method employed to meet the DNB design basis for 17x17 RFA-2 fuel assemblies at Wolf Creek is the Revised Thermal Design Procedure (RTDP), Reference 91. With the RTDP methodology, uncertainties in plant operating parameters, nuclear and thermal parameters, fuel fabrication parameters, computer codes and DNB correlation predictions are considered statistically to obtain DNB uncertainty factors. Based on the DNB uncertainty factors, RTDP design limit DNBR values are determined such that there is at least a 95 percent probability at a 95 percent confidence level that DNB will not occur on the most limiting fuel rod during normal operation and operational transients and during transient conditions arising from faults of moderate frequency (Condition I and II events as defined in ANSI N18.2).

Uncertainties in the plant operating parameters (pressurizer pressure, primary coolant temperature, reactor power, reactor coolant system flow, etc.) have been evaluated. Only the random portion of the plant operating parameter uncertainties is included in the statistical combination. Instrumentation bias is treated as a direct DNBR penalty. Since the parameter uncertainties are considered in determining the RTDP design limit DNBR values, the plant safety analyses are performed using input parameters at their nominal values. The RTDP design limit DNBR for 17x17 RFA-2 fuel and the WRB-2 correlation is 1.24 for both typical and thimble cells. Similarly, the RTDP limit DNBR for 17x17 RFA-2 fuel and the ABB-NV correlation is 1.18 for both typical and thimble cells. The WRB-2 limit is applicable to the region above the first mixing vane grid and the ABB-NV limit is applicable to the region below the first mixing vane grid. The design limit DNBR values are used as a basis for the technical specifications and for consideration of the applicability of safety questions as defined in 10 CFR 50.59.

To maintain DNBR margin to offset DNB penalties such as that due to fuel rod bow (see paragraph 4.4.2.2.5), the safety analyses were performed to DNBR limits higher than the design limit DNBR values. The difference between the design limit DNBRs and the safety analysis limit DNBRs results in available DNBR margin. The net DNBR margin, after consideration of all penalties, is available for operating and design flexibility.

The Standard Thermal Design Procedure (STDP) is used for those analyses where RTDP is not applicable. In the STDP method the parameters used in analysis are treated in a conservative way from a DNBR standpoint. The parameter uncertainties are applied directly to the plant safety analyses input values to give the lowest minimum DNBR. The DNBR limit for STDP is the appropriate DNB correlation limit increased by sufficient margin to offset the applicable DNBR penalties.

By preventing DNB, adequate heat transfer is assured between the fuel clad and the reactor coolant, thereby preventing clad damage as a result of inadequate cooling. Maximum fuel rod surface temperature is not treated as a design basis as it will be within a few degrees of coolant temperature during operation in the nucleate boiling region. Limits provided by the nuclear control and protection systems are such that this design basis will be met for transients associated with Condition II events including overpower transients.

4.4.1.2 Fuel Temperature Design Basis

Basis

During modes of operation associated with Condition I and Condition II events, there is at least a 95-percent probability that the peak kW/ft fuel rods will not exceed the UO_2 melting temperature at the 95-percent confidence level. The melting temperature of UO_2 is taken as 5,080°F (Reference 1), unirradiated and decreasing 58°F per 10,000 MWD/MTU. By precluding UO_2 melting, the fuel geometry is preserved, and possible adverse effects of molten UO_2 on the cladding are eliminated. To preclude center melting and as a basis for overpower protection system setpoints, a calculated centerline fuel temperature of 4,700°F has been selected as the overpower limit. This provides sufficient margin for uncertainties in the thermal evaluations, as described in Section 4.4.2.9.1.

Discussion

Fuel rod thermal evaluations are performed at rated power, maximum overpower, and during transients at various burnups. These analyses assure that this design basis, as well as the fuel integrity design bases given in Section 4.2, are met. They also provide input for the evaluation of Condition III and IV events given in Chapter 15.0.

4.4.1.3 Core Flow Design Basis

Basis

Most of the thermal flow rate will pass through the fuel rod region of the core and be effective for fuel rod cooling. Coolant flow through the thimble tubes, as well as the leakage from the core barrel-baffle region into the core, are not considered effective for heat removal.

Discussion

Core cooling evaluations are based on the thermal flow rate (minimum flow) entering the reactor vessel. A small fraction of this value is allotted as bypass flow. This includes rod cluster control guide thimble cooling flow, head cooling flow, baffle leakage, and leakage to the vessel outlet nozzle. The amount of the bypass flow is a function of the fuel design and is confirmed for each reload.

4.4.1.4 Hydrodynamic Stability Design Basis

Basis

Modes of operation associated with Condition I and II events shall not lead to hydrodynamic instability.

4.4.1.5 Other Considerations

The above design bases, together with the fuel clad and fuel assembly design bases given in Section 4.2.1, are sufficiently comprehensive so no additional limits are required.

Fuel rod diametrical gap characteristics, moderator-coolant flow velocity and distribution, and moderator void are not inherently limiting. Each of these parameters is incorporated into the thermal and hydraulic models used to ensure the above-mentioned design criteria are met. For instance, the fuel rod diametrical gap characteristics change with time (see Section 4.2.3.3), and the fuel rod integrity is evaluated on that basis. The effect of the moderator flow velocity and distribution (see Section 4.4.2.2) and moderator void distribution (see Section 4.4.2.4) are included in the core thermal evaluation and thus affect the design bases.

Meeting the fuel clad integrity criteria covers possible effects of clad temperature limitations. As noted in Section 4.2.3.3, the fuel rod conditions change with time. A single clad temperature limit for Condition I or Condition II events is not appropriate since, of necessity, it would be overly conservative. A clad temperature limit is applied to the loss-of-coolant accident (see Section 15.6.5), control rod ejection accident, and locked rotor accident.

4.4.2 Description of Thermal and Hydraulic Design of the Reactor Core

4.4.2.1 Summary Comparison

Values of pertinent design and operating parameters are presented in Table 4.4-1. The reactor is designed to meet the DNB design basis as no fuel centerline melting during normal operation, operational transients, and faults of moderate frequency.

Fuel densification has been considered in the DNB and fuel temperature evaluations, utilizing the methods and models described in detail in Reference 3.

4.4.2.2 Critical Heat Flux Ratio or Departure from Nucleate Boiling Ratio and Mixing Technology

The minimum DNBRs for the rated power, design overpower, and anticipated transient conditions are given in Table 4.4-1. The minimum DNBR in the limiting flow channel will be downstream of the peak heat flux location (hot spot) due to the increased downstream enthalpy rise.

DNBRs are calculated by using the correlation and definitions described in Sections 4.4.2.2.1 and 4.4.2.2.2. The VIPRE-01 computer code (discussed in Section 4.4.4.5.1) is used to determine the flow distribution in the core and the local conditions in the hot channel for use in the DNB correlation. The use of hot channel factors is discussed in Section 4.4.4.3.1 (nuclear hot channel factors) and in Section 4.4.2.2.4 (engineering hot channel factors).

WRB-2 Correlation

The WRB-2 (Reference 8) correlation has been developed to predict the DNB performance of Westinghouse fuel designs which employ grids with mixing vanes of the same design as the 17X17 standard fuel mixing vane design. This mixing vane design is unique in that the mixing vane area to flow area ratio and the azimuthal extension of the vanes around the rod circumference both differ from the mixing vane designs of other Westinghouse grids. The WRB-2 correlation is also based entirely on rod bundle data. However, the data used to develop the correlation is essentially the 17X17 "R" type grid subset (both STD and OFA fuel) of the WRB-1 data base plus additional DNB test data obtained to quantify the increase in DNB performance due to the addition of Intermediate Flow mixing vane grids (IFM) for the Vantage 5 geometry.

The applicable range of variables for the WRB-2 correlation is:

Pressure	:	$1440 \leq P \leq 2490$ psia
Local Mass Velocity	:	$0.9 \leq G_{loc}/10^6 \leq 3.7$ lb/ft^2-hr
Local Quality	:	$-0.1 \leq X_{loc} \leq 0.3$
Heated Length, Inlet to CHF Location	:	$L_h \leq 14$ feet
Grid Spacing	:	$10 < g_{sp} < 26$ inches
Equivalent Hydraulic Diameter	:	$0.37 \leq d_e \leq 0.51$ inches
Equivalent Heated Hydraulic Diameter	:	$0.46 \leq d_h \leq 0.59$ inches

Figure 4.4-22 shows measured critical heat flux plotted against predicted critical heat flux using the WRB-2 correlation. The 95/95 limit DNBR utilized in thermal/hydraulic analyses has been conservatively set equal to the Westinghouse THINC/WRB-2 code design limit DNBR of 1.17, appropriate for 17X17 standard fuel assemblies. For conditions outside the range of applicability of the WRB-2, the W-3 correlation is used.

W-3 Alternative Correlation

The ABB-NV and WLOP, W-3 Alternative correlations, are based exclusively on DNB data from rod bundle tests. They have a wider applicable range and are more accurate than the W-3 correlation for the prediction of margin to DNB. They are used for DNBR calculations as an alternative to the W-3 correlation and supplement the primary WRB-2 DNB correlation.

The ABB-NV correlation was originally developed for fuel designs of Combustion Engineering designed Pressurized Water Reactors (PWRs) based on a linear relationship between the Critical Heat Flux (CHF) and local quality. The correlation includes the following parameters: pressure, local mass velocity, local equilibrium quality, distance from grid to CHF location, heated length from inlet to CHF location, and heated hydraulic diameter of the subchannel. Supplemental rod bundle data evaluation confirms that ABB-NV, with a 95/95 correlation limit of 1.13, is applicable to the fuel region below the first mixing vane grid for fuel designs that are compatible with Westinghouse designed PWRs (Reference 93). Figure 4.4-23 shows measured critical heat flux plotted against predicted heat flux using the ABB-NV correlation.

The applicable range of the ABB-NV correlation is:

Pressure (psia)	:	1750 to 2415
Local Mass Velocity (Mlbm/hr-ft^2)	:	0.8 to 3.16
Local Quality (fraction)	:	< 0.22
Heated Length, inlet to CHF location (in.)	:	48 (minimum) to 150
Heated Hydraulic Diameter Ratio	:	0.679 to 1.08
Grid Distance (in.)	:	7.3 to 24

The WLOP correlation is a modified ABB-NV correlation specifically developed for low pressure conditions and extended flow range to cover low pressure/low flow conditions. Modifications to ABB-NV were made based on test data from rod bundles containing non-mixing vane grids. The WLOP correlation with a 95/95 DNBR limit has also been validated with test data from rod bundles containing mixing vane grids (Reference 93). The WLOP correlation with a 95/95 DNBR limit of 1.18 has also been validated with test data from rod bundles containing mixing vane grids (Reference 93). Figure 4.4-24 shows measured critical heat flux plotted against predicted heat flux using the WLOP correlation.

The applicable range of the WLOP correlation is:

Pressure (psia)	:	185 to 1800
Local Mass Velocity (Mlbm/hr-ft^2)	:	0.23 to 3.07
Local Quality (fraction)	:	< 0.75
Heated Length, inlet to CHF location (in.)	:	48 (minimum) to 168
Heated Hydraulic Diameter Ratio	:	0.679 to 1.00
Grid Spacing Term (Reference 93)	:	27 to 115

4.4.2.2.1 Departure from Nucleate Boiling Technology

Early experimental studies of DNB were conducted with fluid flowing inside single heated tubes or channels and with single annulus configurations with one or both walls heated. The results of the experiments were analyzed, using many different physical models for describing the DNB phenomenon, but all resultant correlations are highly empirical in nature. The evolution of these correlations is described by Tong (References 4 and 5), including the W-3 correlation which is in wide use in the pressurized water reactor industry.

As testing methods progressed to the use of rod bundles instead of single channels, it became apparent that the bundle average flow conditions could not be used in DNB correlations. As discussed by Tong (Reference 6) test results showed that correlations based on average conditions were not accurate predictors of DNB heat flux, and that a knowledge of the local subchannel conditions within the bundle is necessary.

In order to determine the local subchannel conditions, the VIPRE-01 Code (Reference 9) was developed. VIPRE-01 has been developed for nuclear power utility thermal/hydraulic analysis applications. It is designed to help evaluate nuclear reactor core safety limits, including minimum departure from nucleate boiling ratio (MDNBR), fuel and clad temperature, and coolant state in normal operating steady state and transients and assumed accident conditions.

VIPRE-01 was developed on the strengths of the COBRA code series and has gone through extensive benchmarking against COBRA in Reference 9. Calculations covered a large range of data from comparisons of VIPRE-01 calculations to simple heat-conduction problems having analytical solutions, to complex environments involving flow blockage, two phase pressure drop, void fraction measurements, fuel temperatures and heat transfer.

The basic computational philosophy of VIPRE uses the subchannel analysis concept where a problem is divided into a number of quasi-one-dimensional channels that communicate laterally by diversion crossflow and turbulent mixing. Conservation equations of mass, axial and lateral momentum, and energy are solved for the fluid enthalpy, axial flow rate, lateral flow per unit length, and momentum pressure drop. The flow field is assumed to be incompressible and homogeneous, although models are added to reflect subcooled boiling and co-current liquid/vapor slip.

NRC approval of the EPRI VIPRE-01 computer code is given in Reference 90. WCGS Thermal Hydraulic methodology utilizing the VIPRE-01 code is given in Reference 2.

4.4.2.2.2 Definition of Departure from Nucleate Boiling Ratio

The DNB heat flux ratio (DNBR) as applied to this design when all flow cell walls are heated is:

$$DNBR = \frac{q''_{DNB,N}}{q''_{loc}} \qquad [4.4\text{-}4]$$

where:

$$q''_{DNB,N} = \frac{q''_{DNB,EU}}{F} \qquad [4.4\text{-}5]$$

and $q''_{DNB,EU}$ is the uniform DNB heat flux as predicted by the applicable DNB correlation.

F is the flux shape factor to account for nonuniform axial heat flux distributions (Reference 85) with the "C" term modified as in Reference 5.

q" is the actual local heat flux.

4.4.2.2.3 Mixing Technology

The transverse momentum equation in VIPRE-01 includes terms describing the exchange of momentum between channels due to turbulent mixing. Turbulent mixing is natural eddy diffusion between subchannels which is characterized by eddy diffusivities. However, for numerical applications, such as VIPRE-01, the turbulent mixing is represented by an equivalent lateral mass flow rate. This equivalent lateral flow, defined as W' in VIPRE-01, defines the coolant exchange rate between adjacent channels and thus, specifies the exchange of mass, energy, and momentum between channels.

Turbulent mixing in VIPRE-01 is accounted for with an empirical relation in which the user must specify a form for the turbulent mixing correlation, the turbulent mixing coefficient, and the turbulent momentum factor (FTM).

There are four correlations available in VIPRE-01 for defining the turbulent crossflow. A sensitivity study was performed in Reference 93, showing that VIPRE-01 in insensitive to which correlation is utilized. The correlation used in WCGS analyses is:

$$W' = \beta * S * \bar{G} \qquad [4.4\text{-}9]$$

where:

W' = the calculated turbulent crossflow, lbm*ft/sec

β = the turbulent mixing coefficient (TDC)

S = the gap width, ft

$\bar{G}$ = the average mass velocity in the channels connected by the gap under consideration lbm/sec

The application of the TDC in the VIPRE-01 analysis for determining the overall mixing effect on heat exchange rate is presented in Reference 9 and Reference 93.

As a part of an ongoing research and development program, Westinghouse has sponsored and directed mixing tests at Columbia University (Reference 12). These series of tests, using the "R" mixing vane grid design on 13-, 26-, and 32-inch grid spacing, were conducted in pressurized water loops at Reynolds numbers similar to that of a pressurized water reactor core under the following single and two phase (subcooled boiling) flow conditions:

Pressure	1,500 to 2,400 psia
Inlet temperature	332°to 642°F
Mass velocity	1.0 to 3.5 x 10^6 lb /hr-ft^2
Reynolds number	1.34 to 7.45 x 10^5 m
Bulk outlet quality	-52.1 to -13.5 percent

TDC is determined by comparing the THINC Code predictions with the measured subchannel exit temperatures. Data for 26-inch axial grid spacing are presented in Figure 4.4-4 where the TDC is plotted versus the Reynolds number. TDC is found to be independent of Reynolds number, mass velocity, pressure, and quality over the ranges tested. The two phase data (local, subcooled boiling) fell within the scatter of the single phase data. The effect of two-phase flow on the value of TDC has been investigated by Cadek (Reference 12), Rowe and Angle (References 13 and 14), and Gonzalez-Santalo and Griffith (Reference 15). In the subcooled boiling region, the values of TDC were indistinguishable from the single phase values. In the quality region, Rowe and Angle show that in the case with rod spacing similar to that in pressurized water reactor core geometry, the value of TDC increased with quality to a point and then decreased, but never below the single phase value. Gonzalez-Santalo and Griffith showed that the mixing coefficient (TDC) increased as the void fraction increased.

The data from these tests on the "R" grid showed that a design TDC value of 0.038 (for 26-inch grid spacing) can be used in determining the effect of coolant mixing in thermal-hydraulic analyses.

A mixing test program similar to the one described above was conducted at Columbia University for the 17 x 17 geometry and mixing vane grids on 26-inch spacing (Reference 16). The mean value of TDC obtained from these tests was 0.059, and all data was well above the current design value of 0.038.

Since the actual reactor grid spacing is approximately 20 inches, additional margin is available for this design, as the value of TDC increases as grid spacing decreases (Reference 12). Use of the 0.038 TDC for V5H and RFA fuel with IFM grids is utilized for Wolf Creek. Calculation of the generic DNBR margins for Wolf Creek was performed utilizing this 0.038 TDC (References 11, 92).

The turbulent momentum factor (FTM) in VIPRE-01 controls the efficiency of the momentum mixing due to turbulent crossflow between subchannels. An FTM of 0.0 indicates that crossflow mixes enthalpy only, while an FTM of 1.0 indicates that crossflow mixes momentum equally with enthalpy. Sensitivity studies performed during the VIPRE - 01 qualification effort have shown that VIPRE-01 is relatively insensitive to FTM (Reference 93). However, Reference 9 recommends an FTM of 0.8.

4.4.2.2.4 Hot Channel Factors

The total hot channel factors for heat flux and enthalpy rise are defined as the maximum-to-core average ratios of these quantities. The heat flux hot channel factor considers the local maximum linear heat generation rate at a point (the hot spot), and the enthalpy rise hot channel factor involves the maximum integrated value along a channel (the hot channel).

Each of the total hot channel factors is composed of a nuclear hot channel factor (see Section 4.4.4.3) describing the neutron power distribution and an engineering hot channel factor, which allows for variations in flow conditions and fabrication tolerances. The engineering hot channel factors are made up of subfactors which account for the influence of the variations of fuel pellet diameter, density, enrichment, and eccentricity; fuel rod diameter pitch and bowing; inlet flow distribution; flow redistribution; and flow mixing.

Heat Flux Engineering Hot Channel Factor, F_Q^E

The heat flux engineering hot channel factor is used to evaluate the maximum heat flux. This subfactor is determined by statistically combining the tolerances for the fuel pellet diameter, density, enrichment, eccentricity, and the fuel rod diameter, and has a value of 1.033. Measured manufacturing data on recent Westinghouse 17 x 17 fuel were used to verify that this value was not exceeded for 95 percent of the limiting fuel rods at a 95-percent confidence level. Thus, it is expected that a statistical sampling of the fuel assemblies of this plant will yield a value no larger than 1.033.

Enthalpy Rise Engineering Hot Channel Factor, $F_{\Delta H}^E$

The effect of variations in flow conditions and fabrication tolerances on the hot channel enthalpy rise is directly considered in the core thermal-hydraulic subchannel analysis (see Section 4.4.4.5.1) under any reactor operating condition. The items included in the consideration of the enthalpy rise engineering hot channel factor are discussed below:

a. Pellet diameter, density, and enrichment and fuel rod diameter, pitch, and bowing Design values employed in the VIPRE analysis related to the above fabrication variations are based on applicable limiting tolerances so that these design values are met for 95 percent of the limiting channels at a 95-percent confidence level. Measured manufacturing data on Westinghouse 17 x 17 fuel show that the tolerances used in this evaluation are conservative. In addition, each fuel assembly is inspected to assure that the channel spacing design criteria are met. The effect of variations in pellet diameter, enrichment, and density is considered statistically in establishing the design limit DNBRs (see Subsection 4.4.1.1 for the Revised Thermal Design Procedure (Reference 91) employed in this application.)

b. Inlet flow maldistribution

The consideration of inlet flow maldistribution in core thermal performances is discussed in Section 4.4.4.2.2. A design basis of 5-percent reduction in coolant flow to the hot assembly is used in the core thermal-hydraulic analysis.

c. Flow redistribution

The flow redistribution accounts for the reduction in flow in the hot channel resulting from the high flow resistance in the channel due to the local or bulk boiling. The effect of the nonuniform power distribution is inherently considered in the core thermal-hydraulic analysis for every operating condition that is evaluated.

d. Flow mixing

The subchannel mixing model incorporated in the VIPRE Code and used in reactor design is based on experimental data (References 11 and 17) discussed in Sections 4.4.2.2.3 and 4.4.4.5.1. The mixing vanes incorporated in the spacer grid design induce additional flow mixing between the various flow channels in a fuel assembly as well as between adjacent assemblies. This mixing reduces the enthalpy rise in the hot channel resulting from local power peaking or unfavorable mechanical tolerances.

4 4.2.2.5 Effects of Rod Bow on DNBR

The phenomenon of fuel rod bowing, as described in Reference 83, must be accounted for in the DNBR safety analysis of Condition I and Condition II events for each plant application. Applicable generic credits for margin resulting from retained conservatism in the evaluation of DNBR and/or margin obtained from measured plant operating parameters (such as $F^N_{\Delta H}$ or core flow)--which are less limiting than those required by the plant safety analysis--can be used to offset the effect of rod bow.

For the WCGS safety analysis, sufficient margin was maintained between the VIPRE-01/WRB-2 design limit DNBR and the safety analysis limit DNBR to completely offset any DNBR penalties associated with rod bow.

The maximum rod bow penalties accounted for in the design safety analysis are based on an assembly average burnup of 24,000 MWD/MTU (Reference 85). At burnups greater than 24,000 MWD/MTU, credit is taken for the effect $F^N_{\Delta H}$ burndown, due to the decrease in fissionable isotopes and the buildup of fission product inventory, and no additional rod bow penalty is required.

4.4.2.3 Linear Heat Generation Rate

The core average and maximum linear heat generation rates are given in Table 4.4-1. The method of determining the maximum linear heat generation rate is given in Section 4.3.2.2.

4.4.2.4 Void Fraction Distribution

The calculated core average and the hot subchannel maximum and average void fractions are presented in Table 4.4-3 for operation at full power with design hot channel factors. The void fraction distribution in the core at various radial and axial locations is presented in Reference 21, based on THINC-IV predictions. The void models used in the VIPRE-01 Code are described in Section 4.4.2.7.3.

Since void formation due to subcooled boiling is an important promoter of interassembly flow redistribution, a sensitivity study (Reference 21) was performed with THINC-IV using the void model referenced above.

The results of this study showed that because of the realistic crossflow model used in THINC-IV, the minimum DNBR in the hot channel is relatively insensitive to variations in this model. The range of variations considered in this sensitivity study covered the maximum uncertainty range of the data used to develop each part of the void fraction correlation. The conclusions of the sensitivity study remain applicable to the VIPRE-01 code.

4.4.2.5 Core Coolant Flow Distribution

Assembly average coolant mass velocity and enthalpy at various radial and axial core locations for first core near the beginning of core life power distribution are given in Figures 4.4-5 through 4.4-7. Typical coolant enthalpy rise and flow distributions for the 4-foot elevation (1/3 of core height) are shown in Figure 4.4-5, for the 8-foot elevation (2/3 of core height) in Figure 4.4-6, and at the core exit in Figure 4.4-7. The THINC Code analysis for this case utilized a uniform core inlet enthalpy and inlet flow distribution. No orificing is employed in the reactor design.

4.4.2.6 Core Pressure Drops and Hydraulic Loads

4.4.2.6.1 Core Pressure Drops

The analytical model and experimental data used to calculate the pressure drops shown in Table 4.4-1 are described in Section 4.4.2.7. The core pressure drop includes the fuel assembly (including the effect of inserted core components, such as rod cluster controls), lower core plate, and upper core plate pressure drops. These pressure drops are based on the best estimate flow for estimated plant operating conditions, as described in Section 5.1.4. This section also defines and describes the thermal design flow (minimum flow) which is the basis for reactor core thermal performance and the mechanical design flow (maximum flow) which is used in the mechanical design of the reactor vessel internals and fuel assemblies. Since the best estimate flow is that flow which is most likely to exist in an operating plant, the calculated core pressure drops in Table 4.4-1 are based on this best estimate flow rather than the thermal design flow.

Uncertainties associated with the core and vessel pressure drop values are discussed in Section 4.4.2.9.2.

4.4.2.6.2 Hydraulic Loads

The fuel assembly holddown springs, Figure 4.2-2, are designed to keep the fuel assemblies in contact with the lower core plate under all Condition I and II events, with the exception of the turbine overspeed transient associated with a loss of external load. The holddown springs are designed to tolerate the possible overdeflection associated with fuel assembly liftoff for this case and provide contact between the fuel assembly and the lower core plate following this transient. More adverse flow conditions occur during a loss-of-coolant accident. These conditions are presented in Section 15.6.5.

Hydraulic loads at normal operating conditions are calculated, considering the best estimate flow which is described in Section 5.1 and accounting for the best estimate core bypass flow. Core hydraulic loads at cold plant startup conditions are based on the cold best estimate flow, but are adjusted to account for the coolant density difference. Conservative core hydraulic loads for a pump overspeed transient, which could possibly create flow rates 18 to 20 percent greater than the mechanical design flow, are evaluated to be approximately twice the fuel assembly weight.

Core hydraulic loads were measured during the prototype assembly tests described in Section 1.5. Reference 19 contains a detailed discussion of the results.

4.4.2.7 Correlation and Physical Data

4.4.2.7.1 Surface Heat Transfer Coefficients

The VIPRE-01 code contains a set of heat transfer correlations for each of the four regions of the boiling curve. The user can supply a separate heat transfer correlation for use in the single phase forced convection region, the subcooled and saturated nucleate boiling region, the transition boiling region, and the film boiling region. Each correlation is discussed in detail in Reference 9.

In the single phase forced convection region, forced convection heat transfer coefficients are obtained from the familiar Dittus-Boelter correlation (Reference 20), with the properties evaluated at bulk fluid conditions:

$$\frac{hD_e}{K} = 0.023 \left(\frac{D_e G}{\mu}\right)^{0.8} \left(\frac{C_p \mu}{K}\right)^{0.4} \qquad [4.4\text{-}10]$$

where

h = heat transfer coefficient, (Btu/hr-ft^2-F)
D_e = equivalent diameter, (ft)
K = thermal conductivity, (Btu/hr-ft-F)
G = mass velocity, (lb_m/hr-ft^2)
μ = dynamic viscosity, (lb_m/ft-hr)
C_p = heat capacity, (Btu/lb_m-F)

This correlation has been shown to be conservative (Reference 21) for rod bundle geometries with pitch to diameter ratios in the range used by pressurized water reactors.

The onset of nucleate boiling occurs when the clad wall temperature reaches the amount of superheat predicted by Thom's (Reference 22) correlation. After this occurrence, the outer clad wall temperature is determined by:

$$\Delta T_{sat} = [0.072 \exp(-P/1260)] (q")^{0.5} \qquad [4.4\text{-}11]$$

where:

ΔT_{sat} = wall superheat, $T_w - T_{sat}$ (F)
$q"$ = wall heat flux, (Btu/hr-ft^2)
P = pressure, (psia)
T_w = outer clad wall temperature, (F)
T_{sat} = saturation temperature of coolant at P, (F)

4.4.2.7.2 Total Core and Vessel Pressure Drop

Unrecoverable pressure losses occur as a result of viscous drag (friction) and/or geometry changes (form) in the fluid flow path. The flow field is assumed to be incompressible, turbulent, single-phase water. These assumptions apply to the core and vessel pressure drop calculations for the purpose of establishing the primary loop flow rate. Two-phase considerations are neglected in the vessel pressure drop evaluation because the core average void is negligible (see Table 4.4-3).

Two-phase flow considerations in the core thermal subchannel analyses are considered, and the models are discussed in Section 4.4.4.2.3. Core and vessel pressure losses are calculated by equations of the form:

$$\Delta P_L = \left(K + F\frac{L}{D_e} \right) \frac{\rho v^2}{2g_c\ (144)} \qquad [4.4\text{-}12]$$

where:

ΔP_L = unrecoverable pressure drop, (lb_f/in^2)
ρ = fluid density, (lb_m/ft^3)
L = length, (ft)
D_e = equivalent diameter, (ft)
V = fluid velocity, (ft/sec)
g_c = 32.174, (lb_m-ft/lb_f-sec^2)
K = form loss coefficient, dimensionless
F = friction loss coefficient, dimensionless

Fluid density is assumed to be constant at the appropriate value for each component in the core and vessel. Because of the complex core and vessel flow geometry, precise analytical values for the form and friction loss coefficients are not available. Therefore, experimental values for these coefficients are obtained from geometrically similar models.

Values are quoted in Table 4.4-1 for unrecoverable pressure loss across the reactor core. The results of full-scale tests of core components and fuel assemblies were utilized in developing the core pressure loss characteristic. The pressure drop for the vessel was obtained by combining the core loss with correlation of 1/7th scale model hydraulic test data on a number of vessels (References 23 and 24) and form loss relationships (Reference 25). Moody (Reference 26) curves were used to obtain the single phase friction factors.

Tests of the primary coolant loop flow rates were made (see Section 4.4.5.1) prior to initial criticality to verify that the flow rates used in the design, which were determined in part from the pressure losses calculated by the method described here, were conservative.

4.4.2.7.3 Void Fraction Correlation

VIPRE-01 considers two-phase flow in two steps. First, a quality model is used to compute the flowing vapor mass fraction (true quality) including the effects of subcooled boiling. Then, given the true quality, a bulk void model is applied to compute the vapor volume fraction (void fraction).

VIPRE-01 uses a profile fit model (Reference 9) for determining subcooled quality. It calculates the local vapor volumetric fraction in forced convection boiling by: 1) predicting the point of bubble departure from the heated surface, and 2) postulating a relationship between the true local vapor fraction and the corresponding thermal equilibrium value.

The void fraction in the bulk boiling region is predicted by using homogeneous flow theory and assuming no slip. The void fraction in this region is, therefore, a function only of the thermodynamic quality.

4.4.2.8 Thermal Effects of Operational Transients

DNB core safety limits are generated as a function of coolant temperature, pressure, core power and axial power imbalance. Steady state operation within these safety limits ensures that the DNB design basis is met.

This system provides adequate protection against anticipated operational transients that are slow with respect to fluid transport delays in the primary system. In addition, for fast transients, e.g., uncontrolled rod bank withdrawal at power incident specific protection functions are provided as described in Section 7.2, and the use of these protection functions are described in Chapter 15.0.

4.4.2.9 Uncertainties in Estimates

4.4.2.9.1 Uncertainties in Fuel and Clad Temperatures

As discussed in Section 4.4.2.11, the fuel temperature is a function of crud, oxide, clad, pellet-clad gap, and pellet conductances. Uncertainties in the fuel temperature calculation are essentially of two types: fabrication uncertainties such as variations in the pellet and clad dimensions and the pellet density; and model uncertainties such as variations in the pellet conductivity and the gap conductance. These uncertainties have been quantified by comparison of the thermal model to inpile measurements, (Ref. 30 through 36), by out-of-pile measurements of the fuel and clad properties (Ref. 37 through 48), and by measurements of the fuel and clad dimensions during fabrication. The resulting uncertainties are then used in all evaluations involving the fuel temperature. The effect of densification on fuel temperature uncertainties is also included in the calculation of the total uncertainty.

In addition to the temperature uncertainty described above, the measurement uncertainty in determining the local power and the effect of density and enrichment variations on the local power are considered in establishing the heat flux hot channel factor. These uncertainties are described in Section 4.3.2.2.1.

Reactor trip setpoints, as specified in the Technical Specifications, include allowance for instrument and measurement uncertainties, such as calorimetric error, instrument drift and channel reproducibility, temperature measurement uncertainties, noise, and heat capacity variations.

Uncertainty in determining the cladding temperature results from uncertainties in the crud and oxide thicknesses. Because of the excellent heat transfer between the surface of the rod and the coolant, the film temperature drop does not appreciably contribute to the uncertainty.

4.4.2.9.2 Uncertainties in Pressure Drops

Core and vessel pressure drops based on the best estimate flow, as described in Section 5.1, are quoted in Table 4.4-1. The uncertainties quoted are based on the uncertainties in both the test results and the analytical extension of these values to the reactor application.

A major use of the core and vessel pressure drops is to determine the primary system coolant flow rates, as discussed in Section 5.1. In addition, as discussed in Section 4.4.5.1, tests on the primary system prior to initial criticality were made to verify that a conservative primary system coolant flow rate has been used in the design and analyses of the plant.

4.4.2.9.3 Uncertainties Due to Inlet Flow Maldistribution

The effects of uncertainties in the inlet flow maldistribution criteria used in the core thermal analyses are discussed in Section 4.4.4.2.2.

4.4.2.9.4 Uncertainty in DNB Correlation

The uncertainty in the DNB correlation can be written as a statement on the probability of not being in DNB based on the statistics of the DNB data. This is discussed in Section 4.4.2.2.2.

4.4.2.9.5 Uncertainties in DNBR Calculations

The uncertainties in the DNBRs calculated by core thermal-hydraulic analyses (see Section 4.4.4.5.1) due to uncertainties in the nuclear peaking factors are accounted for by applying conservatively high values of the nuclear peaking factors and including measurement error allowances in the statistical evaluation of the limit DNBR using the RTDP (see Section 4.4.1.1). In

addition, conservative values for the engineering hot channel factors are used as discussed in Section 4.4.2.2.4. The results of a sensitivity study (Reference 18) with THINC-IV, a VIPRE-01 equivalent code, show that the minimum DNBR in the hot channel is relatively insensitive to variations in the core-wide radial power distribution (for the same value of $F^N_{\Delta H}$).

The ability of the VIPRE-01 Code to accurately predict flow and enthalpy distributions in rod bundles is discussed in Section 4.4.4.5.1. Studies have been performed (References 18, 90) to determine the sensitivity of the minimum DNBR in the hot channel to the void fraction correlation (also see Section 4.4.2.4); the inlet velocity and exit pressure distributions assumed as boundary conditions for the analysis; and the grid pressure loss coefficients. The results of these studies show that the minimum DNBR in the hot channel is relatively insensitive to variations in these parameters. The range of variations considered in these studies covered the range of possible variations in these parameters.

4.4.2.9.6 Uncertainties in Flow Rates

The uncertainties associated with loop flow rates are discussed in Section 5.1. For core thermal performance evaluations, a thermal design loop flow is used which accounts for both prediction and measurement uncertainties. In addition, a small fraction of the thermal design flow is assumed to be ineffective for core heat removal capability because it bypasses the core through the various available vessel flow paths described in Section 4.4.4.2.1.

4.4.2.9.7 Uncertainties in Hydraulic Loads

As discussed in Section 4.4.2.6.2, hydraulic loads on the fuel assembly are evaluated for a pump overspeed transient which creates flow rates 18 to 20 percent greater than the mechanical design flow. As stated in Section 5.1, the mechanical design flow is greater than the best estimate or most likely flow rate value for the actual plant operating condition.

4.4.2.9.8 Uncertainty in Mixing Coefficient

The value of the mixing coefficient, TDC, used in VIPRE analyses for this application is 0.038, approved for grid spacing $\leq$ 22 in.

The results of the mixing tests done on 17 x 17 geometry, as discussed in Section 4.4.2.2.3, had a mean value of TDC of 0.059 and standard deviation of 0.007. Calculation of generic DNBR margin was done utilizing a 0.038 TDC.

4.4.2.10 Flux Tilt Considerations

Significant quadrant power tilts are not anticipated during normal operation since this phenomenon is caused by some asymmetric perturbation. A dropped or misaligned rod cluster control assembly could cause changes in hot channel factors. However, these events are analyzed separately in Chapter 15.0. This discussion will be confined to flux tilts caused by x-y xenon transients, inlet temperature mismatches, enrichment variations within tolerances, and so forth.

The design value of the enthalpy rise hot channel factor $F^N_{\Delta H}$, is assumed to be sufficiently conservative such that flux tilts up to and including the alarm point (see the Technical Specifications) will not result in values of $F^N_{\Delta H}$ greater than that assumed in the limiting analysis. The design value of F_Q does not include a specific allowance for quadrant flux tilts.

When the indicated quadrant power tilt ratio exceeds 1.02, corrective action must be taken. The procedure to be followed is explained in detail in the Technical Specifications. The quadrant power tilt ratio limit assures that the radial power distribution satisfies the design values used in the power capability analysis.

4.4.2.11 Fuel and Cladding Temperatures

Consistent with the thermal-hydraulic design bases described in Section 4.4.1, the following discussion pertains mainly to fuel pellet temperature evaluation. A discussion of fuel clad integrity is presented in Section 4.2.3.1.

The thermal-hydraulic design assures that the maximum fuel temperature is below the melting point of UO_2. The temperature distribution within the fuel pellet is predominantly a function of the local power density and the UO_2 thermal conductivity. However, the computation of radial fuel temperature distributions combines crud, oxide, clad gap and pellet conductances. The factors which influence these conductances, such as gap size (or contact pressure), internal gas pressure, gas composition, pellet density, time dependent fuel densification and radial power distribution within the pellet, etc., have been combined into a semi-empirical thermal model. This thermal model enables the determination of these factors and their net effects on temperature profiles. The temperature predictions have been compared to inpile fuel temperature measurements with good results.

As described in Reference 3, fuel rod thermal evaluations (fuel centerline, average and surface temperatures) are determined throughout the fuel rod lifetime with consideration of time dependent densification. To determine the maximum fuel temperatures, various burnup rods, including the highest burnup rod, are analyzed over the rod linear power range of interest.

The principal factors which are employed in the determination of the fuel temperature are discussed below.

4.4.2.11.1 UO_2 Thermal Conductivity

The thermal conductivity of uranium dioxide was evaluated from data reported by Howard, et al. (Ref. 37); Lucks et al. (Ref. 38); Daniel, et al. (Ref. 39); Feith (Ref. 40); Vogt, et al. (Ref. 41); Nishijima, et al. (Ref. 42); Wheeler, et al. (Ref. 43); Godfrey, et al. (Ref. 44); Stora, et al. (Ref.45); Bush (Ref. 46); Asamoto, et al. (Ref. 47); Kruger (Ref. 48); and Gyllander (Ref. 52).

At higher temperatures, thermal conductivity is best obtained by utilizing the integral conductivity to melt, which can be determined with more certainty. From an examination of the data, it has been concluded that the best estimate for the value of $\int_0^{2800^\circ C} Kdt$ is 93 watts/cm. This conclusion is based on the integral values reported by Gyllander (Ref. 52), Lyons, et al. (Ref. 53), Coplin, et al. (Ref. 54), Duncan (Ref. 50), Bain (Ref. 55), and Stora (Ref. 56).

The design curve for the thermal conductivity is shown in Figure 4.4-9. The section of the curve at temperatures between 0° and 1,300°C is in excellent agreement with the recommendation of the IAEA panel (Ref. 57). The section of the curve above 1,300°C is derived for an integral value of 93 watts/cm (Ref. 50, 52 and 56).

Thermal conductivity of UO2 at 95-percent theoretical density can be represented best by the following equation:

$$K = \frac{1}{11.8 + 0.0238T} + 8.775 \times 10^{-13} T^3 \qquad [4.4\text{-}13]$$

where:

K = watts/cm-°C
T = °C

4.4.2.11.2 Radial Power Distribution in UO2 Fuel Rods

An accurate description of the fuel rod radial power distribution as a function of burnup is needed for determining the power level for incipient fuel melting and other important performance parameters, such as pellet thermal expansion, fuel swelling, and fission gas release rates. Radial power distributions in UO_2 fuel rods are determined with the neutron transport theory code, LASER. The LASER Code has been

validated by comparing the code predictions on radial burnup and isotopic distributions with measured radial microdrill data (Ref. 58 and 59). A "radial power depression factor," f, is determined using radial power distributions predicted by LASER. The factor f enters into the determination of the pellet centerline temperature, T_C, relative to the pellet surface temperature, T_S, through the expression:

$$\int_{T_S}^{T_C} K(T)dT = \frac{q'f}{4\pi} \qquad [4.4\text{-}14]$$

where:

K(T) = the thermal conductivity for UO_2 with a uniform density distribution
q' = the linear power generation rate

4.4.2.11.3 Gap Conductance

The temperature drop across the pellet-clad gap is a function of the gap size and the thermal conductivity of the gas in the gap. The gap conductance model is selected such that when combined with the UO_2 thermal conductivity model, the calculated fuel centerline temperatures predict the inpile temperature measurements. The temperature drop across the gap is calculated by assuming an annular gap conductance model of the following form:

$$h = \frac{K_{gas}}{\frac{\delta}{2} + \delta_r}$$

where:

h = contact conductance, (Btu/hr-ft^2-°F)
K_{gas} = thermal conductivity of the gas mixture including a correction factor (Reference 57) for the accommodation coefficient for light gases, e.g., helium, (Btu/hr-ft-°F)
δ = diametral gap size, (ft)
δ_r = effective gap spacing due to surface roughness, (ft)

or an empirical correlation derived from thermocouple and melt radius data.

The larger gap conductance value from these two equations is used to calculate the temperature drop across the gap for noncontact gaps.

For evaluations in which the pellet-clad gap is closed, a contact conductance is calculated. The contact conductance between UO2 and Zircaloy has been measured and found to be dependent on the contact pressure, composition of the gas at the interface, and the surface roughness (References 60 and 61). This information together with the pellet and clad inner surface roughness for Westinghouse fuel leads to the following correlation:

$$h = 0.6P + \frac{K_{gas}}{\delta_r}$$

where:

h = contact conductance, (Btu/hr-ft^2-°F)
K_{gas} = thermal conductivity of the gas mixture including a correction factor (Reference 57) for the accommodation coefficient for light gases, e.g., helium, (Btu/hr-ft-°F)
δ_r = effective gap spacing due to surface roughness, (ft)
P = contact pressure, (psi)

4.4.2.11.4 Surface Heat Transfer Coefficients

The fuel rod surface heat transfer coefficients during subcooled forced convection and nucleate boiling are presented in Section 4.4.2.7.1.

4.4.2.11.5 Fuel Clad Temperatures

The outer surface of the fuel rod at the hot spot operates at a temperature of approximately 660 F for steady state operation at rated power throughout core life due to the presence of nucleate boiling. Initially (beginning-of-life), this temperature is that of the clad metal outer surface.

During operation over the life of the core, the buildup of oxides and crud on the fuel rod surface causes the clad surface temperature to increase. Allowance is made in the fuel center melt evaluation for this temperature rise. Since the thermal-hydraulic design basis limits DNB, adequate heat transfer is provided between the fuel clad and the reactor coolant so that the core thermal output is not limited by considerations of clad temperature.

4.4.2.11.6 Treatment of Peaking Factors

The total heat flux hot channel factor, F_Q, is defined as the ratio of the maximum to core average heat flux. The design value of F_Q as presented in Table 4.3-2 and discussed in Section 4.3.2.2.6, is 2.50 for normal operation. This results in a peak linear power at full power conditions of 14.23 for 3565 MWt operation.

As described in Section 4.3.2.2.6, the peak linear power resulting from overpower transients/operator errors (assuming the maximum overpower value listed in Chapter 15) is limited such that the centerline fuel melt kW/ft limit is never exceeded. The centerline temperature kW/ft must be below the UO_2 melt temperature over the lifetime of the rod, including allowances for uncertainties. The fuel temperature design basis is discussed in Section 4.4.1.2 and results in a maximum allowable calculated centerline temperature of 4,700°F. The centerline temperature at the peak linear power resulting from overpower transients/operator errors (assuming the maximum overpower value listed in Chapter 15) is below that required to produce melting.

4.4.3 DESCRIPTION OF THE THERMAL AND HYDRAULIC DESIGN OF THE REACTOR COOLANT SYSTEM

4.4.3.1 Plant Configuration Data

Plant configuration data for the thermal hydraulic and fluid systems external to the core are provided as appropriate in Chapters 5.0, 6.0, and 9.0. Implementation of the emergency core cooling system (ECCS) is discussed in Chapter 15.0. Some specific areas of interest are the following:

a. Total coolant flow rates for the reactor coolant system (RCS) and each loop are provided in Table 5.1-1. Flow rates employed in the evaluation of the core are presented throughout Section 4.4.

b. Total RCS volume including pressurizer and surge line, RCS liquid volume including pressurizer water at steady state power conditions are given in Table 5.1-1.

c. The flow path length through each volume may be calculated from physical data provided in the above referenced tables.

d. The height of fluid in each component of the RCS may be determined from the physical data presented in Section 5.4. The components of the RCS are water filled during power operation with the pressurizer being approximately 60 percent water filled.

e. Components of the ECCS are to be located so as to meet the criteria for net positive suction head described in Section 6.3.

f. Line lengths and sizes for the safety injection system are determined so as to guarantee a total system resistance which will provide, as a minimum, the fluid delivery rates assumed in the safety analyses described in Chapter 15.0.

g. The parameters for components of the RCS are presented in Section 5.4.

h. The steady state pressure drops and temperature distributions through the RCS are presented in Table 5.1-1.

4.4.3.2 Operating Restrictions on Pumps

The minimum net positive suction head and minimum seal injection flow rate must be established before operating the reactor coolant pumps. With the minimum 6-gpm labyrinth seal injection flow rate established before each pump operation, the operator will have to verify that the system pressure satisfies net positive suction head requirements.

4.4.3.3 Power-Flow Operating Map (BWR)

Not applicable to WCGS.

4.4.3.4 Temperature-Power Operating Map

The relationship between RCS temperature and power is shown in Figure 4.4-10.

The effects of reduced core flow due to inoperative pumps are discussed in Sections 5.4.1, 15.2.5, and 15.3.4. Natural circulation capability of the system is shown in Table 15.2-2.

4.4.3.5 Load Following Characteristics

Load follow using control rod motion and dilution or boration by the boron system is discussed in Section 4.3.2.4.16.

The RCS is designed on the basis of steady state operation at full power heat load. The reactor coolant pumps utilize constant speed drives as described in Section 5.4, and the reactor power is controlled to maintain average coolant temperature at a value which is a linear function of load, as described in Section 7.7.

4.4.3.6 Thermal and Hydraulic Characteristics Summary Table

The thermal and hydraulic characteristics are given in Tables 4.3-1 and 4.4-1.

4.4.4 EVALUATION

4.4.4.1 Critical Heat Flux

The critical heat flux correlation utilized in the core thermal analysis is explained in detail in Section 4.4.2.

4.4.4.2 Core Hydraulics

4.4.4.2.1 Flow Paths Considered in Core Pressure Drop and Thermal Design

The following flow paths for core bypass flow are considered:

a. Flow through the spray nozzles into the upper head for head cooling purposes

b. Flow entering into the rod cluster control guide thimbles to cool the control rods

c. Leakage flow from the vessel inlet nozzle directly to the vessel outlet nozzle through the gap between the vessel and the barrel

d. Flow introduced between the baffle and the barrel for the purpose of cooling these components and which is not considered to be available for core cooling

e. Flow in the gaps between the fuel assemblies on the core periphery and the adjacent baffle wall

The above contributions are evaluated each cycle to confirm that the design value of the core bypass flow is met.

Flow model test results for the flow path through the reactor are discussed in Section 4.4.2.7.2.

4.4.4.2.2 Inlet Flow Distributions

Data from several 1/7 scale hydraulic reactor model tests (Ref. 23, 24, and 62) have been utilized in arriving at the core inlet flow maldistribution criteria to be used in the VIPRE analyses (see Section 4.4.4.5.1). THINC-I analyses made using this data have indicated that a conservative design basis is to consider a 5-percent reduction in the flow to the hot assembly (Ref. 63). The same design basis of 5-percent reduction to the hot assembly inlet is used in VIPRE analyses.

The experimental error estimated in the inlet velocity distribution has been considered as outlined in Reference 18 where the sensitivity of changes in inlet velocity distributions to hot channel thermal performance is shown to be small. Studies (Ref. 18) made with the improved THINC model (THINC-IV) show that it is adequate to use the 5-percent reduction in inlet flow to the hot assembly for a loop out of service based on the experimental data in References 23 and 24.

The effect of the total flow rate on the inlet velocity distribution was studied in the experiments of Reference 23. As was expected, on the basis of the theoretical analysis, no significant variation could be found in inlet velocity distribution with reduced flow rate.

4.4.4.2.3 Empirical Friction Factor Correlations

Two empirical friction factor correlations are used in the VIPRE-01 Code (described in Section 4.4.4.5.1).

The friction factor in the axial direction, parallel to the fuel rod axis, is evaluated using a correlation for the smooth tube (Reference 9). The effect of two-phase flow on the friction loss is expressed in terms of a single-phase friction pressure drop and a two-phase friction multiplier. The multiplier is calculated directly using the homogeneous equilibrium flow model.

The flow in the lateral directions, normal to the fuel rod axis, views the reactor core as a large tube bank. Thus, the lateral friction factor proposed by Idel'chik (Reference 25) is applicable.

This correlation is of the form:

$$F_L = A\,Re_L^{-0.2}$$

where:

A is a function of the rod pitch and diameter as given in Reference 25.
Re_L is the lateral Reynolds number based on the rod diameter.

Extensive comparisons of VIPRE-01 predictions, using these correlations to THINC-IV predictions are given in Reference 9, and verify the applicability of these correlations in pressurized water reactor design.

4.4.4.3 Influence of Power Distribution

The core power distribution, which is largely established at beginning-of-life by fuel enrichment, loading pattern, and core power level, is also a function of variables such as control rod worth and position and fuel depletion throughout lifetime. Radial power distributions in various planes of the core are often illustrated for general interest. However, the core radial enthalpy rise distribution, as determined by the integral of power up each channel, is of greater importance for DNB analyses. These radial power distributions, characterized by $F^N_{\Delta H}$ (defined in Section 4.3.2.2.1) as well as axial heat flux profiles are discussed in the following two sections.

4.4.4.3.1 Nuclear Enthalpy Rise Hot Channel Factor, $F^N_{\Delta H}$

Given the local linear power density q'(kW/ft) at a point x, y, z in a core with N fuel rods and height H,

$$F^N_{\Delta H} = \frac{\text{hot rod power}}{\text{average rod power}} = \frac{\text{Max}\int_0^H q'(x_O,y_O,z_O)dz}{\frac{1}{N}\sum_{\substack{\text{all}\\ \text{rods}}}\int_0^H q'(x,y,z)dz} \qquad [4.4\text{-}18]$$

The location of minimum DNBR depends on the axial profile, and the value of DNBR depends on the enthalpy rise to that point. Basically, the maximum value of the rod integral is used to identify the most likely rod for minimum DNBR. An axial power profile is obtained which, when normalized to the design value of $F^N_{\Delta H}$ recreates the axial heat

flux along the limiting rod. The surrounding rods are assumed to have the same axial profile with rod average powers which are typical distributions found in hot assemblies. In this manner, worst-case axial profiles can be combined with worst-case radial distributions for reference DNB calculations.

It should be noted again that $F^N_{\Delta H}$ is an integral and is used as such in DNB calculations. Local heat fluxes are obtained by using hot channel and adjacent channel explicit power shapes which take into account variations in horizontal power shapes throughout the core. The design radial power distribution discussed in Reference 18 is used in the VIPRE-01 model.

For operation at a fraction P of full power, the design $F^N_{\Delta H}$ used is given by:

$$F^N_{\Delta H} = 1.65\ [1 + 0.3\ (1 - P)] \qquad [4.4\text{-}19]$$

The permitted relaxation of $F^N_{\Delta H}$ with power level is included in the DNB protection setpoints and allows radial power shape changes with rod insertion to the insertion limits (Ref. 66), thus allowing greater flexibility in the nuclear design.

4.4.4.3.2 Axial Heat Flux Distributions

As discussed in Section 4.3.2.2, the axial heat flux distribution can vary as a result of rod motion or power change or due to a spatial xenon transients which may occur in the axial direction. Consequently, it is necessary to measure the axial power imbalance by means of the excore nuclear detectors (as discussed in Section 4.3.2.2.7) and protect the core from excessive axial power imbalance. The reactor trip system provides automatic reduction of the trip setpoint in the Overtemperature ΔT channels on excessive axial power imbalance; that is, when a large axial offset corresponds to an axial shape which could lead to a DNBR which is less than that calculated for the reference DNB design axial shape.

The reference DNB design axial shape used is a chopped cosine shape with a peak to average value of 1.70.

To determine the penalty to be taken in protection setpoints for extreme values of flux difference, this reference shape is supplemented by other axial shapes skewed to the bottom and top of the core. The course of those accidents in which DNB is a concern is analyzed in Chapter 15.0, assuming that the protection setpoints have been set on the basis of these shapes. In many cases, the axial power distribution in the hot channel changes throughout the course of the accident due to rod motion, coolant temperature, and power level changes.

The initial conditions for the accidents for which DNB protection is required are assumed to be those permissible within the relaxed axial offset control strategy for the load maneuvers described in Reference 67. In the case of the loss-of-flow accident, the hot channel heat

flux profile is very similar to the power density profile in normal operation preceding the accident. It is, therefore, possible to illustrate the calculated minimum DNBR for conditions representative of the loss-of-flow accident as a function of the flux difference initially in the core. A plot of this type is provided in Figure 4.4-11 for first core initial conditions. As noted on this figure, all power shapes were evaluated with a full power radial peaking factor ($F^N_{\Delta H}$) of 1.55. The radial contribution to the hot rod power shape is conservative both for the initial condition and for the condition at the time of minimum DNBR during the loss of flow transient. Also shown is the minimum DNBR calculated for the reference power shape at the same conditions.

4.4.4.4 Core Thermal Response

A general summary of the steady state thermal-hydraulic design parameters including thermal output, flow rates, etc., is provided in Table 4.4-1.

As stated in Section 4.4-1, the design bases for the thermal-hydraulic design of the reactor core are to prevent DNB and to prevent fuel melting for Condition I and II events. The protective systems described in Chapter 7.0 are designed to meet these bases. The response of the core to Condition II transients is given in Chapter 15.0.

4.4.4.5 Analytical Techniques

4.4.4.5.1 Core Analysis

The objective of reactor core thermal design is to determine the maximum heat-removal capability in all flow subchannels and to show that the core safety limits are not exceeded using the most conservative power distribution. The thermal design takes into account local variations in dimensions, power generation, flow redistribution, and mixing. VIPRE-01 is a realistic three-dimensional matrix model which has been developed to account for hydraulic and nuclear effects on the enthalpy rise in the core (Reference 9). The behavior of the hot assembly is determined by superimposing the power distribution among the assemblies upon the inlet flow distribution while allowing for flow mixing and flow distribution between assemblies. The local variations in power, fuel rod and pellet fabrication, and mixing within the hottest assembly are superimposed on the average conditions of the hottest assembly in order to determine the conditions in the hot channel. Conservation equations of mass, axial and lateral momentum and energy are solved for the fluid enthalpy, axial flow rate, lateral flow and pressure drop.

4.4.4.5.2 Steady State Analysis

The VIPRE-01 core model as approved by the NRC, Reference 9, is used with the applicable DNB correlations to determine DNBR distributions along the hot channels of the reactor core under all expected operating conditions. The VIPRE-01 code is described in detail in Reference 90, including discussions on code validation with experimental data. The VIPRE-01 modeling method is described in Reference 9, including empirical models and correlations used. The effect of crud on the flow and enthalpy distribution in the core is not directly accounted for in the VIPRE-01 evaluations. However, conservative treatment by the VIPRE-01 modeling method has been demonstrated to bound this effect in DNBR calculations (Reference 9). Estimates of uncertainties are discussed in Section 4.4.2.9.

4.4.4.5.3 Experimental Verification

Experimental verification of VIPRE-01 is presented in References 9 and 90. The VIPRE-01 analysis methodology is based on a knowledge and understanding of the heat transfer and hydrodynamic behavior of the coolant flow and the mechanical characteristics of the fuel elements. VIPRE-01 analysis provides a realistic evaluation of the core performance and is used in the thermal analyses as described above.

4.4.4.5.4 Transient Analysis

The conservation equations in the VIPRE-01 code contain the necessary accumulation of terms for transient DNB calculations. The input description can include one of the following time dependent arrays:

1. Inlet flow variation,
2. Core heat flux variation,
3. Core pressure variation,
4. Inlet temperature or enthalpy variation.

At the beginning of the transient, the calculation procedure is carried out as in the steady state analysis. The time is incremented by an amount determined either by the user or by the time step control options in the code itself. At each new time step the calculations are carried out with the addition of the accumulation terms which are evaluated using the information from the previous time step. This procedure is continued until a preset maximum time is reached. At time intervals selected by the user, a complete description of the coolant parameter distributions as well as DNBR is printed out. In this manner the variation of any parameter with time can be readily determined.

4.4.4.6 Hydrodynamic and Flow Power Coupled Instability

Boiling flows may be susceptible to thermo-hydrodynamic instabilities (Reference 72). These instabilities are undesirable in reactors, since they may cause a change in thermal-hydraulic conditions that may lead to a reduction in the DNB heat flux relative to that observed during a steady flow condition or to undesired forced vibrations of core components. Therefore, a thermal-hydraulic design criterion was developed which states that mode of operation under Condition I and II events shall not lead to thermo-hydrodynamic instabilities.

Two specific types of flow instabilities are considered for Westinghouse PWR operation. These are the Ledinegg or flow excursion type of static instability and the density wave type of dynamic instability. A Ledinegg instability involves a sudden change in flow rate from one steady state to another. This instability occurs (Reference 72) when the slope of the reactor coolant system pressure drop-flow rate curve ($\partial\Delta P/\partial G|_{internal}$) becomes algebraically smaller than the loop supply (pump head) pressure drop-flow rate curve ($\partial\Delta P/\partial G|_{external}$). The criterion for stability is thus $\partial\Delta P/\partial G|_{internal} > \partial\Delta P/\partial G|_{external}$. The Westinghouse pump head curve has a negative slope ($\partial\Delta P/\partial G|_{external} < 0$), whereas the reactor coolant system pressure drop-flow curve has a positive slope ($\partial\Delta P/\partial G|_{internal} > 0$) over the Condition I and Condition II operational ranges. Thus, the Ledinegg instability will not occur.

The mechanism of density wave oscillations in a heated channel has been described in Lahey and Moody (Reference 73). Briefly, an inlet flow fluctuation produces an enthalpy perturbation. This perturbs the length and the pressure drop of the single phase region and causes quality or void perturbations in the two-phase regions which travel up the channel with the flow. The quality and length perturbations in the two-phase region create two-phase pressure drop perturbations. However, since the total pressure drop across the core is maintained by the characteristics of the fluid system external to the core, then the two-phase pressure drop perturbation feeds back to the single phase region. These resulting perturbations can either be attenuated or self-sustained.

A simple method has been developed by Ishii (Reference 74) for parallel closed channel systems to evaluate whether a given condition is stable with respect to the density wave type of dynamic instability. This method had been used to assess the stability of the typical Westinghouse reactor designs similar to Wolf Creek (References 75, 76 and 77), under Condition I and II operation. The results indicate that a large margin to density wave instability exists, e.g., increases on the order of 150 percent of rated reactor thermal power would be required for the predicted inception of this type of instability.

The application of the method of Ishii (Reference 74) to Westinghouse reactor designs is conservative due to the parallel open channel feature of Westinghouse PWR cores. For such cores, there is little resistance to lateral flow leaving the flow channels of high power density. There is also energy transfer from channels of high power density to lower power density channels. This coupling with cooler channels has led to the opinion that an open channel configuration is more stable than the above closed channel analysis under the same boundary conditions. Flow stability tests (Reference 81) have been conducted where the closed channel systems were shown to be less stable than when the same channels were cross connected at several locations. The cross connections were such that the resistance to channel to channel cross flow and enthalpy perturbations would be greater than that which would exist in a PWR core which has a relatively low resistance to cross flow.

Any observed flow instabilities have occurred almost exclusively in closed channel systems operating at low pressure relative to the Westinghouse PWR operating pressures. Kao, Morgan, and Parker (Reference 82) analyzed parallel closed channel stability experiments simulating a reactor core flow. These experiments were conducted at pressures up to 2200 psia. The results showed that for flow and power levels typical of power reactor conditions no flow oscillations could be induced above 1200 psia. Additional evidence that flow instabilities do not adversely affect thermal margin is provided by the data from the rod bundle DNB tests. Many Westinghouse rod bundles have been tested over wide ranges of operating conditions with no evidence of premature DNB or of inconsistent data which might be indicative of flow instabilities in the rod bundle.

In summary, it is concluded that thermo-hydrodynamic instabilities will not occur under Condition I and II modes of operation for Westinghouse PWR designs. A large power margin exists to the predicted inception of such instabilities. Analysis has been performed which shows that minor plant to plant differences in Westinghouse reactor designs such as fuel assembly arrays, core power to flow ratios, fuel assembly length, etc. will not result in gross deterioration of the above power margin.

4.4.4.7 Fuel Rod Behavior Effects from Coolant Flow Blockage

Coolant flow blockages can occur within the coolant channels of a fuel assembly or external to the reactor core. The effects on fuel rod behavior of blockages within the assembly are more pronounced than external blockages of the same magnitude. In both cases, the flow blockages cause local reductions in coolant flow. The amount of local flow reduction, where it occurs, and how far along the flow stream the reduction persists are considerations which will influence the fuel rod behavior. The effects of coolant flow blockages in terms of maintaining rated core performance are determined both by analytical and experimental methods. The experimental data are usually used to augment analytical tools, such as computer programs similar to the THINC-IV or VIPRE-01 program. Inspection of DNB correlations (see Section 4.4.2.2 and Reference 10) shows that the predicted DNBR is dependent upon the local values of quality and mass velocity.

The VIPRE-01 code is capable of predicting the effects of local flow blockages on DNBR within the fuel assembly on a subchannel basis, regardless of where the flow blockage occurs. In Reference 90, it is shown that for a fuel assembly similar to the Westinghouse design, VIPRE-01 accurately predicts the flow distribution within the fuel assembly when the inlet nozzle is completely blocked. Full recovery of the flow was found to occur about 30 inches downstream of the blockage. With the reactor operating at the nominal full power conditions specified in Table 4.4-1, the effects of an increase in enthalpy and decrease in mass velocity in the lower portion of the fuel assembly would not result in the reactor reaching the design DNBR specified in Section 4.4.1.1.

From a review of open literature, it is concluded that flow perturbations caused by flow blockage in "open lattice cores" similar to the Westinghouse cores are confined to the vicinity of the blockage. For a flow blockage in a single flow cell, Ohtsubo, et al. (Reference 78) show that the mean bundle velocity is approached asymptotically about 4 inches downstream from the blockage. Similar results were also found for two and three cells completely blocked. Basmer, et al. (Reference 79) tested an open lattice fuel assembly in which 41 percent of the sub-channels were completely blocked in the center of the test bundle between spacer grids. Their results show the stagnant zone behind the flow blockage essentially disappears after 1.65 L/De or about 5 inches for their test bundle. They also found that leakage flow through the blockage tended to shorten the stagnant zone or, in essence, the complete recovery length. Thus, local flow blockages within a fuel assembly have little effect on sub-channel enthalpy rise. The reduction in local mass velocity is then the main parameter which affects the DNBR and is based on the assumption of fully developed flow along the full channel length. In reality, a local flow blockage is expected to promote turbulence and thus would likely not affect DNBR at all.

Coolant flow blockages induce local crossflows as well as promote turbulence. Fuel rod behavior is changed under the influence of a sufficiently high crossflow component. Fuel rod vibration could occur, caused by this crossflow component, through vortex shedding or turbulent mechanisms. If the crossflow velocity exceeds the limit established for fluid elastic stability, it could result in large amplitude whirling. The limits for a controlled vibration mechanism are established from studies of vortex shedding and turbulent pressure fluctuations. The crossflow velocity required to exceed fluid elastic stability limits is dependent on the axial location of the blockage and the characterization of the crossflow (jet flow or not). These limits are greater than those for vibratory fuel rod wear. Cross-flow velocity above the established limits can lead to mechanical wear of the fuel rods at the grid support locations. Fuel rod wear due to flow induced vibration is considered in the fuel rod fretting evaluation (see Section 4.2.3.1).

4.4.5 TESTING AND VERIFICATION

4.4.5.1 Tests Prior to Initial Criticality

A reactor coolant flow test is performed following fuel loading but prior to initial criticality. Coolant loop elbow differential pressure readings are obtained in this test. This data allows determination of the coolant flow rates at reactor operating conditions. This test verifies that proper coolant flow rates have been used in the core thermal and hydraulic analysis. Chapter 14.0 describes the initial test programs.

4.4.5.2 Initial Power and Plant Operation

Core power distribution measurements are made at several core power levels (see Chapter 14.0). These tests are used to ensure that conservative peaking factors are used in the core thermal and hydraulic analysis.

Additional demonstration of the overall conservatism of the THINC analysis was obtained by comparing THINC predictions to incore thermocouple measurements (Ref. 80). These measurements were performed on the Zion reactor. No further in-reactor testing is planned.

4.4.5.3 Component and Fuel Inspections

Inspections performed on the manufactured fuel are described in Section 4.2.4. Fabrication measurements critical to thermal and hydraulic analysis are obtained to verify that the engineering hot channel factors in the design analyses (see Section 4.4.2.2.4) are met.

4.4.6 INSTRUMENTATION REQUIREMENTS

4.4.6.1 Incore Instrumentation

Instrumentation is located in the core so that by correlating movable neutron detector information with fixed thermocouple information radial, axial, and azimuthal core characteristics may be obtained for all core quadrants.

The incore instrumentation system is comprised of thermocouples, positioned to measure fuel assembly coolant outlet temperatures at preselected positions, and fission chamber detectors positioned in guide thimbles which run the length of selected fuel assemblies to measure the neutron flux distribution. Figure 4.4-21 shows the number and location of instrumented assemblies in the core. The core-exit thermocouples can provide a backup to the flux monitoring instrumentation for monitoring power distribution.

The movable incore neutron detector system would be used for more detailed mapping if the thermocouple system were to indicate an abnormality. These two complementary systems are more useful when taken together than either system alone would be. The incore instrumentation system is described in more detail in Section 7.7.1.9.

The incore instrumentation is provided to obtain data from which fission power density distribution in the core, and fuel burnup distribution may be determined.

4.4.6.2 Overtemperature and Overpower DT Instrumentation

The Overtemperature ΔT trip protects the core against low DNBR. The Overpower ΔT trip protects against excessive power (fuel rod rating protection).

As discussed in Section 7.2.1.1.2, factors included in establishing the Overtemperature ΔT and Overpower ΔT trip setpoints includes the reactor coolant temperature in each loop and the axial distribution of core power through the use of the two section excore neutron detectors.

4.4.6.3 Instrumentation to Limit Maximum Power Output

The output of the three ranges (source, intermediate, and power) of detectors, with the electronics of the nuclear instruments, are used to limit the maximum power output of the reactor within their respective ranges.

There are six radial locations containing a total of eight neutron flux detectors installed around the reactor in the primary shield, two proportional counters for the source range installed on opposite "flat" portions of the core containing the primary startup sources at an elevation approximately 1/4 of the core height. Two compensated ionization chambers for the intermediate range, located in the same instrument wells and detector assemblies as the source range detectors, are positioned at an elevation corresponding to 1/2 of the core height. Four dual section uncompensated ionization chamber assemblies for the power range are installed vertically at the four corners of the core and are located equidistant from the reactor vessel at all points and, to minimize neutron flux pattern distortions, within 1 foot of the reactor vessel. Each power range detector provides two signals corresponding to the neutron flux in the upper and in the lower sections of a core quadrant. The three ranges of detectors are used as inputs to monitor neutron flux from a completely shutdown condition to 120 percent of full power with the capability of recording overpower excursions up to 200 percent of full power.

The output of the power range channels is used for:

a. The rod speed control function

b. Alerting the operator to an excessive power unbalance between the quadrants

c. Protecting the core against the consequences of rod ejection accidents, and

d. Protecting the core against the consequences of adverse power distributions resulting from dropped rods

Details of the neutron detectors and nuclear instrumentation design and the control and trip logic are given in Chapter 7.0. The limits on neutron flux operation and trip setpoints are given in the Technical Specifications.

4.4.6.4 Digital Metal Impact Monitoring System (DMIMS-DX™)

General System Description

The metal impact monitoring system (DMIMS-DX™) at Wolf Creek is designed to detect loose parts in the reactor coolant system. The system consists of sensors preamplifiers, signal conditioners, signal processors and a display. It contains 12 active instrument channels, each comprised of a piezoelectric accelerometer (sensor), signal conditioning and diagnostic equipment.

Redundant sensors are fastened mechanically to the reactor coolant system at each of the following potential loose parts collection regions:

Reactor pressure vessel – upper head region

Reactor pressure vessel – lower head region

Each steam generator – reactor coolant inlet region

The output signal from each accelerometer is passed through a preamplifier and an amplifier. The amplified signal is processed through a discriminator to eliminate noises and signals that are not indicative of loose parts. The processed signal is compared to a preset alarm setpoint. Loose parts detection is accomplished at a frequency range of 1 kHz to 20 kHz, where background signals from the RCS are acceptable. Spurious alarming from control rod stepping is prevented by a module that detects CRDM motion commands and automatically inhibits alarms during control rod stepping.

If a measured signal exceeds the preset alarm level, audible and visible alarms in the control room are activated. Digital signal processors record the times that the first and subsequent impact signals reach various sensors. This timing information provides a basis for locating the loose part. The DMIMS-DX™ also has a provision for audio monitoring of any channel. The audio signal can be compared to a previously recorded audio signal, if desired.

The on-line sensitivity of the LPMS is such that the system will detect a loose part that weighs from 0.25 to 30 pounds and impacts with a kinetic energy of 0.5 feet pounds on the inside surface of the RCS pressure boundary within 3 feet of a sensor.

The DMIMS-DX™ audio and visual alarm capability will remain functional after an Operating Basis Earthquake (OBE). All of the DMIMS-DX™ components are qualified for structural integrity during a Safe Shutdown Earthquake (SSE) and will not mechanically impact any safety-related equipment.

The components of the loose parts monitoring system are designed for the environmental conditions specified in Table 4.4-5. The DMIMS-DX™ components outside containment are located in a mild environment. In addition, the equipment inside containment is designed to remain functional through normal radiation exposures anticipated during a 40-year operating lifetime. Physical separation of the two instrument channels, associated with the redundant sensors at each reactor coolant system location, exists from each sensor to a location accessible during power operation. Capabilities exist for subsequent periodic online channel checks and channel functional tests and for offline channel calibrations at refueling outages.

The loose parts monitoring system complies with NRC Regulatory Guide 1.133, except as noted in USAR Chapter 3, Appendix A, “Conformance to NRC Regulatory Guides”.

Operators were trained in the operation and maintenance of the LPMS prior to Refuel 14 criticality. This consisted of a formal training session onsite by either the onsite training staff or by the vendor using the DMIMS-DX™ that was set up for training in a training lab prior to installation. The vendor can also provide service personnel on short notice to assist the operating staff in operation or maintenance of the equipment and analysis of loose parts signals, as may be required.

4.4.7 REFERENCES

1. Christensen, J. A., Allio, R. J. and Biancheria, A., "Melting Point of Irradiated UO_2," WCAP-6065, February, 1965.

2. Letter from W.D.Reckley (NRC) to B.D.Withers (WCNOC) No. 92-02099, dated Oct. 29, 1992.

3. Weiner, R.A., et al, "Improved Fuel Performance Models for Westinghouse Fuel Rod Design and Safety Evaluations," WCAP-10851-P-A (Proprietary), August 1988.

4. Tong, L. S., "Boiling Heat Transfer and Two-Phase Flow," John Wiley & Sons, New York, 1965.

5. Tong, L. S., "Boiling Crisis and Critical Heat Flux," AEC Critical Review Series, TID-25887, 1972.

6. Tong, L. S., "Critical Heat Fluxes in Rod Bundles," in "Two-Phase Flow and Heat Transfer in Rod Bundles," pp. 31-41, American Society of Mechanical Engineers, New York, 1969.

7. Chelemer, H., Weisman, J. and Tong, L. S., "Subchannel Thermal Analysis of Rod Bundle Cores," WCAP-7015, Revision 1, January, 1969.

8. WCAP-10444-P-A, "Reference Core Report - Vantage 5 Fuel Assembly", S.L.Davidson, Ed., Westinghouse, December 1983.

9. Sung, Y. X., et al., "VIPRE-01 Modeling Qualification for Pressurized Water Reactor Non-LOCA Thermal-Hydraulic Safety Analysis," WCAP-14565-P-A and WCAP-15306-NP-A, October 1999.

10. Tong, L. S., "Prediction of Departure from Nucleate Boiling for an Axially Non-Uniform Heat Flux Distribution," J. Nucl. Energy, 21, 241-248 (1967).

11. "Thermal-Hydraulic Design Procedure Manual", Westinghouse Electric Corporation, Commercial Nuclear Fuel Division, Revision 6.5, 4/90.

12. Cadek, F. F., Motley, F. E. and Dominicis, D. P., "Effect of Axial Spacing on Interchannel Thermal Mixing with the R Mixing Vane Grid," WCAP-7941-P-A (Proprietary) and WCAP-7959-A (Non-Proprietary), January, 1975.

13. Rowe, D. S. and Angle, C. W., "Crossflow Mixing Between Parallel Flow Channels During Boiling, Part II Measurements of Flow and Enthalpy in Two Parallel Channels," BNWL-371, Part 2, December, 1967.

14. Rowe, D. S. and Angle, C. W., "Crossflow Mixing Between Parallel Flow Channels During Boiling, Part III Effect of Spacers on Mixing Between Two Channels," BNWL-371, Part 3, January, 1969.

15. Gonzalez-Santalo, J. M. and Griffith, P., "Two-Phase Flow Mixing in Rod Bundle Subchannels," ASME Paper 72-WA/NE-19.

16. Motley, F. E., Wenzel, A. H. and Cadek, F. F., "The Effect of 17 x 17 Fuel Assembly Geometry on Interchannel Thermal Mixing," WCAP-8298-P-A (Proprietary) and WCAP-8299-A (Non-Proprietary), January, 1975.

17. Cadek, F. F., "Interchannel Thermal Mixing with Mixing Vane Grids," WCAP-7667-P-A (Proprietary) and WCAP-7755-A (Non-Proprietary), January, 1975.

18. Hochreiter, L. E. and Chelemer, H., "Application of the THINC-IV Program to PWR Design," WCAP-8054 (Proprietary) and WCAP-8195 (Non-Proprietary), September, 1973.

19. DeMario, E. E., "Hydraulic Flow Test of the 17 x 17 Fuel Assembly," WCAP-8278 (Proprietary) and WCAP-8279 (Non-Proprietary), February, 1974.

20. Dittus, F. W. and Boelter, L. M. K., "Heat Transfer in Automobile Radiators of the Tubular Type," Calif. Univ. Publication in Eng., 2, No. 13, 443461 (1930).

21. Weisman, J., "Heat Transfer to Water Flowing Parallel to Tube Bundles," Nucl. Sci. Eng., 6, 78-79 (1959).

22. Thom, J. R. S., Walker, W. M., Fallon, T. A. and Reising, G. F. S., "Boiling in Subcooled Water During Flowup Heated Tubes or Annuli," Prc. Instn. Mech. Engrs., 180, Pt. C, 226-46 (1955-66).

23. Hetsroni, G., "Hydraulic Tests of the San Onofre Reactor Model," WCAP-3269-8, June, 1964.

24. Hetsroni, G., "Studies of the Connecticut-Yankee Hydraulic Model," NYO-3250-2, June, 1965.

25. Idel'chik, I. E., "Handbook of Hydraulic Resistance," AEC-TR-6630, 1960.

26. Moody, L. F., "Friction Factors for Pipe Flow," Transaction of the American Society of Mechanical Engineers, 66, pp. 671-684 (1944).

27. Maurer, G. W., "A Method of Predicting Steady State Boiling Vapor Fractions in Reactor Coolant Channels," WAPD-BT-19, pp. 59-70. June, 1960.

28. Griffith, P., Clark, J. A. and Rohsenow, W. M., "Void Volumes in Subcooled Boiling Systems," ASME Paper No. 58-HT-19.

29. Bowring, R. W., "Physical Model, Based on Bubble Detachment, and Calculation of Steam Voidage in the Subcooled Region of a Heated Channel," HPR-10, December, 1962.

30. Kjaerheim, G. and Rolstad, E., "In-Pile Determination of UO_2 Thermal Conductivity, Density Effects and Gap Conductance," HPR-80, December, 1967.

31. Kjaerheim, G., "In-Pile Measurements of Centre Fuel Temperatures and Thermal Conductivity Determination of Oxide Fuels," paper IFA-175 presented at the European Atomic Energy Society Symposium on Performance Experience of Water-Cooled Power Reactor Fuel, Stockholm, Sweden (October 21-22, 1969).

32. Cohen, I., Lustman, B. and Eichenberg, D., "Measurement of the Thermal Conductivity of Metal-Clad Uranium Oxide Rods During Irradiation," WAPD-228, 1960.

33. Clough, D. J. and Sayers, J. B., "The Measurement of the Thermal Conductivity of UO_2 under Irradiation in the Temperature Range 150 C," AERE-R-4690, UKAEA Research Group, Harwell, December, 1964.

34. Stora, J. P., Debernardy, DeSigoyer, B., Delmas, R., Deschamps, P., Ringot, C. and Lavaud, B., Thermal Conductivity of Sintered Uranium Oxide under In-Pile Conditions," EURAEC-1095, 1964.

35. Devold, I., "A Study of the Temperature Distribution in U02 Reactor Fuel Elements," AE-318, Aktiebolaget Atomenergi, Stockholm, Sweden, 1968.

36. Balfour, M. G., Christensen, J. A. and Ferrari, H. M., "In-Pile Measurement of UO_2 Thermal Conductivity," WCAP-2923, March, 1966.

37. Howard, V. C. and Gulvin, T. G., "Thermal Conductivity Determinations on Uranium Dioxide by a Radial Flow Method," UKAEA IG-Report 51, November, 1960.

38. Lucks, C. F. and Deem, H. W., "Thermal Conductivity and Electrical Conductivity of UO_2 " in Progress Reports Relating to Civilian Applications, BMI-1448 (Rev.) for June, 1960; BMI-1489 (Rev.) for December, 1960 and BMI-1518 (Rev.) for May, 1961.

39. Daniel, J. L., Matolich, Jr., J. and Deem, H. W. "Thermal Conductivity of UO_2," HW-69945, September, 1962.

40. Feith, A. D., "Thermal Conductivity of UO_2 by a Radial Heat Flow Method," TID-21668, 1962.

41. Vogt, J., Grandell L. and Runfors, U., "Determination of the Thermal Conductivity of Unirradiated Uranium Dioxide," AB Atomenergi Report RMB-527, 1964, Quoted by IAEA Technical Report Series No. 59, "Thermal Conductivity of Uranium Dioxide."

42. Nishijima, T., Kawada, T. and Ishihata, A., "Thermal Conductivity of Sintered UO_2 and Al_2O_3 at High Temperatures," J. American Ceramic Society, pp. 48, 31, 34 (1965).

43. Ainscough, J. B. and Wheeler, M. J., "Thermal Diffusivity and Thermal Conductivity of Sintered Uranium Dioxide," in Proceedings of the Seventh Conference of Thermal Conductivity, p. 467, National Bureau of Standards, Washington, 1968.

44. Godfrey, T. G., Fulkerson, W., Killie, T. G., Moore, J. P. and McElroy, D. L., "Thermal Conductivity of Uranium Dioxide and Armco Iron by an Improved Radial Heat Flow Technique," ORNL-3556, June, 1964.

45. Stora, J. P., et al., "Thermal Conductivity of Sintered Uranium Oxide Under In-Pile Conditions," EURAEC-1095, August, 1964.

46. Bush, A. J., "Apparatus for Measuring Thermal Conductivity to 2500 C," Westinghouse Research Laboratories Report 64-lP6-401-43 (Proprietary), February, 1965.

47. Asamoto, R. R., Anselin, F. L. and Conti, A. E., "The Effect of Density on the Thermal Conductivity of Uranium Dioxide," GEAP-5493, April, 1968.

48. Kruger, 0. L., Heat Transfer Properties of Uranium and Plutonium Dioxide," Paper 11-N-68F presented at the Fall meeting of Nuclear Division of the American Ceramic Society, September, 1968, Pittsburgh.

49. Hochreiter, L. E., Chelemer, H. and Chu, P. T., "THINC-IV An Improved Program for Thermal-Hydraulic Analysis of Rod Bundle Cores," WCAP-7956, June, 1973.

50. Duncan, R. N., "Rabbit Capsule Irradiation of $U0_2$," CVTR Project, CVNA-142, June, 1962.

51. Not Used.

52. Gyllander, J. A., "In-Pile Determination of the Thermal Conductivity of $U0_2$ in the Range 500-2500 C," AE-411, January, 1971.

53. Lyons, M. F., et al., "UO_2 Powder and Pellet Thermal Conductivity During Irradiation," GEAP-5100-1, March, 1966.

54. Coplin, D. H., et al., "The Thermal Conductivity of $U0_2$ by Direct In-Reactor Measurements," GEAP-5100-6, March, 1968.

55. Bain, A. S., "The Heat Rating Required to Produce Center Melting in Various UO_2 Fuels," ASTM Special Technical Publication, No. 306, pp. 30-46, Philadelphia, 1962.

56. Stora, J. P., "In-Reactor Measurements of the Integrated Thermal Conductivity of UO_2 - Effect of Porosity," Trans. ANS, 13, p.p. 137-138 (1970).

57. International Atomic Energy Agency, "Thermal Conductivity of Uranium Dioxide," Report of the Panel held in Vienna, April, 1965, IAEA Technical Reports Series, No. 59, Vienna, The Agency, 1966.

58. Poncelet, C. G., "Burnup Physics of Heterogeneous Reactor Lattices," WCAP-6069, June, 1965.

59. Nodvick, R. J., "Saxton Core II Fuel Performance Evaluation," WCAP-3385-56, Part II, "Evaluation of Mass Spectrometric and Radiochemical Materials Analyses of Irradiated Saxton Plutonium Fuel," July, 1970.

60. Dean, R. A., "Thermal Contact Conductance Between UO_2 and Zircaloy-2," CVNA-127, May, 1962.

61. Ross, A. M. and Stoute, R. L., "Heat Transfer Coefficient Between UO_2 and Zircaloy-2," AECL-1552, June, 1962.

62. Carter, F. D., "Inlet Orificing of Open PWR Cores," WCAP-7836, January, 1972.

63. Shefcheck, J., "Application of the THINC Program to PWR Design," WCAP-7359-L (Proprietary), August, 1969 and WCAP-7838 (Non-Proprietary), January, 1972.

64. Novendstern, E. H. and Sandberg, R. O., "Single Phase Local Boiling and Bulk Boiling Pressure Drop Correlations," WCAP-2850-L (Proprietary) and WCAP-7916 (Non-Proprietary), April, 1966.

65. Owens, Jr., W. L., "Two-Phase Pressure Gradient," in International Developments in Heat Transfer, Part II, pp. 363-368, ASME, New York, 1961.

66. McFarlane, A. F., "Power Peaking Factors," WCAP-7912-P-A (Proprietary) and WCAP-7912-A (Non-Proprietary), January, 1975.

67. Miller, R. W., et al., "Relaxation of Constant Axial offset Control - FQ Surveillance Technical Specification," WCAP-10216-P-A Rev. 1A, approved version dated February, 1994

68. Vallentine., H. R., "Applied Hydrodynamics," Buttersworth Publishers, London, 1969.

69. Kays, W. M. and London, A. L., "Compact Heat Exchangers," National Press, Palo Alto, 1955.

70. Rowe, D. S., "COBRA-III, a Digital Computer Program for Steady State and Transient Thermal-Hydraulic Analysis of Rod Bundle Nuclear Fuel Elements," BNWL-B-82, 1971.

71. Weisman, J., Wenzel, A. H., Tong, L. S., Fitzsimmons, D., Thorne, W. and Batch, J., "Experimental Determination of the Departure from Nucleate Boiling in Large Rod Bundles at High Pressures," Chem. Eng. Prog. Symp. Ser. 64, No. 82, pp. 114-125 (1968).

72. Boure, J. A., Bergles, A. E., and Tong, L. S, "Review of Two-Phase Flow Instability," Nucl. Engr. Design 25, pgs. 165-192, 1973.

73. Lahey, R. T. and Moody, F. J., "The Thermal Hydraulics of a Boiling Water Reactor," American Nuclear Society, 1977.

74. Ishii, M., Saha, P., and Zuber, N., "An Experimental Investigation of the Thermally Induced Flow Oscillations in Two-Phase Systems," Journal of Heat Transfer, No. 1976, pgs. 612-622.

75. Byron/Braidwood Stations Final Safety Analysis Report, Docket Nos. 50-454, 50-455, 50-456, and 50-457.

76. South Texas Project Units l and 2 Final Safety Analysis Report, Docket Nos. 50-498 and 50-499.

77. Virgil C. Summer Nuclear Station Final Safety Analysis Report, Docket No. 50-395.

78. Ohtsubo, A., and Uruwashi, S., "Stagnant Fluid due to Local Flow Blockage," J. Nucl. Sci. Technol., 9, No. 7, pp. 433-434, (1972).

79. Basmer, P., Kirsh, D. and Schultheiss, G. F., "Investigation of the Flow Pattern in the Recirculation Zone Downstream of Local Coolant Blockages in Pin Bundles," Automwirtschaft, 17, No. 8, pp. 416-417, (1972). (In German).

80. Burke, T. M., Meyer, C. E. and Shefcheck J., "Analysis of Data from the Zion (Unit 1) THINC Verification Test," WCAP-8453-A, May, 1976.

81. Kakac, S., Vexiroglu, T. N., Akyuzlu, K., and Berkol, O, "Sustained and Transient Boiling Flow Instabilities in a Cross-Connected Four-Parallel-Channel Upflow System," Proc of 5th International Heat Transfer Conference, Tokyo, September 3-7, 1974.

82. Kao, H. S., Morgan, C. D., and Parker, W. B., "Prediction of Flow Oscillation in Reactor Core Channel," Trans. ANS Vol. 16, pgs. 212-213, 1973.

83. Skaritka, J. (Ed.), "Fuel Rod Bow Evaluation," WCAP-8691, Rev. l (Proprietary) and WCAP-8692, Rev. 1 (Non-Proprietary), July 1979.

84. Not Used.

85. Letter from C Berlinger, NRC, to E. P. Rahe, Jr., Westinghouse, "Request for Reduction in Fuel Assembly Burnup Limit for Calculation of Maximum Rod Bow Penalty", June 18, 1986.

86. (DELETED)

87. Not Used.

88. Not Used.

89. Neises, G.J, (WCNOC), "WCGS Rerating Program Monthly Status Report for January/February 1992 and the Phase 3 Limiting Events Analysis Report", attachment to NS 92-0278, 2/28/92.

90. Letter from C.E.Rossi, NRC, to J.A.Blaisdell, UGRA, "Acceptance for Referencing of Licensing Topical Report, EPRI NP-2511-CCM, 'VIPRE-01 : A Thermal Hydraulic Code for Reactor Cores,' Volumes 1,2,3 and 4" May, 1986.

91. Friedland, A. J., Ray, S., "Revised Thermal Design Procedure," WCAP-11397-P-A, April, 1989.

92. Letter from Stone, J. C., USNRC, to Carns, N. S., WCNOC, "Wolf Creek Generating Station - Amendment No. 92 to Facility Operationg License No. NPF-42," dated December 8, 1995.

93. Leidich, A., et. al., "Extended Application of ABB-NV Correlation and Modified ABB-NV Correlation WLOP for PWR Low Pressure Applications," WCAP-14565-P-A Addendum 2-P-A, April 2008.

TABLE 4.4-1

THERMAL AND HYDRAULIC COMPARISON TABLE

Design Parameters	WCGS Unit
Reactor core heat output, MWt	3,565
Reactor core heat output, 10^6Btu/hr	12,164
Heat generated in fuel, %	97.4
System pressure, nominal psia	2,250
Minimum DNBR at nominal design conditions	
Typical flow channel	2.39
Thimble (cold wall) flow channel	2.40
Minimum DNBR for design transients	>1.24
DNB Correlation	WRB-2
Coolant Flow	
Total thermal flow rate, gpm	361,200
Effective flow rate for heat transfer, gpm	330,859
Effective flow area for heat transfer, ft^2	51.1
Average velocity along fuel rods, ft/sec	14.4
Average mass velocity, 10^6 lb_m/hr ft^2	2.42

Coolant Temperature	WCGS Unit
Nominal Inlet, °F	555.8
Average rise in vessel, °F	65.2
Average rise in core, °F	70.4
Average in core, °F	593.2
Average in vessel, °F	588.4

TABLE 4.4-1 (Sheet 2)

Design Parameters	WCGS Unit
Heat Transfer	
Active heat transfer surface area, ft^2	59,742
Average Heat Flux, $Btu/hrft^2$	198,315
Average Linear Power, kW/ft	5.691
Peak Linear Power for normal operation, kW/ft	14.23(a)
Pressure drop (b) Across core, psi	28.7

(a) This limit is associated with the value of F_q = 2.50
(b) Based on best estimate reactor flow rate, at discussed in Section 5.1.

Table 4.4-2

This Table has been Deleted

TABLE 4.4-3

VOID FRACTIONS AT NOMINAL REACTOR CONDITIONS
WITH DESIGN HOT CHANNEL FACTORS

	Average (%)	Maximum (%)
Core	0.1	-
Hot Subchannel	-	12.98

TABLE 4.4-4

This Table has been deleted

TABLE 4.4-5

LOOSE PARTS MONITORING SYSTEM

Environmental Conditions

A. Accelerometers

Temperature	40-650°F
Humidity	0-100%
Radiation	10^{18}nvt and 10^{8} rad
Pressure	69 psig
Vibration	OBE
Atmosphere	Air

B. Preamplifiers and Cables (inside containment)

Temperature-electronics	40-150°F
Hardline Cable	40-650°F
Cable inside containment	40-150°F
Humidity	0-100%
Radiation	10^{12}nvt and $6x10^{6}$ rad
Pressure	69 psig
Shock and Vibration	OBE
Atmosphere	Air

C. Signal Conditioning Amplifier, Signal Processor, and Associated Equipment (outside of containment)

Temperature	40-120°F
Radiation	103 rad
Pressure	Atmospheric
Humidity	0-95%
Shock and Vibration	In accordance with good engineering practice
Atmosphere	Air

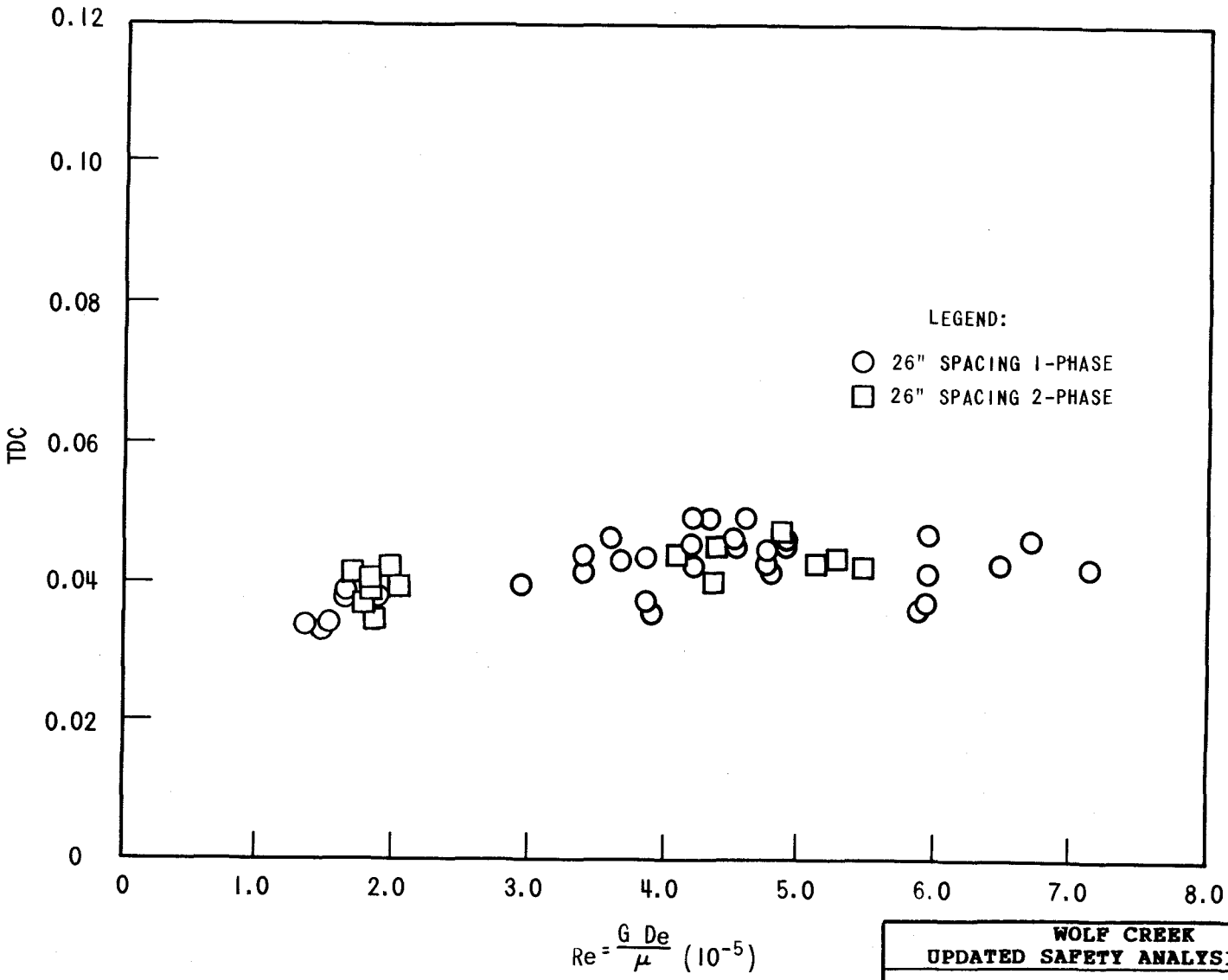

Rev. 0

WOLF CREEK
UPDATED SAFETY ANALYSIS REPORT

FIGURE 4.4-4

TDC VERSUS REYNOLDS NUMBER FOR 26 INCH GRID SPACING

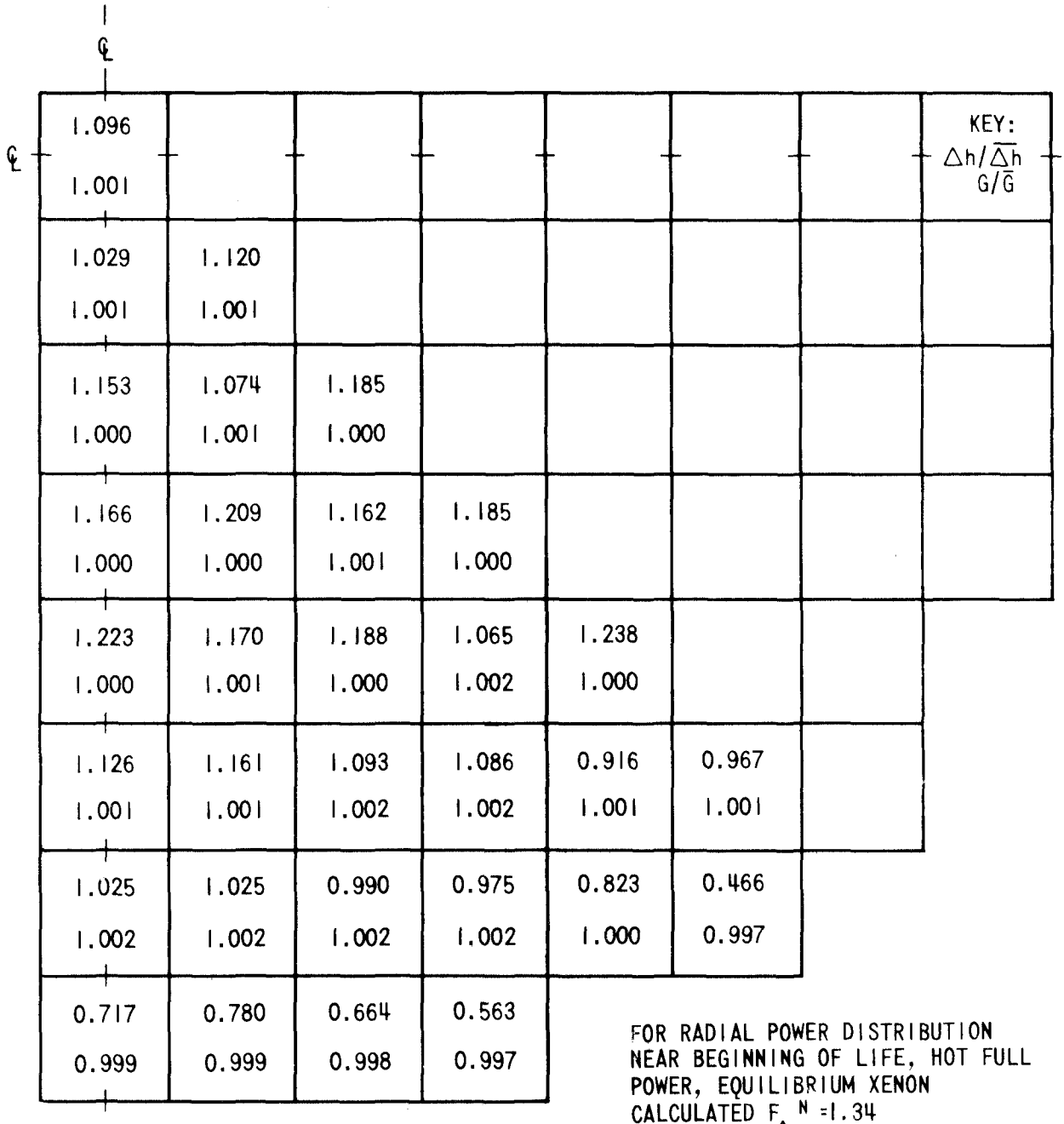

FOR RADIAL POWER DISTRIBUTION NEAR BEGINNING OF LIFE, HOT FULL POWER, EQUILIBRIUM XENON CALCULATED $F_{\Delta H}^{N}$ =1.34

Rev. 0

WOLF CREEK
UPDATED SAFETY ANALYSIS REPORT

FIGURE 4.4-5

NORMALIZED RADIAL FLOW AND ENTHALPY DISTRIBUTION AT 4 FOOT ELEVATION

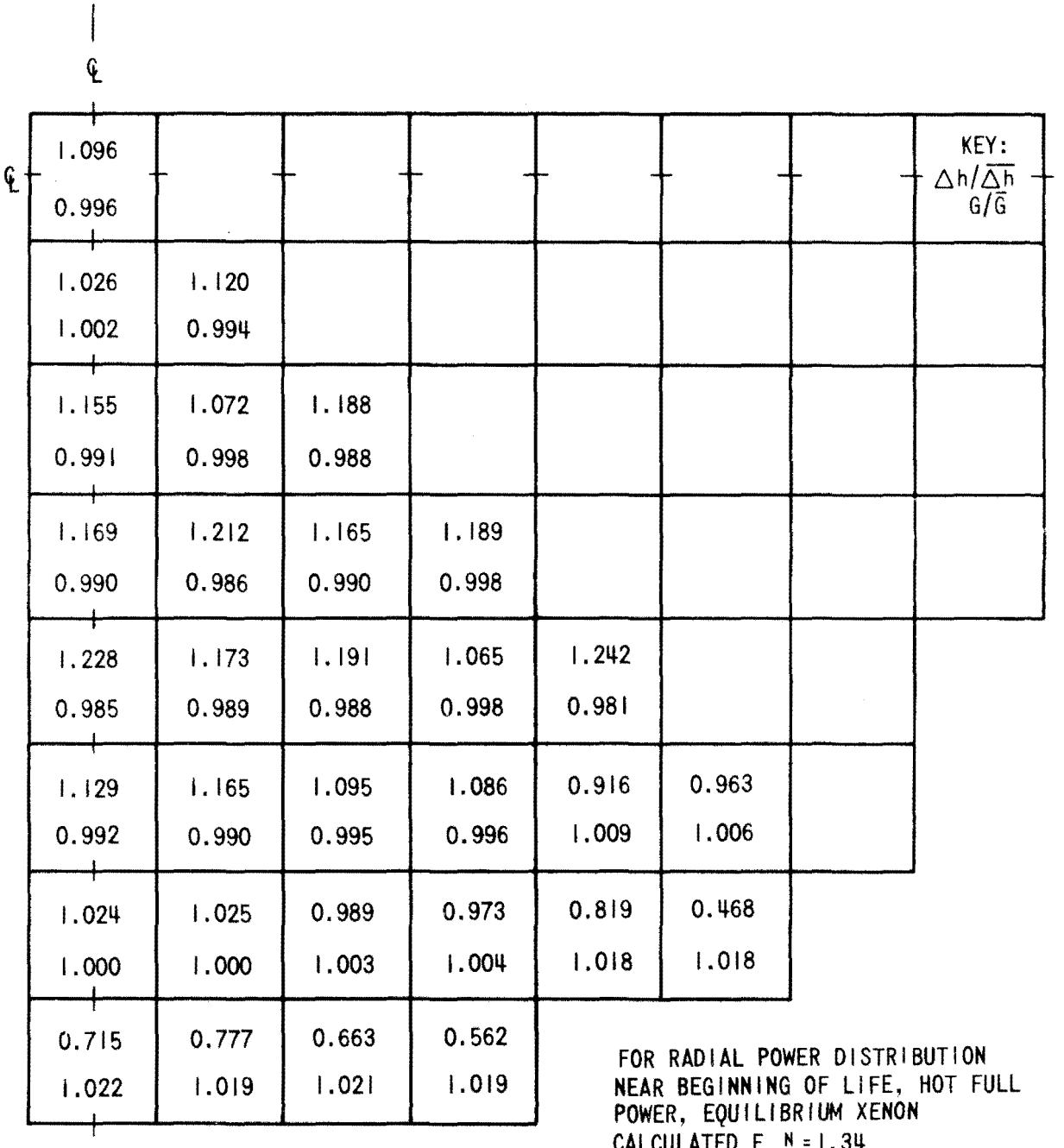

FOR RADIAL POWER DISTRIBUTION
NEAR BEGINNING OF LIFE, HOT FULL
POWER, EQUILIBRIUM XENON
CALCULATED $F_{\Delta H}^{N} = 1.34$

Rev. 0

WOLF CREEK
UPDATED SAFETY ANALYSIS REPORT

FIGURE 4.4-6

NORMALIZED RADIAL FLOW AND ENTHALPY DISTRIBUTION AT 8 FOOT ELEVATION

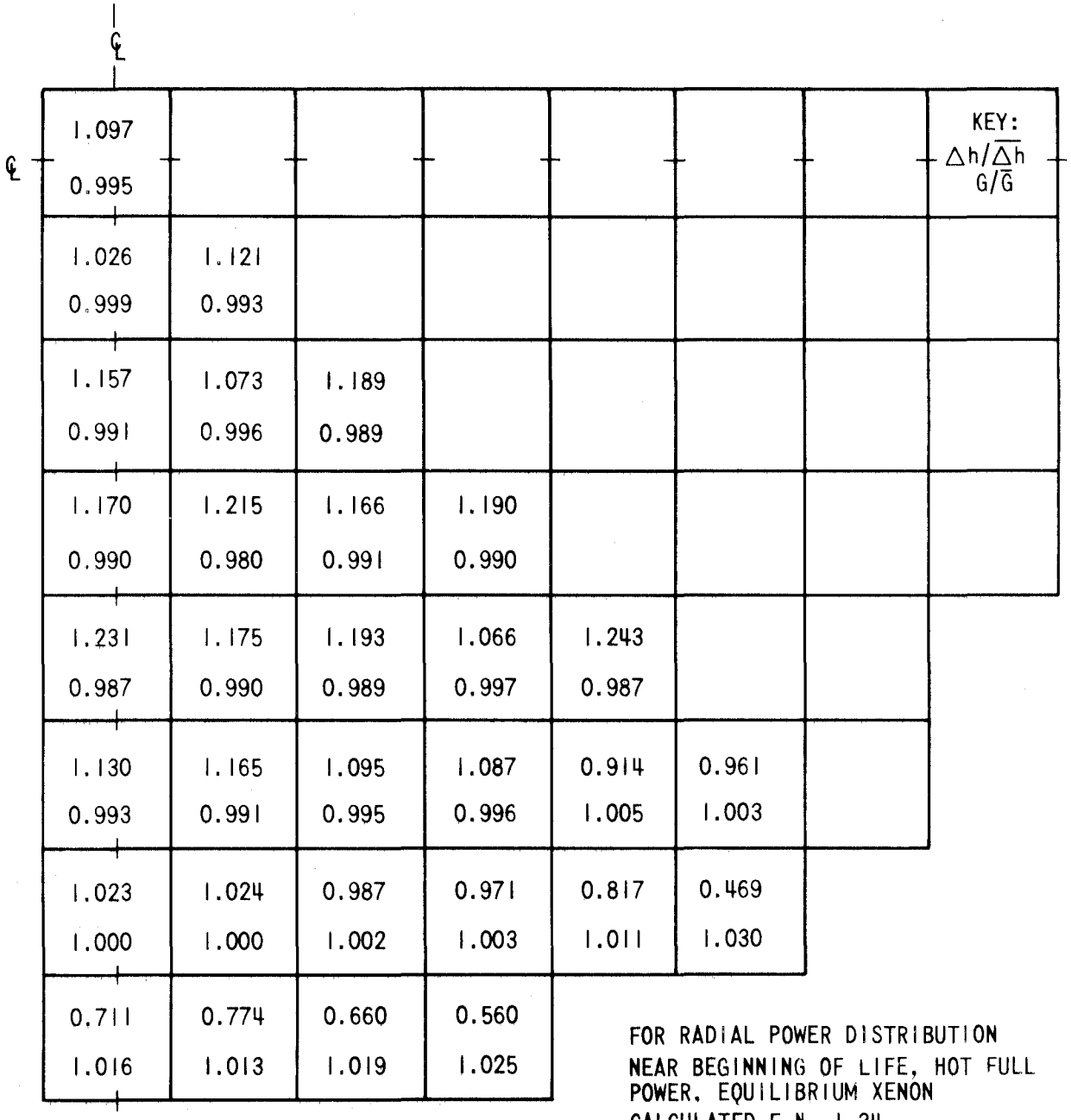

FOR RADIAL POWER DISTRIBUTION
NEAR BEGINNING OF LIFE, HOT FULL POWER, EQUILIBRIUM XENON
CALCULATED $F^N_{\Delta H} = 1.34$

Rev. 0

WOLF CREEK
UPDATED SAFETY ANALYSIS REPORT

FIGURE 4.4-7

NORMALIZED RADIAL FLOW AND ENTHALPY DISTRIBUTION AT 12 FOOT ELEVATION - CORE EXIT

FIGURE 4.4-8 HAS BEEN DELETED

WOLF CREEK
UPDATED SAFETY ANALYSIS REPORT

FIGURE 4.4-8
VOID FRACTION VERSUS
THERMODYNAMIC QUALITY

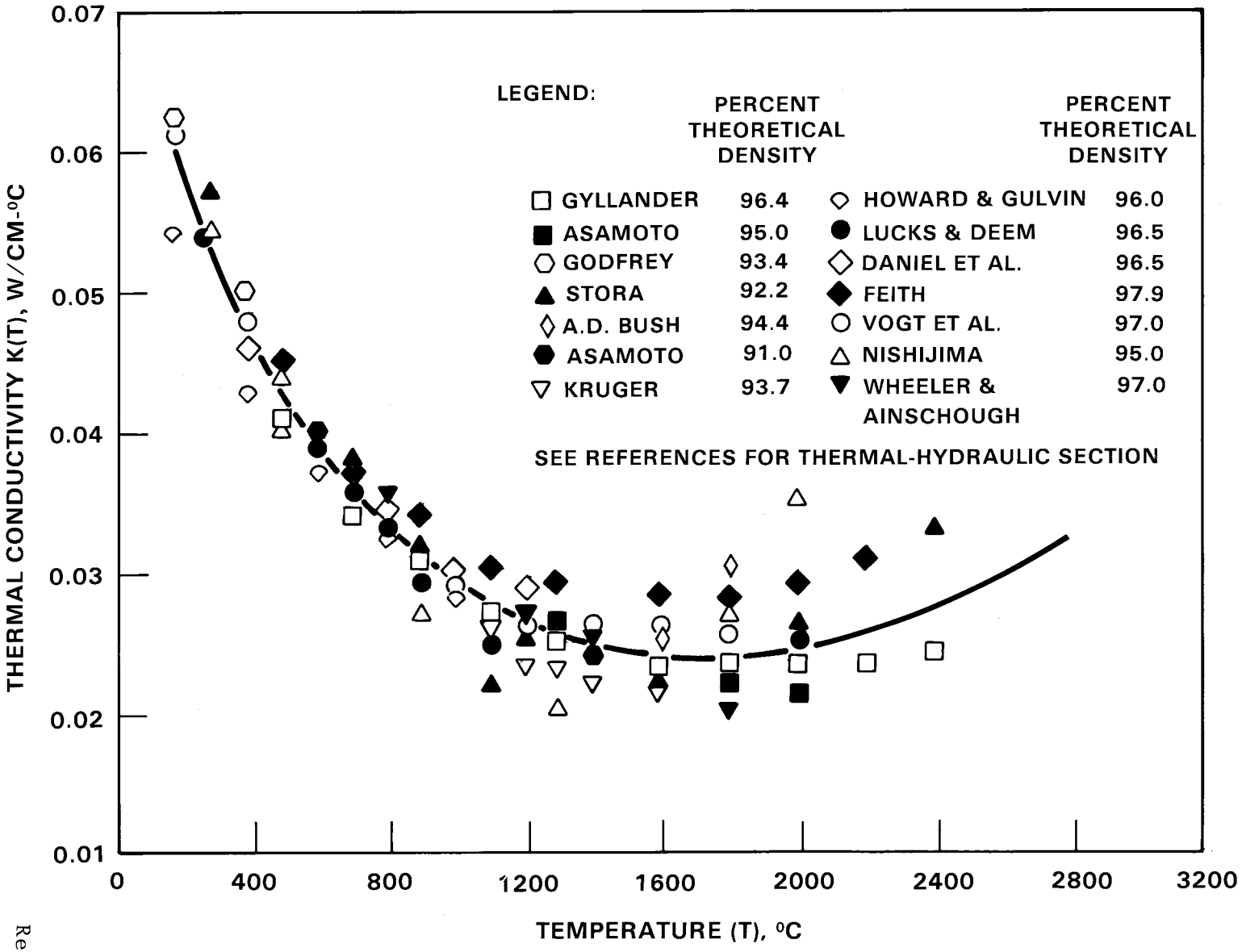

WOLF CREEK
UPDATED SAFETY ANALYSIS REPORT

FIGURE 4.4-9

THERMAL CONDUCTIVITY OF UO_2 (DATA CORRECTED TO 95% THEORETICAL DENSITY)

Rev. 0

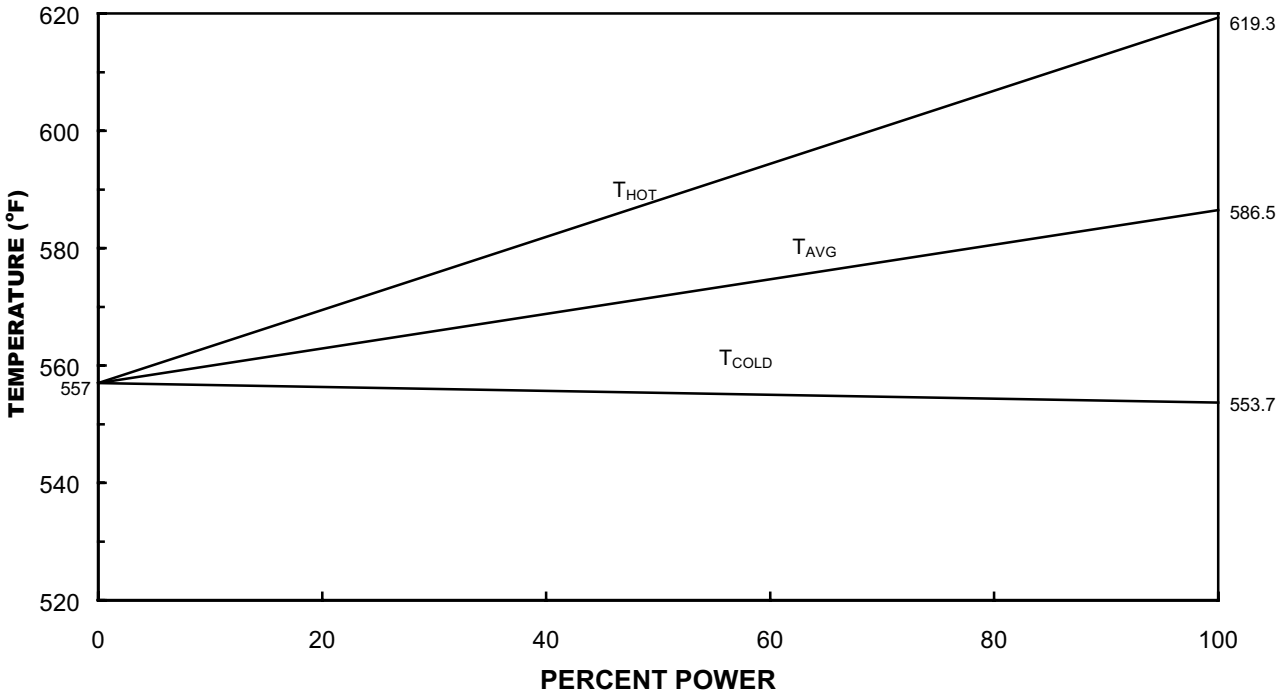

Rev. 13

WOLF CREEK UPDATED SAFETY ANALYSIS REPORT
FIGURE 4.4-10 REACTOR COOLANT SYSTEM TEMPERATURE - PERCENT POWER MAP

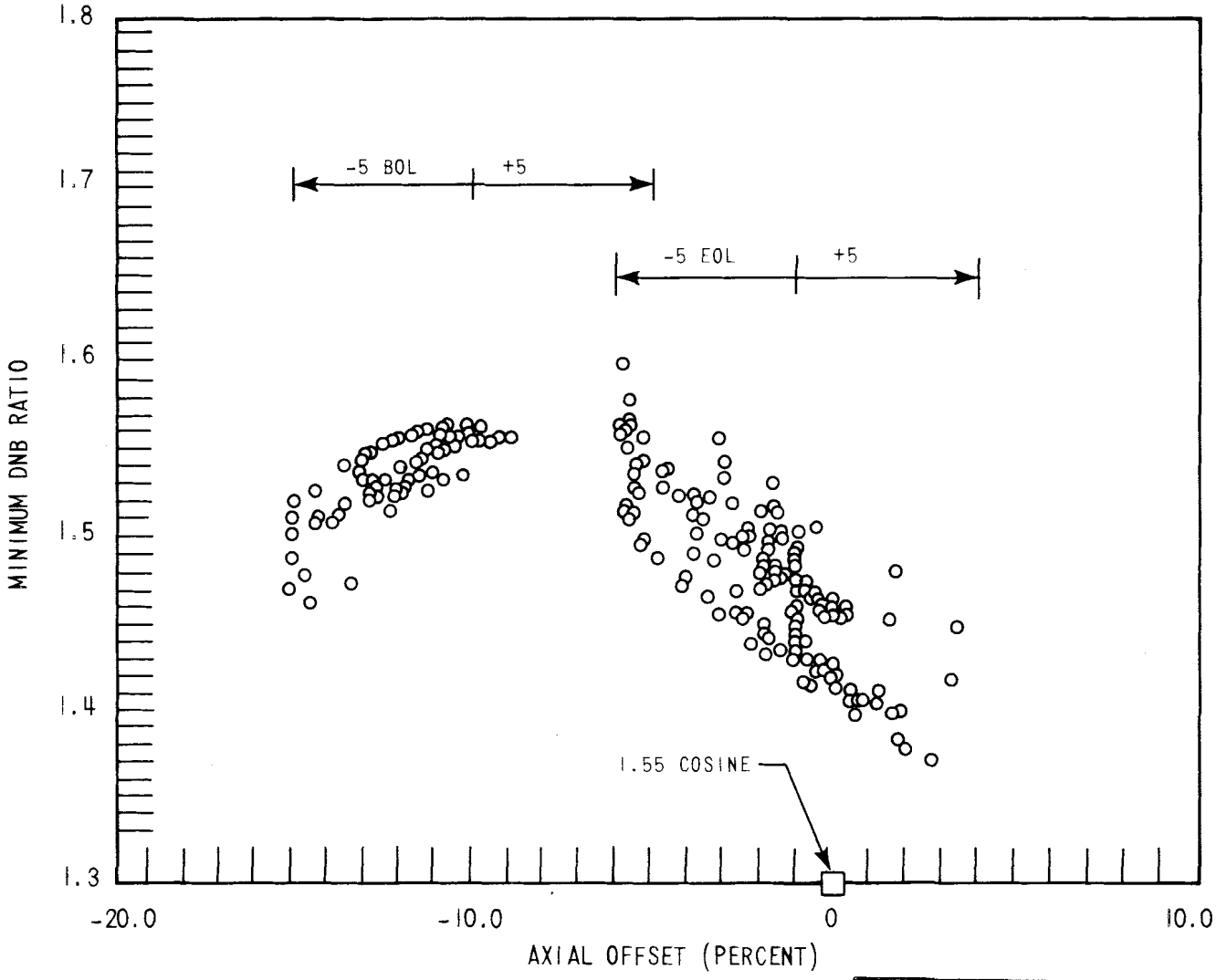

Rev. 0

WOLF CREEK
UPDATED SAFETY ANALYSIS REPORT

FIGURE 4.4-11

100% POWER SHAPES EVALUATED AT CONDITIONS REPRESENTATIVE OF LOSS OF FLOW. ALL SHAPES EVALUATED WITH $F^N_H = 1.55$

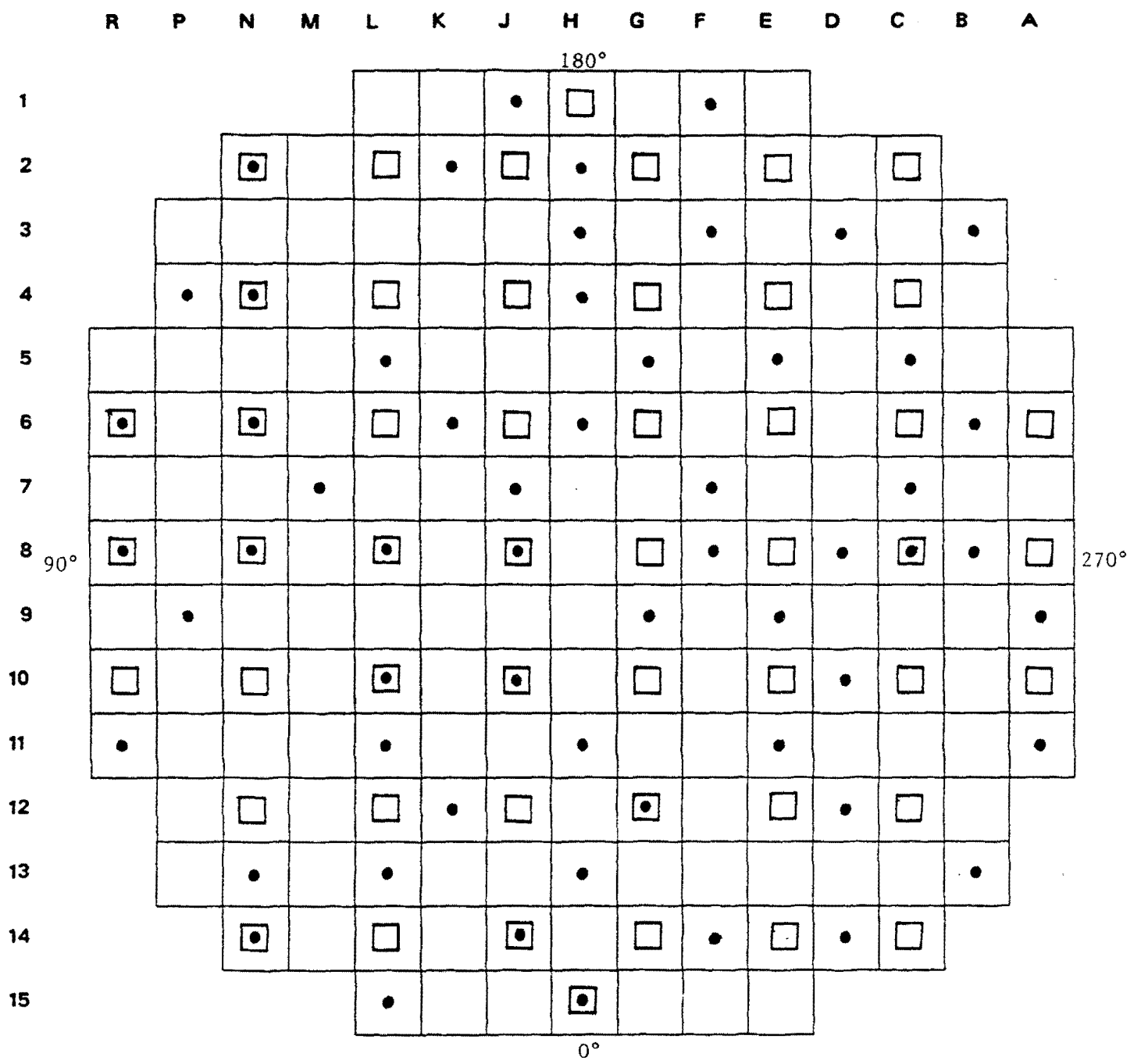

REV. 2

WOLF CREEK
UPDATED SAFETY ANALYSIS REPORT

FIGURE 4.4-21

MOVEABLE DETECTOR AND
THERMOCOUPLE LOCATIONS

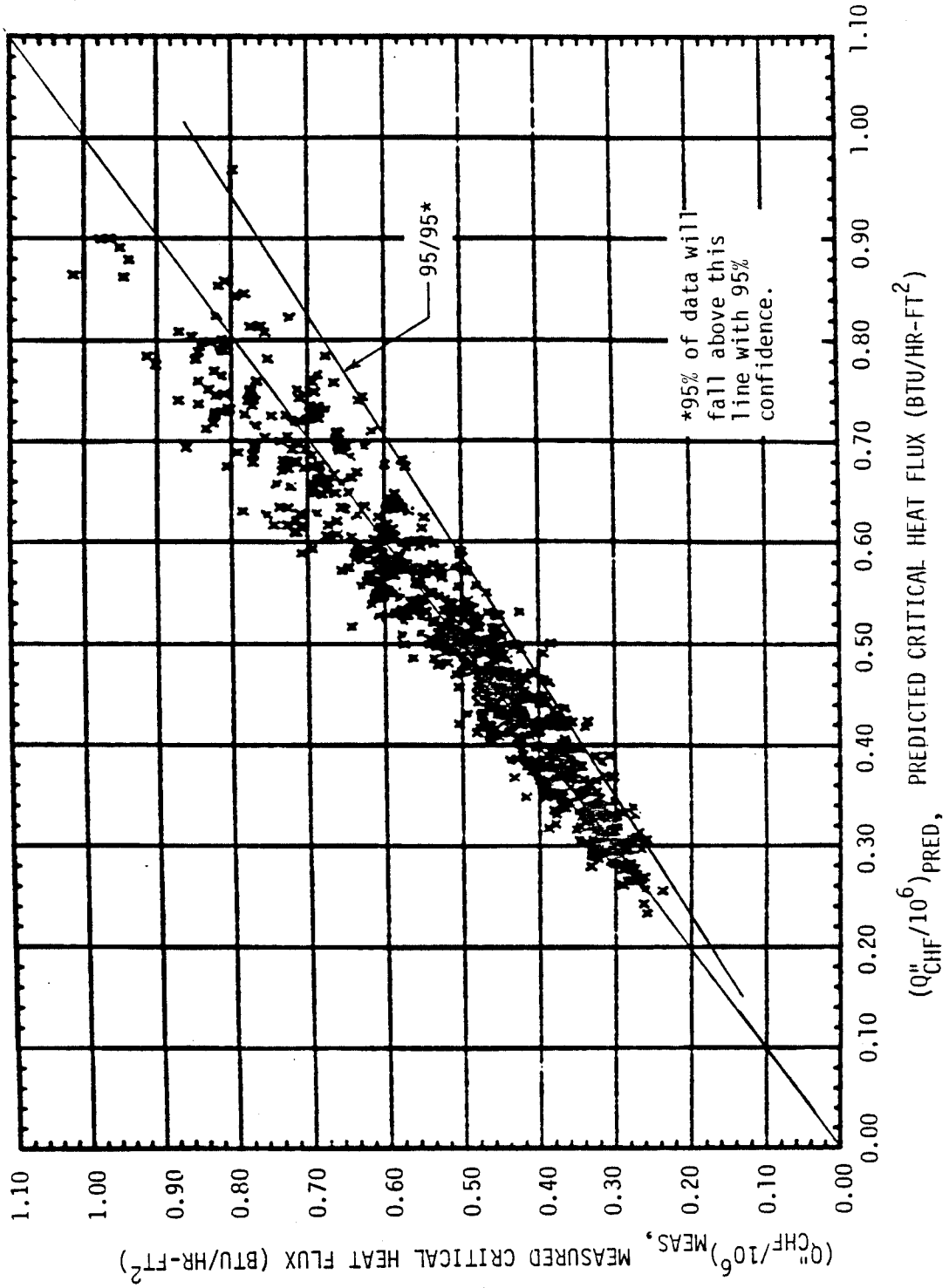

Rev. 7

WOLF CREEK
UPDATED SAFETY ANALYSIS REPORT

FIGURE 4.4-22

MEASURED VERSUS PREDICTED CRITICAL HEAT FLUX WRB-2 CORRELATION

USAR Figure 4.4-23
Measured Versus Predicted Critical Heat Flux – ABB-NV Correlation

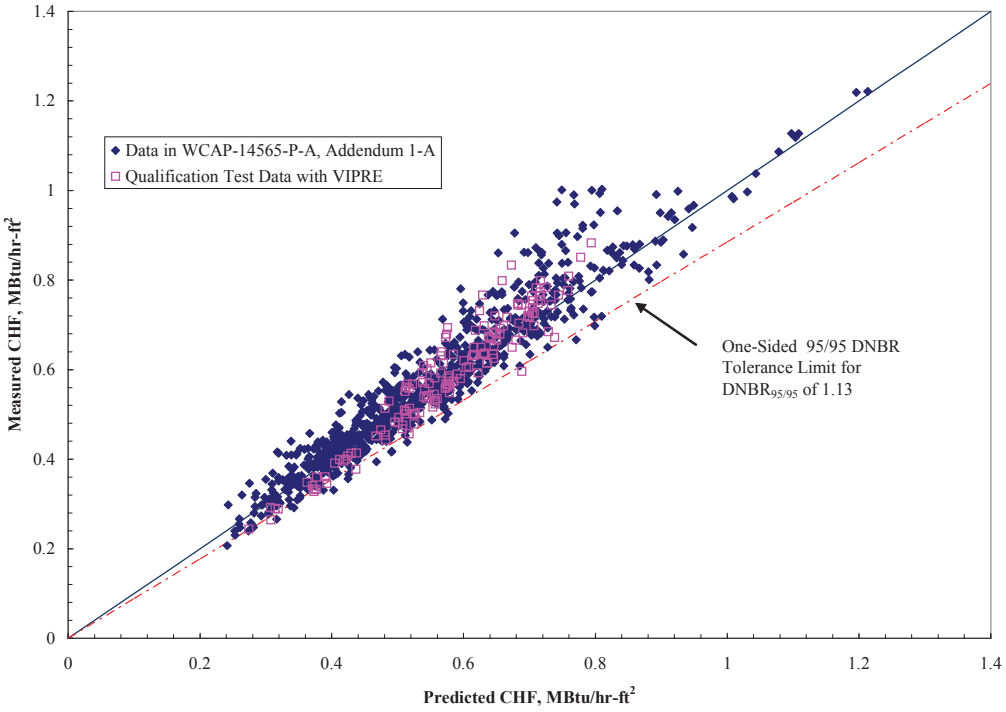

REV. 34

WOLF CREEK UPDATED SAFETY ANALYSIS REPORT
FICURE 4.4-23 MEASURED VERSUS PREDICTED CRITICAL HEAT FLUX-ABB-NV CORRELATION

USAR Figure 4.4-24
Measured Versus Predicted Critical Heat Flux – WLOP Correlation

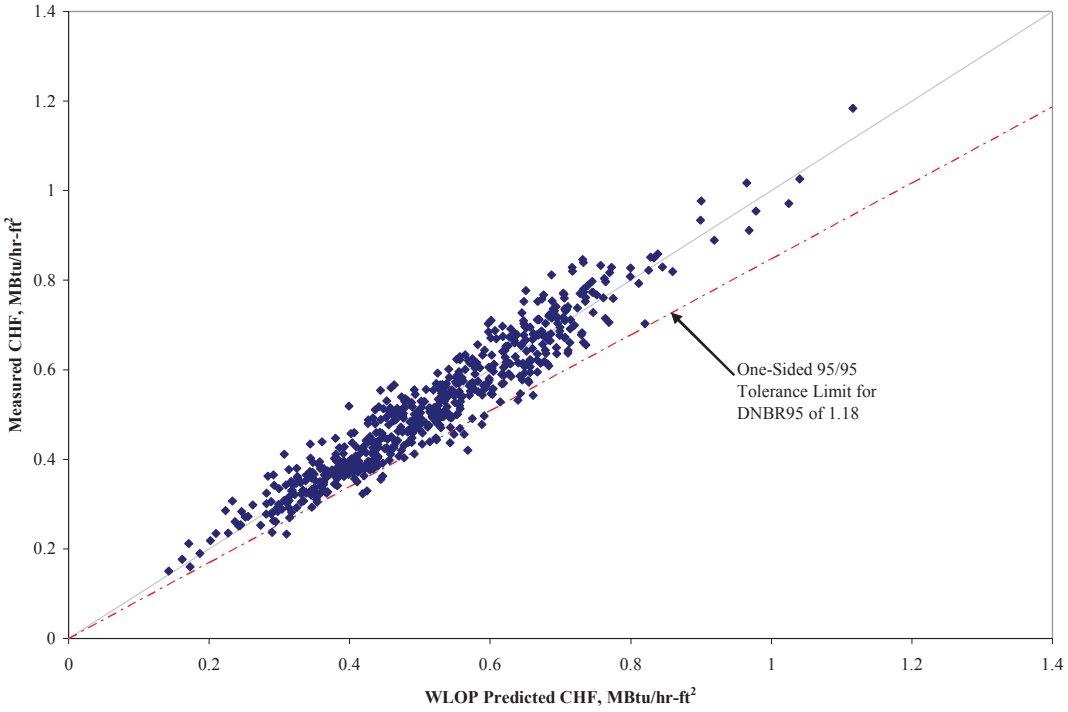

REV. 34

WOLF CREEK UPDATED SAFETY ANALYSIS REPORT
FIGURE 4.4-24 MEASURED VERSUS PREDICTED CRITICAL HEAT FLUX-WLOP CORRELATION

4.5 REACTOR MATERIALS

4.5.1 CONTROL ROD SYSTEM STRUCTURAL MATERIALS

4.5.1.1 Materials Specifications

All parts exposed to reactor coolant are made of metals which resist the corrosive action of the water. Three types of metals are used exclusively: stainless steels, nickel-chromium-iron, and cobalt based alloys. In the case of stainless steels, only austenitic and martensitic stainless steels are used. The martensitic stainless steels are not used in the heat treated conditions which cause susceptibility to stress corrosion cracking or accelerated corrosion in the Westinghouse pressurized water reactor water chemistry.

a. Pressure vessel

   All pressure containing materials comply with Section III of the ASME Boiler and Pressure Vessel Code, and are fabricated from austenitic (Type 304) stainless steel.

b. Coil stack assembly

   The coil housings require a magnetic material. Both low carbon cast steel and ductile iron have been successfully tested for this application. The choice, made on the basis of cost, indicates that ductile iron will be specified on the control rod drive mechanism (CRDM). The finished housings are zinc plated or flame sprayed to provide corrosion resistance.

   Coils are wound on bobbins of molded Dow Corning 302 material, with double glass insulated copper wire. Coils are then vacuum impregnated with silicon varnish. A wrapping of mica sheet is secured to the coil outside diameter. The result is a well insulated coil capable of sustained operation at 200°C.

c. Latch assembly

   Magnetic pole pieces are fabricated from Type 410 stainless steel. All nonmagnetic parts, except pins and springs, are fabricated from Type 304 stainless steel. Haynes 25 is used to fabricate link pins. Springs are made from nickel-chromium-iron alloy (Inconel-X). Latch arm tips are clad with Stellite-6 to provide improved wearability. Hard chrome plate and Stellite-6 are used selectively for bearing and wear surfaces.

d. Drive rod assembly

The drive rod assembly utilizes a Type 410 stainless steel drive rod. The coupling is machined from Type 403 stainless steel. Other parts are Type 304 stainless steel with the exception of the springs, which are nickel-chromium-iron alloy, and the locking button, which is Haynes 25.

4.5.1.2 Fabrication and Processing of Austenitic Stainless Steel Components

The discussions provided in Section 5.2.3 concerning the processes, inspections, and tests on austenitic stainless steel components to ensure freedom from increased susceptibility to intergranular corrosion caused by sensitization, and the discussions provided in Section 5.2.3 on the control of welding of austenitic stainless steels, especially control of delta ferrite, are applicable to the austenitic stainless steel pressure housing components of the CRDM.

4.5.1.3 Contamination Protection and Cleaning of Austenitic Stainless Steel

The CRDMs are cleaned prior to delivery in accordance with the guidance of ANSI N45.2.1. Process specifications in packaging and shipment are discussed in Section 5.2.3. Westinghouse personnel do conduct surveillance to ensure that manufacturers and installers adhere to appropriate requirements, as discussed in Section 5.2.3.

4.5.2 REACTOR INTERNALS MATERIALS

4.5.2.1 Materials Specifications

All the major material for the reactor internals is Type 304 stainless steel. Parts not fabricated from Type 304 stainless steel include bolts and dowel pins, which are fabricated from Type 316 stainless steel, and radial support key bolts, which are fabricated of Inconel-750. These materials are listed in Table 5.2-4. There are no other materials used in the reactor internals or core support structures which are not otherwise included in ASME Code, Section III, Appendix I.

4.5.2.2 Controls on Welding

The discussions provided in Section 5.2.3 are applicable to the welding of reactor internals and core support components.

4.5.2.3 Nondestructive Examination of Wrought Seamless Tubular Products and Fittings

The nondestructive examination of wrought seamless tubular products and fittings is in accordance with Section III of the ASME Code.

4.5.2.4 Fabrication and Processing of Austenitic Stainless Steel Components

The discussions provided in Section 5.2.3 and Appendix 3A verify conformance of reactor internals and core support structures with Regulatory Guide 1.44.

The discussions provided in Section 5.2.3 and Appendix 3A verify conformance of reactor internals and core support structures with Regulatory Guide 1.31.

The discussion provided in Appendix 3A verifies conformance of reactor internals with Regulatory Guide 1.34.

The discussion provided in Appendix 3A verifies conformance of reactor internals and core support structures with Regulatory Guide 1.71.

4.5.2.5 Contamination Protection and Cleaning of Austenitic Stainless Steel

The discussions provided in Section 5.2.3 and Appendix 3A are applicable to the reactor internals and core support structures and verify conformance with ANSI N45 specifications and Regulatory Guide 1.37.

4.6 FUNCTIONAL DESIGN OF REACTIVITY CONTROL SYSTEMS

4.6.1 INFORMATION FOR CONTROL ROD DRIVE SYSTEM (CRDS)

The CRDS is described in Section 3.9(N).4.1. Figures 3.9(N)-5 and 3.9(N)-6 provide the details of the control rod drive mechanisms, and Figure 4.2-8 provides the layout of the CRDS. No hydraulic system is associated with its functioning. The instrumentation and controls for the reactor trip system are described in Section 7.2, and the reactor control system is described in Section 7.7.

4.6.2 EVALUATION OF THE CRDS

The CRDS has been analyzed in detail in a failure mode and effects analysis (Ref. 1). This study, and the analyses presented in Chapter 15.0, demonstrates that the CRDS performs its intended safety function, reactor trip, by putting the reactor in a subcritical condition when a safety system setting is approached, with any assumed credible failure of a single active component. The essential elements of the CRDS (those required to ensure reactor trip) are isolated from nonessential portions of the CRDS (the rod control system) as described in Section 7.2.

Despite the extremely low probability of a common mode failure impairing the ability of the reactor trip system to perform its safety function, analyses have been performed in accordance with the requirements of WASH-1270. These analyses, documented in References 2 and 3, have demonstrated that acceptable safety criteria would not be exceeded even if the CRDS were rendered incapable of functioning during a reactor transient for which their function would normally be expected.

The design of the control rod drive mechanism is such that failure of the control rod drive mechanism cooling system will, in the worst case, result in an individual control rod trip or a full reactor trip (see Section 9.2).

4.6.3 TESTING AND VERIFICATION OF THE CRDS

The CRDS is extensively tested prior to its operation. These tests may be subdivided into five categories: 1) prototype tests of components, 2) prototype CRDS tests, 3) production tests of components following manufacture and prior to installation, 4) onsite preoperational and initial startup tests, and 5) periodic inservice tests. These tests, which are described in Sections 3.9(N).4.4, 4.2, 14.2, and the Technical Specifications , are conducted to verify the operability of the CRDS when called upon to function.

4.6.4 INFORMATION FOR COMBINED PERFORMANCE OF REACTIVITY SYSTEMS

As is indicated in Chapter 15.0, the only postulated events which assume credit for reactivity control systems other than a reactor trip to render the plant subcritical are the steam line break, feedwater line break, and loss-of-coolant accident. The reactivity control systems for which credit is taken in these accidents are the reactor trip system and the safety injection system (SIS). Additional information on the CRDS is presented in Section 3.9(N).4 and on the SIS in Section 6.3. Note that no credit is taken for the boration capabilities of the chemical and volume control system (CVCS) as a system in the analysis of transients presented in Chapter 15.0. Information on the capabilities of the CVCS is provided in Section 9.3.4. The adverse boron dilution possibilities due to the operation of the CVCS are investigated in Section 15.4.6. Prior proper operation of the CVCS has been presumed as an initial condition to evaluate transients, and appropriate Technical Specifications have been prepared to ensure the correct operation or remedial action.

4.6.5 EVALUATION OF COMBINED PERFORMANCE

The evaluations of the steam line break, feedwater line break, and the loss-of-coolant accident, which presume the combined actuation of the reactor trip system to the CRDS and the SIS, are presented in Sections 15.1.5, 15.2.8, and 15.6.5. Reactor trip signals and safety injection signals for these events are generated from functionally diverse sensors and actuate diverse means of reactivity control, i.e., control rod insertion and injection of soluble poison.

Nondiverse but redundant types of equipment are utilized only in the processing of the incoming sensor signals into appropriate logic, which initiates the protective action. This equipment is described in detail in Sections 7.2 and 7.3. In particular, note that protection from equipment failures is provided by redundant equipment and periodic testing. Effects of failures of this equipment have been extensively investigated as reported in Reference 4. The failure mode and effects analysis described in this reference verifies that any single failure will not have a deleterious effect on the engineered safety features actuation system. Adequacy of the emergency core cooling system and SIS performance under faulted conditions is verified in Section 6.3.

4.6.6 REFERENCES

1. Shopsky, W. E., "Failure Mode and Effects Analysis (FMEA) of the Solid State Full Length Rod Control System," WCAP-8976, August 1977.

2. "Westinghouse Anticipated Transients Without Trip Analysis," WCAP-8330, August 1974.

3. Gangloff, W. C. and Loftus, W. D., "An Evaluation of Solid State Logic Reactor Protection in Anticipated Transients," WCAP-7706-L (Proprietary) and WCAP-7706 (Non-Proprietary), July 1971.

4. Mesmeringer, J.C., "Failure Mode and Effects Analysis (FMEA) of the Engineered Safety Features Actuation System," WCAP-8584, Revision 1 (Proprietary) and WCAP-8760, Revision 1 (Non-Proprietary), February 1980.